QUESTIONING THE SPHINX: STRUCTURAL AND FUNCTIONAL STUDIES OF SPHINGOSINE-1-PHOSPHATE LYASE

DISSERTATION

ZUR
ERLANGUNG DER NATURWISSENSCHAFTLICHEN DOKTORWÜRDE
(DR. SC. NAT.)

VORGELEGT DER
MATHEMATISCH-NATURWISSENSCHAFTLICHEN FAKULTÄT
DER
UNIVERSITÄT ZÜRICH

VON
FLORENCE EVELYNE BOURQUIN

VON
BUTTES, LES VERRIÈRES, LA CÔTE-AUX-FÉES (NE)

PROMOTIONSKOMITEE
PROF. DR. MARKUS G. GRÜTTER (VORSITZ + LEITUNG)
PROF. DR. ANTONIO BAICI
PROF. DR. RAIMUND DUTZLER
DR. GUIDO CAPITANI

ZÜRICH 2010

Die vorliegende Arbeit wurde von der Mathematisch-naturwissenschaftlichen Fakultät der Universität Zürich im SS10 als Dissertation angenommen.
Promotionskomitee: Prof. Dr. Markus G. Grütter (Vorsitz), Prof. Dr. Antonio Baici, Prof. Dr. Raimund Dutzler und Dr. Guido Capitani (Leitung der Dissertation).

TABLE OF CONTENTS

RESEARCH SUMMARY

Sphingolipids play crucial roles in eukaryotic cells both as membrane components and as mediators of signalling events. Sphingosine and ceramide promote apoptosis while sphingosine-1-phosphate (S1P) is involved in the regulation of cell growth, survival, proliferation and migration as well as in inflammation and angiogenesis. The relative balance between sphingosine and ceramide on one side and S1P on the other side has been found to play a key role in the determination of cell fate. The metabolism of S1P is often deregulated in pathologies like cancer, allergic response, diabetes and multiple sclerosis. The intracellular concentration of S1P is tightly regulated by a set of three enzymes, sphingosine kinase, S1P phosphatase and S1P lyase (SPL), the biochemistry of which is at present poorly understood. SPL carries out the irreversible degradation of S1P into hexadecenal and phosphoethanolamine (PE). Eukaryotic SPL is a single-pass membrane protein located in the endoplasmic reticulum (ER) with the active site situated in the cytosol. The enzyme requires pyridoxal 5'-phosphate (PLP) as a cofactor. Yeast SPL is involved in the response to heat stress and nutrient deprivation, in calcium homeostasis and in endocytosis. In mammals, SPL plays a crucial role in the maintenance of the immune system, in cell turnover and development.

In this thesis work, a thorough structural characterization of eukaryotic SPL and of a prokaryotic orthologue was successfully carried out, together with a detailed functional analysis. The prokaryotic enzyme, originating from the thermophilic bacterium *Symbiobacterium thermophilum* exhibited a dimer-tetramer equilibrium on size-exclusion chromatography. We solved the structure of a homodimer at 1.8 Å and of a homotetramer at 3.4 Å. The tetramer interface was analysed and categorized as a crystal contact. The protein was active in a preliminary spectrophotometric activity assay validated using mass spectrometry. The structure of the protein inactivated with semicarbazide, a "classical" inhibitor of PLP-dependent enzymes, was solved at 2.1 Å resolution and provided a clear insight into the mode of SPL inhibition. Additionally we solved the structure of a homodimer with conformational heterogeneities at a resolution of 3 Å: one active site lacked PLP and several surrounding loops were conformationally disordered. This active site was assumed to represent an inactive state of the enzyme. The structure of an inactive mutant of the protein in complex with the reaction product PE was solved at 2.9 Å. This and the previous structures served as a basis for the design of active site mutants, which allowed the identification of key residues for activity.

Importantly, the structure of a truncated variant of yeast SPL was solved at 3.1 Å. Despite the striking similarity between the active sites of bacterial and yeast SPLs, truncated yeast SPL turned out to be inactive *in vitro*. Thus, the missing residues appear to be needed for activity, possibly for recruiting the substrate.

An *in vivo* activity assay was carried out on mutants of full-length yeast SPL in collaboration with Prof. Howard Riezman, University of Geneva. The results of the *in vitro* activity tests on bacterial SPL and of the *in vivo* activity test on yeast SPL are in good agreement with each other and provide a solid basis for the proposed reaction mechanism of the enzyme.

ZUSAMMENFASSUNG

Sphingolipide haben in Eukaryoten nicht nur als Membrankomponente eine zentrale Funktion, sondern auch als Mediatoren innerhalb des Signalübertragungsweges der Zelle. Während Sphingosin und Ceramid den programmierten Zelltod auslösen, reguliert Sphingosin-1-phosphat (S1P) nicht nur das Zellwachstum sondern steuert auch die Zelllebensdauer, sowie die Zellteilung und spielt bei Entzündungen und beim Gefässwachstum eine wichtige Rolle. Es hat sich herausgestellt, dass das relative Konzentrationsverhältnis von Sphingosin-Ceramid zu S1P für die Überlebenschance einer Zelle bestimmend ist. Zum Beispiel bei Krebs, Allergie, Diabetes und Multiple Sklerosis ist der S1P Metabolismus sehr oft aus dem Gleichgewicht geraten. Die intrazelluläre Konzentration von S1P wird von den drei Enzymen Sphingosin-Kinase, S1P-Phosphatase und S1P-Lyase (SPL) reguliert. Die damit verbundenen biochemischen Abläufe dieser Regulierung sind jedoch nur zum Teil bekannt. SPL ist für den irreversiblen Abbau von S1P zu Hexadecenal und Phosphoethanolamin (PE) verantwortlich. Eukaryotisches SPL ist ein singlepass Transmembranprotein welches im endoplasmatischen Reticulum (ER) positioniert ist. Das aktive Zentrum liegt im Cytosol. Dieses Enzym benötigt Pyridoxal-5'-Phosphat (PLP) als Enzym-Cofaktor. SPL aus Hefe ist mitverantwortlich für die Reaktion der Zelle auf Wärmestress und Nährstoffmangel, und spielt eine Rolle in der Aufrechterhaltung des zellulären Calciumspiegels sowie in der Endozytose. SPL in Säugetieren spielt eine zentrale Rolle in der Aufrechterhaltung des Immunsystems, im Zellumsatz und in der Entwicklung des Gewebes.
In dieser Dissertation wird eine umfassende strukturelle Charakterisierung und detaillierte funktionelle Analyse des eukariotischen SPL-Enzyms sowie eines prokaryotischen Orthologs präsentiert. Das prokaryotische Enzym des thermophilen Bakteriums *Symbiobacterium thermophilum* zeigte in Gelfiltrations Experimenten ein Equilibrium zwischen dem Dimer und dem Tetramer. Es ist uns gelungen die Struktur des Homodimers auf 1.8Å und die des Homotetramers auf 3.4Å zu lösen. Das Interface der tetrameren Form wurde analysiert und als Kristallkontakt klassiert. Die zuvor gemessene Aktivität in einem spektophotometrischen Assay konnte in der anschliessenden massenspektrometrischen Analyse bestätigt werden. Die Struktur des mit N-Aminoharnstoff (Semicarbazid) inhibierten Proteins konnte bis auf 2.1Å gelöst werden. Die hohe Auflösung erlaubte einen vertieften Einblick in die Funktionsweise der SPL-Inhibition. Zusätzlich konnten wir die homodimere Struktur mit konformationellen Heterogenität bis auf eine Auflösung von 3Å bestimmen. Bei dieser Struktur fehlte im aktiven Zentrum das PLP und mehrere Stellen zeigten eine veränderte konformationelle Anordnung. Es ist naheliegend, dass das aktive Zentrum in dieser Form den inaktiven Zustand des Enzymes darstellt. Die Proteinstruktur einer inaktiven Mutante im Komplex mit dem Reaktionsprodukt PE konnte bis auf 2.9Å gelöst werden. Diese und alle vorhergehenden Proteinstrukturen dienten als Basis für den Entwurf von Varianten mit Mutationen im aktiven Zentrum. Dies sollte die präzise Lokalisierung der für die Aktivität verantwortlichen Aminosäureresten ermöglichen.
Wichtig für das Projekt war auch die Strukturbestimmung auf 3.1Å einer gekürzten Variante von SPL aus Hefe. Trotz der verblüffenden Ähnlichkeit des aktiven Zentrums zum bakteriellen SPL, zeigte die gekürzte Variante aus Hefe keine Aktivität *in vitro*. Das ist ein Hinweis dafür, dass die fehlenden Aminosäuren eine Funktion haben müssen, welche sich auf die Aktivität des Proteins auswirkt. Es wird vermutet, dass diese Aminosäurenresten eine wichtige Rolle bei der Rekrutierung des Substrates übernehmen.
Ein *in vivo* Aktivitätstest an Mutanten mit komplettem SPL aus Hefe wurde in Kollaboration mit Prof. Howard Riezman von der Universität in Genf durchgeführt. Die sehr gut übereinstimmenden Resultate des *in vitro* Aktivitätstests mit bakteriellem SPL und dem *in vivo* Aktivitätstest mit SPL aus Hefezellen bilden eine solide Basis für mögliche Erklärungen des Reaktionsmechanismus dieses Enzyms.

ABBREVIATIONS

ABC, ATP-binding cassette
AC, adenylyl cyclase-cyclic AMP
ADP, adenosine 5'-diphosphate
AET, S-(2-aminoethyl)isothiouronium bromide hydrobromide
AMP, adenosine 5'-monophosphate
ATP, adenosine 5'-triphosphate
a.u., asymmetric unit
AU, absorbance unit
AUC, analytical ultracentrifugation

BSA, bovine serum albumin

CAPS, 3-(cyclohexylamino)-1-propanesulfonic acid
CD, circular dichroism
CER, ceramide
CER'ase, ceramidase
CERT, ceramide transport protein
CFTR, cystic fibrosis transmembrane regulator
CHAPS, 3-[(3-cholamidopropyl)dimethylammonio]-1-propanesulfonate
CHES, 2-(cyclohexylamino)ethanesulfonic acid
CHOL, cholesterol
CMC, critical micelle concentration
COS7, **C**V-1 (cell line derived from kidney cells of the African green monkey) in **O**rigin carrying **S**V40 (Simian-Virus 40) genetic material
C1P, ceramide-1-phosphate
CPT2, carnitine palmitoyl-transferase 2

Da, dalton (g/mol)
DAG, diacylglycerol
DDM, dodecylmaltoside
DHS1P, dihydrosphingosine-1-phosphate
DMSO, dimethyl sulfoxide
DNA, deoxyribonucleic acid
DNPH, dinitrophenylhydrazine
Dpl1p, dihydrosphingosine-1-phosphate lyase 1
DTT, dithiothreitol

EDG, endothelial differentiation gene
EDTA, ethylenediaminetetraacetic acid
EG, ethylene glycol
ER, endoplasmic reticulum
ERK, extracellular signal-regulated kinase
ESI, electrospray

FL, full-length
FTY720 (fingolimod), 2-amino-2-[2-(4-octylphenyl)ethyl]propane-1,3-diol

GABA, γ-amino butyric acid
Gad/GAD, glutamate decarboxylase
GLTP, glycolipid transfer protein
GSL, glycosphingolipids
GTP, guanosine 5'-triphosphate

HEPES, 4-(2-hydroxyethyl)-1-piperazineethanesulfonic acid
HPLC, high performance (or high-pressure) liquid chromatography
Hs, *Homo sapiens*

IGF, insulin-like growth factor
IL, interleukin
IMAC, immobilized metal affinity chromatography
IPTG, isopropyl β-D-1-thiogalactopyranoside
ITC, isothermal titration calorimetry

JNK, Jun amino-terminal kinase

L, litre
LB, Luria broth
LCB, long-chain base
LDAO, lauryldimethylamine-oxide
LL-DAP-AT, LL-diaminopimelate aminotransferase
LPA, lysophosphatidic acid

MAMs, mitochondria-associated membranes
MME, monomethyl ether (PEG)
MPD, 2-methyl-2,4-pentanediol
MS, mass spectrometry
MW, molecular weight
MWCO, molecular weight cut-off

NDA, naphthalene-2,3-dicarboxaldehyde
NEM, N-ethylmaleimide
NF-κB, nuclear factor κB
Ni-NTA, nickel-nitriloacetic acid

OD, optical density

PA, phosphatidic acid
PARP, poly-ADP-ribose polymerase
PC, phosphatidylcholine
PCR, polymerase chain reaction
PDB, protein data bank
PDGF, platelet-derived growth factor
PE, phosphoethanolamine
PEG, polyethylene glycol
PG, phosphatidylglycerol
PH, pleckstrin homology
PI, phosphatidylinositol
PIDD, p53-inducible death domain protein
PI3K, phosphatidylinositol-3 kinase

PIP / PIP2 / PIP3, phosphatidylinositol phosphate / biphosphate / triphosphate
PI4P, phosphatidylinositol 4-monophosphate
PKC, protein kinase C
PLC, phospholipase C
PLP, pyridoxal 5'-phosphate
PM, plasma membrane
PRR, proline-rich repeat (or region)
PS, phosphatidylserine
PS1P, phytosphingosine-1-phosphate
PtE, phosphatidylethanolamine
PVDF, polyvinylidene fluoride

rmsd, root mean square deviation

SAXS, small-angle X-ray scattering
Sc, *Saccharomyces cerevisiæ*
SDS-PAGE, sodium dodecyl sulphate polyacrylamide gel electrophoresis
SEC, size-exclusion chromatography
SK, sphingosine kinase
SM, sphingomyelin
SM'ase, sphingomyelinase
S1P, sphingosine-1-phosphate
SPH, sphingosine
SPL, sphingosine-1-phosphate lyase
SPP, sphingosine-1-phosphate phosphatase
SPR, surface plasmon resonance
SPT, serine palmitoyl-transferase
SQR, sulphide:quinine oxidoreductase
SREBP, sterol regulatory element binding protein
St, *Symbiobacterium thermophilum*
START, steroidogenic acute regulatory protein-related lipid transfer

TAPS, N-[tris(hydroxymethyl)methyl]-3-aminopropanesulfonic acid
TB, terrific broth
TCEP, tris(2-carboxyethyl)phosphine
THI, 2-acetyl-4-tetrahydroxybutyl-imidazole
TLC, thin-layer chromatography
TM, transmembrane
TNF, tumour-necrosis factor
TOF, time-of-flight
Tris, tris(hydroxymethyl)aminomethane

VEGF, vascular endothelial growth factor

WT, wild-type

1. INTRODUCTION

1.1. MEMBRANE LIPIDS

Lipids perform three main functions in living organisms: they are an energy source, they form cellular membranes and they act as signalling molecules (1). Approximately 5% of a eukaryotic genome encodes lipid-related proteins, tuned by evolution to generate, degrade and transport more than a thousand different lipids. The lipid repertoire of an organism is highly conserved across evolution. Failure in lipid metabolism or transport is associated with severe dysfunctions. Moreover, specific lipids are connected to viral and bacterial infection (2). In spite of the importance of this class of molecules, biochemical investigations are hindered by the difficulty of handling these hydrophobic compounds in aqueous solutions.

1.1.1. METABOLISM AND LOCALISATION

Cellular membranes are composed by amphipathic lipids, molecules exhibiting both a hydrophobic and a hydrophilic portion. The formation of a lipid bilayer is spontaneous. The hydrophobic moiety of the lipid self-associates and the hydrophilic part interacts with an aqueous environment. This enables cells to segregate their internal constituents from the external environment and to create specialized compartments where specific chemical or enzymatic reactions take place.
Importantly, the lipid composition of membranes exerts an influence on the activity of integral and peripheral membrane proteins. Some lipids, by arranging into defined membrane domains, are able to recruit proteins that mediate signalling events, transport of solutes and nutrients or provide enzymatic activity. The major structural lipids in eukaryotic membranes are glycerophospholipids: phosphatidic acid (PA), phosphatidylethanolamine (PtE), phosphatidylserine (PS), phosphatidylinositol (PI), and phosphatidylcholine (PC), the most abundant phospholipid in eukaryotic cells (**figure 1-1**). Their hydrophobic portion, diacylglycerol (DAG), features a variable length and degree of insaturation. This allows a further degree of specialization in addition to the polar head group. Due to its relatively small polar head, PtE does not spontaneously associate into a bilayer, but rather interacts with membrane proteins and modulates their activity. Additionally, PtE allows for membrane curvature, a property required for membrane budding, fission, and fusion (3). Another class of structural lipids is that of sphingolipids (**figure 1-2**). They possess saturated or *trans*-insaturated hydrophobic tails and pack together more tightly than PC does. Glycosphingolipids are located at the cell surface and are involved in cell-to-cell recognition and cellular communication. The hydrolysis (or phosphorylation) of glycerophospholipids and sphingolipids produces bioactive lipids: PA, DAG, sphingosine (SPH), sphingosine-1-phosphate (S1P), ceramide (CER) and ceramide-1-phophate (C1P) (**figures 1-1** & **1-2**). Since SPH and S1P contain only one aliphatic chain and are thus presumably less tightly bound to the membrane than CER and C1P, they might be involved in signalling events through interaction with cognate membrane receptors (4). Sterols are non-polar membrane lipids (**figure 1-3**). These molecules are able to intercalate between sphingolipid tails, thus increasing the fluidity of sphingolipid-rich domains. In yeast cell membranes the predominant sterol is ergosterol, while cholesterol predominates in mammals.
The various kinds of lipids specifically distribute into given organelles. The enzymes involved in the synthesis of lipids are distributed in several cellular compartments. The endoplasmic reticulum (ER) is the major site of synthesis of cholesterol, phospholipids and ceramides. The

enzymes of lipid metabolism are subcompartmentalized in defined regions of the ER called mitochondria-associated membranes (MAMs). The newly synthesized lipids are quickly transported to other organelles. The Golgi apparatus is specialized in sphingolipid synthesis. It produces phosphosphingolipids like sphingomyelin, glycosphingolipids like glucosylceramide and lactosylceramide, as well as gangliosides, which are glycosphingolipids with a terminal sialic acid. Most of the lipids synthesized in the Golgi will be further transported to the plasma membrane (PM). The PM is enriched in sphingolipids and sterols, which are densely packed and make it resistant to mechanical stress. Numerous reactions of lipid metabolism take place in this part of the cell, for example the degradation of sphingomyelin to ceramide by sphingomyelinase. The synthesis of phosphoinositides occurs in the PM as well as in early and late endosomes (**figure 1-1**). Phosphoinositides are signalling molecules specialized in membrane recognition and sorting of membrane proteins to organelles. Late endosomes are specialized in lipid catabolism. For example, one isoform of sphingomyelinase located in late endosomes and possessing an acidic pH optimum, is responsible for the turnover of plasma membrane sphingomyelin. Sterols and PS are also degraded in late endosomes. The mitochondrion synthesizes phosphatidylglycerol (PG), the building block for cardiolipin, a lipid unique to the inner membrane of mitochondria and to bacterial membranes (5) (**figure 1-4**). This organelle also synthesizes lysophosphatidic acid (LPA), PA, and PtE. Moreover, mitochondria are involved in the metabolism of cholesterol together with the ER (6).

Figure 1-1. Glycerophospholipids

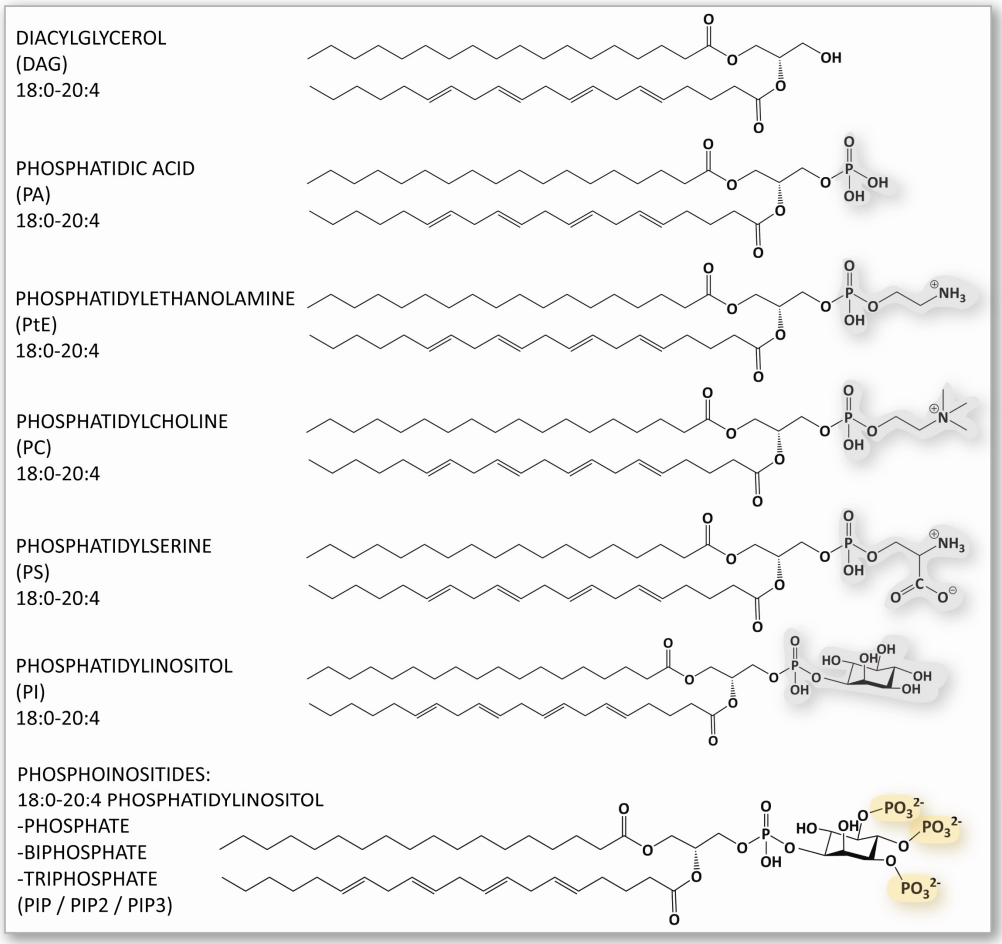

Figure 1-2. Sphingolipids

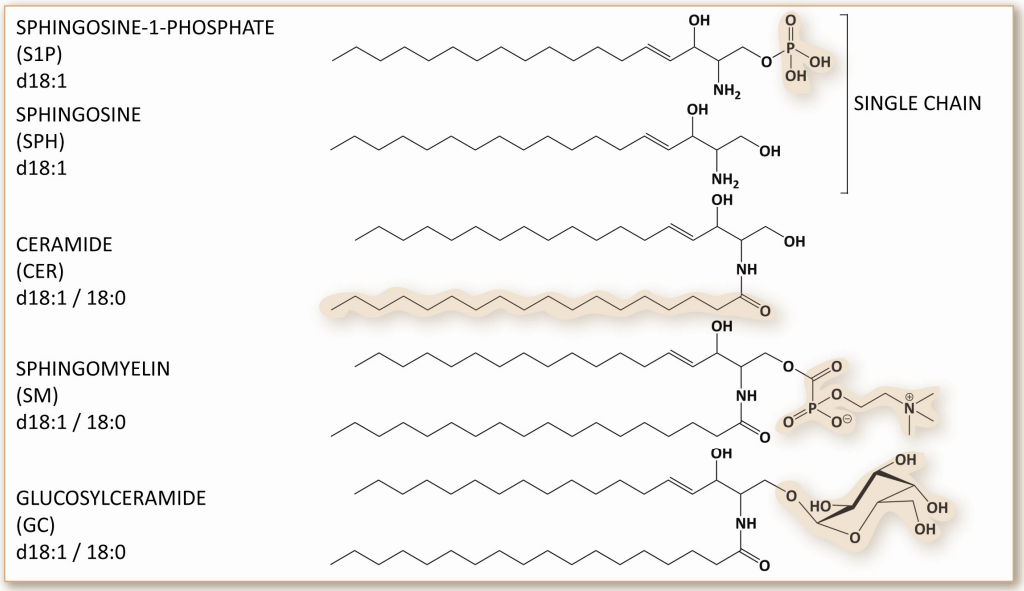

Figure 1-3. Sterols

Figure 1-4. Mitochondrion lipids

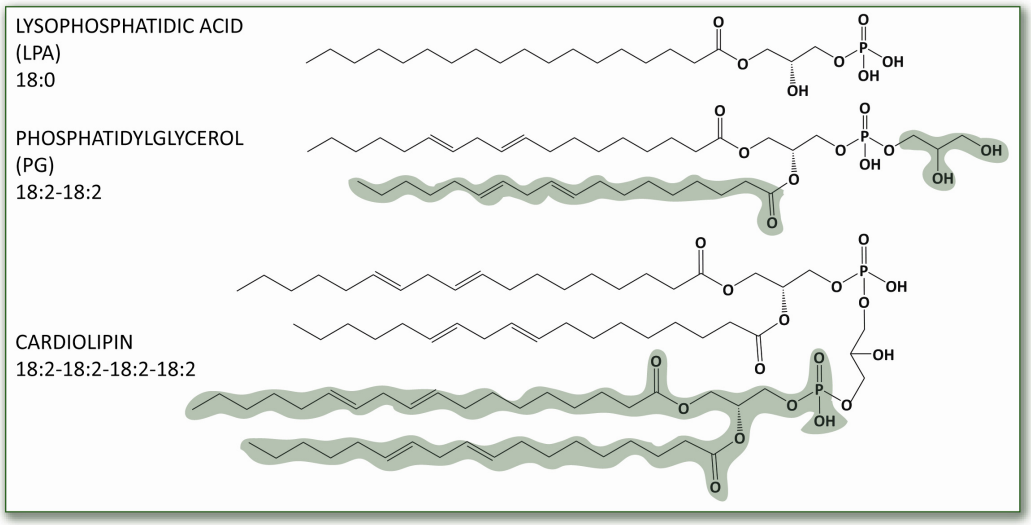

1.1.2. TRANSMEMBRANE DISTRIBUTION

The lipid composition of the two leaflets of the ER membrane and the inner membrane of Gram-negative bacteria is symmetric. This is not true for the two leaflets of the Golgi, endosomal and plasma membranes. Sphingomyelin and glycosphingolipids are found in the external leaflet of the PM, whereas the cytosolic leaflet is enriched in PS and PtE (7). Lipid asymmetry has functional consequences. For example, phagocytosis is mediated by sensing of PS exposed to the cell surface. Furthermore, an imbalance in lipid quantity is required for vesicle budding (8).

Lipid asymmetry results from three main phenomenona. First, some lipids are able to spontaneously cross the hydrophobic core of the membrane depending on the size, charge and polarity of the molecule (9). PS and PtE are known to equilibrate between the two leaflets of the ER membrane. Second, lipids can be retained in one leaflet *via* specific interactions with proteins or other lipids (10). This is presumably the case for cholesterol, which is assumed to be more abundant in the exoplasmic leaflet of the cell membrane due to its affinity with sphingolipids, despite controversial data on its orientation in the PM (11) (7). Third, the lipids can undergo membrane protein-mediated transport from one leaflet to the other (12). In the ER, ATP-independent transport occurs, resulting in the equilibration of lipids in the two leaflets. Specific or aspecific ATP-dependent transport involves members of the P4 family of lipid flippases and of ABC (ATP-binding cassette) transporters, known as floppases (**figure 1-5**). The flippases commonly carry out the import of lipids, whereas the export is achieved by the floppases. Other membrane proteins, the plasma membrane scramblases (also called lipid translocases) are involved in Ca^{2+}-dependent and ATP-independent randomization of lipid location between the two leaflets.

Figure 1-5. The three major classes of lipid transporters (adapted from (12))

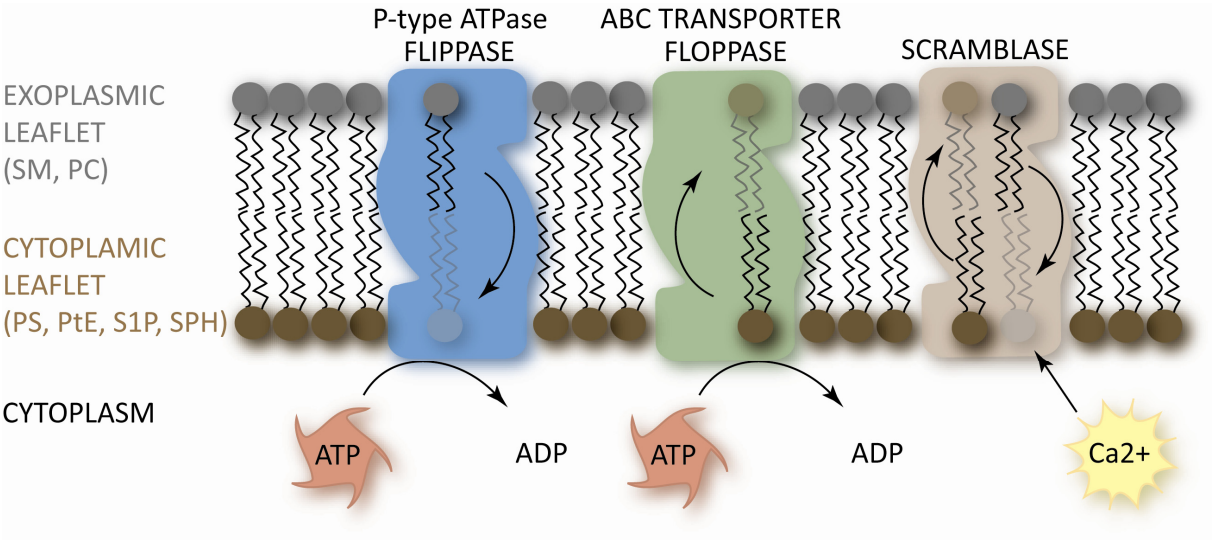

1.1.3. TRANSPORT BETWEEN ORGANELLES

Transport of specific lipids from organelles is mandatory for their metabolism and is most commonly mediated by budding and fusion of membrane vesicles. Specific lipid transport covers the ER, the Golgi, the PM, the endosomes, and the lysosomes. Some lipids are preferentially incorporated into anterograde vesicles (that is, the vesicles targeted to the PM) and are excluded from retrograde transport. This phenomenon contributes to enriching the PM in certain lipids, like sphingolipids and sterols.
In contrast, the import and export of lipids from and to the mitochondria and the peroxisomes are not connected to the vesicular transport system. There, proteins are likely responsible for lipid transport, presumably through contact sites between organelles. Non-vesicular transport of lipids between organelles has been demonstrated (13) (14) (15) (16) (17) (18) (**figure 1-6**). It involves specialized proteins such as CERT (ceramide transport protein). CERT is a protein harbouring a START lipid transfer domain and additional domains required for the identification of donor and acceptor membranes (19) (20) (see section 1.5.3.).

Figure 1-6. Cellular distribution of cholesterol, phospholipids and sphingolipids

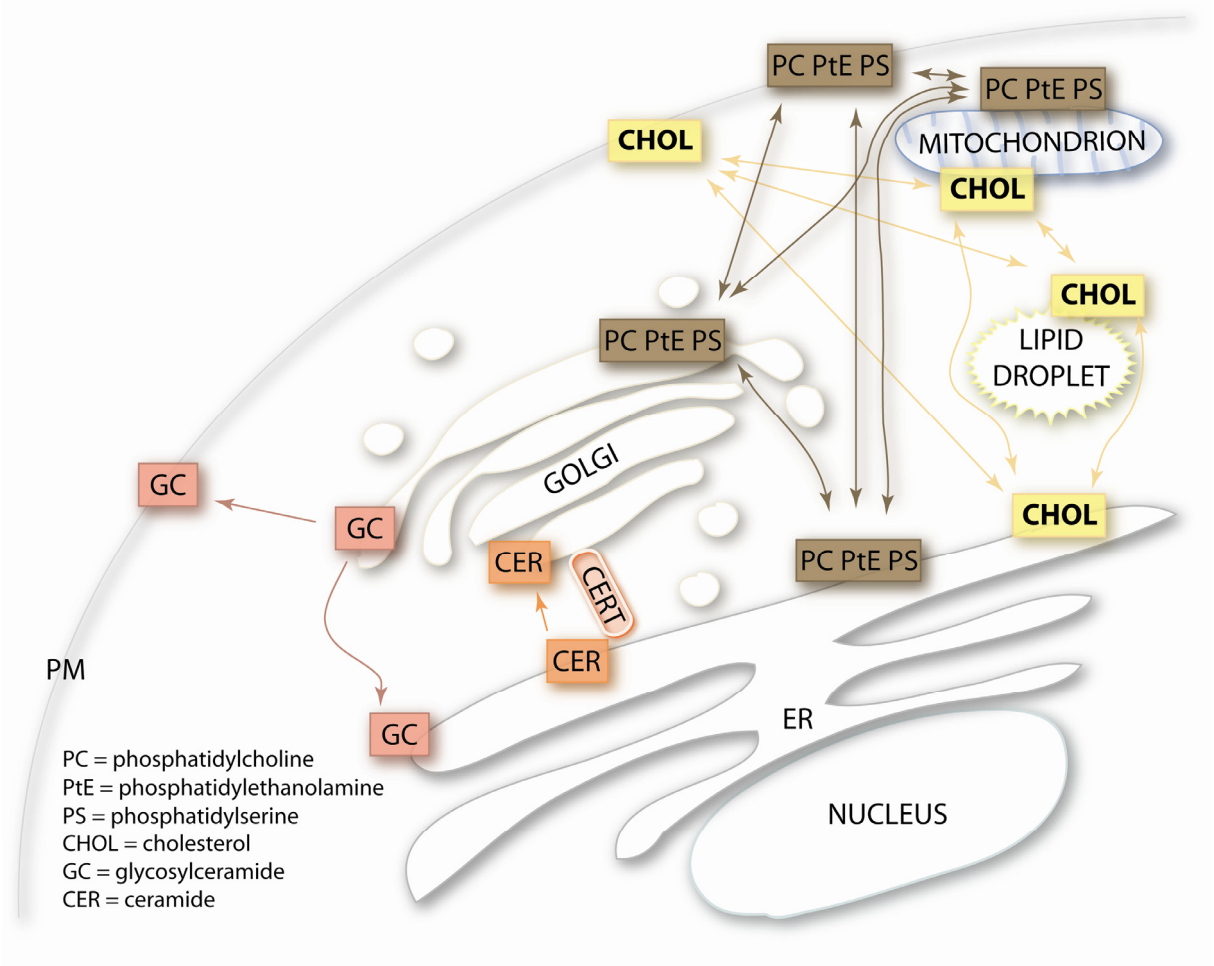

1.2. SPHINGOLIPIDS

Sphingolipids were first isolated in 1884 by J.L.W. Thudichum and named with the prefix sphingo- due to their enigmatic behaviour. In fact, they exhibited at the same time some features of hydrophilic and hydrophobic compounds, and their function was a riddle. They are strictly found in eukaryotes, with the exception of the *Sphingomonas* bacterial genus.

1.2.1. CHEMICAL STRUCTURE

Sphingolipids are composed of three modules: a sphingosine backbone called long-chain base (LCB), a polar head group, and an amine-linked fatty acid chain (**figures 1-7** & **1-2**). The common structure of the sphingosine backbone, 2-amino-1,3-diol-alkane, is unique in nature and possesses two optical centres at carbon atoms 2 and 3. The naturally occurring diastereoisomers of sphingolipids have the (2D,3D) [or D(+)-*erythro*-] configuration (21). The sphingosine backbone and the fatty acid chain are variable in length, degree of insaturation and substitution. The most common sphingosine backbone has 18 carbon atoms and one 4-*trans* double bond (abbreviated d18:1) (**table 1-1**). The length of the fatty acid chain usually ranges from 14 to 30 carbon atoms and can also carry one single insaturation as well as hydroxyl groups. In mammals alone, there are a couple of dozen types of LCB and fatty acid chains and more than 400 polar head groups exist: they combine in tens of thousands of various sphingolipids (22).

Figure 1-7. Chemical structure of sphingolipids

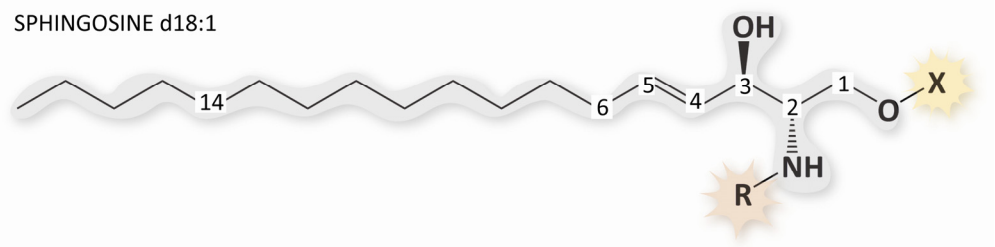

NAME	ABBREVIATION	- R	- X
SPHINGOSINE	SPH	H	H
SPHINGOSINE-1-PHOSPHATE	S1P		Phosphate
CERAMIDE	CER	Fatty acid	H
CERAMIDE-1-PHOSPHATE	C1P		Phosphate
GLUCO- / GALACTO-CEREBROSIDE	GlcCer / GalCer		Glucose / Galactose
SPHINGOMYELIN	SM		Phosphocholine
GLOBOSIDE			Several neutral sugars: Glucose / Galactose / N-acetyl galactosamine
GANGLIOSIDE			Several Glucose / Galactose / N-acetyl galactosamine + 1 to 4 N-acetyl neuraminic acid (NANA)

Table 1-1. Examples of sphingosine backbones

NAME	LENGTH	INSATURATION	ADDITIONAL HYDROXYL GROUP	CODE
SPHINGOSINE (SPHINGENINE)	18 C	4-*trans*		d18:1
DIHYDOSPHINGOSINE (SPHINGANINE)				d18:0
PHYTOSPHINGOSINE (4-HYDROXYSPHINGANINE)			4-Hydroxy-	t18:0
SPHINGADIENE		4-*trans* 14-*cis*		d18:2

1.2.2. METABOLISM

Sphingolipids can either be produced *via* the degradation of existing sphingolipids or *de novo* in a synthesis pathway initiated by serine palmitoyl-transferase (SPT) (**figure 1-8**) (23). SPT catalyzes the condensation of serine and palmitoyl-CoA to the first sphingolipid, 3-keto-dihydrosphingosine (24). This reaction is the entry point of sphingolipid metabolism. Acylation of dihydrosphingosine generates dihydroceramide (25), which is subsequently desaturated to form ceramide (CER) (26), a sphingolipid metabolic hub. CER is the building block of glycosphingolipids (27), ceramide-1-phosphate (C1P) (28) and sphingomyelin (SM) (29). CER deacylation by various ceramidases produces sphingosine (SPH) (30) (31), a single-chain sphingolipid. SPH is the substrate of sphingosine kinase (SK) (32), which produces sphingosine-1-phosphate (S1P). S1P can be reversibly dephosphorylated by S1P phosphatase (SPP) (33) or irreversibly degraded by S1P lyase (SPL) in one long-chain aldehyde and phosphoethanolamine (PE), a polar compound (34). The cleavage of S1P catalyzed by SPL is the exit point of the sphingolipid metabolism. PE can be reintroduced into the lipid metabolic pathway by phophoethanolamine transferase, which produces phosphatidylethanolamine (PtE) from PE and diacylglycerol (35). In fruit fly PtE, in addition to being a plasma membrane phospholipid, is required for the processing of SREBP (sterol regulatory element binding protein), a key regulator of lipid biosynthetic gene transcription (36).
A second route for the generation of ceramide consists in the breakdown of complex sphingolipids by specific hydrolases (37) and of sphingomyelin by specific sphingomyelinases (30).

Figure 1-8. Sphingolipid metabolism (adapted from (23))

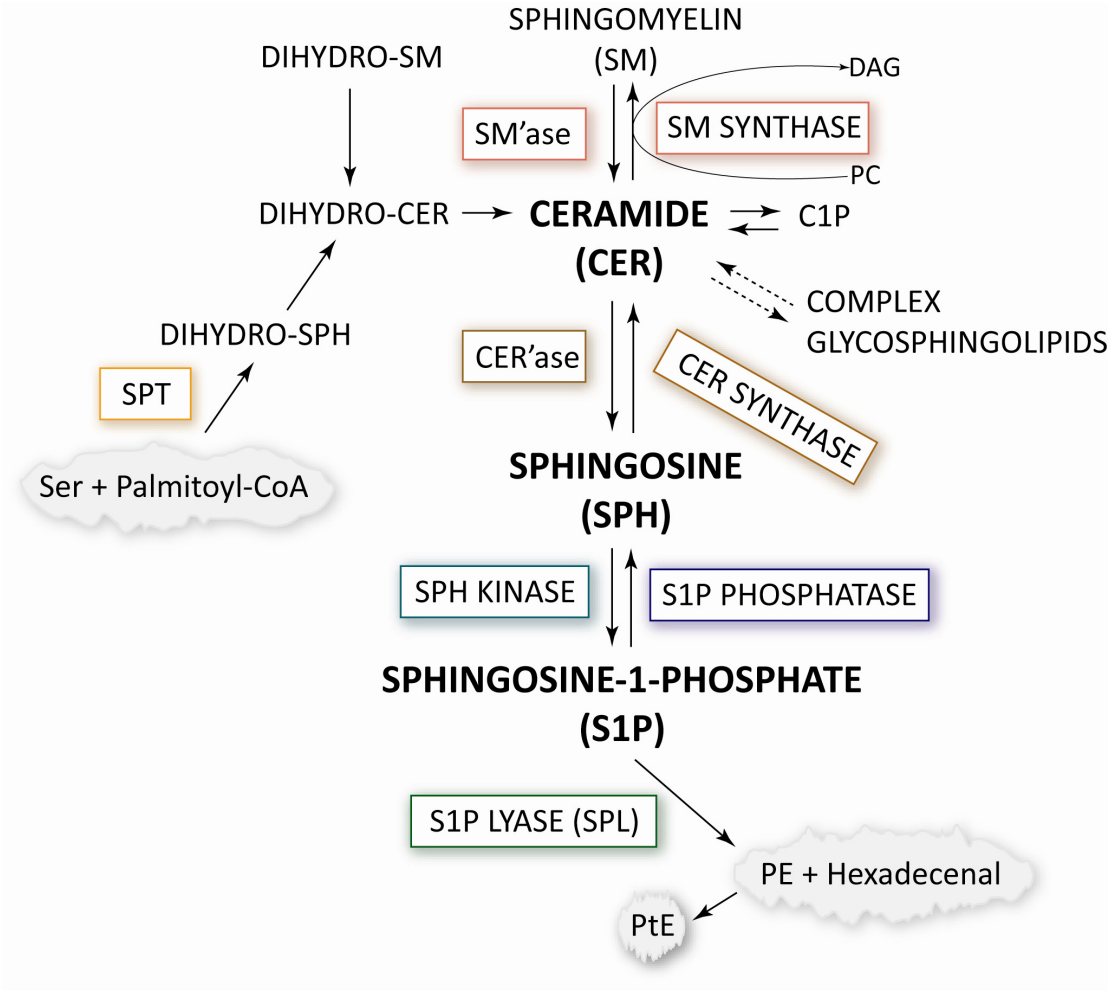

1.2.3. LOCALISATION

The subcellular localisation of sphingolipids and of the proteins involved in their metabolism is an important parameter influencing the function and regulation of a given lipid or protein. Neutral hydrophobic sphingolipids such as ceramide may be able to flip-flop across membrane (10), while charged sphingolipids are most likely to be confined in their site of synthesis or transported by an active mechanism from one to the other leaflet or to their target organelle.

CER is produced in the ER and transported to the Golgi and the PM where it serves to build SM and complex sphingolipids (**figure 1-9**) (38). The transport is carried out by vesicular transport and by CERT, a multi-domain protein able to specifically translocate a sphingolipid molecule from the ER to the Golgi (19) (see section 1.5.3.). The six known ceramide synthases show distinct affinities for different fatty acyl-CoA substrates and locate in different cell compartments (**table 1-2**) (25). CER is also produced from the breakdown of SM, by three types of sphingomyelinase (SM'ase) featuring different pH optima, primary sequence and localisation. Acid SM'ase is mainly found in the endolysosomal pathway, but can be primed to relocate to the outer leaflet of the PM, whereas the neutral isoform localizes to the inner leaflet of the PM (39). The third isoform, alkaline SM'ase, is a secreted enzyme responsible for the digestion of dietary sphingomyelin in the gut (40).

Sphingosine kinase 1 (SK1) translocates to the PM from the cytosol and interacts with anionic phospholipids (41). The nature of the second isoform (SK2) seems to be more elusive, as it was reported either sharing SK1 properties and localisation or being more tightly associated to membranes (42) (43). S1P is a pivotal cell signalling molecule, which is located in various cell compartments and cell types. S1P is transported into the blood stream by lipoproteins and albumin, a non-specific lipid adsorbent. Platelets and erythrocytes lack the S1P degrading enzymes and can release S1P in response to certain stimuli (44) (45). Within the cell, S1P is produced in the inner leaflet of the PM and can be transported to the outer leaflet by ABCC1, an ABC transporter (46). Cystic fibrosis transmembrane regulator (CFTR) is another ABC transporter that facilitates S1P transport from the outer to the inner leaflet of the membrane (47).

Figure 1-9. Spatial organisation of the sphingolipid metabolism (adapted from (23))

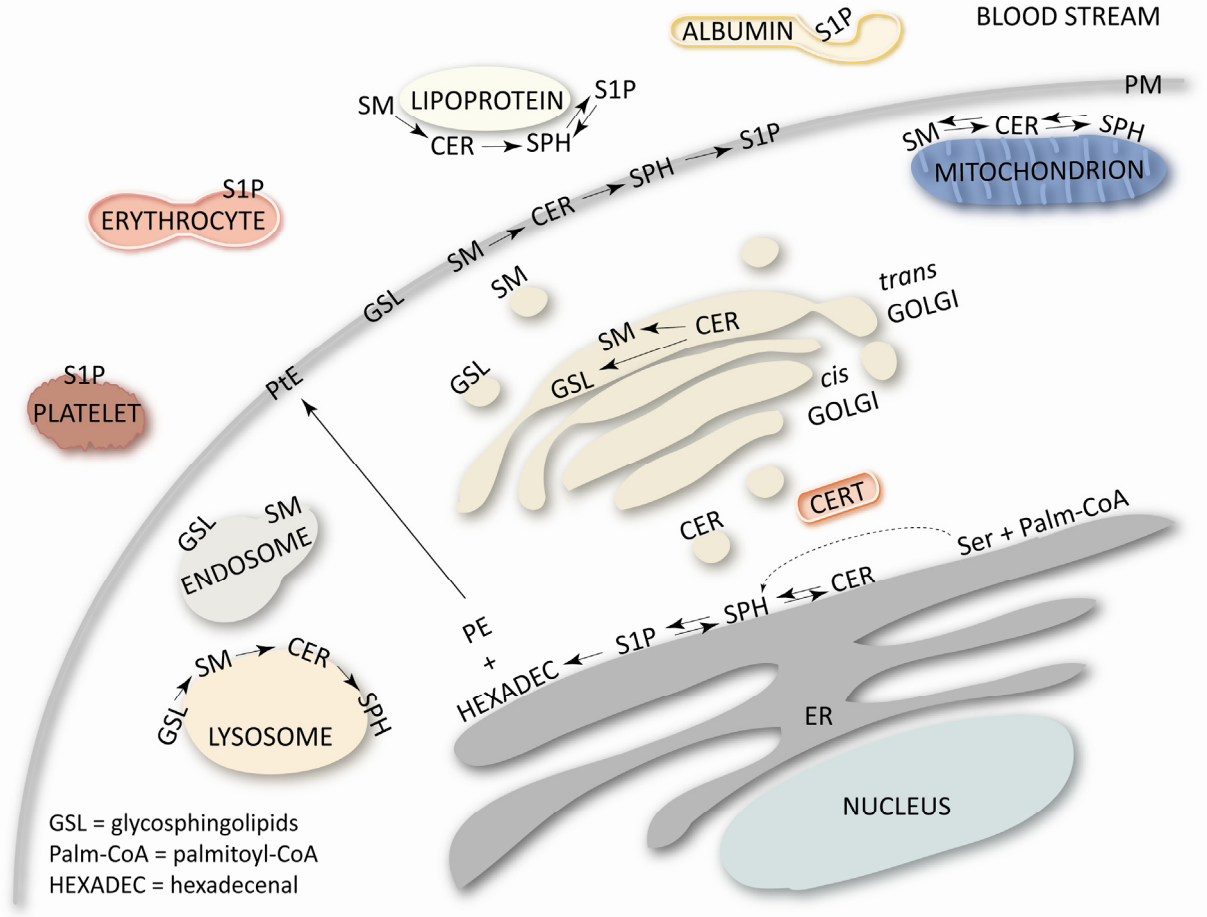

Table 1-2. Human sphingolipid-related proteins locations and properties

NAME	ISOFORM	TYPE	LOCALISATION	REFERENCE
SPHINGOMYELINASE (SM'ASE)	Acid	Soluble	Lysosome Secreted Outer PM	(38) (48)
	Neutral -2	Integral membrane protein	Debated (Golgi, ER, nucleus, PM)	(48)
	Alkaline	Soluble or membrane-anchored	Secreted (Intestine) Outer PM	(38) (40)
SM SYNTHASE	1	Integral membrane protein	Golgi	(29)
	2		Golgi PM	(29) (49)
	r		ER	(29) (50)
CERAMIDASE (CER'ASE)	Acid	Not determined	Lysosome	(51) (52)
	Neutral	Integral membrane protein	Secreted (Intestine) Outer PM Mitochondria	(38) (53)
	Alkaline	Integral membrane protein	Golgi	(31)
CERAMIDE SYNTHASE	1-6	Integral membrane protein	ER	(25) (25, 54)
SERINE PALMITOYL-TRANSFERASE (SPT)	(1)	Debated (1-2 TMH)	ER	(55) (56) (57)
S1P PHOSPHATASE (SPP)	1-2	Integral membrane protein	ER	(58)
SPH KINASE (SK)	1	Soluble but recruited to the membrane	Cytosol PM	(41) (59) (60)
	2	Debated: Similar to SK1 or Integral membrane protein	Cytosol or ER and Nucleus	(42) (43)
S1P LYASE (SPL)	(1)	N-terminal TMH	ER	(61)
CERAMIDE TRANSPORT PROTEIN (CERT)		Soluble with membrane-interacting domains	ER and Golgi	(18) (19)

1.2.4. FUNCTIONS

Sphingolipids play crucial roles in living cells.
Together with cholesterol, sphingomyelin and glycosphingolipids form lipid detergent-resistant membrane microdomains called "lipid rafts". Lipid rafts are involved in the clustering of membrane proteins, for example during signal transduction, in vesicular budding, and in the entry of pathogens. Sphingolipids can directly interact with domains of membrane proteins, thereby modifying their activity. An example is the inhibition of the EGF (epidermal growth factor) receptor tyrosine kinase by a ganglioside (62). Some pathogenic bacteria like *Escherichia coli*, *Mycobacterium tuberculosis*, *Vibrio cholerae*, *Clostridium tetani*, *Salmonella typhimurium* and some viruses like *Influenzavirus*, *HIV*, *Ebolavirus* use rafts as a gateway to the host cell. The same is true for various parasites like trypanosomes, *Plasmodium falciparum*, *Leishmania*, *Toxoplasma* and even for *prions* (63) (64).
Some sphingolipids are “bioactive”, that is a change in their concentration brings about functional consequences (65). The enzymes of the sphingolipid metabolism are biochemically interconnected, meaning that an increase in synthesis of one compound is related to a decrease in the other. Such interconnectivity increases the complexity of the signalling pathway and allows the cell to modulate the levels of a signalling molecule and its antagonist. An example is the interconversion of sphingosine to S1P. Phosphorylation of sphingosine increases the level of S1P and decreases at the same time the level of sphingosine. Moreover, the relative levels of ceramide, sphingosine, and S1P differs tremendously (**figure 1-10**). As a consequence, phosphorylation of 1% of the sphingosine pool may lead to a doubled amount of S1P (65). In addition, the location and transport of metabolites and enzymes, allowing pathways to operate in parallel, add another level of complexity. The balance of the concentrations of ceramide and sphingosine on one side and of S1P on the other side has been proposed to form a "sphingolipid rheostat" that controls cell fate (**figure 1-10**) (66). The relative amounts of sphingolipids and imbalances in their metabolism have been univocally linked to allergic response, colon and breast cancer, diabetes mellitus type II and multiple sclerosis. In particular, glucosylceramide is involved in drug resistance (67). Sphingosine modulates the activity of various kinases involved in the regulation of the cytoskeleton, endocytosis, cell cycle, and apoptosis (68). Ceramide regulates stress-induced senescence (69) and apoptosis (70), whereas ceramide-1-phosphate is involved in inflammation, vesicular trafficking and phagocytosis (71) (72). S1P mediates cell survival, cell migration and inflammation (73).

Figure 1-10. The sphingolipid rheostat (adapted from (65))

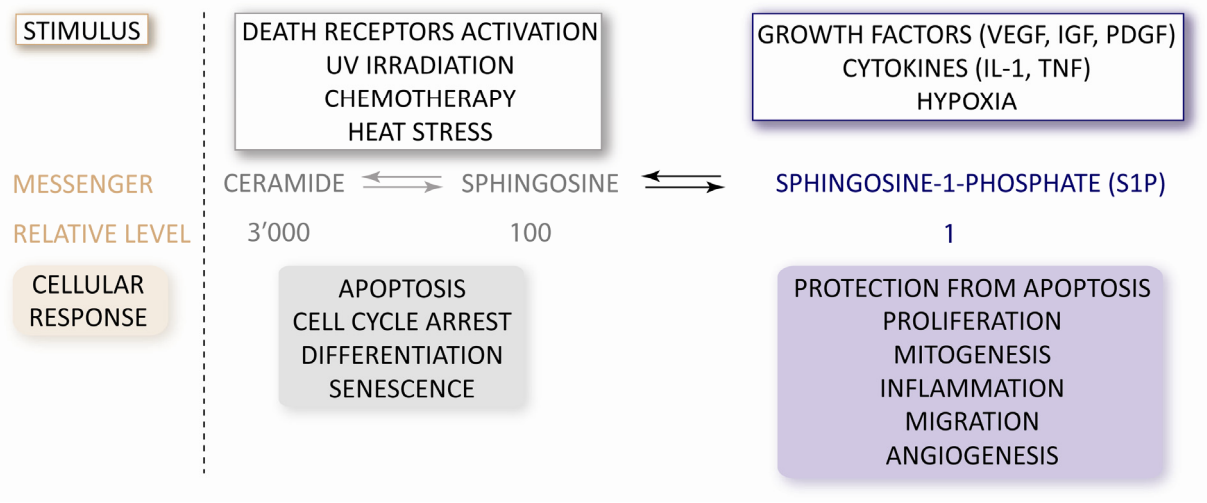

1.3. SPHINGOSINE-1-PHOSPHATE (S1P)

S1P is a bioactive lipid involved in the regulation of proliferation, cell growth, cell survival, cell migration, inflammation, angiogenesis and resistance to apoptosis. It is a tumour-promoting agent antagonist to the cellular response primed by ceramide and sphingosine (**figure 1-10**) (43). Elevated amounts of S1P are found in cancer cells (74). Inhibitors of the enzyme responsible for S1P synthesis, sphingosine kinase, are currently used as antitumor drugs (75) (76). S1P is a unique messenger in that it shows both an intracellular and extracellular mode of action. This latter is made possible through the binding to its five yet identified cognate receptors $S1PR_{1-5}$ (77).

1.3.1. INTRACELLULAR MESSENGER

Consistently with its function in signalling, S1P is present in nanomolar amounts in cells (78) and its concentration is tightly regulated by a set of three enzymes: sphingosine kinase (SK), sphingosine-1-phophate phosphatase (SPP) and sphingosine-1-phosphate lyase (SPL) (see 1.2.2. and 1.4.) (**figure 1-11**).
Two isoforms of sphingosine kinase are known in mammals, SK1 and SK2. SK1 is the main enzyme responsible for the synthesis of S1P at the PM (79). SK1 is activated subsequently to PDGF (platelet-derived growth factor) (80) and VEGF (vascular endothelial growth factor) receptors activation (81), by cytokines like tumour necrosis factor-α (TNF- α), and by numerous other growth and survival factors (66). One known activation scheme involves the phosphorylation of SK1 on a critical serine residue by protein kinase C (PKC), promoting the interaction of SK1 with phosphatidylserine located in the cytoplasmic leaflet of the PM (60). Other studies highlight the role of Ca^{2+} and calmodulin in the translocation of SK1 to the PM (59) (82). The fate of the newly synthesized S1P is unclear: it might interact with a specific carrier, might undergo vesicular transport or might associate to a yet unknown specific target. An increase in S1P concentration correlates with the activation of nuclear factor κB (NF-κB) (83) and of GTPases of the Ras family (81), with the inactivation of the Jun amino-terminal kinase (JNK) (84), and with an increase in intracellular calcium concentration (85).

Figure 1-11. S1P modes of action (adapted from (86))

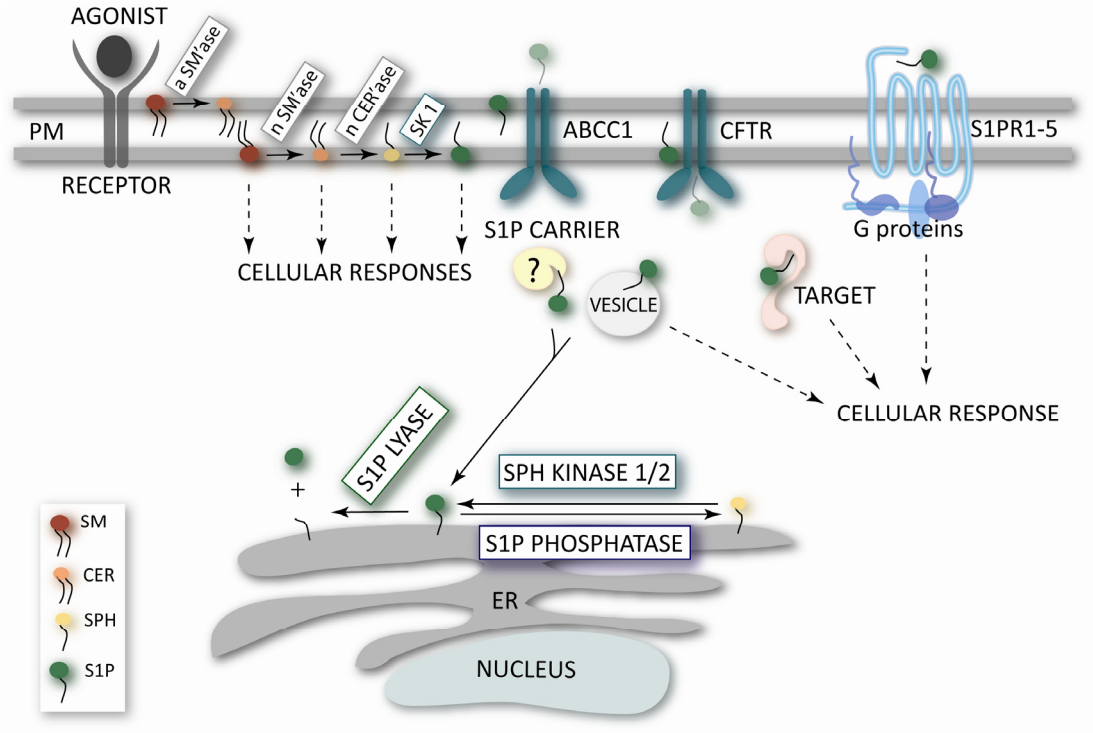

1.3.2. EXTRACELLULAR MESSENGER

In addition to its intracellular signalling mode, S1P can act extracellularly in an autocrine or a paracrine way (86). Newly discovered ABC transporters are involved in the translocation of S1P to the external leaflet of the PM or to the extracellular space, as well in its import into the cytosol or in the cytosolic leaflet of the PM (46) (87) (88) (89). The precise translocation mechanism has not yet been deciphered (90).

S1P receptors were originally named EDG, standing for endothelial differentiation gene and were first described in 1998 (91). S1P receptors 1-5 are differentially expressed and coupled to various G-proteins (**figure 1-11**, right), themselves involved in various signalling pathways (**table 1-3**): extracellular signal-regulated kinase (ERK), Jun amino terminal kinase (JNK), small GTPases of the Rho family (Rho and Rac), phospholipase C (PLC), adenylyl cyclase-cyclic AMP (AC), phosphatidylinositol-3 kinase (PI3K) (66) (4). Typical cellular responses following activation of S1P receptors are: angiogenesis and vascular maturation (92), heart development (93) and immunity (94) (95) (96).

S1P receptor 1 plays a crucial role in the maintenance of the immune system (86). T-cells exhibit chemotaxis against a gradient of S1P actively maintained between the lymphoid tissues and the blood stream by S1P lyase (SPL) (97) (78). In lymphoid tissues the concentration of S1P is kept low (in the nanomolar range) by high SPL activity, whereas it reaches micromolar range in the blood. The main sources of S1P in the blood are the vascular endothelium (98), the erythrocytes (45), and the platelets (44). S1P is also present in bound form to lipoproteins and to albumin (99). S1P receptor 1 is externalized in lymphoid tissues and permits the egress of T-cells to the blood along the S1P gradient. Disruption of this gradient by inhibiting SPL results in lymphopænia (100). Interestingly, following inflammation, tissue S1P concentration increases, modifying the immune cells trafficking (101).

Table 1-3. S1PR signalling pathways

S1PR	COUPLED G-PROTEIN	ACTIVATED DOWNSTREAM PATHWAYS
1	G_i	AC PLC
2	G_i G_q $G_{12/13}$	Rac PI3K AC PLC Rho
3		
4	G_i ? $G_{12/13}$	ERK PLC ? Rho
5	G_i $G_{12/13}$	ERK PLC Rho JNK

1.4. S1P METABOLYZING ENZYMES

The enzymes directly involved in the regulation of S1P are sphingosine kinase, catalysing the synthesis of S1P, S1P phosphatase, responsible for the reverse reaction, and S1P lyase for its irreversible degradation (**figure 1-12**).

Figure 1-12. S1P metabolism

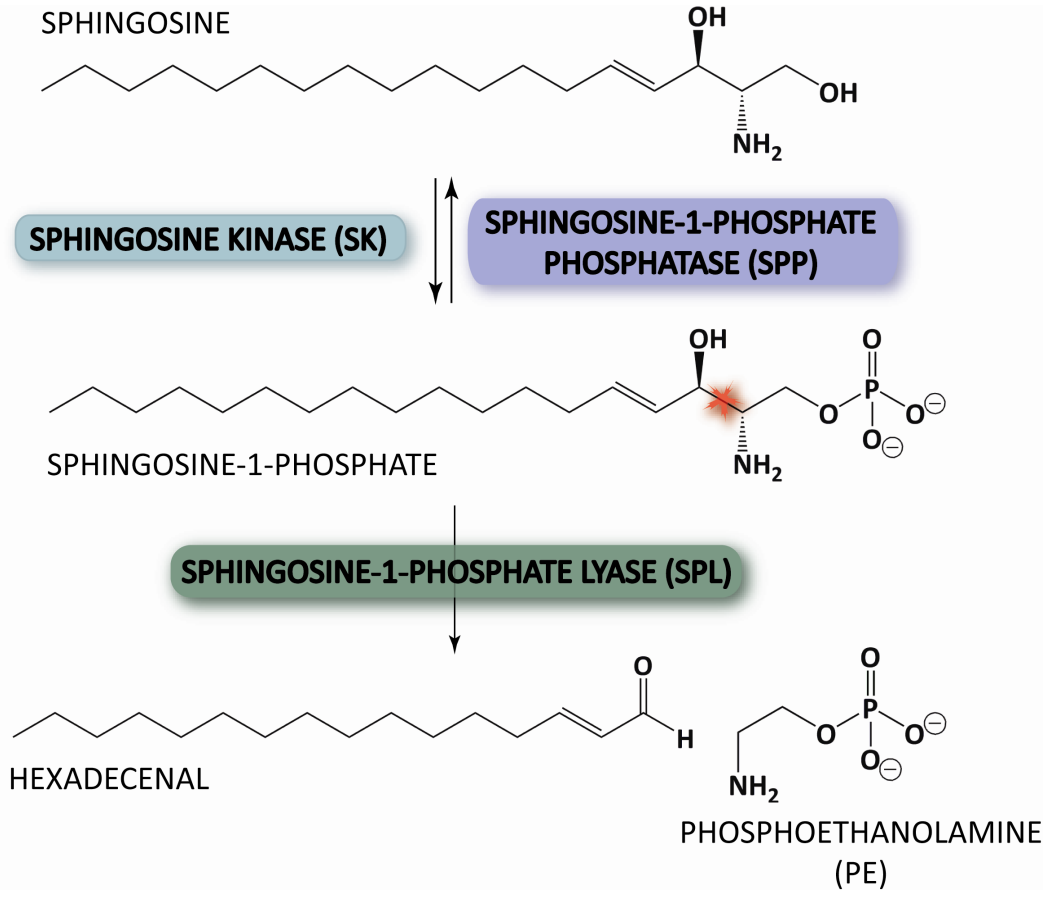

1.4.1. SPHINGOSINE KINASE (SK)

SK is evolutionary conserved, with activity detected in humans, mice, yeast and plant. Both mammalian isoforms 1 and 2 possess five conserved domains (**figure 1-13**) termed C1-C5. The domains C1-3 encompass the catalytic core of the enzyme, where the C2 domain binds ATP. The catalytic core displays high sequence similarity with the diacylglycerol kinase family. The presence of transmembrane domains in SK2 is still a matter of debate (43) (42) and its role is not well understood. It has been shown to phosphorylate the competitive inhibitor FTY720 (fingolimod), an immunosuppressive drug (102). SK1 and SK2 display different kinetic properties, tissue distribution and temporal expression patterns during development. Thus, they may carry out different functions (43).

Figure 1-13. SK topology (adapted from (43))

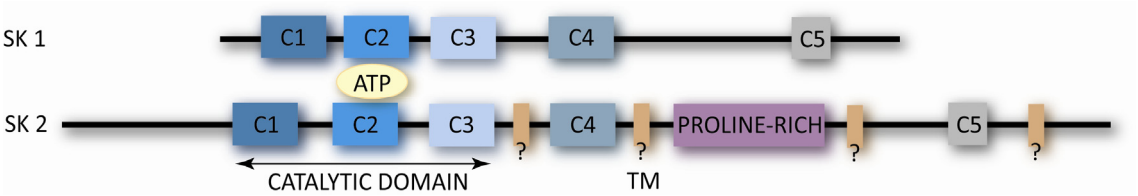

1.4.2. SPHINGOSINE-1-PHOSPHATE PHOSPHATASE (SPP)

S1P phosphatase activity was first detected in yeast, where it plays a role in heat-stress response (103) (104) (105). Two isoforms of SPP were identified in mammals (106) (107) (108) based on sequence similarity to the lipid phosphate phosphatase (LPP) family. Both mammalian SPP isoforms, similarly to their yeast counterpart, are integral membrane proteins located in the ER (**figure 1-14**). SPP1 and 2 are differentially expressed in tissues, where SPP1 is most expressed in liver, kidney and placenta and SPP2 in kidney and heart (109). This indicates that, despite their overall similarities, SPP1 and 2 might be differently regulated and carry out different cellular functions. With regard to substrate specificity, SPP1 and 2 are more specific to S1P than to dihydro-S1P (58). Overexpression of SPP1 in mammalian cells induces accumulation of ceramide by the inhibition of ceramide trafficking from the ER to the Golgi. The regulation of ceramide levels in the ER by SPP1 is not well understood (109). SPP2 has a shorter N-terminus compared to SPP1 (**figure 1-14**) but this does not exert any effect on activity, since both isoforms display similar substrate specificity and activity (107).

Figure 1-14. SPP topology (adapted from (43))

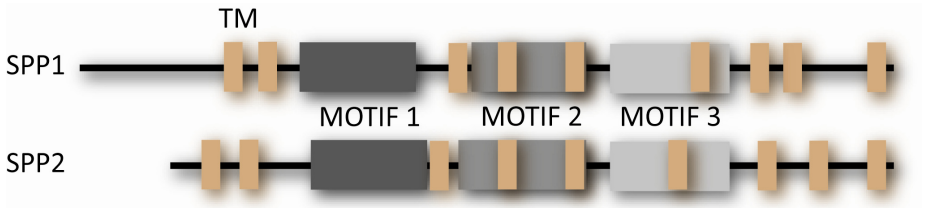

1.4.3. SPHINGOSINE-1-PHOSPHATE LYASE (SPL)

Localisation and topology

The SPL gene has been first identified in budding yeast (*Saccharomyces cerevisæ*) (110) and the human gene was cloned in 2000 (61). The SPL gene is present in many organisms including fungi, plants and mammals (111). Yeast and mammalian SPL are predicted single-pass membrane proteins with the transmembrane helix residing within the first fifth of the protein (**figure 1-15**, beige box). Mammalian and yeast SPL are located in the ER membrane (112) but may localize to other organelles (113) (114) (115). Their N-terminus is situated in the ER lumen, where it undergoes glycosylation in yeast (112) and their active site is exposed to the cytosol (115). Mammalian SPL can be functionally expressed in yeast (116).

Recently, a SPL gene from the facultative intracellular pathogen *Legionella pneumophila* (named LegS2) has been cloned and could be functionally expressed in yeast (117). Interestingly, a phylogenetic analysis indicates that LegS2 has a eukaryotic origin but the protein surprisingly localizes in the mitochondria when expressed in mammalian cells. In addition, LegS2 contains a C-terminal extension that is absent in eukaryotic SPLs and is required for infection, even if the precise role of the enzyme in the pathogenicity of the bacterium remains elusive. Other bacteria, for example *Myxococcus xanthus* and *Symbiobacterium thermophilum* also carry a gene coding for a S1P lyase.

Figure 1-15. SPL topology (adapted from (43))

Function and regulation

Yeast SPL, called Dpl1p (dihydrosphingosine-1-phosphate lyase 1), is involved in resistance to heat stress (105) (118) and nutrient deprivation (119), in calcium homeostasis (85) as well as in endocytosis (120). In mammals, SPL plays a crucial role in the migration of T-cells from lymphoid tissues by maintaining the S1P gradient necessary for T-cells to egress from the lymph nodes into the blood stream (see section 1.3.2.) (78). SPL activity is also linked with an increase in ceramide levels in response to stress factors and is involved in apoptosis (114). The SPL gene is a transcriptional target of platelet-derived growth factor (PDGF) (121). PDGF regulates critical cellular events like cell growth, differentiation and migration and is involved in cancer, inflammation, wound healing and production of the extracellular matrix (122). The SPL gene is ubiquitously expressed with the exception of erythrocytes (123) and platelets (44) and its expression is linked to tissues undergoing rapid cell turnover, like the intestine, the colon, the thymus and the liver (111). SPL gene expression is down-regulated in colon cancer (124), whereas it is high in enterocytes under normal conditions, where the protein is involved in metabolizing dietary sphingolipids (125). SPL triggers p53-dependent activation of PIDD (p53-inducible death domain protein), which in turn activates caspase 2. Caspase 2 primes the apoptotic cascade (activation of caspase 3, release of cytochrome *c* from mitochondria, PARP (poly-ADP-ribose polymerase) cleavage, exposure of phosphatidylserine at the cell surface, and cell death). Consistently with the powerful effects SPL exerts, the transcription of its gene is tightly regulated (111). Notably, SPL is up-regulated in certain malignant tissues, for example in ovarian cancers (126). Up-regulation of SPL is also found in the skin of patients suffering from atopic dermatitis (127). Additionally, SPL is involved in

developmental events, especially in vascular maturation (111). Furthermore, the human protein is nitrosylated, a modification that probably alters the cofactor or substrate binding to the enzyme (128).

Reaction, substrate and inhibition

SPL is a pyridoxal 5'-phosphate (PLP)-dependent enzyme. PLP is covalently bound to the enzyme *via* a Schiff base between the aldehyde group of the PLP and the side chain amine of a nearby lysine. The PLP-lysine complex is called an internal aldimine (**figure 1-16**).

Figure 1-16. Internal aldimine lysine-PLP

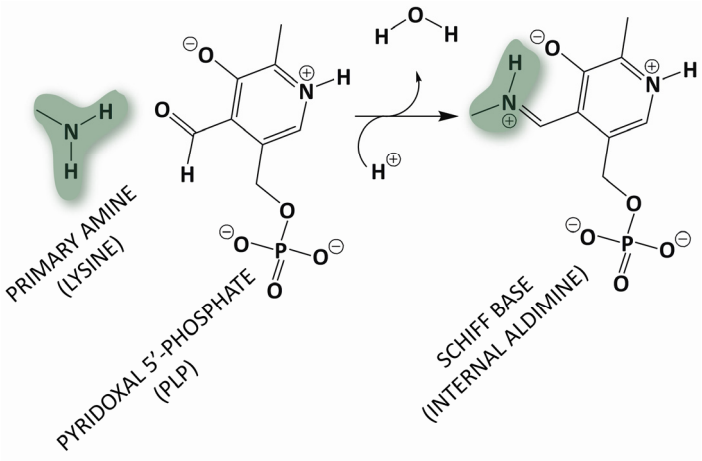

SPL is a member of the carbon-carbon lyase subclass of aldehyde-lyases. SPL cleaves its substrate between carbon atoms 2 and 3 yielding a hydrophobic product, a so-called long chain aldehyde, and a hydrophilic product, invariably phosphoethanolamine (PE) (**figure 1-12**). The function of SPL was initially considered to be restricted to S1P degradation. Interestingly, it has recently been proposed that the products of the cleavage of S1P may be involved in further metabolic pathways, like the synthesis of phospholipids (129) (130) (35) (see section 1.2.2.). Hexadecenal, the long-chain aldehyde, is thought to be in equilibrium with the corresponding long-chain alcohol and carboxylic acid (**figure 1-17**) (131).

Figure 1-17. Irreversible cleavage of S1P by SPL and stability of hexadecenal

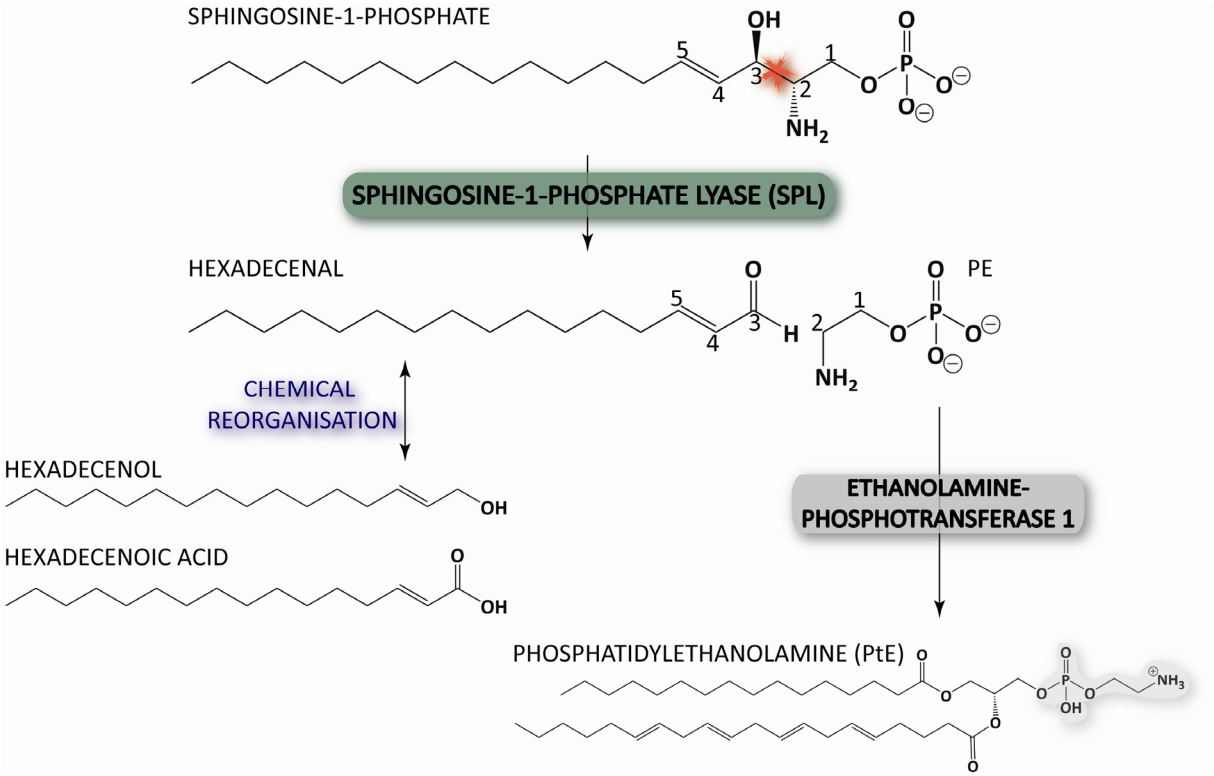

The pH optimum of SPL is in the range of 7.2 to 7.4. The enzyme is poorly active in Tris buffer, or in any kind of buffer containing a primary amine, which can compete with the substrate for binding to PLP (21). SPL shows a high level of specificity toward the stereochemistry of the substrate and cleaves exclusively the naturally occurring D-*eythro* (2D,3D configuration) sphingolipids. On the other hand, the enzyme exhibits very little specificity with respect to chain length, degree of insaturation and substitution, as it cleaves sphingosine-1-phosphate, dihydrosphingosine-1-phosphate, phytosphingosine-1-phosphate, as well as methyl- or dimethylsphingosine-1-phosphate (**figure 1-18**) (132) (133) (111). When the amino group of phosphosphingolipids is modified, for example by acetylation (N-acetyldihydrosphingosine-1-phosphate) or by methylation (N,N-dimethylsphingosine-1-phosphate), the substrate is not cleaved (132).

Figure 1-18. Known substrates of SPL

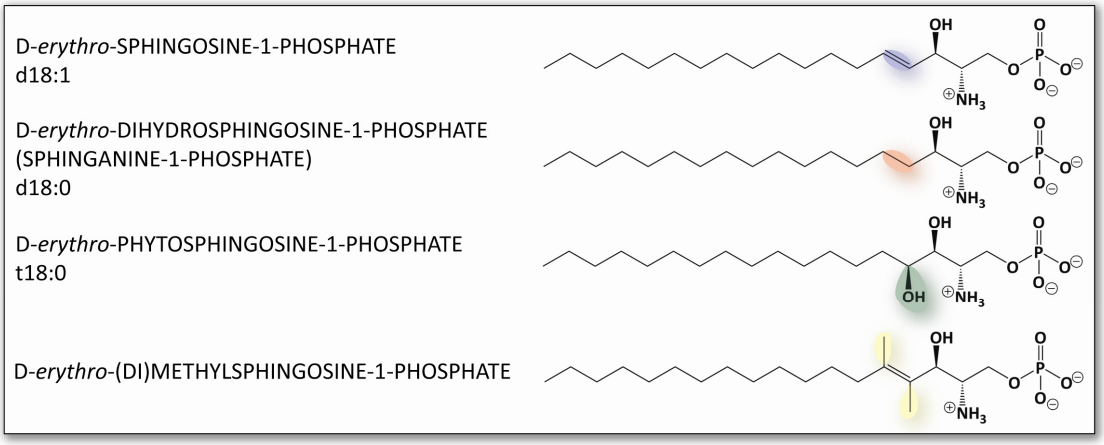

The classical PLP-dependent enzyme inhibitors semicarbazide, iodoacetamide, N-methylmaleimide (**figure 1-19**) inhibit SPL to various extent, presumably by binding to either the cofactor (for semicarbazide) or a sulfhydryl group from a cysteine (111). Deoxypyridoxine also inhibits SPL, possibly by competing with PLP (21).

Figure 1-19. PLP-dependent enzyme inhibitors

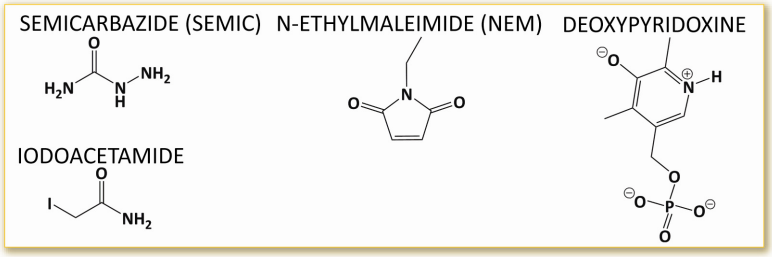

There are known substrate analogues that inhibit SPL (**figure 1-20**), for example 1-deoxydihydrosphingosine-1-phosphonate (134), the *threo* isomer of dihydro-S1P (135), and 2-vinyldihydro-S1P (136). FTY720 (also called fingolimod as recommended International Nonproprietary Name) (**figure 1-20**) is an immunomodulatory drug phosphorylated by sphingosine kinases 1 & 2 (137) (138) that targets the S1P receptors 1, 3, 4 and 5 (139). Interestingly, cell exposure to an extracellular concentration of 1 µM S1P and of P-FTY720, the phosphorylated form of the drug, leads to the internalization of $S1PR_1$, which does not impair G_i protein-mediated signalling (139). P-FTY720 might bind and maintain the receptor in an active conformation. Hence, FTY720 and its phosphorylated form have a complex mechanism of action on S1P receptors. FTY720 inhibits SPL *in vivo*, when orally administered to mice, and *in vitro* (the assay uses a cell extract of mammalian cells expressing SPL). Inhibition by FTY720 modifies neither SPL gene expression levels nor S1P levels in tissues (140). THI (2-acetyl-4-tetrahydroxybutyl-imidazole), found in the food colorant caramel colorant III, (**figure 1-20**) also inhibits SPL *in vivo* (78) although the mechanism of inhibition is not understood (111). The divalent cations Ca^{2+} and Zn^{2+} have also been reported to inhibit the activity of SPL (113). SPL activity is also sensitive to non-ionic and zwitterionic detergents even at concentrations below their critical micelle concentration. Octylglucoside (OG), lauryldimethylammonium oxide (LDAO), octanoyl-N-methylglucamide and CHAPS all inhibit SPL (113).

Figure 1-20. SPL inhibitors

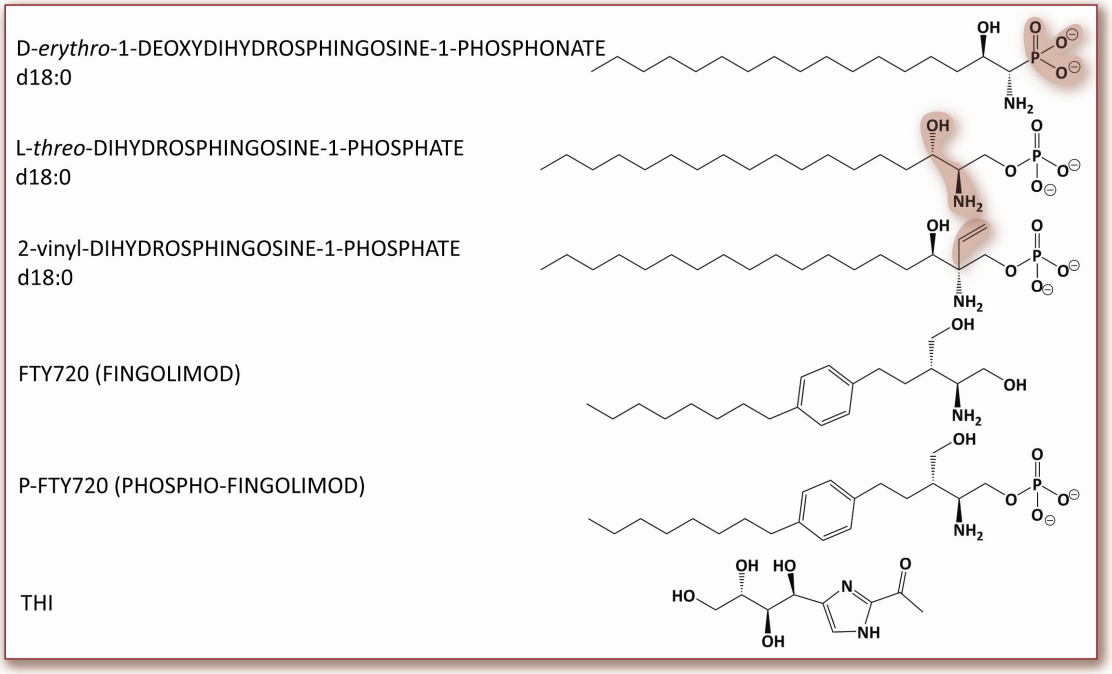

It should be noted that biochemical results in the literature have been so far nearly invariably obtained using crude extracts or cell fractionation samples. Given the tight interconnectivity of the S1P-related enzymes, this approach might introduce non-negligible bias.

Mechanism

SPL is associated with the ER membrane *via* a single predicted transmembrane helix, while its active site is located in the cytosol. The mechanism of accommodation and cleavage of the substrate and of release of the hydrophilic and hydrophobic products is not yet elucidated. The protein might contain a hydrophobic recognition site that interacts with the hydrophobic moiety of the substrate while the hydrophilic head might be accommodated within the active site and can be then cleaved (**figure 1-21**) (21).

Figure 1-21. Schematic view of eukaryotic membrane-bound SPL (adapted from (21))

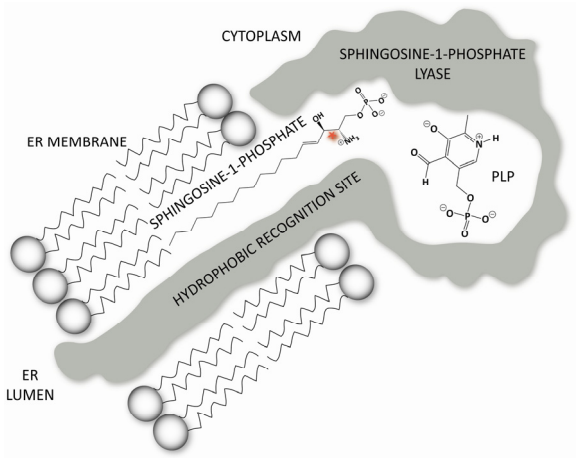

Recent results on yeast SPL (Dpl1p) mutagenesis support the view that part of the lumenal domain and the transmembrane helix (residues 59-81) are required for *in vivo* but not *in vitro* activity (112). A lumenal domain truncation of human SPL (HsSPL) has been previously reported as active (61) (**figure 1-22**), even if the results might be controversial (hence "active" is italicized in the figure). The transmembrane domain of Dpl1p contains three polar (C65, S70, N71) and one charged (K67) residues, proposed to mediate the formation of an active oligomer and to retain the protein in the ER. A lysine side chain adjacent to the cytoplasmic side of the ER membrane might interact with the phosphate head of the substrate and help directing it to the active site.

Figure 1-22. *In vivo* and *in vitro* activity of N-terminal truncations of Dpl1p and HsSPL

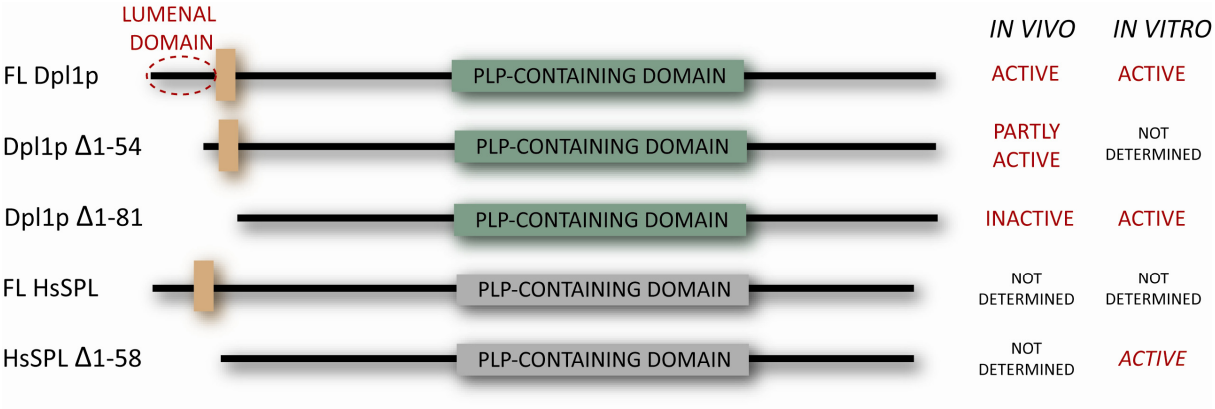

Biochemical studies are hindered by the poor solubility of phosphorylated sphingolipids, albeit zwitterionic in nature (21). Electrostatic and hydrophobic intermolecular interactions are presumably responsible for this phenomenon (141). Triton X-100 is so far considered the best detergent and is widely used to solubilise phosphorylated sphingolipids, since a number of other neutral and zwitterionic detergents inhibit enzymes of their metabolism (21). Development of new biochemical tools will hopefully allow in-depth analysis of the kinetics of the cleavage of S1P by SPL (142) (143) (131).

Already in 1976 and 1993 a reaction mechanism was proposed based on general knowledge of the biochemistry of PLP-dependent enzymes. Moreover, SPL is sensitive toward sulfhydryl reagents, its reaction is stereospecific, and one proton is stereospecifically added in phosphoethanolamine (PE) (144) (21). The mechanism proposed in 1993 encompasses the following steps: once the substrate is in the active site, its primary amine replaces the lysine residue of the enzyme in the Schiff base with the PLP, forming a species called an external aldimine (**figure 1-23, *step III***). The substrate is held in place and ready to undergo a nucleophilic attack carried out by the sulfhydryl anion of a cysteine (***step IV***). The attack is proposed to be on carbon 3 of S1P, carrying the hydroxyl group. Mutating conserved cysteines in human SPL is deleterious for activity (61). The formed thiohemiacetal decomposes into a long-chain aldehyde that is released from the active site (***step V***) and a sulfhydryl. PE is still bound to the PLP and forms a quinonoid intermediate (***step VI***). A solvent proton is stereospecifically incorporated (***step VII***) onto PE (***step VIII***) before hydrolysis takes place, releasing PE from the active site (***step IX***) and reforming the native state internal aldimine (***step I***).

This mechanism is partly supported by a recent mutagenesis study of Dpl1p using an *in vivo* complementation activity assay. The mutants were designed based on bioinformatic analysis and structure prediction (112). The internal aldimine mutant (K380A) is fully inactive, as expected. Another lysine (K386) is strictly required for activity. Surprisingly, the mutant targeting the predicted nucleophile cysteine (C344A) shows only partly impaired activity. Interestingly, a tyrosine (Y554) located on the very C-terminus of the protein is involved in enzymatic function, because mutating it to either alanine or phenylalanine reduces the activity.

Figure 1-23. SPL reaction mechanism proposed in the literature (adapted from (21))

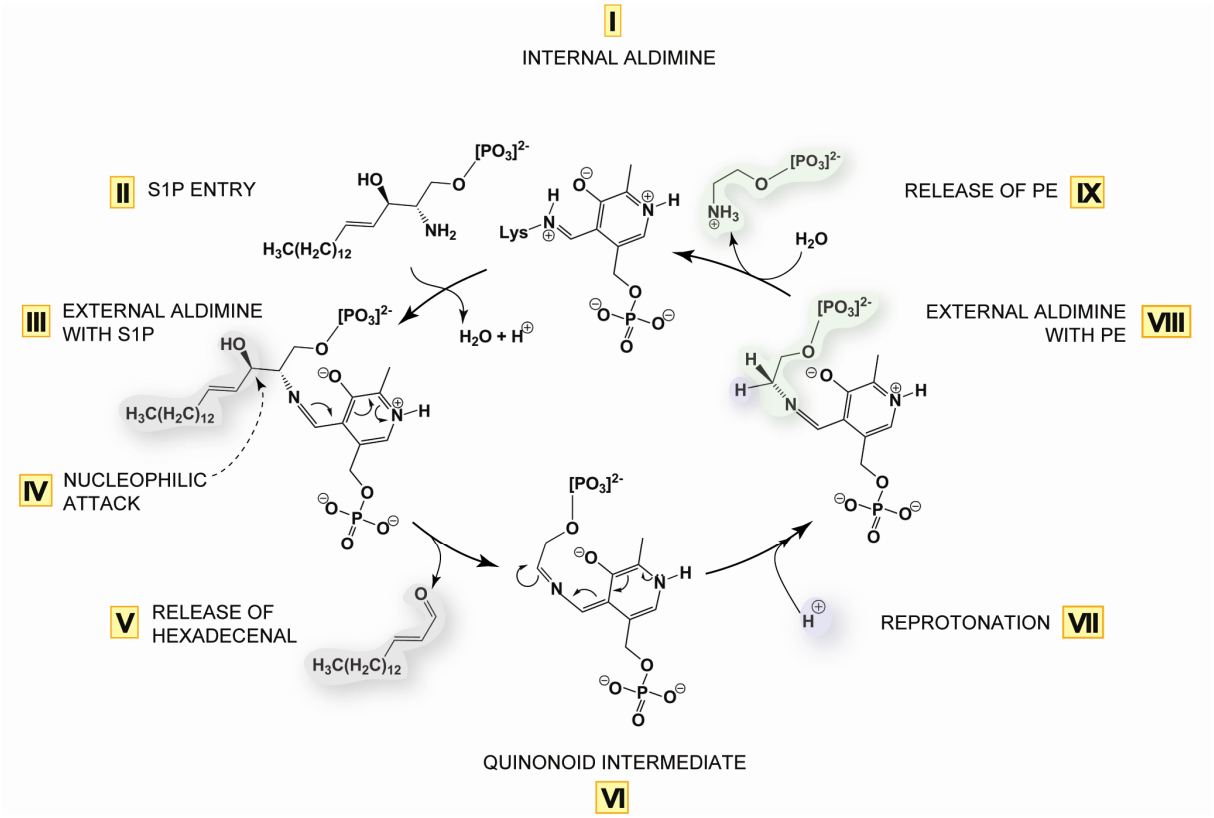

1.5. X-RAY STRUCTURES OF SPHINGOLIPID-RELATED ENZYMES

1.5.1. SPHINGOMYELINASE (SM'ase)

The structure of *Listeria ivanovii* SM'ase C (SmcL) was determined at 1.9 Å resolution in 2005 (145). Unlike the mammalian neutral SM'ase which is bound to the membrane *via* either N- or C-terminal extensions (**table 1-2**), SmcL is a secreted neutral SM'ase acting as a membrane-damaging virulence factor and interfering with the sphingomyelin-ceramide signalling pathway. The protein adopts a DNase I-fold, that is a central β-sandwich flanked by helices and loops (**figure 1-24**). The active site is located in a solvent-accessible pocket and is surrounded by hydrophobic loops that help accommodating sphingomyelin into the active site. One phosphate ion presumably mimics the position of the substrate. (145). Mutagenesis studies carried out with *Bacillus cereus* SM'ase (see below) revealed that mutating the nearby residues H185 and H325 (corresponding to *B. cereus* SM'ase residues H151 and H296) knocks the activity out (146). Two aspartate residues, D282 and D229 (*B. cereus* SM'ase D254 and D195, not shown) are strictly conserved among sphingomyelinases and are found in the vicinity of the catalytic histidine pair. The protein lacks predicted transmembrane helices but a β-hairpin (coloured brown in **figure 1-24**) and a loop containing exposed tryptophan, tyrosine and phenylalanine residues (in green) have been proposed to penetrate the lipid bilayer and allow the transport of the substrate into the active site. Similarly, three structures of *Bacillus cereus* sphingomyelinases (Bc-SMase) were solved in 2006 in complex with Mg^{2+}, Co^{2+}, Ca^{2+} at 1.8, 1.8 and 1.4 Å resolution, respectively (147) (not shown). The enzyme shows a very similar fold to SmcL. The metal ions bind to two clefts within the active site and a variable number of them can bind in one cleft. The enzyme complexed with Co^{2+}, Mn^{2+}, Mg^{2+} has a higher catalytic activity than with Ca^{2+} or Sr^{2+}. A bound molecule of MES provides an additional hint on the substrate binding mode.

Figure 1-24. X-ray structure of SmcL

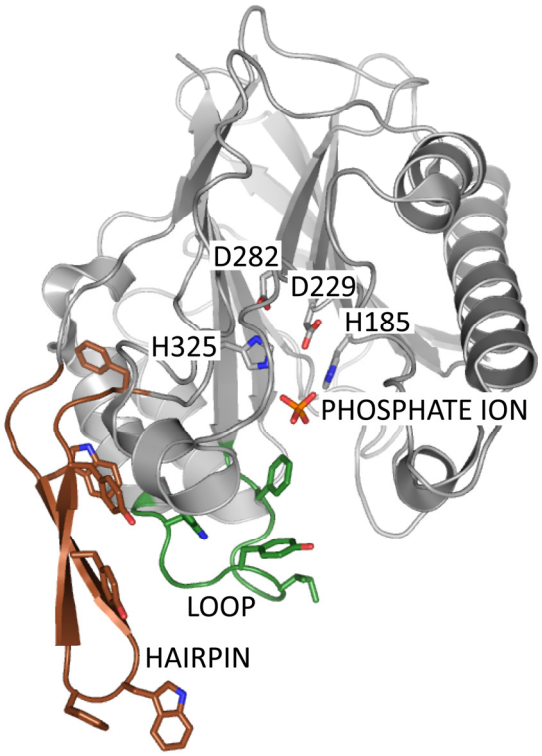

In 2005 also two structures of sphingomyelinase D from spider (*Loxosceles laeta*) venom were solved at 1.85 Å (148) and 1.75 Å (149) resolution in complex with Mg^{2+}. This cation may stabilize the phosphonate intermediate formed during sphingomyelin catalysis. In contrast to its bacterial counterparts, the arachnidan protein is a distorted $(\alpha/\beta)_8$ barrel (TIM barrel) (**figure 1-25**). A flexible loop (coloured blue) close to the sulphate binding site adopts various conformations in the sulphate-free (not shown) and sulphate-bound forms. The catalytic loop (coloured green) contains a disulfide bridge and forms a hairpin. It carries H47, one of the two catalytic histidines found in the conserved active site pocket. In addition to H47 the active site pocket is composed of H12, D34, D91, E32, K93 and W230 (149).

Figure 1-25. X-ray structure of spider SM'ase D

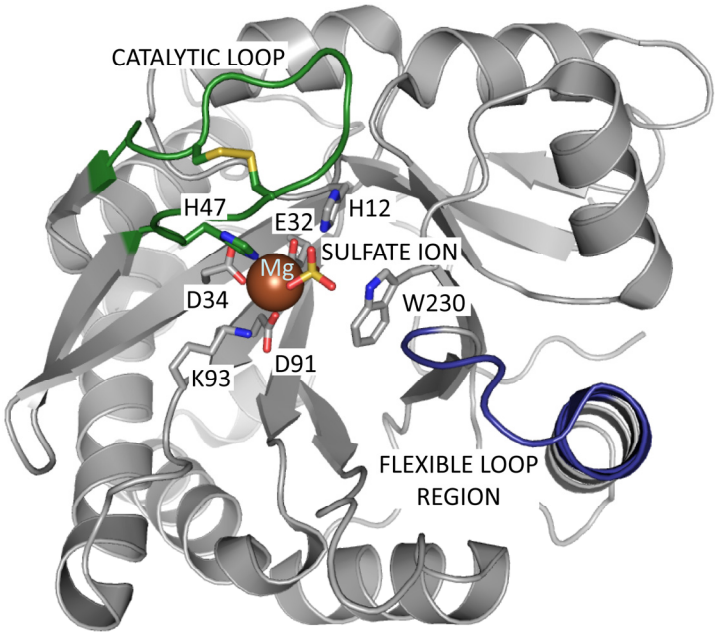

1.5.2. CERAMIDASE (CER'ase)

The structure of neutral CER'ase from *Pseudomonas aeruginosa* (PaCD), unbound and bound to an artificial substrate C2-ceramide, has been solved very recently at 1.4 and 2.2 Å resolution, respectively (150). Neutral ceramidases from different origins exist in either soluble form or as type II integral membrane proteins. Unlike its mammalian counterparts (**table 1-2**) and similarly to bacterial sphingomyelinases (see section 1.5.1.), prokaryotic ceramidase is a soluble protein secreted in the external *milieu* and functions as exotoxin. The membrane retention of mammalian neutral ceramidases is effected by a mucin-like domain at the N-terminus, domain that is absent in the bacterial ceramidases. Mammalian ceramidases can be secreted after processing of their N-terminal membrane anchor (151). PaCD consists of an N-terminal and a C-terminal domain (**figure 1-26**). Divalent cations, Zn^{2+} and Mg^{2+} or Ca^{2+}, are found at their interface. Mg^{2+} or Ca^{2+} may stabilize the two domains whereas Zn^{2+} is directly involved in catalysis. The highly conserved residues H97, H204, Y448, E411 either bind or coordinate Zn^{2+} and are strictly required for activity, as indicated by mutagenesis studies (150). The active site is covered by flexible loops (I and II) sitting above the Zn^{2+} binding site. The loops are moved aside in the substrate-bound structure (**figure 1-26**, blue and green, respectively). Interestingly, the sphingoid base of ceramide points towards the surface whereas its fatty acid chain is more buried in the active site cavity.

Figure 1-26. X-ray structure of PaCD

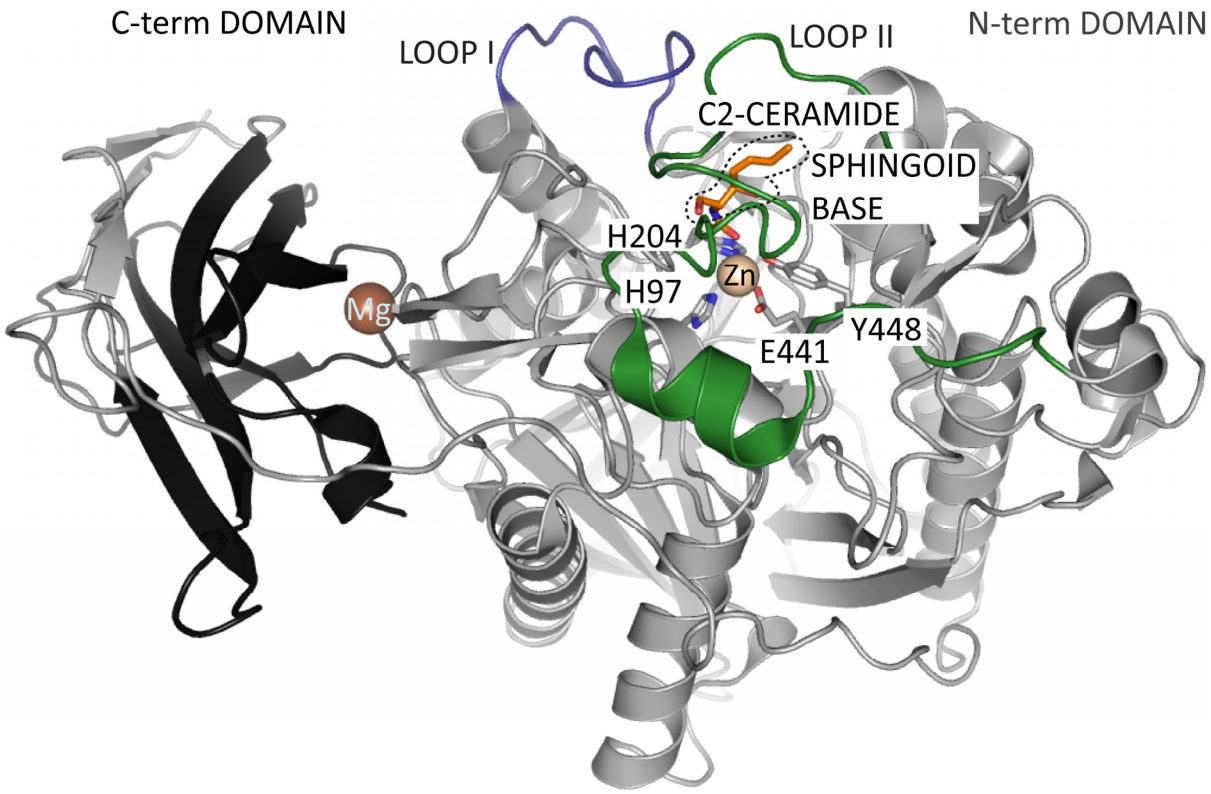

1.5.3. CERAMIDE TRANSPORT PROTEIN (CERT)

CERT is only found in Metazoa and carries out the non-vesicular transport of ceramide from the ER to the Golgi, where ceramide is converted to sphingomyelin (19). CERT consists of an N-terminal pleckstrin homology (PH) domain that specifically recognizes the phosphatidylinositol 4-monophosphate (PI4P) of the Golgi membrane, a middle region containing a FFAT motif able to bind the ER marker protein VAP, and a START (steroidogenic acute regulatory protein-related lipid transfer) domain that specifically extracts ceramide from the ER (**figure 1-27**).

Figure 1-27. CERT topology

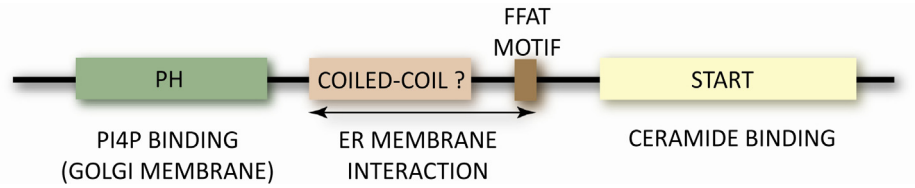

Although the precise mechanism of transfer remains unknown, two models were proposed (19). The first one involves swinging of the C-terminal domain containing the START domain while CERT remains bound to the Golgi and the ER *via* the PH domain and the FFAT motif, respectively (**figure 1-28**). The second model implies that CERT detaches from the ER after ceramide binding and shuttles to the Golgi (not shown). In both cases, CERT must undergo large conformational changes upon binding and transfer of ceramide.

Figure 1-28. Proposed mechanism for the transfer of ceramide from the ER to the Golgi (adapted from (19))

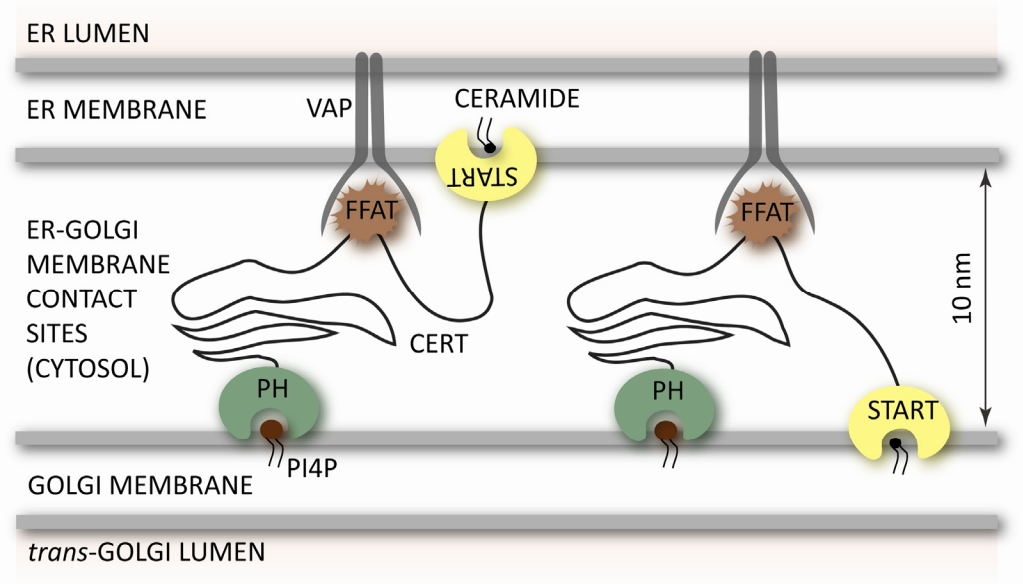

The structure of the START domain of CERT bound to ceramides of various chain lengths was solved in 2008 at resolutions ranging from 1.4 to 2.2 Å (20). Ceramide is buried in an amphiphilic cavity in the centre of the protein. The sphingoid chain is invariably more exposed to the solvent than the fatty acid chain (**figure 1-29**). Surprisingly, the C_α chains of START bound to a ceramide and unbound do not exhibit any significant differences, indicating that the START domain alone does not undergo large rearrangements upon ceramide binding.

Figure 1-29. X-ray structure of the START domain of CERT bound to C_{18}-ceramide

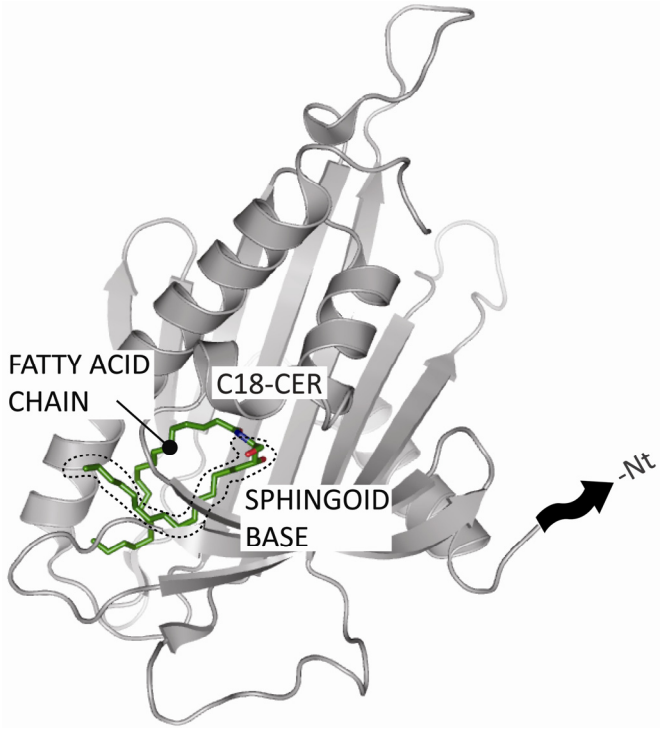

1.5.4. GLYCOLIPID TRANSFER PROTEIN (GLTP)

Glycolipid transfer protein (GLTP) is involved in the non-vesicular trafficking of glycosylceramide from the cytosolic leaflet of the Golgi membrane to the inner leaflet of the PM and its fold is conserved among mammals (152) (153) (154). The structures of bovine and human GLTP in complex with various glycosylceramides have been solved recently at resolutions ranging from 1.36 to 2.3 Å (152) (153) (154). The protein exhibits a 2-layer all-α-helix fold and possesses a conserved sugar binding pocket and a flexible hydrophobic channel (**figure 1-30**).

Mutagenesis studies of the residues W96, N52, D48 and H140 revealed that they play crucial roles in binding of the sugar head of lactosylceramide. Residues K55 and Y207 are also involved in activity, but seem less critical (152). Those residues presumably also mediate the conformational changes undergone by the hydrophobic channel to bind substrates of various lengths and degrees of insaturation (**figure 1-31**). Mutating L136, L165, F148, F103, I45 and F183 into polar residues impairs binding of lactosylceramide (**figure 1-32**) but the effect is less pronounced than for the sugar binding residues (152). Interestingly, like in CERT and neutral ceramidases, the sphingosine moiety of the substrate is the last to enter the channel, and is thus more exposed to the external *milieu* than the fatty acid chain and may even point outside the protein when the sphingoid bases are longer than 18 carbon atoms (**figure 1-30**).

Figure 1-30. Sugar head binding pocket of the human GLTP bound to 18:1 lactosylceramide and to 24:1 galactosylceramide

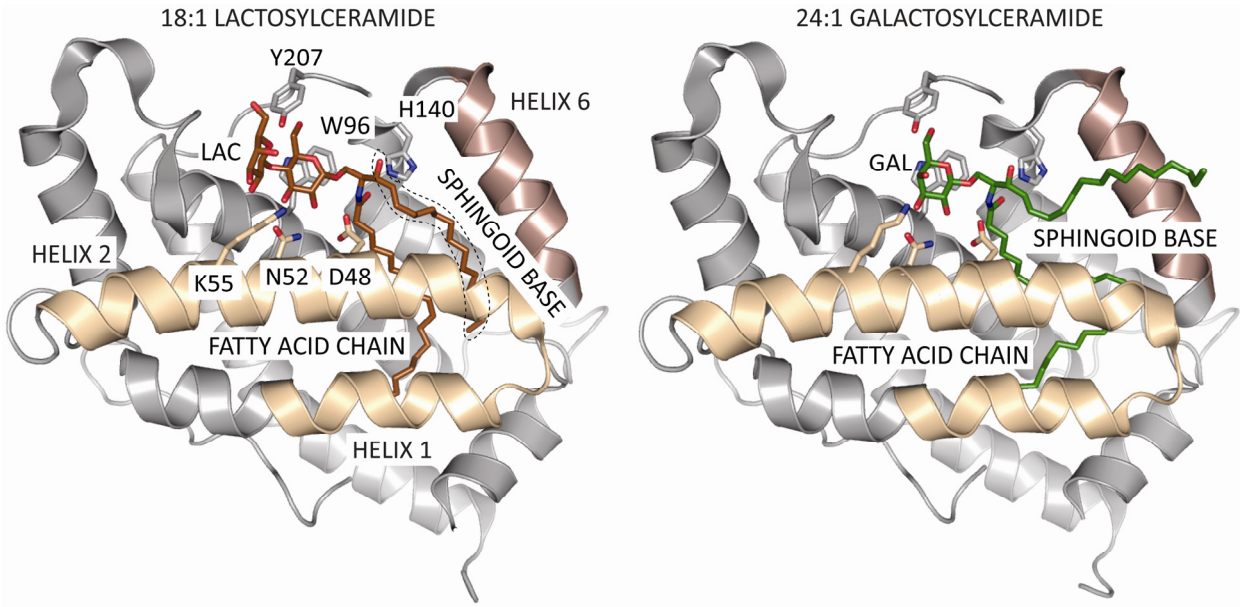

Figure 1-31. GLTP hydrophobic channel gating and conformational changes

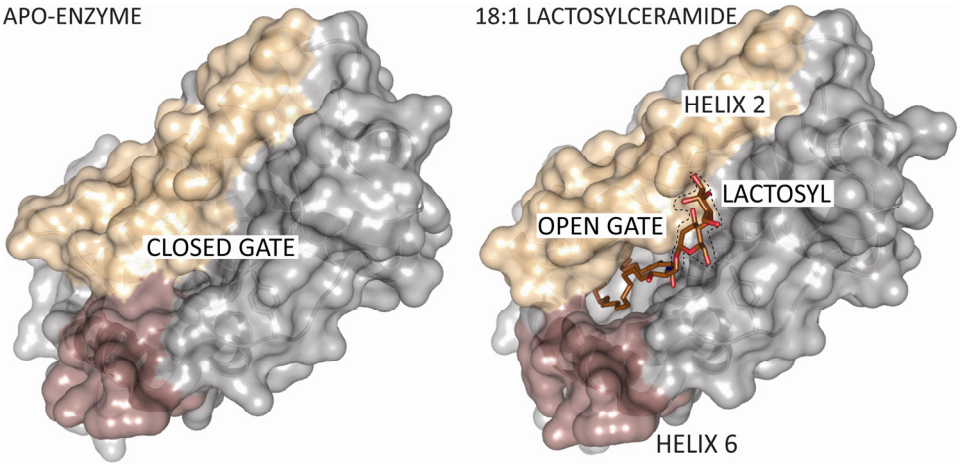

Figure 1-32. 18:1 lactosylceramide hydrophobic chain accommodation in human GLTP

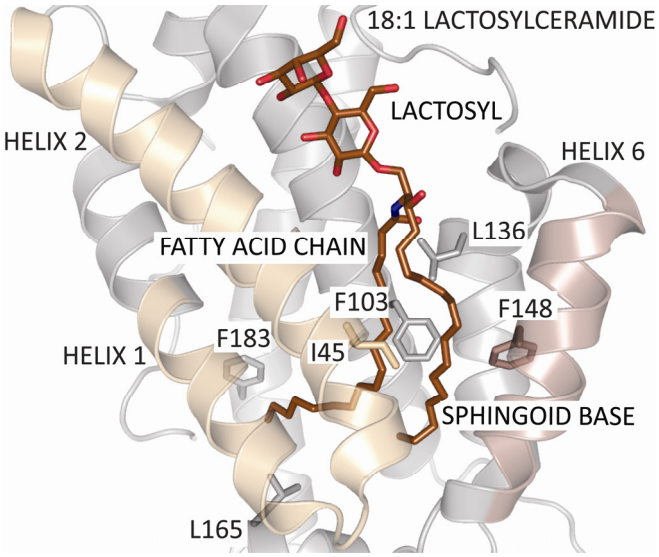

1.5.5. SERINE PALMITOYL-TRANSFERASE (SPT)

Serine palmitoyl-transferase (SPT) belongs to the type I fold family of PLP-dependent enzymes. The enzyme catalyzes the formation of 3-keto-dihydrosphingosine from serine and palmitoyl-coA, the rate-limiting step in sphingolipid synthesis. In yeast and mammals, SPT is an ER membrane-associated complex. It consists of a heterodimer of two strictly related subunits plus a third subunit that confers substrate specificity (56) (155). One subunit of the heterodimer lacks the residues involved in the accommodation of PLP and is thus catalytically inactive, albeit strictly required for activity. The single catalytic site is located on the cytoplasmic side of the membrane, at the interface between two monomers. Heterodimers might form a higher-order complex, presumably an octamer (55).
The bacteria *Sphingomonas paucimobilis* EY2395^{T}, *Sphingobacterium multivorum, Sphingobacterium spiritivorum* and the bacteria-predating bacterium *Bdellovibrio stolpii* carry SPT homologues that have recently been identified and characterized (156) (157). Unlike *Sphingomonas paucimobilis* SPT, which is a cytosolic enzyme, the latter two SPTs are peripheral inner membrane proteins. Notably, the physiological function of the sphingolipids in bacteria is unknown.

The structure of *Sphingomonas paucimobilis* EY2395^{T} SPT (SpSPT) was solved in 2007 at 1.3 Å resolution (158) (**figure 1-33**). The first twenty and the last nine residues of the SpSPT sequence are not visible in the electron density map. Unlike eukaryotic SPTs, the enzyme is a homodimer with one active site per monomer. The active site is composed of residues from both subunits. The role of the Mg^{2+} ions remains to be clarified.

Figure 1-33. X-ray structure of SpSPT (adapted from (158))

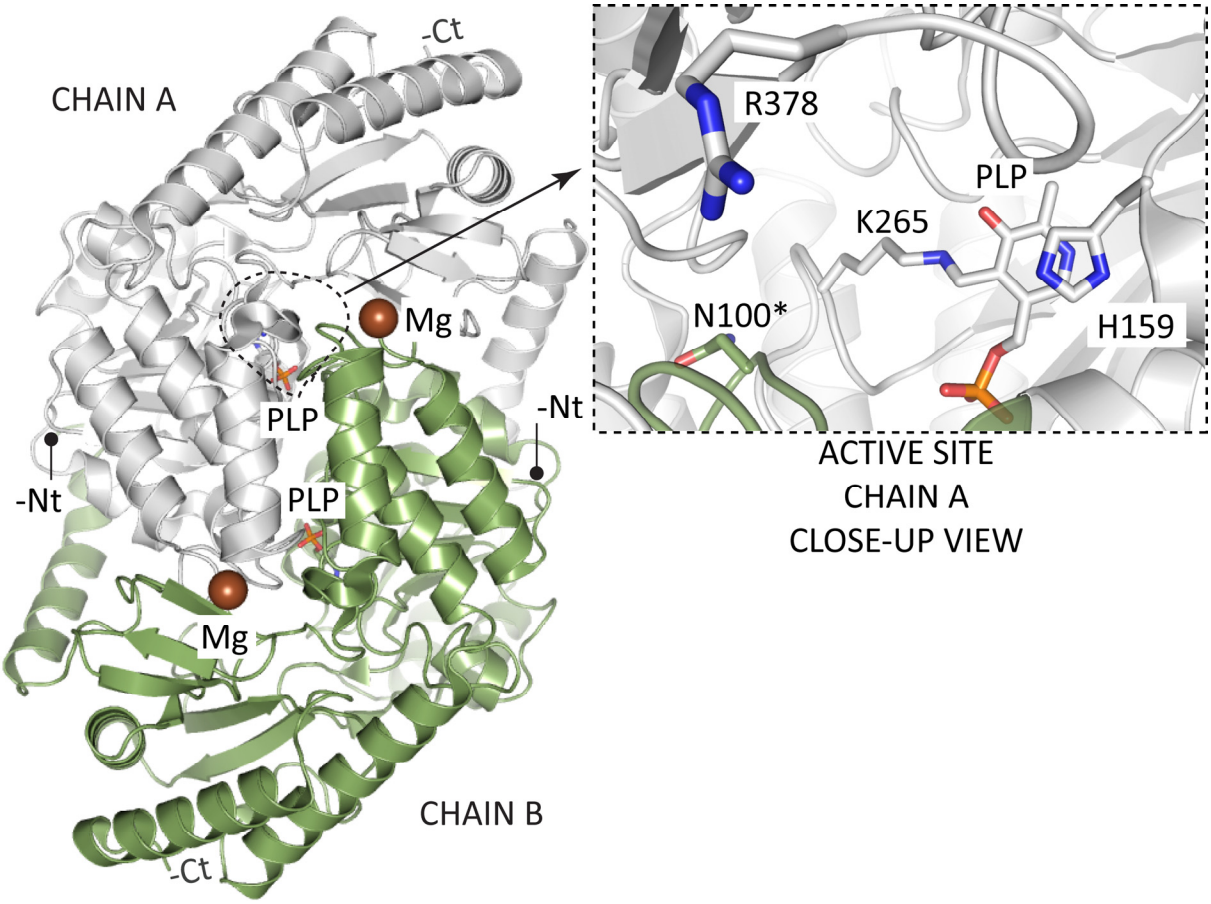

The enzyme produces an absorption spectrum characteristic of PLP-dependent enzymes, featuring a 416-426 nm- (ketoenamine) and a 332-338 nm-peak (enolimine), the ratio of which is modified upon addition of serine, the hydrophilic substrate. The two peaks correspond to the two tautomers of the internal aldimine that PLP forms with K265 of the enzyme (**figure 1-16**, section 1.4.3. & **figure 1-34**). Addition of serine causes decrease of the enolimine peak. In some instances also a transient 505-515 nm-peak, characteristic of a quinonoid intermediate, is observed. This peak invariably occurs upon addition of the fatty acyl-CoA substrate (159) (157) (160).

Figure 1-34. The PLP forms different species in the absence of substrate and upon reaction: the two tautomers (left and centre) of the internal aldimine with K265 and the quinonoid intermediate (right).

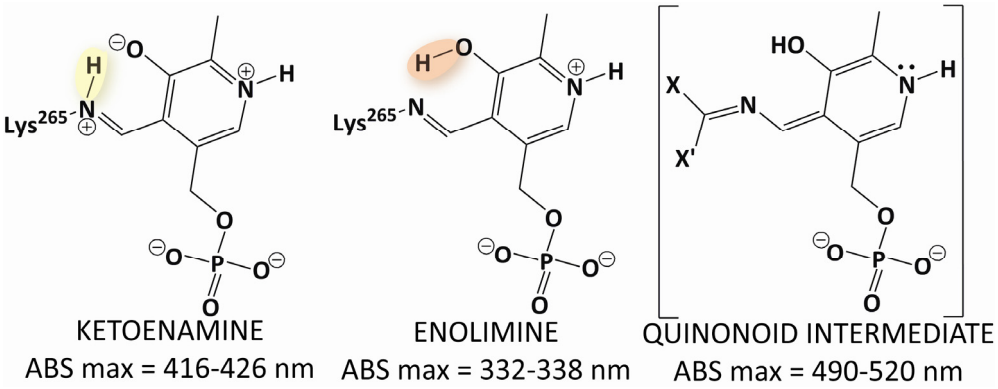

The reaction mechanism of SPT has been extensively studied, mainly using the characteristic UV-visible spectra of the protein at various stages of the enzymatic reaction of the wild-type and mutant proteins (161) (160) (159). Briefly, the internal aldimine between PLP and K265 undergoes transaldimination with L-serine to yield PLP-L-serine external aldimine. Binding of the second substrate, a fatty acyl-CoA, triggers the α-deprotonation of serine yielding a first quinonoid intermediate. The resulting carbanion attacks the fatty acyl-CoA to generate a condensation product, which is then decarboxylated to yield a second quinonoid intermediate. Protonation at C_α gives the external aldimine with the product, 3-keto-dihydrosphingosine, which is released from the active site. The conserved residue H159 plays crucial roles in catalysis (**figure 1-33**) (159). It stacks the pyridine ring of PLP, recognizes and anchors the carboxylate group of serine, regulates the conformation of the serine-PLP external aldimine to prevent unwanted reactions, and acts as acid catalyst in the condensation reaction. In June 2009, the structure of the external aldimine PLP-L-serine of *Sphingomonas paucimobilis* SPT was reported (160), highlighting the crucial role of N100* from the neighbouring subunit in binding the carboxylate of the external aldimine (160). The residue R378 is involved in the stabilization of the quinonoid intermediate although it is not conserved in all SPTs (160).

At the same time, a structural and functional study of *Sphingobacterium multivorum* SPT (SmSPT) was published (162). The structure, solved at 2.3 Å resolution, displays similar features as those previously described for SpSPT, with the exception of minor differences in the N-terminal region (158).

1.5.6. SUMMARY TABLE

PROTEIN	NAME	ORGANISM	TYPE	FIG.	REF.	PDB[(1)]
NEUTRAL SPHINGOMYELINASE (SM'ASE)	SmcL	*Listeria ivanovii* (Prokaryotes)	Soluble (Secreted)	**1-24**	(145)	**1ZWX**
	Bc-SMase	*Bacillus cereus* (Prokaryotes)	Soluble (Secreted)		(147)	2DDT (Mg^{2+}) 2DDR (Ca^{2+}) 2DDS (Co^{2+})
	SMase D	*Loxoceles sp.* (Arachnida)	Soluble	**1-25**	(148) **(149)**	2F9R **1XX1**
NEUTRAL CERAMIDASE (CER'ASE)	PaCD	*Pseudomonas aeruginosa* (Prokaryotes)	Soluble (Secreted)	**1-26**	(150)	2ZWS **2ZXC**
START DOMAIN OF CERAMIDE TRANSPORT PROTEIN (CERT)	CERT START	*Homo sapiens* (Mammals)	Soluble	**1-29**	(20)	2E3S (C_{24}-CER) **2E3Q** & 2E3R (C_{18}-CER) 2E3O & 2E3P (C_{16}-CER) 2E3N (C_6-CER) 2E3M (apo form)
GLYCOLIPID TRANSFER PROTEIN	GLTP	*Homo sapiens* (Mammals)	Soluble	**1-30**	(152) (153)	**1SWX** (apo form) **1SX6**(18:1 Lacto-CER) 2EUM (8:0 Lacto-CER) 2EVD (12:0 Lacto-CER) 2EVL (18:2 Gal-CER) **2EUK** (24:1 Gal-CER)
		Bos Taurus (Mammals)	Soluble		(154)	1WBE (apo form) 2BV7 (GM3) 1TFJ (fatty acid)
SERINE PALMITOYL-TRANSFERASE (SPT)	SpSPT	*Sphingomonas paucimobilis* (Prokaryotes)	Soluble (membrane-associated)	**1-33**	(158)	**2JG2** 2JGT
	SmSPT	*Sphingobacterium multivorum* (Prokaryotes)			(162)	3A2B

[(1)] The structure shown in the respective figure is highlighted in **bold**.

2. BACKGROUND & AIMS

2.1. STRUCTURE OF *Escherichia coli* GLUTAMATE DECARBOXYLASE (GadB)

Glutamate decarboxylase (GadB) is a PLP-dependent enzyme that plays a key role in the glutamate-based acid resistance system of *Escherichia coli* (163). The enzyme consumes protons in the decarboxylation of glutamate to γ-amino butyric acid (GABA). The structure of *E. coli* GadB was solved in 2003 at pH 4.6 and 7.6 (164). The protein is a two-layered, disc-shaped trimer of dimers (dimers are the basic functional units of PLP-dependent enzymes) (**figures 2-1** & **2-2**). Upon activation by a decrease of pH in the cytosol, GadB undergoes conformational changes causing it to migrate to the PM (164). This behaviour is mediated by the first 14 residues of the protein, which group to form two triple α-helical bundles in an acidic environment (**figure 2-1**). Truncating the first 14 residues produces a protein that is unable to interact with the membrane (164). At neutral pH the N-termini are disordered (**figure 2-2**). *In cristallo* pH shift experiments of GadB revealed that at pH 5.9 only one triple helical bundle exists, whereas the other three N-termini are disordered (165). At neutral pH (7.6) the last 14 C-terminal residues are ordered and enter the active site of the cognate subunit, thereby preventing the entry of the substrate (164).

Figure 2-1. X-ray structure of *E. coli* GadB at pH 4.6 (PBD code 1PMM)

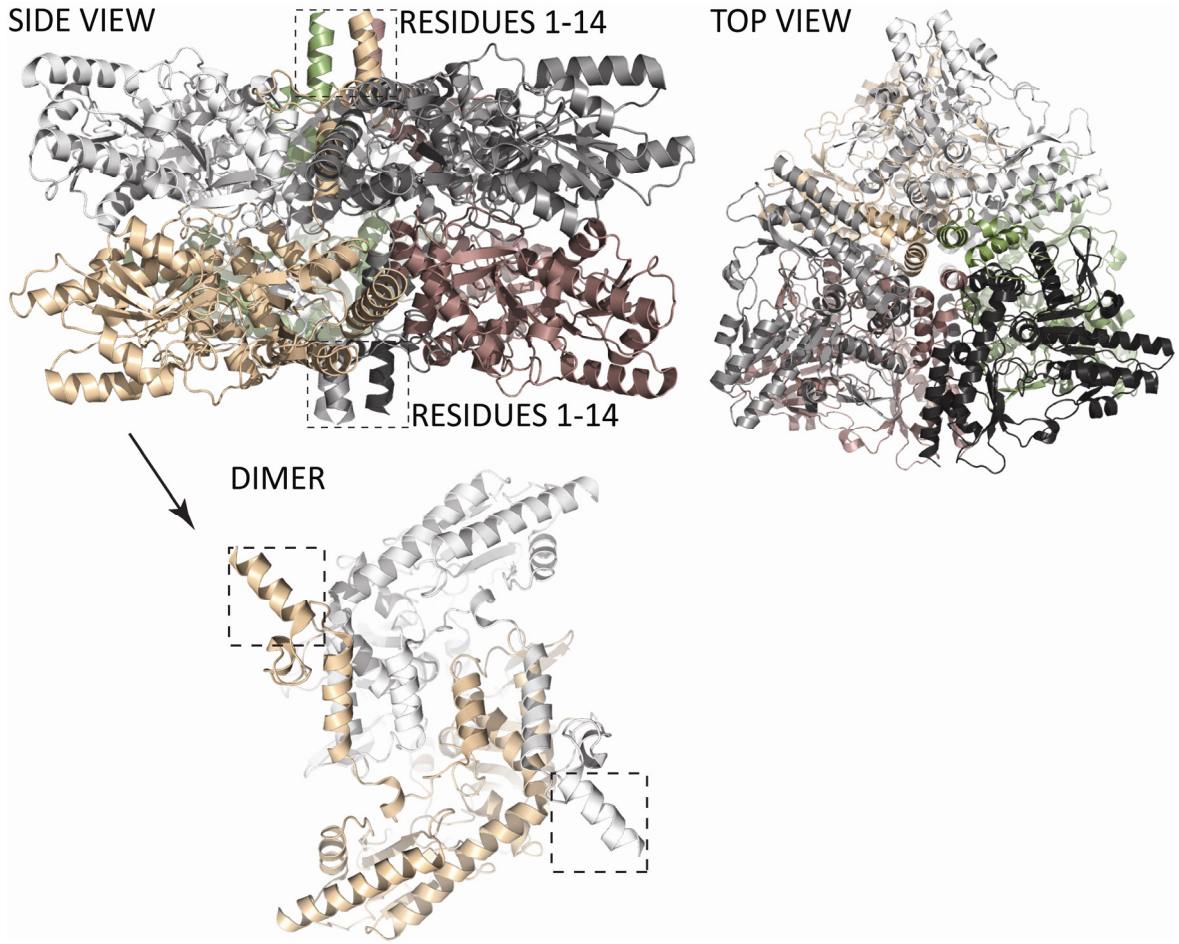

Figure 2-2. X-ray structure of *E. coli* GadB at pH 7.6 (PBD code 1PMO)

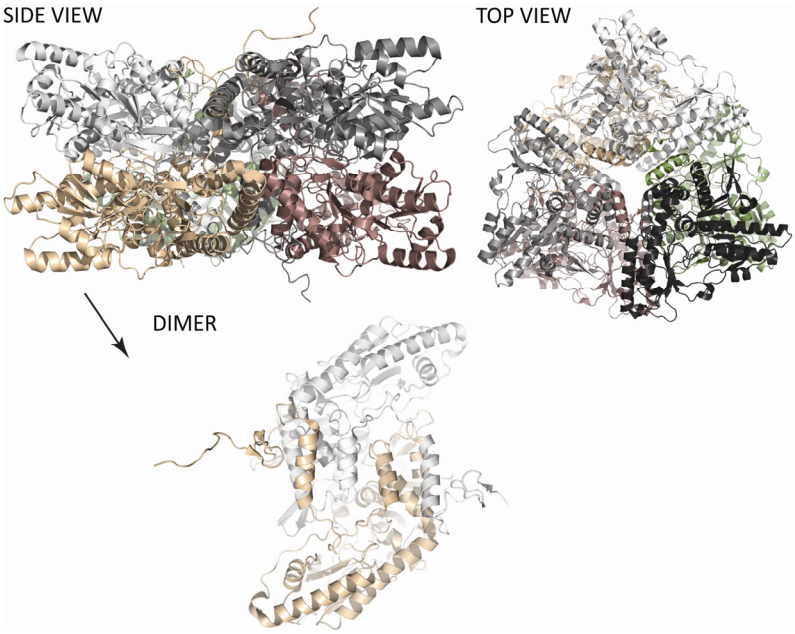

The penultimate residue of the C-terminal tail, H465, forms a substituted aldamine with the cofactor, acting as a covalent lock (**figure 2-3**) [3] (PDB code 2DGK). When the pH drops, protonation causes the aldamine to dissociate and the C-terminal tail (**figure 2-4**, coloured brown) is released, taking a flexibly disordered conformation. Thus, at pH 4.6 the active site is accessible to glutamate.

Figure 2-3. PLP-H465 substituted aldamine of *E. coli* GadB Δ1-14 (PDB code 2DGK)

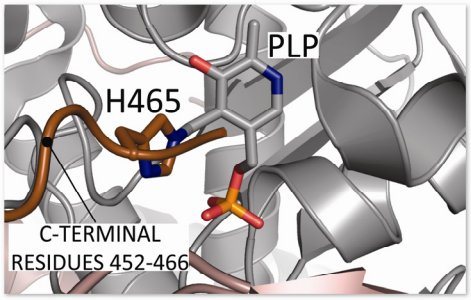

Figure 2-4. Conformation of the C-termini of *E. coli* GadB at pH 7.6 and 4.6

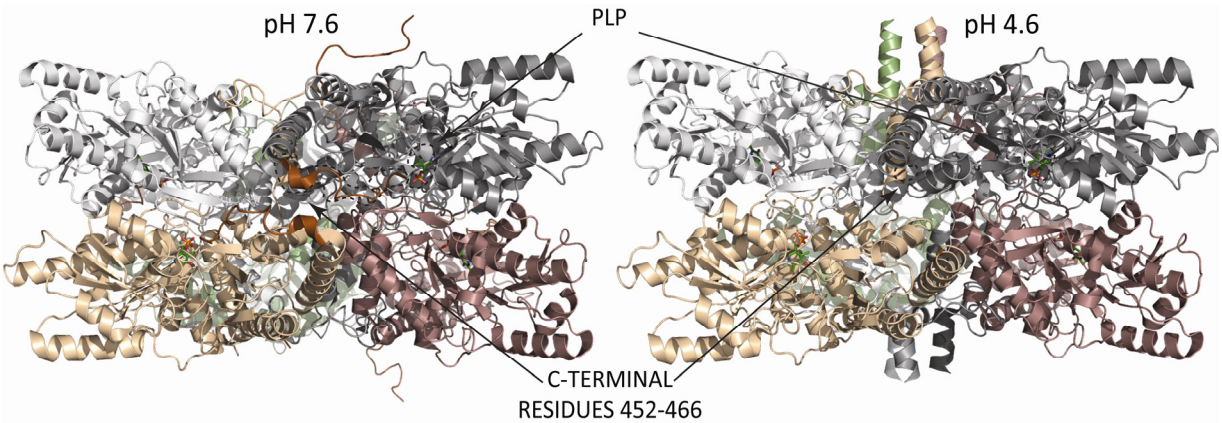

2.2. SEARCH FOR *E. coli* GadB STRUCTURAL RELATIVES AMONG METAZOA

Putative structural relatives of *E. coli* GadB in animals were searched for by running Blastp (166) versus the UniProt database (http://www.uniprot.org) (167). The search was carried out with a taxonomic filter to limit the search to animals. The top non-fragment hits in the search were proteins annotated as sphingosine-1-phosphate lyase (SPL) and sharing about 25% sequence identity with *E. coli* GadB.

2.3. SEARCH FOR PROKARYOTIC HOMOLOGUES OF SPL

Prokaryotic putative homologues of *Saccharomyces cerevisiæ* (yeast) Dpl1p were searched for by running Blastp (166) versus the UniProt database (http://www.uniprot.org) (167). The search was carried out with a taxonomic filter to exclude eukaryotic or archæal proteins. A 507-residue long protein from the thermophilic bacterium *Symbiobacterium thermophilum* (UniProt entry name Q67PY4_SYMTH / accession number Q67PY4) was the top hit in the search, sharing 37% identity and 57% similarity with Dpl1p (UniProt entry name SGPL_YEAST / accession number Q05567) over 517 aligned residues. **Table 2-1** summarizes the identity and similarity values for bacterial, yeast and human SPLs, obtained from BLAST alignments.

Table 2-1. Identity and similarity of *S. thermophilum*, yeast and human SPLs

1st Protein	**2nd Protein**	**Identity (%)**	**Similarity (%)**	**Number of aligned residues** (including gaps)
S. thermophilum SPL Q67PY4	Yeast Dpl1p Q05567	37	57	517
	Human SPL O95470	45	62	477
Yeast Dpl1p Q05567		41	61	501

The research question arose, whether the *S. thermophilum* protein was a real homologue of Dpl1p. Unlike its yeast and human counterparts, *Symbiobacterium thermophilum* SPL lacks a predicted transmembrane helix, while the PLP-containing catalytic domain is well conserved in the three organisms (**figure 2-5**). Compared to *E. coli* GadB, all three SPLs have a 30- to 50-residue long C-terminal extension (**figure 2-5**). The experiments showing that Q67PY4_SYMTH is a prokaryotic SPL are described in part 3 and chapter 4.7. of this thesis.

Figure 2-5. Predicted topology of *E. coli* GadB and SPLs

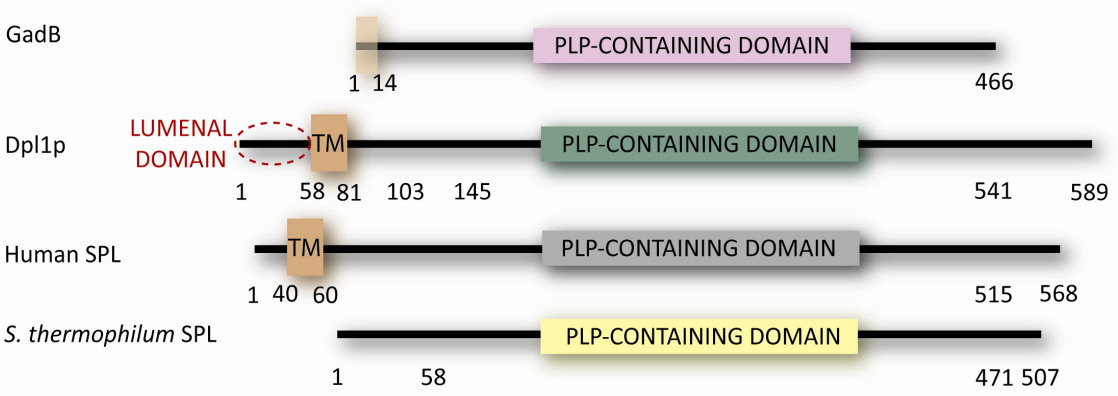

Symbiobacterium thermophilum is an obligately symbiotic thermophile originally isolated from compost at Hiroshima (Japan) in a mixed culture with a *Bacillus* strain. The bacterium lacks carbonic anhydrase and consumes the carbon dioxide produced by its symbiont (168) (169). *Symbiobacterium thermophilum* is also found in soil, animal faeces, intestinal tract, feeds (170) and seashells and other marine samples from the Pacific coast of Japan (171). Molecular taxonomy using the 16S rRNA gene indicates that the bacterium represents a novel phylogenetic branch in the Gram-positive bacterial group although it is negative by traditional Gram stain, which makes it unique in terms of taxonomy (171). Its membrane, viewed by electron microscopy, has a three-layered structure outside the cytoplasmic membrane: an electron-transparent layer is flanked by two electron-dense layers (168). The bacterium is able to form endospore-like structures under specific culture conditions (**figure 2-6**) (172). Its genome was sequenced in 2004 and displays a high (nearly 70%) GC content, typical for thermophilic organism (172).

Figure 2-6. Formation of endospore-like cellular structures in *Symbiobacterium thermophilum* viewed by optical micrography (source: (172))

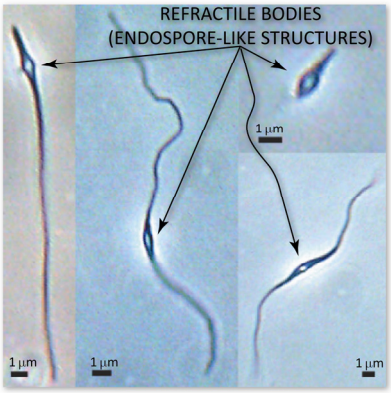

2.4. RESEARCH AIMS

In spite of their biological relevance, the enzymes of sphingolipid metabolism are biochemically not well characterized. Only few structures of sphingolipid-related proteins have been determined (see chapter 1.5.). The aim of this thesis work was to produce, purify, biochemically characterize and determine the X-ray structure of prokaryotic and eukaryotic SPLs. For this purpose, three target proteins were chosen: a prokaryotic homologue, *Symbiobacterium thermophilum* SPL, *Saccharomyces cerevisiæ* (yeast) Dpl1p and *Homo sapiens* (human) SPL.
The above research aims have been achieved to a very large degree; the next chapters of this thesis describe in detail the results and their interpretation.

3. PUBLISHED RESULTS

The following manuscript was published in *Structure* the 11th of August 2010.

Structure and function of sphingosine-1-phosphate lyase, a key enzyme of sphingolipid metabolism

Florence Bourquin, Howard Riezman, Guido Capitani and Markus Gerhard Grütter

Structure 18, 1054-1065, August 11, 2010

Structure
Article

Structure and Function of Sphingosine-1-Phosphate Lyase, a Key Enzyme of Sphingolipid Metabolism

Florence Bourquin,[1] Howard Riezman,[2] Guido Capitani,[1,3,*] and Markus G. Grütter[1]
[1]Department of Biochemistry, University of Zurich, Winterthurerstrasse 190, 8057 Zurich, Switzerland
[2]Department of Biochemistry, University of Geneva, 30 Quai E. Ansermet, 1211 Geneva 4, Switzerland
[3]Biomolecular Research, Paul Scherrer Institut, 5232 Villigen, Switzerland
*Correspondence: guido.capitani@psi.ch
DOI 10.1016/j.str.2010.05.011

SUMMARY

Sphingosine-1-phosphate lyase (SPL), a key enzyme of sphingolipid metabolism, catalyzes the irreversible degradation of sphingoid base phosphates. Its main substrate sphingosine-1-phosphate (S1P) acts both extracellularly, by binding G protein-coupled receptors of the lysophospholipid receptor family, and inside the cell, as a second messenger. There, S1P takes part in regulating various cellular processes and its levels are tightly regulated. SPL is a pivotal enzyme regulating S1P intracellular concentrations and a promising drug target for the design of immunosuppressants. We structurally and functionally characterized yeast SPL (Dpl1p) and its first prokaryotic homolog, from *Symbiobacterium thermophilum*. The Dpl1p structure served as a basis for a very reliable model of *Homo sapiens* SPL. The above results, together with in vitro and in vivo studies of SPL mutants, reveal which residues are involved in activity and substrate binding and pave the way to studies aimed at controlling the activity of this pivotal enzyme.

INTRODUCTION

Sphingolipids are ubiquitous constituents of cell membranes and their metabolites play the role of signaling molecules in eukaryotic cells (Hannun and Obeid, 2008). A very important sphingolipid is sphingosine-1-phosphate (S1P), which acts as a second messenger and takes part in the regulation of cell proliferation, motility, invasiveness, and apoptosis (Hait et al., 2009; Spiegel and Milstien, 2003). The effects of S1P have been described in a wide spectrum of organisms, ranging from *Arabidopsis thaliana* (Dunn et al., 2004; Pata et al., 2009; Tsegaye et al., 2007), *Saccharomyces cerevisiae* to *Caenorhabditis elegans* (Oskouian and Saba, 2004), *Mus musculus* (Forrest et al., 2004), and *Homo sapiens* (Oskeritzian et al., 2007; Rivera et al., 2008; Saba and Hla, 2004). S1P is unique in that it can act both as an intracellular second messenger (Hait et al., 2009) and as a ligand for G protein-coupled cell-surface receptors belonging to the lysophospholipid receptor family (Hla et al., 2001; Takabe et al., 2008).

The intracellular levels of S1P are kept under tight control by three enzymes, the first of which, sphingosine kinase, catalyzes S1P synthesis, while the other two, sphingosine-1-phosphate phosphatase and sphingosine-1-phosphate lyase (SPL, EC 4.1.2.27), catabolize it. While sphingosine-1-phosphate phosphatase catalyzes the reversible dephosphorylation of S1P, SPL degrades it irreversibly to phosphoethanolamine (PE) and hexadecenal (Bandhuvula and Saba, 2007). This complex regulation of S1P levels is biologically very significant in light of the so-called "sphingolipid rheostat," whereby cell fate depends on the ratio of intracellular S1P, which is a proliferative stimulus, and sphingosine and ceramide, which induce apoptosis (Spiegel and Milstien, 2003).

Notably, SPL was found to play an important role in regulating the immune system. Schwab and Cyster (2007) and Schwab et al. (2005) showed that 2-acetyl-4-tetrahydroxybutylimidazole (THI), a component of the food colorant caramel III, inhibits SPL, which normally maintains a steep S1P concentration gradient between the lymphoid tissues and the vascular circulation. T cells egress from lymphoid tissues by navigating along the S1P gradient. SPL inhibition by THI leads to disruption of the S1P gradient, thus preventing the egress of T cells into the blood stream and causing a logjam in lymphoid tissues (Schwab and Cyster, 2007; Schwab et al., 2005). There is also evidence of SPL involvement in tumor-suppressor and cancer surveillance pathways (Oskouian et al., 2006) and resistance to cisplatin. Control of SPL expression and activity may prove useful in the future in adjuvant and reproductive cell-protecting approaches to cancer therapy (Bandhuvula and Saba, 2007).

SPL belongs to the superfamily of PLP (pyridoxal 5′-phosphate)-dependent enzymes. Its activity was first characterized more than 40 years ago (Stoffel et al., 1968); more recently, the genes for *C. elegans* (Mendel et al., 2003), yeast (Saba et al., 1997), mouse (Zhou and Saba, 1998), plant (Nishikawa et al., 2008), and human SPL (Van Veldhoven et al., 2000) were cloned. To date, there is scarce data about the structure and biochemistry of SPL. The enzyme is known to be located in the ER (endoplasmic reticulum) and to possess an N-terminal lumenal domain, a transmembrane segment and a soluble PLP-binding domain, responsible for the catalytic activity (Ikeda et al., 2004; Van Veldhoven and Mannaerts, 1991).

The biological relevance and the growing amount of interest around SPL as a drug target (Bandhuvula and Saba, 2007; Fyrst and Saba, 2008; Han et al., 2009; Kumar and Saba, 2009) mandated, as the next step, high-resolution structural characterization of this enzyme, which had to date been shown to exist

Table 1. Data Collection and Refinement Statistics for the Structures St_1-4 and Dpl1p

Structure code	St_1	St_2	St_3	St_4	Dpl1p
Space group	$P2_12_12_1$	$P2_12_12_1$	$C222_1$	$P2_12_12_1$	F222
Unit cell parameters (Å)	a = 57.6 b = 126.8 c = 137.1	a = 84.2 b = 84.9 c = 131.3	a = 64.4 b = 243.4 c = 280.7	a = 57.7 b = 127.0 c = 136.8	a = 151.1 b = 156.9 c = 201.6
Number of polypeptide chains per a.u.	2	2	4	2	2
Resolution range[a] (Å)	29.5–2.0 (2.1–2.0)	30.0–2.97 (3.10–2.97)	29.9–2.9 (3.0–2.9)	30.0–2.05 (2.2–2.05)	48.0–3.15 (3.32–3.15)
Completeness[a] (%)	98.8 (98.6)	98.7 (92.8)	97.6 (92.7)	98.9 (95.0)	99.9 (100.0)
Redundancy	4.4	5.4	6.0	6.7	6.5
Unique reflections	67,856	19,779	48,405	63,157	20,848
I/σ [a]	9.6 (2.5)	13.7 (4.3)	11.9 (2.8)	16.4 (4.5)	15.1 (2.6)
R_{sym} [a] (%)	9.2 (60.3)	11.0 (44.2)	12.6 (57.9)	7.9 (43.1)	8.7 (70.7)
No. of reflections (test)	67,794 (950)	19,768 (988)	48,401 (2420)	63,122 (875)	20,686 (610)
No. of atoms	7268	6480	13845	7478	6634
R_{work} (%)	21.0	20.0	22.9	18.1	24.1
R_{free} (%)	24.7	26.5	25.2	21.8	30.0
rmsd bonds (Å)	0.005	0.006	0.005	0.007	0.002
rmsd angles (°)	0.98	0.97	0.96	1.09	0.52
NCS restraints applied	No	Yes	Yes	No	Yes
Ramachandran plot regions (MolProbity)					
Favored (%)	97.5	95.4	96.7	97.8	92.3
Allowed (%)	100.0	99.9	100	100	99.0
Number of outliers	0	1 (K311 B)	0	0	8[b]

See also Table S2.
[a] Values for the outermost resolution shell in brackets.
[b] S233, G312, S347, G415 in each of the two chains.

only in eukaryotes. To this end, we first used a bioinformatically identified putative prokaryotic homolog, the product of gene *STH1274* from the commensal thermophilic bacterium *Symbiobacterium thermophilum* (Ueda et al., 2004), which we characterized as a bona fide sphingosine-1-phosphate lyase and named StSPL. This in turn allowed us to solve the structure of *Saccharomyces cerevisiae* SPL, called Dpl1p, and obtain a reliable homology model of the human counterpart, SPL. Both StSPL and Dpl1p exhibit flexible stretches in regions surrounding the active site. These flexible regions carry crucial residues for activity, as shown by our thorough mutagenesis-based functional analysis. Altogether, our structural and functional studies of StSPL and Dpl1p allowed us to propose a reaction mechanism for the cleavage of long-chain base phosphates by SPL.

RESULTS AND DISCUSSION

Structure of Full-Length StSPL: Symmetries and Asymmetries

In a previous study (Mukhopadhyay et al., 2008), we had described a parsed homology model of the active site of Dpl1p, based on the active site of *Escherichia coli* glutamate decarboxylase (GadB) (Capitani et al., 2003; Gut et al., 2006), which shares 23% sequence identity with Dpl1p over a 251 residue stretch. Mutations based on that limited model and assumed to influence the enzyme activity were confirmed by cell biology data (Mukhopadhyay et al., 2008). As the next step, we embarked on a structure determination program, encompassing not only Dpl1p but also a putative prokaryotic SPL homolog in *Symbiobacterium thermophilum* (Uniprot code Q67PY4), which we had identified by a BLAST search (Altschul et al., 1997) of Dpl1p taxonomically limited to prokaryotes and named StSPL. We cloned the gene encoding Q67PY4 from the genome of *S. thermophilum*, expressed it in *E. coli*, and obtained pure protein and diffraction-quality crystals. The structure of StSPL was solved first, with a molecular replacement approach. A dimer from the GadB hexamer was used as the search model. Two StSPL structures were refined at 2.0 and 3.0 Å resolution (Table 1), respectively, from two different crystal forms, the first (St_1) (Figure 1A) containing a symmetric StSPL dimer in the asymmetric unit (a.u.), the second (St_2) (Figure 4) also containing one dimer per a.u. but featuring clear conformational asymmetry between subunits A and B. The asymmetry was not only limited to the protein chains but involved cofactor binding as well. While in St_1 both active sites contain a PLP molecule covalently bound to K311 to form an internal aldimine, in St_2 one active site is PLP-free and contains a phosphate ion at the place of the cofactor phosphate moiety (Figure 4B). The following structural description of the StSPL structure refers to St_1 (Figure 2A): each subunit can be divided into a N-terminal disordered region (called hereafter Nt-FLEX), spanning residues 1–57 and corresponding to absent or poor electron density, and a folded core encompassing residues 58–507. The core exhibits a typical type 1 PLP-dependent enzyme fold, attributed by the

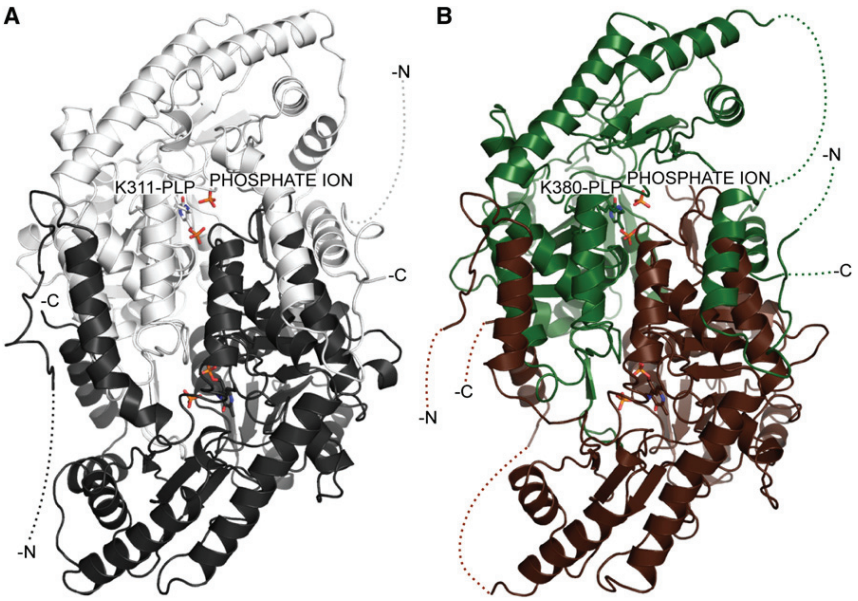

Figure 1. Cartoon Representation of FL WT StSPL (Structure St_1) and Dpl1p Δ1-102 (Structure Dpl1p-S)

(A) Subunit A of St_1 appears in light gray, subunit B in dark gray. The cofactor (PLP) and phosphate ion of both subunits, together with the covalently bound side chain of K311 (see Figure 2), are in ball-and-stick representation in the color of the respective subunit and atom colors. Nt-FLEX (residues 1–57) is not visible and its end is represented by dashed lines in the color of the corresponding subunit. The N and C termini of each subunit are indicated.

(B) Subunit A of Dpl1p-S is in green, subunit B in dark brown. Color coding is as above. StSPL K311 corresponds to Dpl1p K380. The end of Nt-FLEX (corresponding to residues 103–130) and stretches 541–563, as well as residues 580–589, are represented by dashed lines of the color of the corresponding subunit. All structural figures were prepared with PyMOL (DeLano, 2002).

SCOP database (Andreeva et al., 2008) to the pyridoxal-dependent decarboxylases subfamily. Its closest structural relative is GadB, with a rmsd of 2.2 Å over 363 common C_α atoms. The StSPL core can be divided into an N-terminal domain (residues 58–97), a large domain containing the cofactor binding K311 (residues 98–382) and a small C-terminal domain (residues 383–471). This domain structure is common with pyridoxal-dependent decarboxylases like GadB. StSPL, however, possesses a fourth C-terminal domain, dubbed C-terminal extension (Ct-EXT, residues 472–507).

Structure of Dpl1p Δ1-102: Similarities and Differences to StSPL

Using the structure of the K311A StSPL mutant (Bourquin, 2010) (at the time it was the highest quality structure of StSPL available) as search model, we could solve and refine the structure of Dpl1p Δ1-102 at 3.15 Å resolution (Table 1) (space group F222, with two Dpl1p Δ1-102 subunits per a.u., creating two different dimers by crystallographic symmetry). The use of a high-resolution, well-refined model of StSPL was instrumental to locating the two Dpl1p Δ1-102 subunits with Phaser (McCoy, 2007). The solution found refined well in Phenix (Zwart et al., 2008). The two refined Dpl1p Δ1-102 dimers are conformationally very similar but differ by cofactor binding, since one of them (Dpl1p-S) contains PLP in both active sites (Figure 1B), while the other (Dpl1p-A, mainly *apo*) exhibits very low occupancy of the cofactor (not modeled) (Figure 3A). As in subunit B of St_2 (Figure 4B), the missing cofactor is partly replaced by a phosphate ion.

The overall structure of Dpl1p Δ1-102 is very similar to that of StSPL, with a rmsd between the Dpl1p-S and St_1 dimers of 1.2 Å over 399 common C_α atoms (Figure 3B) and of 1.2 Å over 396 common C_α atoms between the Dpl1p-A and St_1 dimers and 42% sequence identity. Notably, even though the Nt-FLEX of StSPL and Dpl1p differ substantially, with the latter containing a predicted lumenal domain, followed by a transmembrane region and a cytoplasmic spacer (Figure 7A), their end is spatially very well conserved: the observed folded core of Dpl1p Δ1-102 starts with residue N131, superimposing well onto residue K58 of St_1 (Figure 3B). The same degree of conservation is observed also with respect to the domain structure. In the folded core of Dpl1p Δ1-102, the N-terminal domain spans residues 131–167, the large domain containing the cofactor-binding K380 extends from 168 to 451, the small domain from 452 to 540 and the Ct-EXT from 541 to 589 (Figure 2B). The only significant structural difference between St_1 and Dpl1p Δ1-102 resides in Ct-EXT, where Dpl1p-S residues 541 to 563 (566 in Dpl1p-A) and 580 to 589 are conformationally disordered and correspond to absent or very poor electron density (Figures 1B, 2B, 2D, and 3). This difference appears to have important functional implications as Dpl1p Δ1-102 was found to be inactive in vitro (see section on activity and mutagenesis studies) even though its boundaries correspond perfectly to those of the folded core of StSPL (Figure 3B), which is active in vitro. Since full-length (FL) Dpl1p is active in vivo (Figure 7B), we assume that Nt-FLEX (residues 1–130) plays a key role for activity, presumably in substrate presentation to the active site, and the absence of its first 102 residues may be correlated with the disorder of Ct-EXT. This is corroborated by the observation that in StSPL residues 473–488 constitute the "bottom wall" of a long hydrophobic pocket adjacent to the active site, which is not present in GadB and most likely accommodates the long hydrophobic chain of the substrate before its entrance into the active site (Figure 2C). In the crystal structure of Dpl1p Δ1-102 the aforementioned hydrophobic pocket lacks the "bottom wall" (Figure 2D) since residues 541–563 are disordered.

The Region around the Active Site in StSPL: More Asymmetries and Comparison to Other Enzymes

As mentioned above, the St_2 structure of FL WT (wild-type) StSPL exhibits clear asymmetries between subunits A and B, in contrast to the symmetry shown by the St_1 dimer. The

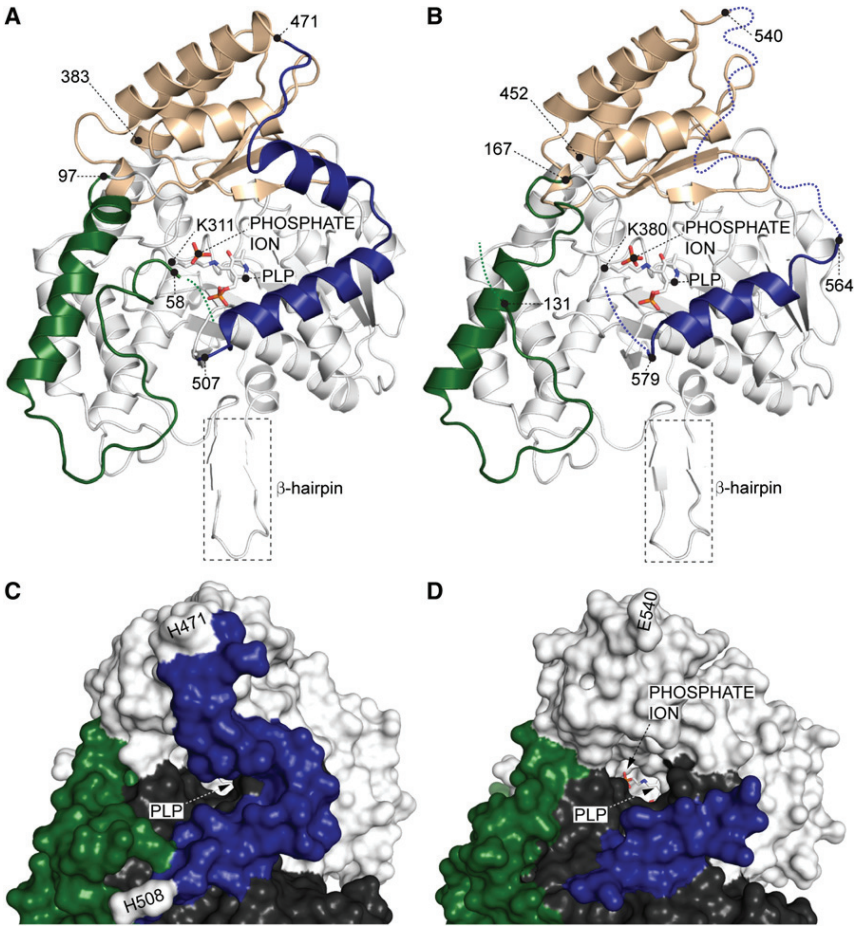

Figure 2. Subunit Structure and Domains of StSPL and Dpl1p Δ1-102

(A) Cartoon representation of subunit A of FL WT StSPL (structure St_1). The cofactors, together with the covalently bound side chain of K311 (in StSPL) and K380 (in Dpl1p), appear as described in Figure 1. The end of Nt-FLEX is depicted as dotted green line; the N-terminal domain is colored green, the large domain white, the C-terminal domain beige and Ct-EXT blue. The b-hairpin of subunit A, covering the active site of subunit B (not shown), is boxed with a dashed line. (B) Cartoon representation of subunit A of Dpl1p Δ1-102 (structure Dpl1p-S). Details as in (A). (C and D) Surface representation of StSPL (structure St_1) and Dpl1p Δ1-102 (structure Dpl1p-S) showing the active site entry channel. (C) Subunit A of St_1. The N-terminal domain is colored green while Ct-EXT is colored blue. The first histidine of the C-terminal His-tag is labeled. K311, PLP, and phosphate ion are shown as sticks. (D) Subunit A of Dpl1p-S. Color coding is as in (C).

asymmetries of St_2 are not limited to the lack of PLP in subunit B but involve the protein conformation around the active site (Figure 4): while in subunit A the regions surrounding the active site are ordered and a chloride ion is found at the position occupied by a phosphate ion in St_1 (Figure 2A), in subunit B no chloride or phosphate ion is observed and the loop comprising residues 90–107 is mostly disordered, with only residues G102 to Y105 corresponding to interpretable density (Figure 4B). The Ct-EXT of subunit A is again partly disordered, with only residues 475–483 and 490–507 corresponding to interpretable density. The entire Ct-EXT of subunit B is disordered. As a consequence, the hydrophobic pocket of subunit B of St_2 partly lacks its "bottom wall" (Figure 2C), while its counterpart in subunit A is nearly complete since its Ct-EXT is partly ordered. Yet another element of asymmetry in St_2 is the S123*-S135* loop (residues followed by an asterisk belong to the neighboring subunit), exhibiting markedly higher B-factors in chain A (lining the active site of subunit B) than in chain B (<B > = 60 $Å^2$ in the former versus 41 $Å^2$ in the latter).

Crystallographic and biochemical studies of the two isoforms of human glutamate decarboxylase, GAD65 and GAD67 (Fenalti et al., 2007), showed the importance of a "catalytic loop" (residues 432*–442* in GAD67) being ordered or disordered for the control of enzyme activity. The active site loop of human GAD is not conserved in SPL, where it is replaced by a β-hairpin (residues 334*–349* in StSPL) (Figure 2A), but it suggests a functional role for the aforementioned asymmetric elements of St_2, all of which are located nearby.

Another enzyme involved in sphingolipid metabolism, serine palmitoyl-transferase (SPT), exhibits peculiar asymmetry with respect to PLP binding: it is a heterodimer composed of two strictly related subunits plus a third subunit conferring substrate specificity (Han et al., 2009; Hornemann et al., 2009). One of the two subunits of the heterodimer lacks the residues for PLP binding even though it is required for activity, as modeled from the structures of *Sphingomonas paucimobilis* (Yard et al., 2007) and *Sphingobacterium multivorum* (Ikushiro et al., 2009) SPTs. St_2 features asymmetry in cofactor binding in spite of being a homodimer. Modulation of cofactor binding thus appears to be a feature common to several eukaryotic PLP-dependent enzymes.

Altogether, our structural studies of StSPL and Dpl1p Δ1-102 reveal that both proteins share the same fold and that the disorder in the N terminus (Nt-FLEX domain) is a conserved feature. Moreover, variations are found in the cofactor occupancy in some forms of both enzymes. One significant difference between StSPL and Dpl1p Δ1-102 is that the latter lacks part of Ct-EXT covering the active site. Asymmetries between both subunits of one crystal form of StSPL were mapped in three regions surrounding the active site. We assumed that this flexibility is functionally relevant and performed mutagenesis studies of residues carried by these loops (see below).

Cofactor Binding Mode and Active Site in FL StSPL and Dpl1p Δ1-102 and Model of Substrate Accommodation

The cofactor binding mode and the active site in general are very well conserved between StSPL and Dpl1p: in both cases the phosphate moiety of PLP is held in place by a classical "phosphate cup" motif (Denesyuk et al., 2003) with residues

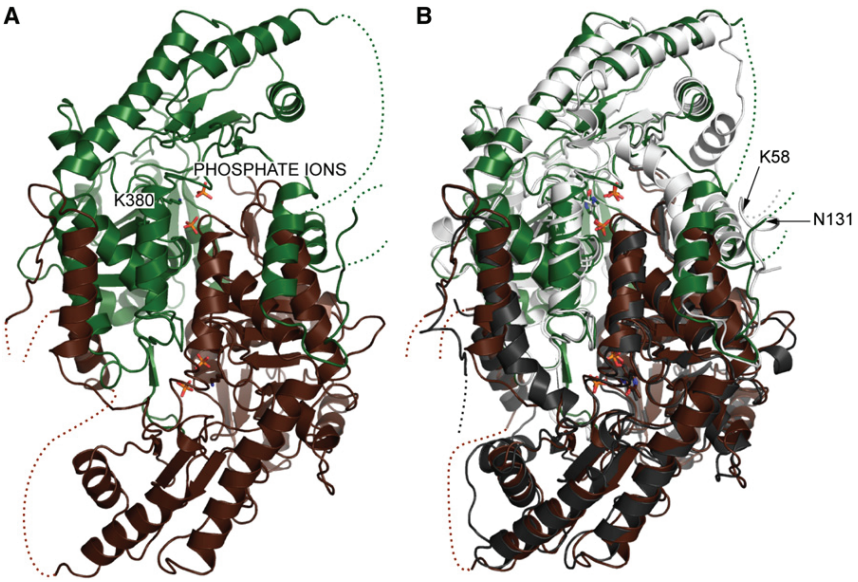

Figure 3. Dpl1p-A, Dpl1p-S and StSPL
(A) Cartoon representation of Dpl1p-A dimer. Subunit C appears in green, subunit D in dark brown. Color coding is as in Figure 1.
(B) Superposition, in cartoon representation, of the Dpl1p-S dimer structure onto StSPL (structure St_1). The color coding is as in Figure 1. The first ordered residue of each protein (K58 for StSPL and N131 for Dpl1p-S) is denoted by an arrow.

(StSPL numbering) G168, T169, H310, and S353* hydrogen-bonding the phosphate oxygen atoms (see Figures S1A and B available online). The pyridinium ring of PLP is sandwiched between residues C276 and H201 in StSPL, corresponding to residues C344 and H268 in Dpl1p. Another common feature is a phosphate ion found at the same position in both proteins, in the vicinity of the cofactor. The ion interacts with the phenolic moiety of Y105, the imidazolium ring of H129*, the main chain amide nitrogen of A103 and the carboxamide group of N126* (distances 2.6, 2.7, 2.8, and 3.2 Å, respectively, in subunit A of St_1). The corresponding phosphate-binding residues in the active site of Dpl1p are Y174, H198*, and A172. The conserved binding mode of the phosphate ion mimics the binding mode of the phosphate moiety of the natural substrate of the enzyme, S1P. This is confirmed by the structure of StSPL K311A in complex with the product PE at 2.9 Å resolution (structure St_3) (Table 1; Figure 5A). PE is one of the two products of the SPL reaction and contains the polar part of the substrate. No significant conformational changes were observed between St_1 and St_3 (rmsd value of 0.3 Å over 446 common C_α atoms). PE was seen to form a Schiff base with PLP and its phosphate group replaced the phosphate ion found in the active sites of St_1 and Dpl1p Δ1-102 (Figures 2A and 2B). Based on St_3, we modeled the substrate S1P bound in WT StSPL (Figure S1C) and carried out mutagenesis studies on residues A103, Y105, H129*, C276, K311, K317, and Y482 (Figure 5B). The mutants were designed on the basis of the well-described biochemistry of PLP-dependent enzymes (Eliot and Kirsch, 2004; Toney, 2005) as well as by taking into account the mechanism proposed in Van Veldhoven and Mannaerts (1993) and by assuming that residues found in flexible stretches of Dpl1p Δ1-102 and St_2 (Figures 2B and 2D, and Figure 4, respectively) might be involved in activity (see previous sections). Residues A103 and Y105 (StSPL numbering) are located on the active-site flanking loop that is disordered in subunit B of St_2 (Figure 4, dark brown loop). H129* and K317 sit near the phosphate moiety of the active site-bound substrate, even though K317 is too distant (nearly 5 Å) to hydrogen-bond the phosphate. In an early study of SPL (Van Veldhoven et al., 2000), the residue corresponding to C276 had been proposed to be the nucleophile required for bond cleavage and was therefore included into our mutagenesis study. The activity of mutants of the corresponding residues in Dpl1p (A172, Y174, H198*, C344, K380, K386, and

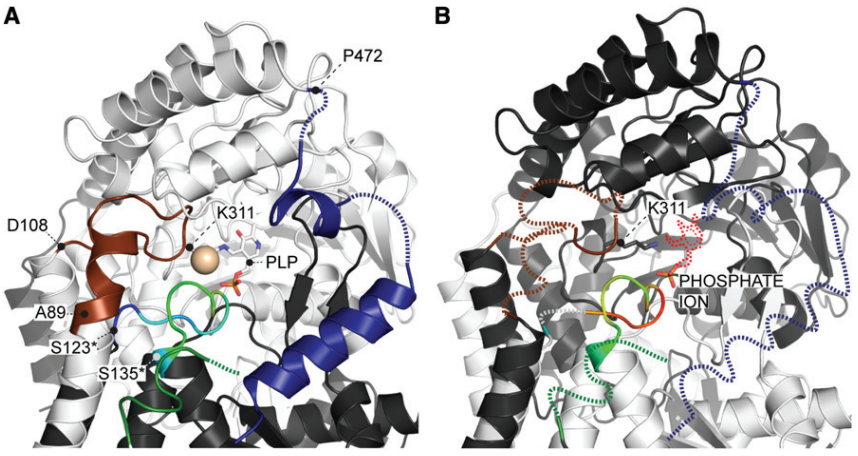

Figure 4. Cartoon Representation of the Two Subunits of the Asymmetric Form of StSPL (Structure St_2)
(A) Subunit A appears in light gray with the same color conventions as in Figure 1. Additionally, structural elements exhibiting asymmetry between the two subunits of St_2 are depicted as follows: residues A89–D108 in brown, P472–V507 (Ct-EXT) in blue, and K58–F64 in green. The chloride ion bound in the active site of subunit A is shown in beige in space-fill model. The loop S123*–S135*, which completes the active site environment, is colored according to its B-factors (blue corresponds to lower B-factors). Disordered regions are represented by dashed lines.
(B) Same as above with view vertically rotated by 180° and focusing on subunit B. The active site lacks the cofactor (the trace of PLP in the subunit A is depicted by a red dashed line), which is partly replaced by a phosphate ion.

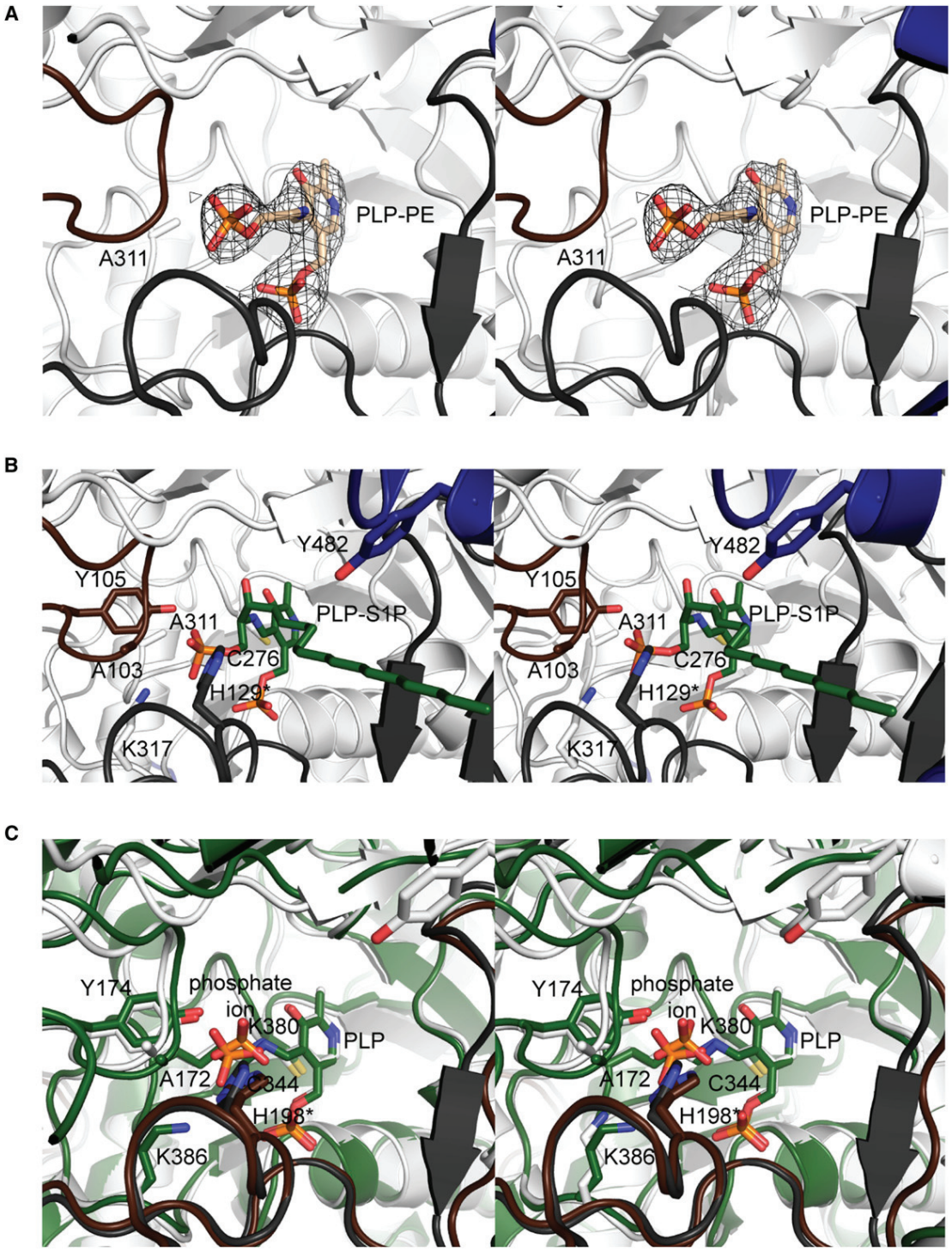

Figure 5. Close-up View of the Active Sites of StSPL and Dpl1p Δ1-102

(A) Stereo representation of the reaction product PE bound to PLP (PLP-PE) in the active site of StSPL K311A (structure St_3). Color coding is as in Figure 1A.

(B) Same as (A), showing the modeled external aldimine intermediate with S1P (PLP-S1P). Color coding is as in Figure 4. The residues studied by mutagenesis are labeled. The model, based on the structure of St_3, is to be considered tentative, especially with respect to the C2-C3 (see Figure 8, step II) torsion angle and to the conformation of the hydrophobic chain. The optimal conformation for retro-aldol cleavage is with the C3-hydroxyl moiety of S1P antiperiplanar to the amino group of the aldimine (Dunathan, 1966). In our modeling attempt, such a conformation led to steric clashes with Y249 (Figure S1C).

(C) Stereo representation of a superposition of Dpl1p Δ1-102 (Dpl1p-S) onto FL WT StSPL (structure St_1), showing the residues of Dpl1p presumably involved in activity. Color coding is as in Figure 1. See also Figures S1 and S2.

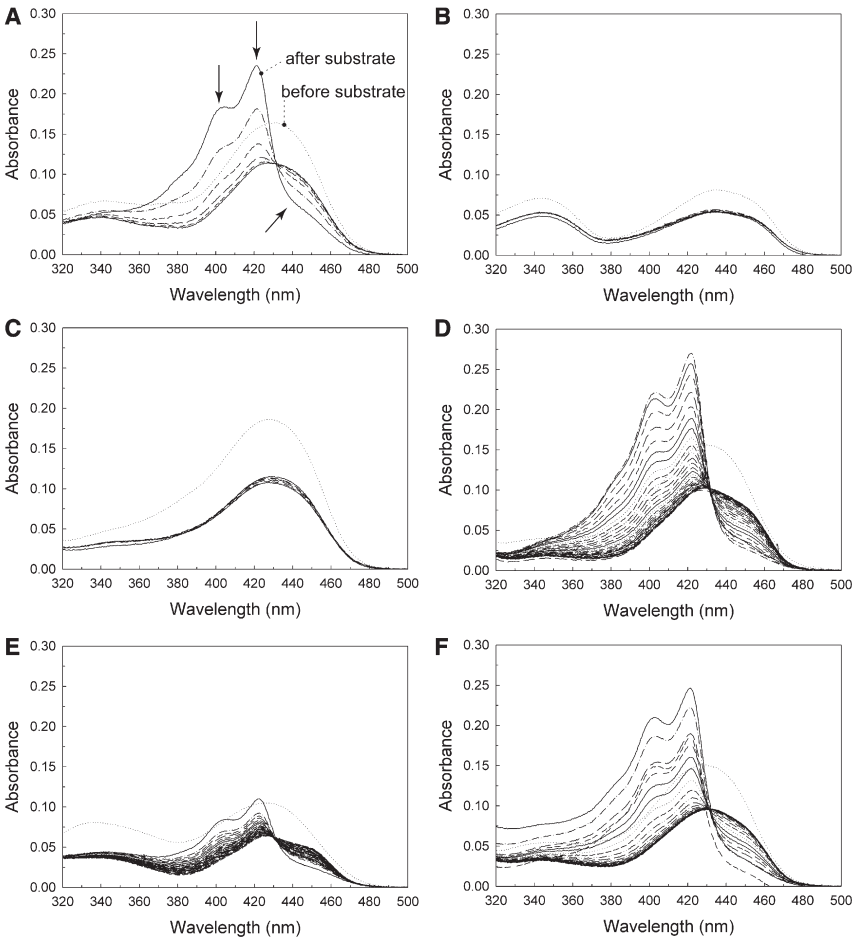

Figure 6. Spectrophotometric Activity Assay of StSPL Using S1P As Substrate

(A) FL WT control for (B) and (C). The visible spectrum (320–500 nm) of the enzyme before and after addition of substrate is depicted by a dotted and a solid line respectively. Spectra were recorded each min over 5 min. The transient peaks at 403 and 420 nm as well as changes in the 450 nm regions are indicated with arrows.

(B) Same as (A) for K311A.

(C) Same as (A) for Y105F.

(D) Same as (A) for Y482F except that the spectra were recorded during 30 min. FL WT control is shown in (F).

(E) C276A. FL WT control is shown in (F).

(F) FL WT control for (D) and (E). Spectra of (E) and (F) were recorded as in (D). See also Figures S3, S4, and S5.

Y554) was compared using an in vivo assay (Mukhopadhyay et al., 2008). The active sites of St_1 and Dpl1p-S superimpose very well and the above-mentioned residues occupy structurally equivalent positions in both enzymes, except for Y554 (Y482 in StSPL), which is found in the disordered region of Ct-EXT of Dpl1p (Figure 5C).

Importantly, Dpl1p Δ1-102 shares 45% sequence identity over 420 residues with its medically important human counterpart, SPL (UniProt code O95470): we could calculate a reliable homology model of SPL (Figure S1D), showing that the active site is conserved between the two proteins, with the exception of T148 in SPL (A172 in Dpl1p). A multiple sequence alignment of StSPL, Dpl1p and SPL with the predicted secondary structure elements can be found in Figure S2. The structural features and the functionally important residues described in this study provide a solid basis for future mutagenesis and inhibition studies of SPL.

Activity and Mutagenesis Studies of StSPL and Dpl1p

The visible spectrum of FL WT StSPL exhibits a shoulder at 340 nm and a broad peak at 420–460 nm, presumably resulting from the contribution of two species centered at 425 and 450 nm (Figure 6A, dotted line), respectively. The 340 and 425 nm species correspond to tautomers of the internal aldimine (Gut et al., 2009), while the 450 nm band represents an unknown species. The spectra of mutants K311A and C276A (Figures 6B and 6E, dotted lines) and of construct ΔCt-EXT (lacking residues 472–507) (Figure S3B, dotted lines) differ markedly from that of FL WT. They feature a peak at 345 nm, which may correspond to the hydrated form of PLP, as seen in the structure of StSPL K311A (Bourquin, 2010).

Mutagenesis studies were carried out on the residues listed above as well as on Nt-FLEX and Ct-EXT truncation variants of StSPL (Figure 2A). There are many SPL activity assays available, based on the detection of fluorescent species (Bedia et al., 2009; Bandhuvula et al., 2007, 2009). In the present work, the activity of StSPL mutants and variants compared with FL WT was assessed by spectrophotometry and mass spectrometry (MS). The first method monitors variations occurring in the environment of PLP upon catalysis, as shown for serine palmitoyltransferase (Ikushiro et al., 2009; Raman et al., 2009; Shiraiwa et al., 2009), and thereby indirectly monitors the activity of the protein, while the latter monitors substrate cleavage. Both tests provided qualitative information. Quantitative analysis was hindered by variations in the amount of soluble material, presumably due to discrepancies in the purity of S1P from various batches of chemical synthesis or of extraction from natural sources, to the inherently poor solubility of S1P (García-Pacios et al., 2009) and to the challenging reproducibility of the solubilization procedure, as well as by variations when desalting the sample before MS. As a consequence, an accurate concentration of S1P was difficult to obtain, resulting in different response intensities in the activity assays. Therefore, the activity of mutants or variants of StSPL has to be compared with that of the FL WT StSPL purified in parallel and tested under similar conditions.

The spectrophotometric activity assay monitors the appearance and disappearance of transient peaks at 403 and 420 nm, accompanied by a decrease in the absorption at 450 nm, that appeared upon mixing FL WT StSPL with S1P (Figures 6A

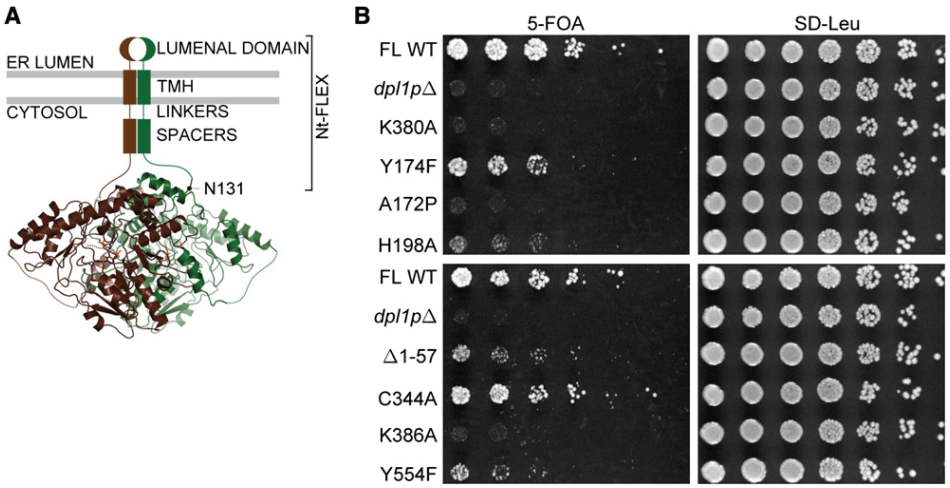

Figure 7. Function of Dpl1p Variants In Vivo

(A) Proposed arrangement of the catalytic domain of Dpl1p with respect to the ER membrane. The two subunits are depicted as in Figure 1B. TMH, transmembrane helix.

(B) Yeast strain RH4863 carrying FL WT Dpl1p, Dpl1p Δ1-57, FL mutants A172P, Y174F, H198A, C344A, K380A, K386A, and Y554F or an empty vector (designated *dpl1p*Δ) were 5-fold serially diluted and spotted onto SD plates without leucine or on SD plates with uracil and 5-fluoroorotic acid (5-FOA). Only strains carrying a functional Dpl1p can grow in presence of 5-FOA (Mukhopadhyay et al., 2008). The colonies were photographed after 3 days of incubation at 30°C.

and 6F; Figures S3C and S3G), dihydrosphingosine-1-phosphate (DHS1P) (Figure S3H) or phytosphingosine-1-phosphate (PS1P) (Figure S3I). We tentatively interpret those peaks as the external aldimine species PLP-S1P and PLP-PE (Figure 8, steps III and VII). The 420 nm band may correspond to the external aldimine with PE, since a spectrum of StSPL K311A incubated with PE shows a slowly appearing, broad band centered at about 425–430 nm (Bourquin, 2010). It is noteworthy that no similar changes were observed upon incubating StSPL WT and PE (Bourquin, 2010). The above transient spectrophotometric changes correlate with the cleavage of S1P, as shown by MS (Figures S4C and S4D). The time elapsed until disappearance of the peaks (relaxation time) is assumed to be proportional to the amount of enzyme and its degree of activity. When FL WT StSPL was incubated with semicarbazide, a general PLP-dependent enzyme inhibitor, the 420–460 nm peak disappeared and was replaced by a 360 nm peak with a clear isosbestic point (Figure S5C), and only very faint transient peaks were observed upon substrate addition (Figure S5D). The PLP-semicarbazone adduct (Figure S5B) formed by the inhibitor with the cofactor was found by crystallography (structure St_4) to have left the active site (Figure S5A). This correlates with the observation that cocrystals of StSPL with 10-fold molar excess of semicarbazide are colorless, while the native crystals are bright yellow (Bourquin, 2010). In St_4, the nearby residue Y249 (Figure S1C) partly replaces the pyridinium ring of the PLP but is likely not involved in catalysis, since mutant Y249F behaves similarly as FL WT (Figures S5E and S5F, respectively). StSPL mutants K311A and Y105F did not exhibit significant time-dependent changes in the spectrophotometric (Figures 6B and 6C, respectively) and MS (Figures S4H and S4I, respectively) assays and were categorized as inactive. Mutants A103P and K317A (Figures S3E and S3F, respectively) exhibited no transient peaks at 403 and 420 nm and no activity in the MS assay (Figure S4J and S4K, respectively). All the above mutants were categorized as inactive. StSPL Y482F, C276A (Figures 6D and 6E, respectively), H129A and ΔCt-EXT (Figures S3D and S3B, respectively) exhibited a significantly longer relaxation time and much less intense transient peaks (especially for H129A) and were thus assumed to be partly active. StSPL ΔNt-FLEX behaved similarly (albeit with an altered relaxation time) as FL WT (Figure S3A). The Dpl1p truncation Δ1-102 used for structure determination did not exhibit any visible spectrum alterations upon addition of S1P, DHS1P nor PS1P (Figures S3J, S3K, and S3L, respectively) and was therefore considered as inactive in vitro.

The Nt-FLEX of FL Dpl1p (residues 1–130) is assumed to consist, from its N to C terminus, of a lumenal domain (residues 1–57), a transmembrane helix (residues 58–82), a linker and a spacer (Figure 7A). A yeast synthetic lethality test (Mukhopadhyay et al., 2008) was used to assess the activity of mutants and of the lumenal domain truncation of Dpl1p. Dpl1p Δ1-57 and FL Dpl1p Y174F, H198A, Y554F are partly active, C344A is probably slightly less active as the WT, while K380A, A172P, and K386A are inactive (Figure 7B). The mutagenesis results of Dpl1p are in good agreement with those of StSPL, except for Y174F (corresponding to StSPL Y105F). This single difference might arise from the very different time scale of the in vitro experiments compared with the in vivo experiments or from other sources of bias. For instance, we do not know which enzymatic parameters (K_m, K_{cat}) are most crucial for the in vivo experiment. Alternatively, the precise role of this residue might not be conserved between StSPL and Dpl1p, as a result of different modes of regulation. Importantly, Y174 of Dpl1p is conserved in SPL (Y150). Dpl1p Y174F was found to be partly active: a possible role for this residue is that of influencing the protonation state of K386 and this might represent a regulation mechanism of eukaryotic SPLs.

Further analysis is required to confirm that StSPL Y105F is fully inactive since our in vitro assays are not quantitative. Based on

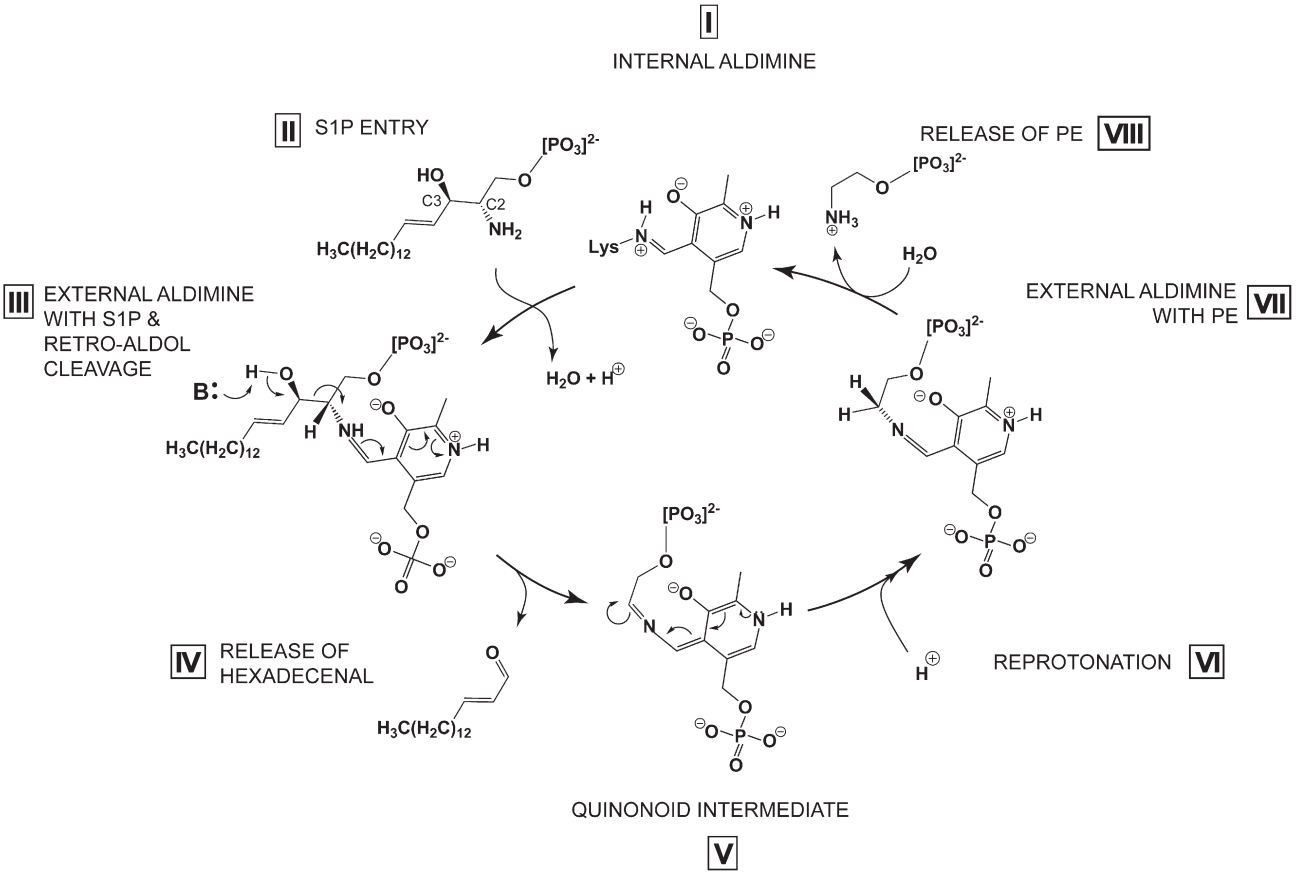

Figure 8. Proposed Mechanism of S1P Cleavage by SPL

The incoming S1P (step II) replaces the catalytic lysine (311 in StSPL and 380 in Dpl1p) as Schiff base partner of PLP, forming an external aldimine (step III). Retro-aldol cleavage occurs at the hydroxyl group of carbon atom 3 of S1P (step III) and the long-chain aldehyde product (called hexadecenal in case S1P is the substrate) is released (step IV). The second external aldimine (step VII) results from reprotonation (step VI) of the quinonoid intermediate (step V). PE is then released (step VIII) and the internal aldimine is re-formed (step I): the enzyme is now ready for a second turnover.

our model (Figure 5B) residues (StSPL numbering) Y105 and H129*, found close to the phosphate head of the substrate, are important for substrate binding. The side-chain amino group of K317 is also close to the phosphate location but not within hydrogen-bonding distance (4.8 Å in St_1, subunit A). A103 appears to keep the loop 89–108, containing Y105 (Figure 4A, dark brown), in a conformation able to bind the phosphate moiety of the cofactor. The corresponding residue of SPL, T148, might provide additional stabilization by interacting with H174* and N171* (Figure S1D).

Figure 8 summarizes the reaction mechanism we propose based on the structural, biochemical and literature information available. Step III is a retro-aldol cleavage whereby a base (depicted as B:) nucleophilically attacks the proton of the hydroxyl moiety of the substrate. Based on our current model of the external aldimine with S1P (Figure 5B) the identity of that base is not clear and its elucidation will require further structural and biochemical studies. Notably, for serine hydroxymethyl-transferase, another PLP-dependent enzyme catalyzing a retro-aldol cleavage, finding the corresponding base has proved similarly difficult (Schirch and Szebenyi, 2005). The quinonoid reprotonation step (step VI), resulting in the formation of the external aldimine PE-PLP and in the subsequent release of PE (steps VII and VIII, respectively) may be carried out by StSPL K311 or by the nearby Y105 (K380 and Y174 in Dpl1p, K353 and Y150 in SPL). K317 of StSPL (K386 in Dpl1p and K359 in SPL) for sure electrostatically contributes to the binding of the phosphate moiety of the substrate and may also play an indirect role in the reprotonation. The partial activity of the alanine mutant of C276 (C344 and C317), a PLP stacking residue, indicates that its role is mostly structural, keeping the cofactor in an optimal position for reactivity. This is consistent with the observation that the side chain thiol of C276 points away from the substrate instead of toward it. Y482 (Y554 and Y526) appears to play an important role in activity, possibly in substrate accommodation since it belongs to the ''bottom wall'' region discussed above. Further analysis is required to decipher the precise role of all residues involved in the reaction mechanism of SPL.

As mentioned above, the extent of disorder or flexibility of the N termini (Nt-FLEX) seems to be conserved from StSPL to Dpl1p Δ1-102 (Figure 3B) and may reflect a functional role, presumably in accommodating the substrate embedded in

the membrane. Since StSPL lacks a transmembrane helix, the precise mechanism of accommodation is most probably not conserved, because StSPL ΔNt-FLEX behaves as FL WT in the in vitro activity test (Figure S3A), and Dpl1p Δ1-102 is inactive in vitro, while Dpl1p Δ1-57 is only partly active in vivo (Figure 7B).

The N and C termini of StSPL, and most probably of Dpl1p, surround the active site entry channel (Figures 2C and 2D, respectively) and might act as a gate that isolates the substrate-bound active site from solvent and thus promotes catalysis. Indeed, StSPL ΔCt-EXT appears to be less active than FL WT StSPL (Figure S3B).

Our functional analysis of StSPL and Dpl1p clearly indicates that the flexible regions described in the first sections carry residues crucial for activity. Our results allow a better understanding of the mode of action of this very important enzyme. Given the similarity of the active sites and the high degree of conservation between StSPL, Dpl1p and SPL (Figures 5C, S1 and S2), the proposed mechanism can serve as basis for further studies on the human counterpart.

In conclusion, this study provides the first structural characterization of a eukaryotic SPL, identifies critical residues for activity, sheds light on the reaction mechanism, and demonstrates the existence and functionality of a prokaryotic homolog of the enzyme. Modulating the cofactor occupancy seems to be a common feature of both StSPL and Dpl1p. Moreover, our results allowed the generation of a high-quality homology model of the human enzyme, pinpointing the conservation of the above described residues. Most importantly, they provide a solid foundation for structure-based drug design on SPL.

EXPERIMENTAL PROCEDURES

Chemicals

All chemicals and reagents were of the highest commercially available grade.

Plasmid Constructs and Protein Expression and Purification

Plasmid construction and expression and purification of StSPL and Dpl1p Δ1-102 are described in Supplemental Information.

Activity Assays

UV-visible spectra were recorded on a Cary-50 spectrophotometer (Varian) using 1 cm light path quartz precision cells (Hellma). Protein concentration was estimated using an average value of the extinction coefficient of a fully reduced and a fully oxidized protein as calculated with ProtParam (Gasteiger et al., 2005). The value used for FL WT StSPL was 79′400 $M^{-1}cm^{-1}$ and 50′500 $M^{-1}cm^{-1}$ for Dpl1p Δ1-102. S1P was purchased from Acros, Alexis Biochemicals or Avanti Polar Lipids, while DHS1P and PS1P were from Avanti Polar Lipids. The phosphosphingolipids were solubilized in 1% (w/v) Triton X-100 (Fluka or Acros) to 1 mg/ml (corresponding to 2.6 mM). The suspension was incubated at 37°C for 30 min with 1 min vortexing every 4 min. After 10 min sonification and further vortexing, insoluble material was separated by a 10 min centrifugation step at 14,000 × g at room temperature. Protein concentration in the cell was set at 22 μM (1.2 mg/ml), for a total volume of 100 μl. Seventy microliters of phosphosphingolipid solution was added to the protein and briefly homogenized with a pipette. The buffer corresponded to the SEC buffer containing 1 mM KPi. Spectra were recorded every minute from 500 to 320 nm until no or only slight spectral changes could be observed.

The yeast synthetic lethality test was carried out as described in Mukhopadhyay et al. (2008).

Semicarbazide (Fluka) was mixed to FL WT StSPL set at 14 μM to a molar excess of 100-fold over active sites and spectra were recorded as described above. After 1 hr incubation, S1P was added and the spectra recorded as described above.

For MS activity assay, S1P cleavage by StSPL was carried out under the same conditions as the spectrophotometric activity assay except that S1P was solubilized in 100% ethanol. The reaction mixture was desalted using C_{18} ZipTip® pipettes tips (Millipore) and diluted in 50% acetonitrile, 0.2% formic acid (pH 2) before injection. Masses were measured in the positive mode on a quadrupole mass spectrometer equipped with an electrospray (ESI) ionization source and a time of flight (TOF) ion separation device (Q-TOF Ultima API, Waters Corporation). Multiple-charged protein ion signals were deconvoluted to produce zero-charge spectra using the Maximum EntropyTM 1 (MaxEnt1) algorithm in the Micromass MassLynx software package (Thermo Scientific).

Protein Crystallization and Structure Determination

Native StSPL and Dpl1p were crystallized by vapor diffusion (sitting drop) at 20°C. For cocrystallization with PE, StSPL K311A (7 mg/ml) was incubated for 10 min on ice with an equimolar amount of PLP. StSPL K311A and PE (Fluka) at a 10-fold molar excess over protein subunit were then incubated overnight at 4°C and concentrated prior to crystallization. Bright yellow (structures St_1, St_2 and Dpl1p), pale yellow (structure St_3) or colorless (structure St_4) crystals appeared after 2–15 days. Crystallization conditions are listed in Table S2. Crystals were cryoprotected by adding ethylene glycol (EG) to the well solution (which, in cocrystallization experiments, was supplemented with the corresponding compound at the appropriate concentration) (Table S2). Crystals were flash-frozen by rapid immersion in liquid propane. Data sets were collected at 100K at the X06SA beamline of the Swiss Light Source (SLS; Villigen, Switzerland). Data were processed with XDS (Kabsch, 1993). The first structure of StSPL (code St_2) was solved by molecular replacement with Phaser (McCoy, 2007) using a polyserine dimer of GadB (PDB entry 2DGK) as search model. FL WT StSPL set at 3 mg/ml was cocrystallized with semicarbazide according to the same procedure as for PE omitting the initial incubation with PLP and with 45 min incubation at 4°C prior to crystallization.

Crystallographic Refinement and Validation

Refinement was carried out with CNS (Brünger et al., 1998) and Phenix (Zwart et al., 2008). The structure of Dpl1p Δ1-102 was solved with Phaser (McCoy, 2007) using a refined dimeric model of StSPL K311A (Bourquin, 2010). NCS restraints were employed by default and manually edited during refinement, unless data resolution was high enough to render them superfluous (Table 1). Models were rebuilt with Coot (Emsley and Cowtan, 2004) and validated with ProCheck (Laskowski et al., 1993) and MolProbity (Davis et al., 2007). PDB entry codes are 3MAD (St_1), 3MAF (St_2), 3MAU (St_3), 3MBB (St_4), and 3MC6 (Dpl1p).

Modeling of SPL and of StSPL K311A in Complex with S1P

A dimeric homology model of the folded core of SPL was computed based on the structure of Dpl1p Δ1-102 using the program Modeller 9v6 (Sali, 1995). The PLP cofactor was also included in the calculation as a rigid-body residue. The model, including the internal aldimine linkage of the cofactor with K353, was geometry minimized with Phenix (Zwart et al., 2008).

A tentative model of StSPL K311A containing the external aldimine intermediate with the substrate S1P was prepared with Coot based on the structure of St_3 (Figure S1C). The S1P ligand was obtained from PDB entry 3I9G (Wojciak et al., 2009), manually coupled with PLP and optimized with the PRODRG server (http://davapc1.bioch.dundee.ac.uk/prodrg/). The S1P hydrophobic chain was positioned such that it interacts with a hydrophobic region encompassing residues L128*, Y249, L344*, Y345*, F346*, V496, L497, and F500. The model was energy-minimized with Phenix.

SUPPLEMENTAL INFORMATION

Supplemental Information includes Supplemental Experimental Procedures, five figures, and two tables and can be found with this article online at doi:10.1016/j.str.2010.05.011.

ACKNOWLEDGMENTS

We are grateful to D. De Biase for critical reading of the manuscript. We thank the staff of beamline X06SA at the Swiss Light Source (Villigen, CH) for excellent support in X-ray data collection. We also thank Martin A. Schärer (Paul Scherrer Institut), B. Blattmann and C. Stutz-Ducommun (University of Zurich), Drs. Serge Chesnov and Bernd Roschitzki (Functional Genomics Center Zurich). The *S. thermophilum* genome was a kind gift from Dr. K. Ueda, Nihon University, Japan. This project was funded by the Forschungskredit of the University of Zurich (grant to G.C.), the Swiss National Science Foundation (grants to H.R., M.G.G.) and the Swiss NCCR Structural Biology program.

Received: February 5, 2010
Revised: April 1, 2010
Accepted: May 9, 2010
Published: August 10, 2010

REFERENCES

Altschul, S.F., Madden, T.L., Schäffer, A.A., Zhang, J., Zhang, Z., Miller, W., and Lipman, D.J. (1997). Gapped BLAST and PSI-BLAST: a new generation of protein database search programs. Nucleic Acids Res. *25*, 3389–3402.

Andreeva, A., Howorth, D., Chandonia, J.M., Brenner, S.E., Hubbard, T.J., Chothia, C., and Murzin, A.G. (2008). Data growth and its impact on the SCOP database: new developments. Nucleic Acids Res. *36*, D419–D425.

Bandhuvula, P., Fyrst, H., and Saba, J.D. (2007). A rapid fluorescence assay for sphingosine-1-phosphate lyase enzyme activity. J. Lipid Res. *48*, 2769–2778.

Bandhuvula, P., and Saba, J.D. (2007). Sphingosine-1-phosphate lyase in immunity and cancer: silencing the siren. Trends Mol. Med. *13*, 210–217.

Bandhuvula, P., Li, Z., Bittman, R., and Saba, J.D. (2009). Sphingosine 1-phosphate lyase enzyme assay using a BODIPY-labeled substrate. Biochem. Biophys. Res. Commun. *380*, 366–370.

Bedia, C., Camacho, L., Casas, J., Abad, J.L., Delgado, A., Van Veldhoven, P.P., and Fabriàs, G. (2009). Synthesis of a fluorogenic analogue of sphingosine-1-phosphate and its use to determine sphingosine-1-phosphate lyase activity. ChemBioChem *10*, 820–822.

Bourquin, F. (2010). Questioning the Sphinx: structural and functional studies of sphingosine-1-phosphate lyase. PhD thesis, Department of Biochemistry, University of Zurich, Zurich, Switzerland.

Brünger, A.T., Adams, P.D., Clore, G.M., DeLano, W.L., Gros, P., Grosse-Kunstleve, R.W., Jiang, J.S., Kuszewski, J., Nilges, M., Pannu, N.S., et al. (1998). Crystallography & NMR system: a new software suite for macromolecular structure determination. Acta Crystallogr. D Biol. Crystallogr. *54*, 905–921.

Capitani, G., De Biase, D., Aurizi, C., Gut, H., Bossa, F., and Grutter, M.G. (2003). Crystal structure and functional analysis of Escherichia coli glutamate decarboxylase. EMBO J. *22*, 4027–4037.

Davis, I.W., Leaver-Fay, A., Chen, V.B., Block, J.N., Kapral, G.J., Wang, X., Murray, L.W., Arendall, W.B., 3rd, Snoeyink, J., Richardson, J.S., et al. (2007). MolProbity: all-atom contacts and structure validation for proteins and nucleic acids. Nucleic Acids Res. *35*, W375–W383.

DeLano, W.L. (2002). The PyMOL Molecular Graphics System (Palo Alto, CA: DeLano Scientific).

Denesyuk, A.I., Denessiouk, K.A., Korpela, T., and Johnson, M.S. (2003). Phosphate group binding "cup" of PLP-dependent and non-PLP-dependent enzymes: leitmotif and variations. Biochim. Biophys. Acta *1647*, 234–238.

Dunathan, H.C. (1966). Conformation and reaction specificity in pyridoxal phosphate enzymes. Proc. Natl. Acad. Sci. USA *55*, 712–716.

Dunn, T.M., Lynch, D.V., Michaelson, L.V., and Napier, J.A. (2004). A post-genomic approach to understanding sphingolipid metabolism in Arabidopsis thaliana. Ann. Bot. *93*, 483–497.

Eliot, A.C., and Kirsch, J.F. (2004). Pyridoxal phosphate enzymes: mechanistic, structural, and evolutionary considerations. Annu. Rev. Biochem. *73*, 383–415.

Emsley, P., and Cowtan, K. (2004). Coot: model-building tools for molecular graphics. Acta Crystallogr. D Biol. Crystallogr. *60*, 2126–2132.

Fenalti, G., Law, R.H., Buckle, A.M., Langendorf, C., Tuck, K., Rosado, C.J., Faux, N.G., Mahmood, K., Hampe, C.S., Banga, J.P., et al. (2007). GABA production by glutamic acid decarboxylase is regulated by a dynamic catalytic loop. Nat. Struct. Mol. Biol. *14*, 280–286.

Forrest, M., Sun, S.Y., Hajdu, R., Bergstrom, J., Card, D., Doherty, G., Hale, J., Keohane, C., Meyers, C., Milligan, J., et al. (2004). Immune cell regulation and cardiovascular effects of sphingosine 1-phosphate receptor agonists in rodents are mediated via distinct receptor subtypes. J. Pharmacol. Exp. Ther. *309*, 758–768.

Fyrst, H., and Saba, J.D. (2008). Sphingosine-1-phosphate lyase in development and disease: sphingolipid metabolism takes flight. Biochim. Biophys. Acta *1781*, 448–458.

García-Pacios, M., Collado, M.I., Busto, J.V., Sot, J., Alonso, A., Arrondo, J.L., and Goñi, F.M. (2009). Sphingosine-1-phosphate as an amphipathic metabolite: its properties in aqueous and membrane environments. Biophys. J. *97*, 1398–1407.

Gasteiger, E., Hoogland, C., Gattiker, A., Duvaud, S., Wilkins, M.R., Appel, R.D., and Bairoch, A. (2005). Protein identification and analysis tools on the ExPASy server. In The Proteomics Protocols Handbook, J.M. Walker, ed. (Totowa, NJ: Humana Press), pp. 571–607.

Gut, H., Pennacchietti, E., John, R.A., Bossa, F., Capitani, G., De Biase, D., and Grutter, M.G. (2006). Escherichia coli acid resistance: pH-sensing, activation by chloride and autoinhibition in GadB. EMBO J. *25*, 2643–2651.

Gut, H., Dominici, P., Pilati, S., Astegno, A., Petoukhov, M.V., Svergun, D.I., Grütter, M.G., and Capitani, G. (2009). A common structural basis for pH- and calmodulin-mediated regulation in plant glutamate decarboxylase. J. Mol. Biol. *392*, 334–351.

Hait, N.C., Allegood, J., Maceyka, M., Strub, G.M., Harikumar, K.B., Singh, S.K., Luo, C., Marmorstein, R., Kordula, T., Milstien, S., et al. (2009). Regulation of histone acetylation in the nucleus by sphingosine-1-phosphate. Science *325*, 1254–1257.

Han, G., Gupta, S.D., Gable, K., Niranjanakumari, S., Moitra, P., Eichler, F., Brown, R.H.J., Harmon, J.M., and Dunn, T.M. (2009). Identification of small subunits of mammalian serine palmitoyltransferase that confer distinct acyl-CoA substrate specificities. Proc. Natl. Acad. Sci. USA *106*, 8186–8191.

Hannun, Y.A., and Obeid, L.M. (2008). Principles of bioactive lipid signalling: lessons from sphingolipids. Nat. Rev. Mol. Cell Biol. *9*, 139–150.

Hla, T., Lee, M.J., Ancellin, N., Paik, J.H., and Kluk, M.J. (2001). Lysophospholipids—receptor revelations. Science *294*, 1875–1878.

Hornemann, T., Penno, A., Rutti, M.F., Ernst, D., Kivrak-Pfiffner, F., Rohrer, L., and von Eckardstein, A. (2009). The SPTLC3 subunit of serine-palmitoyltransferase generates short chain sphingoid bases. J. Biol. Chem. *284*, 26322–26330.

Ikeda, M., Kihara, A., and Igarashi, Y. (2004). Sphingosine-1-phosphate lyase SPL is an endoplasmic reticulum-resident, integral membrane protein with the pyridoxal 5′-phosphate binding domain exposed to the cytosol. Biochem. Biophys. Res. Commun. *325*, 338–343.

Ikushiro, H., Islam, M.M., Okamoto, A., Hoseki, J., Murakawa, T., Fujii, S., Miyahara, I., and Hayashi, H. (2009). Structural insights into the enzymatic mechanism of serine palmitoyltransferase from Sphingobacterium multivorum. J. Biochem. *146*, 549–562.

Kabsch, W. (1993). Automatic processing of rotation diffraction data from crystals of initially unknown symmetry and cell constants. J. Appl. Crystallogr. *26*, 795–800.

Kumar, A., and Saba, J.D. (2009). Lyase to live by: sphingosine phosphate lyase as a therapeutic target. Expert Opin. Ther. Targets *13*, 1013–1025.

Laskowski, R.A., Moss, D.S., and Thornton, J.M. (1993). Main-chain bond lengths and bond angles in protein structures. J. Mol. Biol. *231*, 1049–1067.

McCoy, A.J. (2007). Solving structures of protein complexes by molecular replacement with Phaser. Acta Crystallogr. D Biol. Crystallogr. *63*, 32–41.

Mendel, J., Heinecke, K., Fyrst, H., and Saba, J.D. (2003). Sphingosine phosphate lyase expression is essential for normal development in Caenorhabditis elegans. J. Biol. Chem. *278*, 22341–22349.

Mukhopadhyay, D., Howell, K.S., Riezman, H., and Capitani, G. (2008). Identifying key residues of sphinganine-1-phosphate lyase for function in vivo and in vitro. J. Biol. Chem. *283*, 20159–20169.

Nishikawa, M., Hosokawa, K., Ishiguro, M., Minamioka, H., Tamura, K., Hara-Nishimura, I., Takahashi, Y., Shimazaki, K., and Imai, H. (2008). Degradation of sphingoid long-chain base 1-phosphates (LCB-1Ps): functional characterization and expression of AtDPL1 encoding LCB-1P lyase involved in the dehydration stress response in Arabidopsis. Plant Cell Physiol. *49*, 1758–1763.

Oskeritzian, C.A., Milstien, S., and Spiegel, S. (2007). Sphingosine-1-phosphate in allergic responses, asthma and anaphylaxis. Pharmacol. Ther. *115*, 390–399.

Oskouian, B., and Saba, J.D. (2004). Death and taxis: what non-mammalian models tell us about sphingosine-1-phosphate. Semin. Cell Dev. Biol. *15*, 529–540.

Oskouian, B., Sooriyakumaran, P., Borowsky, A.D., Crans, A., Dillard-Telm, L., Tam, Y.Y., Bandhuvula, P., and Saba, J.D. (2006). Sphingosine-1-phosphate lyase potentiates apoptosis via p53- and p38-dependent pathways and is down-regulated in colon cancer. Proc. Natl. Acad. Sci. USA *103*, 17384–17389.

Pata, M.O., Hannun, Y.A., and Ng, C.K. (2009). Plant sphingolipids: decoding the enigma of the Sphinx. New Phytol. *185*, 611–630.

Raman, M.C., Johnson, K.A., Yard, B.A., Lowther, J., Carter, L.G., Naismith, J.H., and Campopiano, D.J. (2009). The external aldimine form of serine palmitoyltransferase: structural, kinetic, and spectroscopic analysis of the wild-type enzyme and HSAN1 mutant mimics. J. Biol. Chem. *284*, 17328–17339.

Rivera, J., Proia, R.L., and Olivera, A. (2008). The alliance of sphingosine-1-phosphate and its receptors in immunity. Nat. Rev. Immunol. *8*, 753–763.

Saba, J.D., and Hla, T. (2004). Point-counterpoint of sphingosine 1-phosphate metabolism. Circ. Res. *94*, 724–734.

Saba, J.D., Nara, F., Bielawska, A., Garrett, S., and Hannun, Y.A. (1997). The BST1 gene of Saccharomyces cerevisiae is the sphingosine-1-phosphate lyase. J. Biol. Chem. *272*, 26087–26090.

Sali, A. (1995). Comparative protein modeling by satisfaction of spatial restraints. Mol. Med. Today *1*, 270–277.

Schirch, V., and Szebenyi, D.M. (2005). Serine hydroxymethyltransferase revisited. Curr. Opin. Chem. Biol. *9*, 482–487.

Schwab, S.R., and Cyster, J.G. (2007). Finding a way out: lymphocyte egress from lymphoid organs. Nat. Immunol. *8*, 1295–1301.

Schwab, S.R., Pereira, J.P., Matloubian, M., Xu, Y., Huang, Y., and Cyster, J.G. (2005). Lymphocyte sequestration through S1P lyase inhibition and disruption of S1P gradients. Science *309*, 1735–1739.

Shiraiwa, Y., Ikushiro, H., and Hayashi, H. (2009). Multifunctional role of his159in the catalytic reaction of serine palmitoyltransferase. J. Biol. Chem. *284*, 15487–15495.

Spiegel, S., and Milstien, S. (2003). Sphingosine-1-phosphate: an enigmatic signalling lipid. Nat. Rev. Mol. Cell Biol. *4*, 397–407.

Stoffel, W., Sticht, G., and LeKim, D. (1968). Metabolism of sphingosine bases. IX. Degradation in vitro of dihydrospingosine and dihydrospingosine phosphate to palmitaldehyde and ethanolamine phosphate. Hoppe Seylers Z. Physiol. Chem. *349*, 1745–1748.

Takabe, K., Paugh, S.W., Milstien, S., and Spiegel, S. (2008). "Inside-out" signaling of sphingosine-1-phosphate: therapeutic targets. Pharmacol. Rev. *60*, 181–195.

Toney, M.D. (2005). Reaction specificity in pyridoxal phosphate enzymes. Arch. Biochem. Biophys. *433*, 279–287.

Tsegaye, Y., Richardson, C.G., Bravo, J.E., Mulcahy, B.J., Lynch, D.V., Markham, J.E., Jaworski, J.G., Chen, M., Cahoon, E.B., and Dunn, T.M. (2007). Arabidopsis mutants lacking long chain base phosphate lyase are fumonisin-sensitive and accumulate trihydroxy-18:1 long chain base phosphate. J. Biol. Chem. *282*, 28195–28206.

Ueda, K., Yamashita, A., Ishikawa, J., Shimada, M., Watsuji, T.O., Morimura, K., Ikeda, H., Hattori, M., and Beppu, T. (2004). Genome sequence of Symbiobacterium thermophilum, an uncultivable bacterium that depends on microbial commensalism. Nucleic Acids Res. *32*, 4937–4944.

Van Veldhoven, P.P., and Mannaerts, G.P. (1991). Subcellular localization and membrane topology of sphingosine-1-phosphate lyase in rat liver. J. Biol. Chem. *266*, 12502–12507.

Van Veldhoven, P.P., and Mannaerts, G.P. (1993). Sphingosine-phosphate lyase. Adv. Lipid Res. *26*, 69–98.

Van Veldhoven, P.P., Gijsbers, S., Mannaerts, G.P., Vermeesch, J.R., and Brys, V. (2000). Human sphingosine-1-phosphate lyase: cDNA cloning, functional expression studies and mapping to chromosome 10q22(1). Biochim. Biophys. Acta *1487*, 128–134.

Wojciak, J.M., Zhu, N., Schuerenberg, K.T., Moreno, K., Shestowsky, W.S., Hiraiwa, M., Sabbadini, R., and Huxford, T. (2009). The crystal structure of sphingosine-1-phosphate in complex with a Fab fragment reveals metal bridging of an antibody and its antigen. Proc. Natl. Acad. Sci. USA *106*, 17717–17722.

Yard, B.A., et al. (2007). The structure of serine palmitoyltransferase; gateway to sphingolipid biosynthesis. J. Mol. Biol. *370*, 870–886.

Zhou, J., and Saba, J.D. (1998). Identification of the first mammalian sphingosine phosphate lyase gene and its functional expression in yeast. Biochem. Biophys. Res. Commun. *242*, 502–507.

Zwart, P.H., Afonine, P.V., Grosse-Kunstleve, R.W., Hung, L.W., Ioerger, T.R., McCoy, A.J., McKee, E., Moriarty, N.W., Read, R.J., Sacchettini, J.C., et al. (2008). Automated structure solution with the PHENIX suite. Methods Mol. Biol. *426*, 419–435.

Structure *18*

Supplemental Information

Structure and Function of Sphingosine-1-Phosphate Lyase, a Key Enzyme of Sphingolipid Metabolism

Florence Bourquin, Howard Riezman, Guido Capitani, and Markus Gerhard Grütter

Figure S1 related to Figure 5

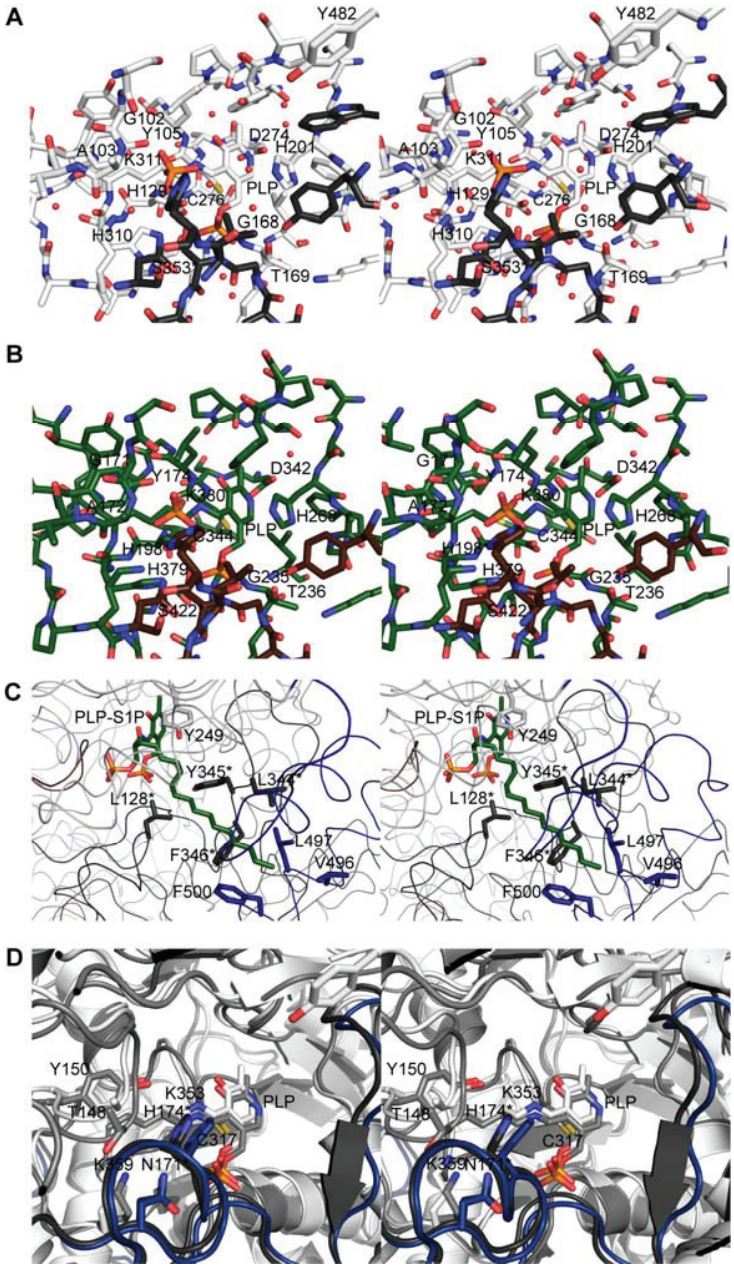

Figure S1. Close-up view of the active sites of StSPL, Dpl1p Δ1-102 and SPL
(A) Active site of StSPL (structure St_1) showing residues involved in the accommodation of PLP. Color coding is as in Figure 1A.
(B) Same as in (A) for Dpl1p Δ1-102 (structure Dpl1p-S). Color coding is same as Figure 1B.
(C) Stereo representation of a model of StSPL K311A containing the external aldimine intermediate with the substrate S1P (PLP-S1P, in green and atom color). The peptide backbone is represented as ribbon. Subunits A and B are in light and dark gray, respectively. Ct-EXT is colored blue. Several hydrophobic residues likely interacting with the hydrophobic moiety of the substrate are shown in stick representation and labeled.
(D) Stereo representation of a superposition of SPL onto FL WT StSPL (structure St_1). Color coding is as in Figure 5C, except that the subunit A and B of SPL, colored medium grey and blue, respectively, are depicted instead of Dpl1p Δ1-102. Note that SPL T148 replaces StSPL A103 (A172 in Dpl1p).

Figure S2 related to Figure 5

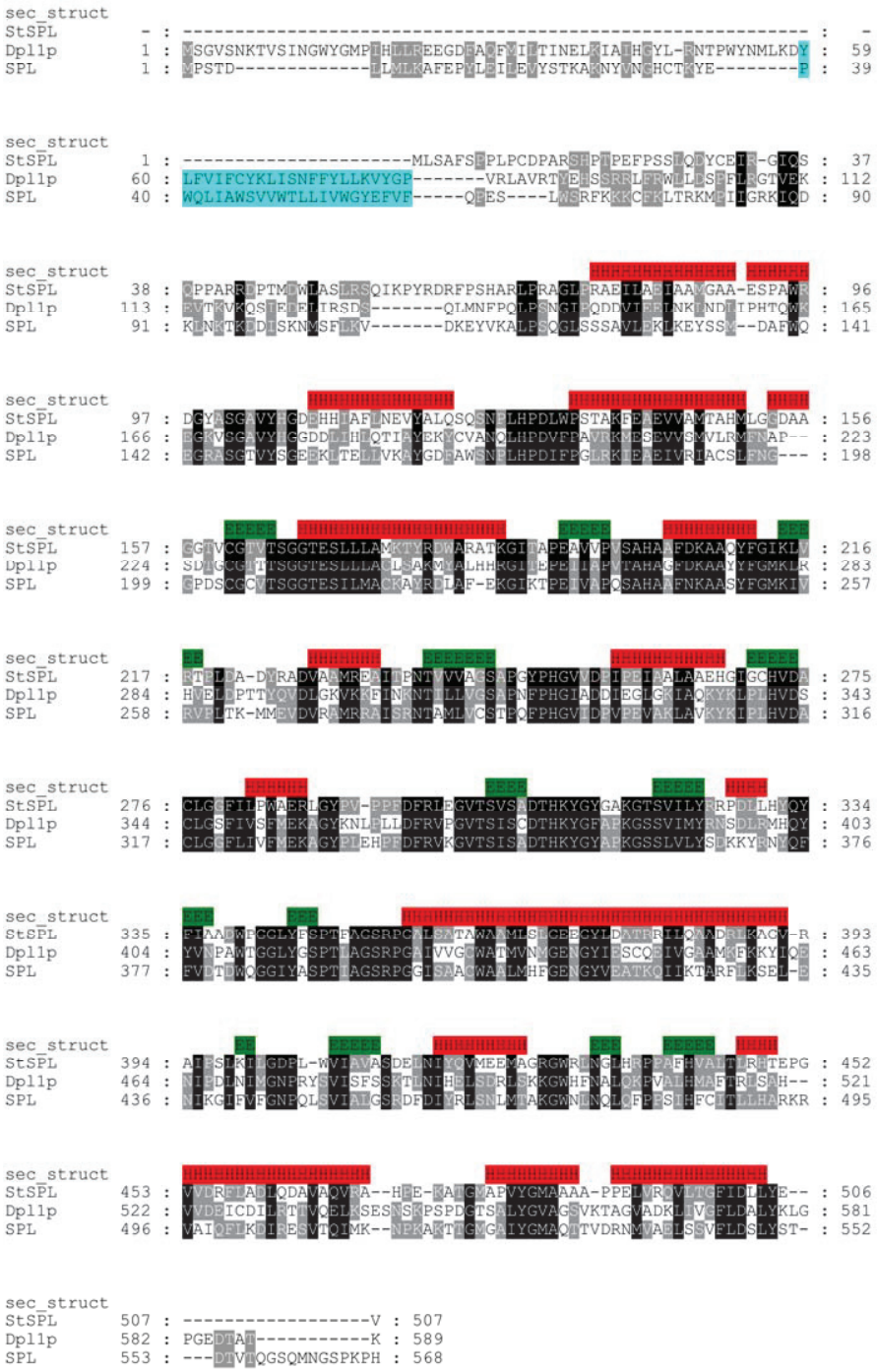

Figure S2. Multiple sequence alignment of StSPL, Dpl1p and SPL
The predicted transmembrane helices of Dpl1p and SPL are highlighted in blue. The observed α-helices and β-strands of StSPL, assigned with PROMOTIF (Hutchinson et al., 1996) are shown in red and in green, respectively, in the top line. The sequences were aligned with T-Coffee (Notredame et al., 2000) and the figure was prepared with Genedoc (http://www.psc.edu/biomed/genedoc).

Figure S3 related to Figure 6

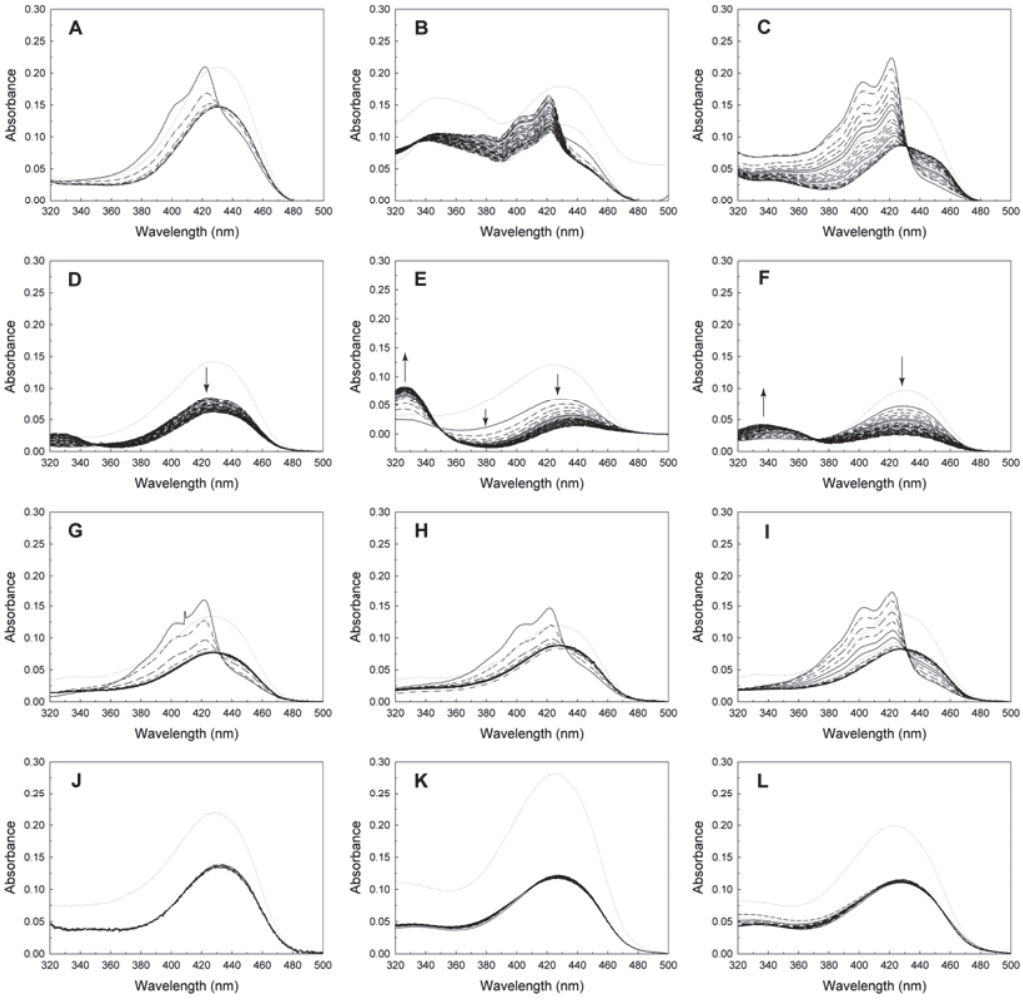

Figure S3. StSPL and Dpl1p Δ1-102 spectrophotometric activity assay using S1P, DHS1P and PS1P as substrate

(A-G) Assay of StSPL FL WT, variants and mutants with S1P used as substrate.
(A) Same as Figure 6A for StSPL ΔNt-FLEX. The FL WT control is depicted in (C).
(B) Same as (A) for StSPL ΔCt-EXT except that the spectra were recorded during 30 min. For clarity, the spectrum before addition of S1P (dotted line) is raised by 0.06 absorbance units with respect to the other curves.
(C) FL WT StSPL control for (A) and (B).
(D-I) 15 µM of StSPL was used instead of 22 and the changes upon addition of substrate were recorded over 30 min (D-F) or 20 min (G-I). FL WT control for (D), (E) and (F) is depicted in (G). The arrow in (D) shows the faint peaks at 420 nm appearing after addition of substrate. Arrows in (E) and (F) indicate alterations in the visible spectrum in the 430 nm, 380 nm and 330-340 nm regions, which did not correlate with S1P cleavage (Figure S4J and K respectively).
(D) StSPL H129A.
(E) StSPL A103P.
(F) StSPL K317A.
(G) FL WT StSPL control for (D-F).
(H) Same as (G) except that DHS1P was used as substrate.
(I) Same as (G) except that PS1P was used as substrate.

(J-L) same as (G-I) for Dpl1p Δ1-102. The protein concentration in (K) was set to 36 μM, while it was 29 μM in (J) and (L). The spectra in (J) were recorded 1, 2, 5, 10 and 20 min after addition of S1P.

Figure S4 related to Figure 6

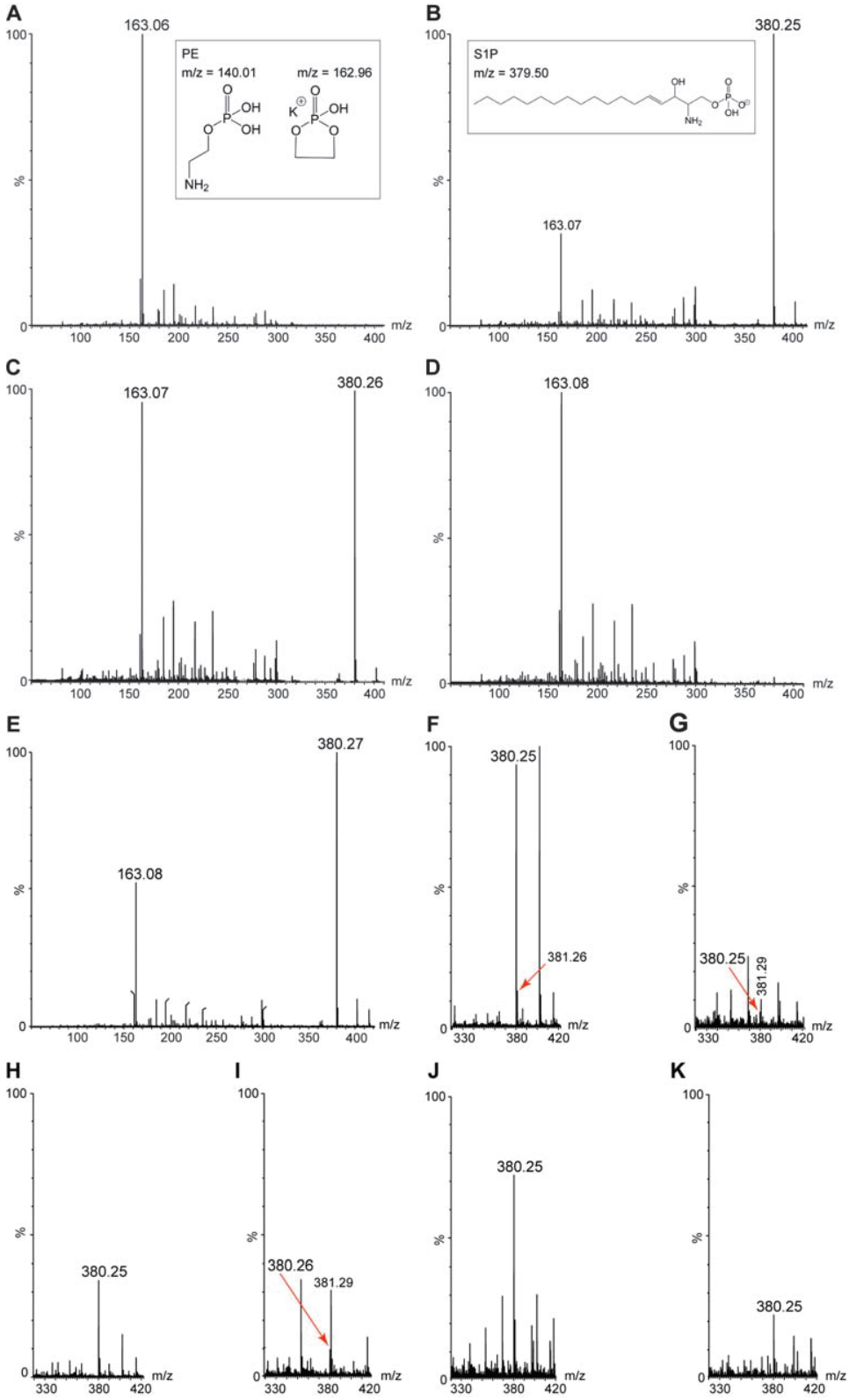

Figure S4. In vitro activity assay of FL WT StSPL and mutants K311A, Y105F, A103P and K317A by MS

(A) Chromatogram of PE. Under the ionization conditions, PE exhibits a peak at 163.06 Da, which may correspond to a potassiated 5-membered cyclophosphane (Han et al., 1996).

(B) Chromatogram of S1P. Under the ionization conditions, S1P produced a peak at 163.07 Da, presumably corresponding to PE. The ratio between the 380 and 163 Da peaks was constant during the time of the experiment, as shown in (E).

(C) Chromatogram of a mixture of S1P and FL WT StSPL immediately after addition of S1P to the enzyme.

(D) Same as (C) after 75 min incubation at 20°C. The disappearance of the 380 Da peak reflects the activity of the protein.

(E) Same as in (B) after 105 min at 20°C.

(F) S1P control for (G-K), measured as in (B) with another S1P batch.

(G) FL WT StSPL control for (H-K). The experiment was performed under the same conditions as in (D), except for the incubation time (4 h).

(H-K) Same as (G) for the mutants K311A (H), Y105F (I), A103P (J) and K317A (K).

Note that only the mutants which did not exhibit the 420 and 403 nm peaks upon substrate addition (Figure 6 and Figure S3) were analyzed by MS.

Figure S5 related to Figure 6

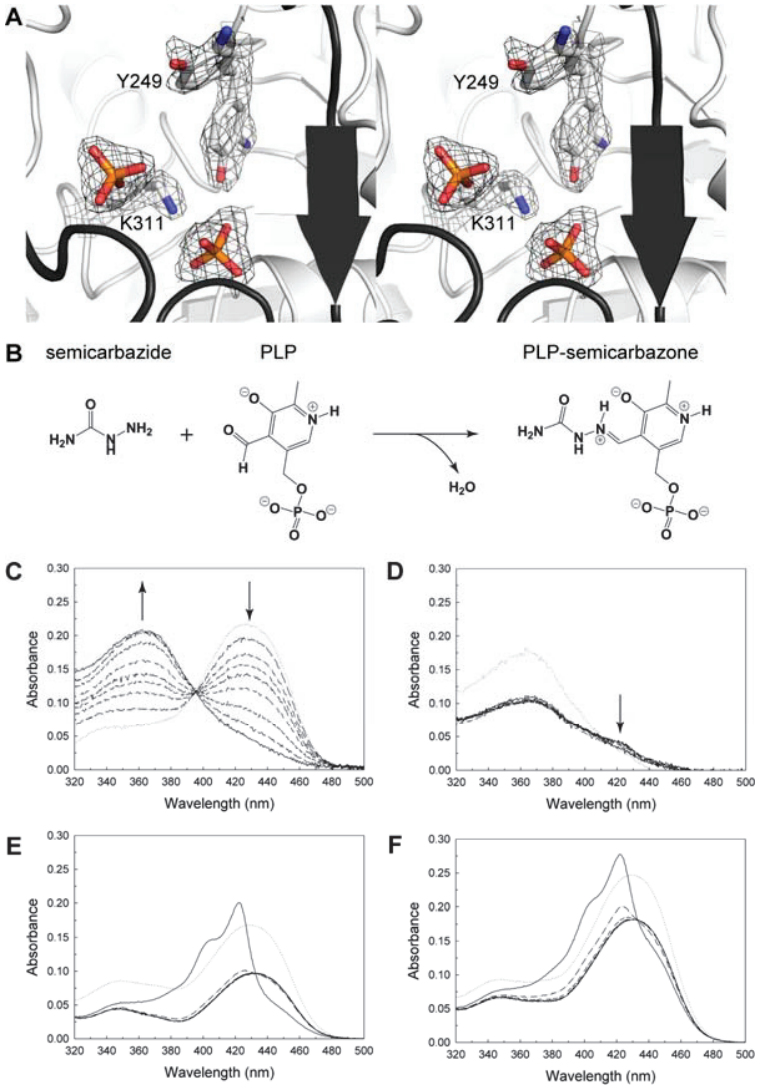

Figure S5. StSPL inhibition with semicarbazide.
(A) Stereo representation of the active site of StSPL crystallized in presence of a 10-fold molar excess of semicarbazide (structure St_4). The phenol ring of Y249 encountered a modification in *ortho*, most likely an amination resulting from the attack by semicarbazide.
(B) Scheme of the condensation reaction yielding to PLP-semicarbazone.
(C) Semicarbazide-induced spectral changes. A 100-fold molar excess of semicarbazide over StSPL active site was added to the protein and the spectra were recorded between 320 and 500 nm at regular intervals over 1 h.
(D) Same as (C) except that S1P was added to a mixture of StSPL and semicarbazide incubated 1 h at room temperature.
(E-F) Same as Figure 6 except that 33 µM of enzyme subunit was used. The spectra were recorded over 5 min.
(E) Y249F.
(F) FL WT control.

Table S1. Primer sequences for StSPL and Dpl1p constructs
The sequences are written from 5' to 3'.

Construct name	Forward (5') primer	Reverse (3') primer
pQE60-StSPL FL WT	GGAAGATCTCTTTCGGCGTTTTCCCCGC	CCCAAGCTTACTAGTGATGGTGATGGTGATGCACCTCGTACAGCAGGTCG
pQE70-StSPL FL WT	CATGCATGCCACTTTCGGCGTTTTCCCCGC	CCCAAGCTTACTAGTGATGGTGATGGTGATGCACCTCGTACAGCAGGTCG
pQE70-StSPL ΔNt-FLEX WT	CATGGCATGCCAAAGCCTTACCGCGACCGCT	CCCAAGCTTACTAGTGATGGTGATGGTGATGCACCTCGTACAGCAGGTCG
pQE70-StSPL ΔCt-EXT WT	GGAAGATCTCTTTCGGCGTTTTCCCCGC	AGCTAAGCTTACTAGTGATGGTGATGGTGATGGGCCCGGACCTGAGCCAC
pQE70-StSPL FL A103P	CTCCGGCCCCGTCTACC	GGTAGACGGGGCCGGAG
pQE70-StSPL FL Y105F	CGCCGTCTTCCACGGCG	CGCCGTGGAAGACGGCG
pQE70-StSPL FL H129A	AACCCGCTCGCCCCGGACCTC	GAGGTCCGGGGCGAGCGGGTT
pQE70-StSPL FL Y249F	GCCGGGCTTCCCCCACG	CGTGGGGGAAGCCCGGC
pQE70-StSPL FL C276A	GGACGCCGCCCTGGGCG	CGCCCAGGGCGGCGTCC
pQE70-StSPL FL K311A	GCGTACGGCTACGGGGCCAA	GTGGGTGTCGGCCGAGAC
pQE70-StSPL FL K317A	CGGGGCCGCGGGAACGT	ACGTTCCCGCGGCCCCG
pQE70-StSPL FL Y482F	CCCCGGTCTTCGGCATGGC	GCCATGCCGAAGACCGGGG
pET28a+-Dpl1p Δ1-102	CATGCCATGGGATCACCATTTTTGAGGGGTACC	CCGCTCGAGCTTGGTGGCGGTATCCTCT
pRS415-Dpl1p FL A172P	GGAAAGGTCTCTGGTCCCGTTTACCACGGTGGTGATGATTTG	CAAATCATCACCACCGTGGTAAACGGGACCAGAGACCTTTCC
pRS415-Dpl1p FL Y174F	GGTCTCTGGTGCCGTTTTCCACGGTGGTGATGATTTGATCC	GGATCAAATCATCACCACCGTGGAAAACGGCACCAGAGACC
pRS415-Dpl1p FL H198A	GCGTTGCCAATCAATTAGCTCCCGATGTCTTTCCTGCCG	CGGCAGGAAAGACATCGGGAGCTAATTGATTGGCAACGC
pRS415-Dpl1p FL WT	(Mukhopadhyay et al., 2008)	(Mukhopadhyay et al., 2008)
pRS415-Dpl1p Δ1-57 WT	(Mukhopadhyay et al., 2008)	(Mukhopadhyay et al., 2008)
pRS415-Dpl1p FL C344A	(Mukhopadhyay et al., 2008)	(Mukhopadhyay et al., 2008)
pRS415-Dpl1p FL K380A	(Mukhopadhyay et al., 2008)	(Mukhopadhyay et al., 2008)
pRS415-Dpl1p FL K386A	(Mukhopadhyay et al., 2008)	(Mukhopadhyay et al., 2008)
pRS415-Dpl1p FL Y554F	(Mukhopadhyay et al., 2008)	(Mukhopadhyay et al., 2008)

Table S2, related to Table 1. Crystallization conditions for the structures St_1-4 and Dpl1p

Protein code	Sample	Protein concentration	Ratio protein-to-well solution	Well solution	% EG
St_1	pQE70-StSPL FL WT native	21 mg/ml	1:1 (2 µl : 2 µl)	0.1 M Tris (HOAc) pH 8.4 0.15 M KSCN 16 % PEG 5K MME	22
St_2	pQE60-StSPL FL WT native	28 mg/ml	1:1 (400 nl : 400nl)	0.1 M Tris (HOAc) pH 8.3 0.2 M $MgCl_2$ 25 % PEG 2K MME	20
St_3	pQE70-St SPL FL K311A PE	15 mg/ml	2:1 (2 µl :1 µl)	0.1 M Tris (HOAc) pH 8.2 0.15 M KSCN 17 % PEG 5K MME	20
St_4	pQE70-StSPL FL WT semicarbazide	21 mg/ml	1:1 (2 µl : 2 µl)	0.1 M Tris (HOAc) pH 8.6 0.15 M KSCN 17 % PEG 5K MME	20
Dpl1p	pET28a+-Dpl1p Δ1-102	10 mg/ml	1:1 (2 µl : 2 µl)	0.1 M Na-cacodylate (HOAc) pH 6.7 0.2 M Li_2SO4 18 % PEG 4K	18

SUPPLEMENTAL EXPERIMENTAL PROCEDURES

Plasmid constructs

The gene of FL (omitting to first methionine, that is corresponding to residues 2-507) WT *Symbiobacterium thermophilum* SPL (NCBI database accession number YP_075103 (Ueda et al., 2004)) was amplified by PCR from genomic DNA according to standard procedure and cloned into pQE60 (Qiagen) using BglII and HindIII and into pQE70 using SphI and HindIII with the primers listed in Table S1. Truncations of the protein were obtained with the same procedure, except that the plasmid pQE70-StSPL FL WT was used as PCR template. The Dpl1p Δ1-102 gene (NCBI database accession number Q05567 (Saba et al., 1997)) was amplified by PCR using a whole cell lysate of baker's yeast purchased from a local supermarket. This construct comprised residues 103-589. Yeast cells were suspended in water, vortexed with 425-600 µm glass beads (Sigma) and frozen/thawed. The cell lysate was serially diluted and various amounts were used as PCR template. The PCR product was cloned into pET28a+ (Novagen) using NcoI and XhoI with the primers listed in Table S1. The construct contains point mutations I308V and N469D possibly originating from lack of homogeneity of the yeast strains used for PCR. StSPL WT FL and variants as well as Dpl1p Δ1-102 were fused to a C-terminal 6x His-tag. The QuikChange Site directed-mutagenesis kit (Stratagene) was used to insert the desired mutations into pQE70-StSPL FL WT and into pRS415 Dpl1p FL WT for the synthetic lethality test (see below) according to the manufacturer's instructions with the primers listed in Table S1.

Protein expression and purification

Variants and mutants of StSPL carried by pQE60 or pQE70 transformed into *Escherichia coli* M15 competent cells (Qiagen) were grown for 3 h at 37°C in LB

(Luria broth) medium (Invitrogen) containing 100 µg/ml of ampicillin, 50 µg/ml of kanamycin and 0.1 g/l pyridoxine. The culture was then cooled down to 30°C and protein expression was induced at an $OD_{600\ nm}$ (optical density) of 0.8 by adding ethanol to 2 %, pyridoxine to 0.1 g/l and IPTG to 0.1 mM. The cells were harvested after 4 h, resuspended in 50 mM KP_i pH 7.2 and frozen overnight at -20°C. The cell suspension was thawed and diluted with an equal volume of 50 KP_i pH 7.2, 2 mM DTT, 0.4 mM PLP, 200000 U/ml lysozyme (Fluka), 0.02 mg/ml DNase I (Roche) and 2x Protease inhibitor cocktail (Roche). The suspension was incubated for 30 min on an orbital shaker at room temperature. DTT was supplemented to a total concentration of 1.5 mM and cells were disrupted with a high pressure homogenizer (AVESTIN, Canada). EDTA was immediately added after lysis to a final concentration of 1 mM. The sample was then incubated at 60°C for 1 h and spun down 30 min at 50000 *g* at 25°C. The supernatant was incubated with Ni^{2+}-NTA agarose beads (Qiagen) for 30 min at room temperature on an orbital shaker prior to purification according to the manufacturer's instructions. The protein was eluted in 50 or 1 mM KP_i pH 7.2, 100 mM imidazole, 5 mM EDTA, 1 mM DTT, 0.2 mM PLP and 1x Protease inhibitor cocktail. StSPL was then concentrated using an Amicon Ultra-15 centrifugal filter unit (Millipore) with a MW (molecular weight) cut-off of 50 kDa according to the manufacturer's instructions with gradually decreasing the temperature from 15 to 4°C. The concentrated protein was injected on a SEC (size-exclusion chromatography) column (Superdex-200 10/300 HR, GE Healthcare) and eluted at 4°C in 50 or 1 mM KP_i pH 7.2, 100 mM NaCl, 1 mM EDTA, 1 mM DTT and 0.01 mM PLP at a flow rate of 0.5 ml/min. The protein MW was estimated using the calibration curve of known molecular mass standards (GE Healthcare) and by analytical ultracentrifugation (Bourquin, 2010). The fractions of the two peaks eluting at 11 (corresponding to approximately 200 kDa, *i.e.* a tetramer) and 13 ml (corresponding to approximately 100 kDa) were analyzed by 10 % SDS-PAGE (sodium dodecyl sulfate polyacrylamide gel electrophoresis). The fractions of the peak eluting at 13 ml were pooled and concentrated at 4°C as mentioned above. Dpl1p Δ1-102 was expressed in *Escherichia coli* HMS174(DE3) in LB containing 50 µg/ml of kanamycin and 10 mM glucose according to the same protocol as for StSPL with the following modifications: the culture was carried out at 30°C throughout, ethanol was not added at induction and cells were harvested 24 h after induction. The cell pellets were resuspended in 50 mM KP_i pH 7.2, 1 mM DTT, 0.1 mM PLP, 100000 U/ml lysozyme (Fluka), 0.01 mg/ml DNase I (Roche) and 1x Protease inhibitor cocktail (Roche) and incubated for 1 h at 4°C prior to overnight storage at -20°C. Subsequent purification steps were exclusively carried out at 4°C in the same way as for StSPL, except that cell debris and unbroken cells were removed by a 45-min centrifugation step at the same speed and all buffers contained 50 mM KPi. The fractions corresponding to the single peak eluting at 13 ml were pooled and concentrated prior to crystallization.

SUPPLEMENTAL REFERENCES

Bourquin F. (2010). Questioning the Sphinx: structural and functional studies of sphingosine-1-phosphate lyase. Ph.D. Thesis, Institute of Biochemistry, University of Zurich, Zurich, Switzerland.

Han X., Gross R.W. (1996). Structural Determination of Lysophospholipid Regioisomers by Electrospray Ionization Tandem Mass Spectrometry. J Am Chem Soc *118*, 451–457.

Hutchinson E.G., Thornton J.M. (1996). PROMOTIF--a program to identify and analyze structural motifs in proteins. Protein Sci *5*, 212-220.

Mukhopadhyay D., Howell K.S., Riezman H., Capitani G. (2008). Identifying key residues of sphinganine-1-phosphate lyase for function in vivo and in vitro. J Biol Chem *283*, 20159-20169.

Notredame C., Higgins D.G., Heringa J. (2000). T-Coffee: A novel method for fast and accurate multiple sequence alignment. J Mol Biol *302*, 205-217.

Saba J.D., Nara F., Bielawska A., Garrett S., Hannun Y.A. (1997). The BST1 gene of Saccharomyces cerevisiae is the sphingosine-1-phosphate lyase. J Biol Chem *272*, 26087-26090.

Ueda K., Yamashita A., Ishikawa J., Shimada M., Watsuji T.O., Morimura K., Ikeda H., Hattori M., Beppu T. (2004). Genome sequence of Symbiobacterium thermophilum, an uncultivable bacterium that depends on microbial commensalism. Nucleic Acids Res *32*, 4937-4944.

4. RESULTS & DISCUSSION *Symbiobacterium thermophilum* SPL (StSPL)

4.1. FULL-LENGTH (FL) SPL CONSTRUCTS DESIGN

Full-length wild-type SPL from *Symbiobacterium thermophilum* (named thereafter FL WT StSPL) was successfully cloned and expressed as described in Materials & Methods (sections 8.2.1. and 8.3.1.) and in part 3 (manuscript) SI *Text*. The protein carries a C-terminal 6x His tag directly after the last residue of the WT sequence and various additional residues at the N-terminus due to the cloning procedure (**figure 4-1**).

Figure 4-1. FL WT StSPL cloned in pQE60 or pQE70

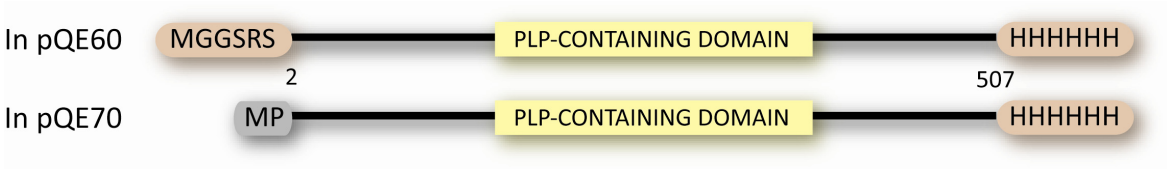

4.2. EXPRESSION IN *E. coli* AND SOLUBILITY ASSAY

4.2.1. EXPRESSION

The expression conditions were optimized as described in Materials & Methods: the resulting optimized conditions are summarized in **table 4-1**. Protein production was monitored by 10 % SDS-PAGE and anti-His tag protein immuno-detection (Western blot) (**figure 4-2**). The protocol includes addition of pyridoxine, which is a precursor of the cofactor of SPL, PLP. Ethanol supplemented to the medium at induction of protein expression elicits a stress-response in *E. coli* that apparently triggers the production of the chaperones groEL and groES together with the protein of interest (173).

Table 4-1. Optimized expression conditions for FL WT StSPL

Expression system	pQE
***E. coli* strain**	M15
Medium composition	LB (10 g tryptone, 5 g yeast extract, 10 g NaCl) 0.1 g/l pyridoxine Appropriate antibiotics
Starting $OD_{600\ nm}$ (500 ml medium)	0.02
$OD_{600\ nm}$ at induction	0.8
IPTG concentration	0.1 mM
Chemicals added at induction	2% (v/v) ethanol 0.1 g/l pyridoxine
Temperature during protein expression	30°C
Expression duration	4 hours

Figure 4-2. Expression of pQE60 and pQE70 FL WT StSPL in *E. coli*

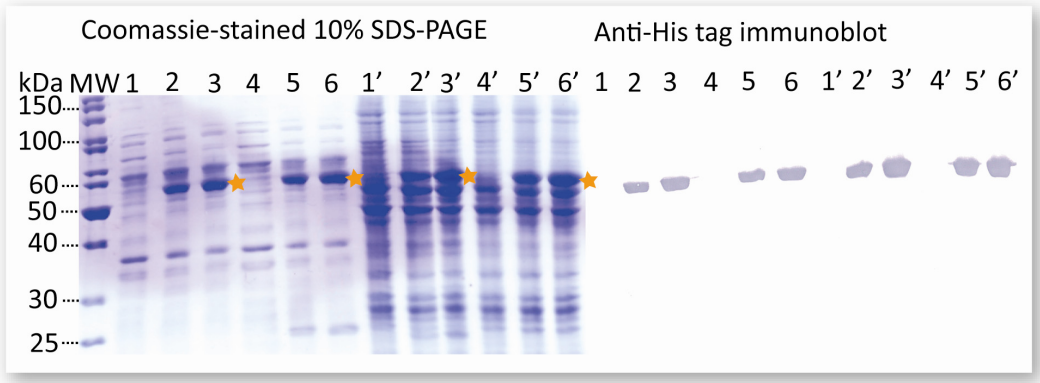

Legend
MW: Molecular weight marker
 # & #': Soluble & insoluble fraction respectively
1 & 1': in pQE60 before induction
2 & 2': in pQE60 2 h after induction
3 & 3': in pQE60 4 h after induction
4 & 4': in pQE70 before induction
5 & 5': in pQE70 2 h after induction
6 & 6': in pQE70 4 h after induction
★ FL StSPL

4.2.2. CELL LYSIS BUFFER COMPOSITION AND SAMPLE TREATMENT

The composition of the cell lysis buffer was screened for with the aim of increasing the yield of soluble protein. The optimal buffer composition is summarized in **table 4-2**. The amount of soluble protein is significantly decreased in 50 mM KP_i pH 6.5 and 6.0, in 50 mM KOAc at pH 5.0 and 3.6 and in the presence of 1, 10 and 100 mM $MgCl_2$ and $CaCl_2$. Adding 300 mM NaCl does not have an effect on the amount of soluble protein (not shown). It has to be mentioned that this test cannot discriminate between an impaired solubility of SPL and a decreased activity of lysozyme, which lyses the cell wall and helps cell lysis. Both factors, in fact, result in a decreased amount of soluble protein.

Table 4-2. Optimal cell lysis buffer for FL WT StSPL in small-scale assays

KP_i	50 mM pH 7.2 (20°C, KOH)
DTT	1 mM
PLP	200 µM
Protease inhibitor cocktail without EDTA (Roche)	1x
Chicken egg white lysozyme	100000 U/ml
DNase I	10 µg/ml

Heating the samples after cell lysis positively influences the amount of soluble protein. An incubation of 30 min at 60°C results in a several-fold increase of soluble material compared to incubation on ice (**figure 4-3** lanes 1 and 1' compared to 4 and 4', respectively). Moreover, heating denatures host cellular components and significantly increases the purity of the sample, an effect that has often been exploited in the purification of thermophilic and hyperthermophilic proteins. One hour incubation at 60°C was routinely used as a purification step after cell lysis and prior to immobilized metal affinity chromatography (IMAC) purification.

Figure 4-3. Effect of heating on the amount of soluble FL WT StSPL after cell lysis

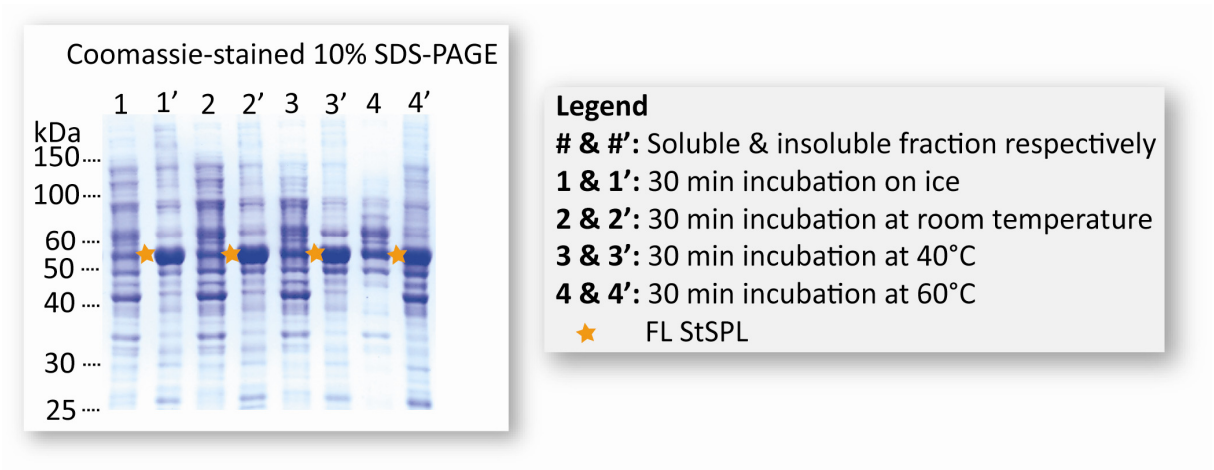

4.3. PURIFICATION

FL WT StSPL was purified according to a three-step purification protocol. The protocol involved sample heating at 60°C followed by IMAC with Ni-NTA (nitrilotriacetic acid) agarose beads, performed at room temperature, and size-exclusion chromatography (SEC) (gel filtration) at 4°C (see Materials & Methods, section 8.3.1. and part 3 (manuscript) SI *Text*).
The heating step alone leads to a many-fold purification of the protein (lane 1 compared with 2 in **figure 4-4**). A non-negligible amount of protein does not bind to the Ni-NTA agarose beads and is found in the flow-through (lane 3). This stems either from unfolded protein or from an excess of protein compared to the available binding sites on the beads. Washing the beads with 20 bead volumes of buffer containing 0 and 10 mM imidazole further increases protein purity (lanes 4 and 5). The protein is eluted with 100 mM imidazole and 5 mM EDTA (lane 6). Only a small amount of protein cannot be eluted under these conditions (lane 7), due either to an alternative stronger protein binding mode or to protein precipitation. The amount of pure and soluble material is strongly decreased when the IMAC step is performed at 4°C (data not shown). After IMAC, the protein is immediately concentrated at gradually decreasing temperatures of 15 to 4°C and kept on ice or at 4°C in all subsequent steps. The concentrated sample (lane 9) is loaded on a SEC column.
In addition to the main 55 kDa band (yellow star), a faint 110 kDa band (green star) and a 30 kDa band (black star) are visible on the Coomassie-stained SDS-PAGE. The 110 kDa species reacts with anti-His tag antibodies (lane 10), indicating that this species is either a SDS-resistant dimer (most likely, given its apparent molecular mass), or a covalently modified StSPL species, or an impurity that binds to the Ni-NTA beads and likewise reacts with the anti-His tag antibodies.

Figure 4-4. pQE70 FL WT StSPL purification steps 1 and 2: 60°C heating and IMAC

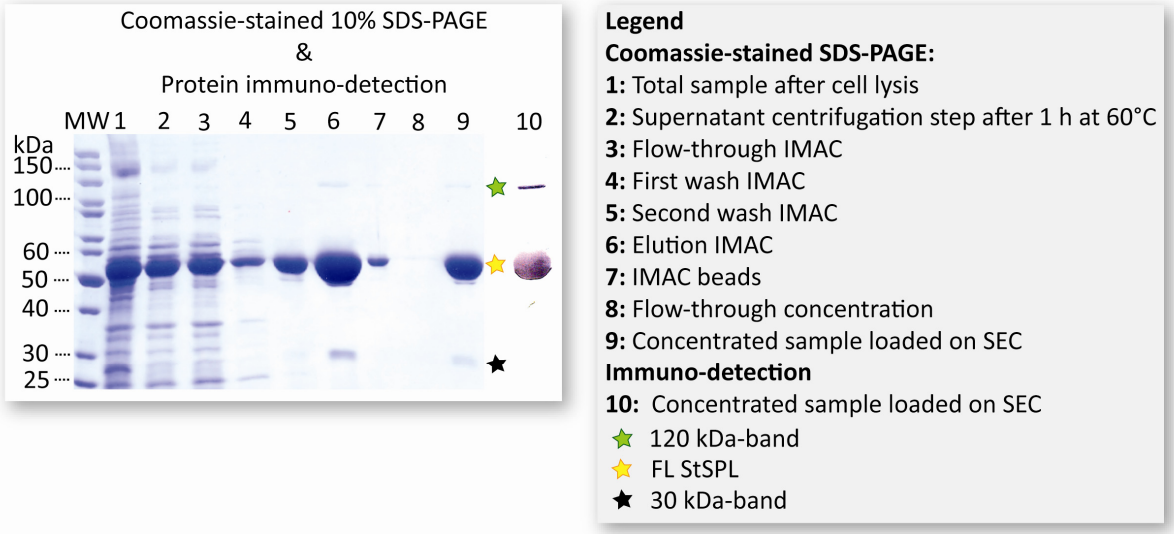

Two peaks elute from the SEC column (**figure 4-5**), a Superdex-200 10/300. Both peaks contain FL StSPL, as confirmed by Coomassie-staining SDS-PAGE, protein immunodetection (inlet **figure 4-5**), N-terminal sequencing of the respective 55 kDa bands and mass spectrometry (data not shown). The calculated mass of the protein from the primary sequence is 55.8 and 55.4 kDa depending on the expression vector (in pQE60 and pQE70, respectively). The peaks eluting at 11 and 13 ml correspond to a 320 kDa and a 140 kDa globular species, respectively, and can be assigned to a tetramer and a dimer of StSPL respectively. These molecular masses derive from calibration runs carried out with soluble protein mass standards. Pooled fractions of the 11 ml- (called thereafter the tetramer peak) and 13 ml-peak (dimer peak), as indicated with the stars in the inlet of **figure 4-5**, respectively contain an additional 120 kDa band, as seen on SDS-PAGE, and a 30 kDa smeared band. Nevertheless, the estimated purity of each sample exceeds 98%.

Figure 4-5. FL WT StSPL purification step 3: SEC

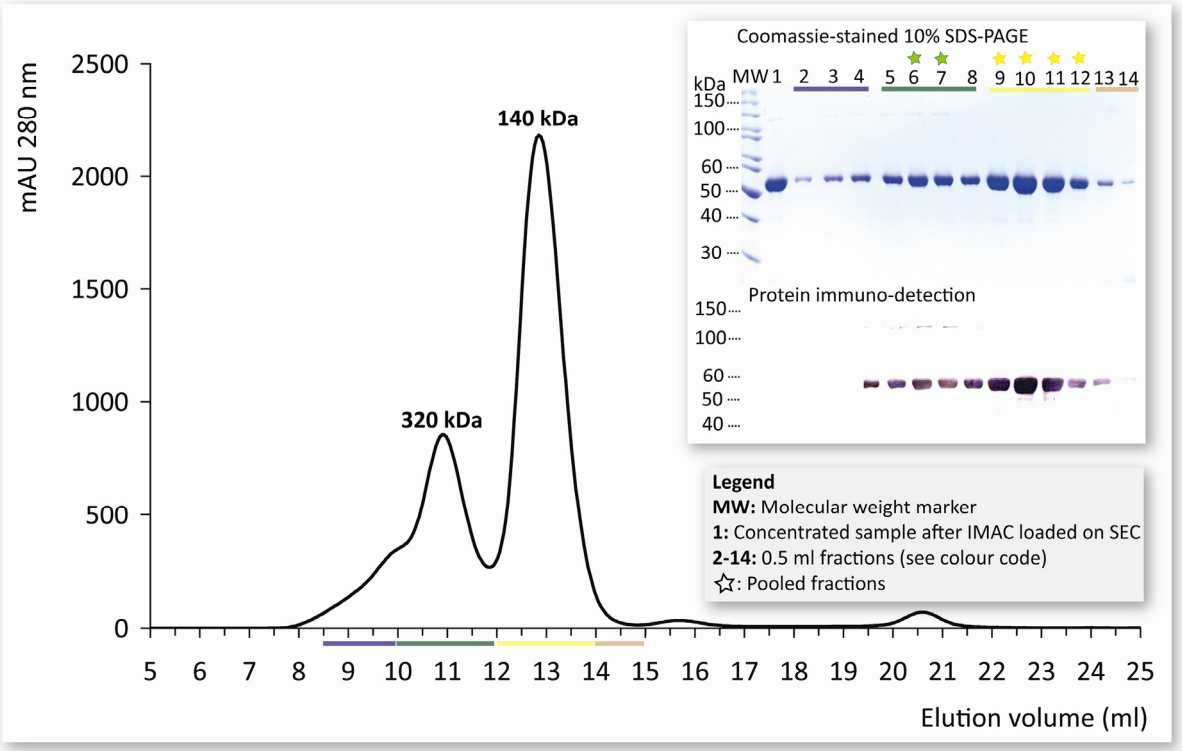

The tetramer-to-dimer peak (abbreviated 4mer-to-2mer) ratio increases with sample concentration. Interestingly, the two peaks exhibit a different behaviour or overall stability upon concentration. Pooled fractions of the tetramer peak concentrated to 6 mg/ml and subjected again to SEC generate a significant peak at 13 ml retention volume, whereas pooled fractions of the dimer peak concentrated to 25 mg/ml mainly run as a sharp 13 ml peak (**table 4-3**). The tetramer species thus seems more prone to dissociate into dimers than the dimer species is prone to oligomerize into a tetramer.

Table 4-3. Influence of the concentration on the intensity of the tetramer and dimer peaks

	Concentration[(1)]	**4mer-to-2mer ratio**
Sample after **IMAC**	16	40 : 100
Tetramer peak reloaded	6	100 : 30
Dimer peak reloaded	3	1 : 100
Dimer peak reloaded	25	2 : 100

[(1)] Indicated as mg/ml of monomer (peptide chain).

The purification outcomes are similar for FL WT StSPL expressed in pQE60 or pQE70, meaning that the additional residues at the N-terminus, MGGSRS in case of pQE60 and MP in case of pQE70, do not alter the biophysical properties of the FL protein. Adding 1 mM EDTA, using HEPES or NaP_i instead of KP_i (at the same concentration and pH), replacing NaCl by KCl, running the SEC without pH-buffering agents have no effect on the elution profile (data not shown). When pooled fractions of the 13 ml-peak kept for one week at 4°C, -20°C or -80°C

either in non-concentrated or in five-fold concentrated form are subjected to SEC, the protein runs as a single sharp peak eluting at 13 ml. This indicates that the protein does not aggregate or unfold upon storage. Nevertheless, all crystallisation trials and activity assays were performed with material as fresh as possible, unless otherwise stated. Both SEC peaks were subjected to crystallisation trials.

4.4. BIOPHYSICAL CHARACTERIZATION

4.4.1. UV-VIS SPECTRUM

Free PLP (vitamine B_6) exhibits two peaks in the visible range, the main one being centred at 385 nm with a shoulder at 330 nm (**figure 4-6** orange trace). The features of the visible spectrum of PLP-dependent enzymes depend on the protonation state and microenvironment of the cofactor (174) (175). The UV-Vis spectrum of FL WT StSPL is characterized by a broad peak located at 420-460 nm (**figure 4-6**) presumably resulting from two contributions, one centred at 425 nm and the other at 450 nm. The latter species is unknown. The 425-nm species presumably corresponds to the ketoenamine form of the internal aldimine, which is the covalent complex between K311 and PLP (see section 1.5.5. **figure 1-34**). Mutating the internal aldimine lysine is known to alter the spectrum and to inactivate the enzyme. The spectrum of StSPL K311A (FL) shows a 350 nm peak which probably corresponds to the hydrated form of PLP in one of the active sites of structure St_10 (**figures 4-7** & **4-8**) (176) (177).

Figure 4-6. UV-Vis spectra of free PLP, StSPL FL WT and K311A

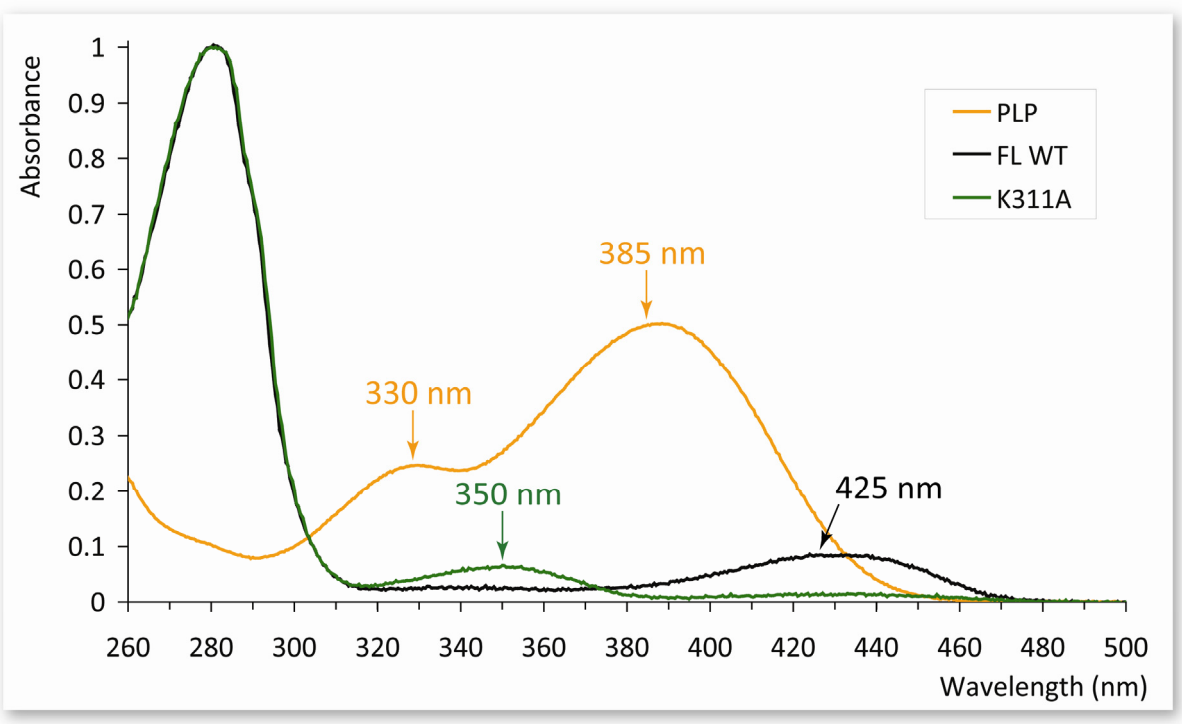

Note: the protein spectra were normalized to 1 at 280 nm whereas the maximal absorbance of PLP was adjusted to 0.5 at 385 nm.

Figure 4-7. PLP internal aldimine and hydrated form

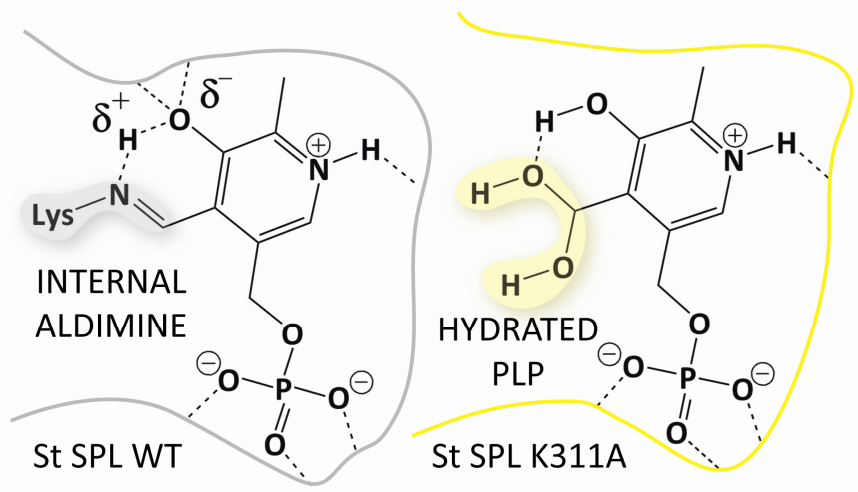

Figure 4-8. Hydrated form of PLP in one active site of StSPL K311A (structure St_10)

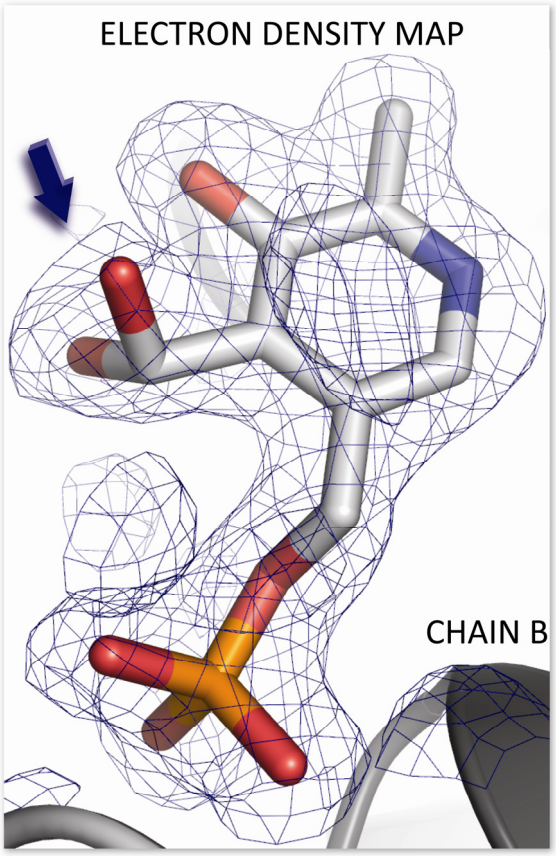

Note: the crystallisation and the structure are described in sections 4.5.4. and 4.6.7., respectively.

4.4.2. PRIMARY SEQUENCE ANALYSIS

FL WT StSPL expressed in pQE60 and pQE70 was subjected to N-terminal sequencing and mass spectrometry after SEC. Both methods indicate that the first methionine (Met1) was cleaved off of the protein and are in full agreement with the expected sequences and molecular masses (**table 4-4**).

Table 4-4. Calculated and experimental MWs of FL WT StSPL constructs lacking Met1

	N-terminal sequence	**Calculated** (without Met1)	**Measured**
In pQE60	GGSRSLSAFS	55 781 Da	55 784 Da
In pQE70		55 434 Da	55 436 Da

Note: the molecular masses were calculated from the primary sequences including all additional residues except Met1 using ProtParam (http://www.expasy.org/tools/protparam.html (178)).

Mass spectrometry reveals the presence of two species under the conditions tested, the protein lacking its cofactor (called apo-form) and the protein with the covalently bound cofactor (called holo-form) (**figure 4-9**).

Figure 4-9. pQE70 FL WT StSPL mass spectrometry analysis

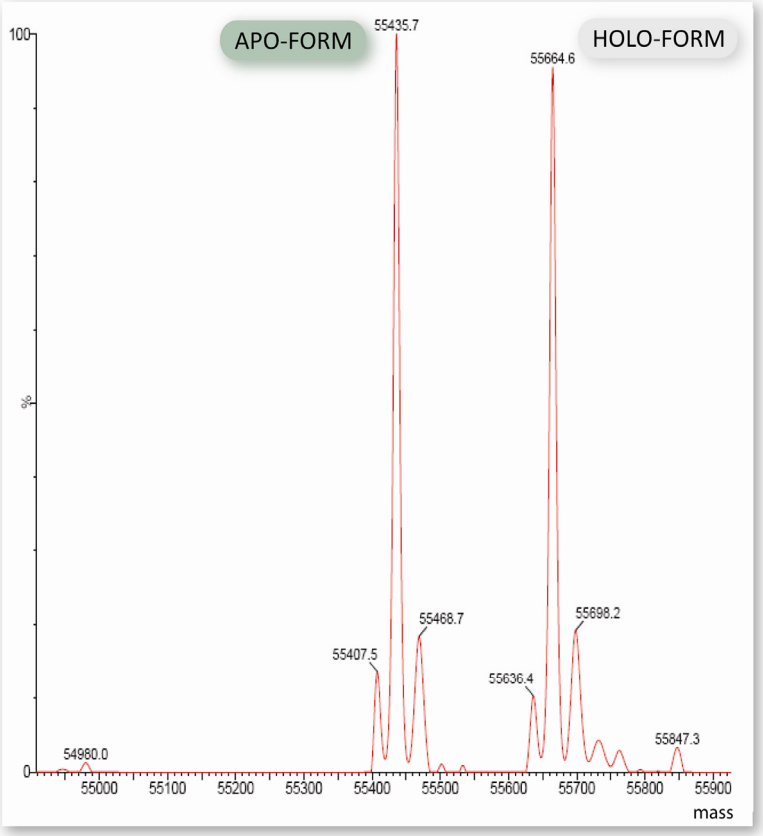

4.4.3. ANALYTICAL ULTRACENTRIFUGATION

The 11 ml- (tetramer) and 13 ml-peak (dimer) of the SEC purification step were analysed by AUC with the aim of confirming their oligomeric state. After pooling (see chapter 4.3. **figure 4-5** green and yellow stars) the respective fractions of the 11 ml- and 13 ml-peaks, part of each sample was diluted to 0.4 mg/ml whereas the other part was concentrated to 15 and 33 mg/ml, respectively. The sedimentation of the 0.4 mg/ml samples was monitored by their absorbance at 320 nm whereas the sedimentation of the more concentrated samples was monitored using interference. The data obtained using the latter detection method were too noisy to be analysed in a reproducible way and are therefore not shown. The outcomes of the data analysis of the low concentration samples are presented in **figure 4-10**. Three species are present in the SEC tetramer peak sample, corresponding to a dimer, a tetramer and probably to a hexamer whereas only one tailed peak appears in the SEC dimer sample with a mass corresponding to a dimer. These results are in good agreement with the molecular masses estimated from the SEC column calibration runs.

Figure 4-10. AUC analysis of pQE60 FL WT StSPL SEC tetramer and dimer peaks (0.4 mg/ml)

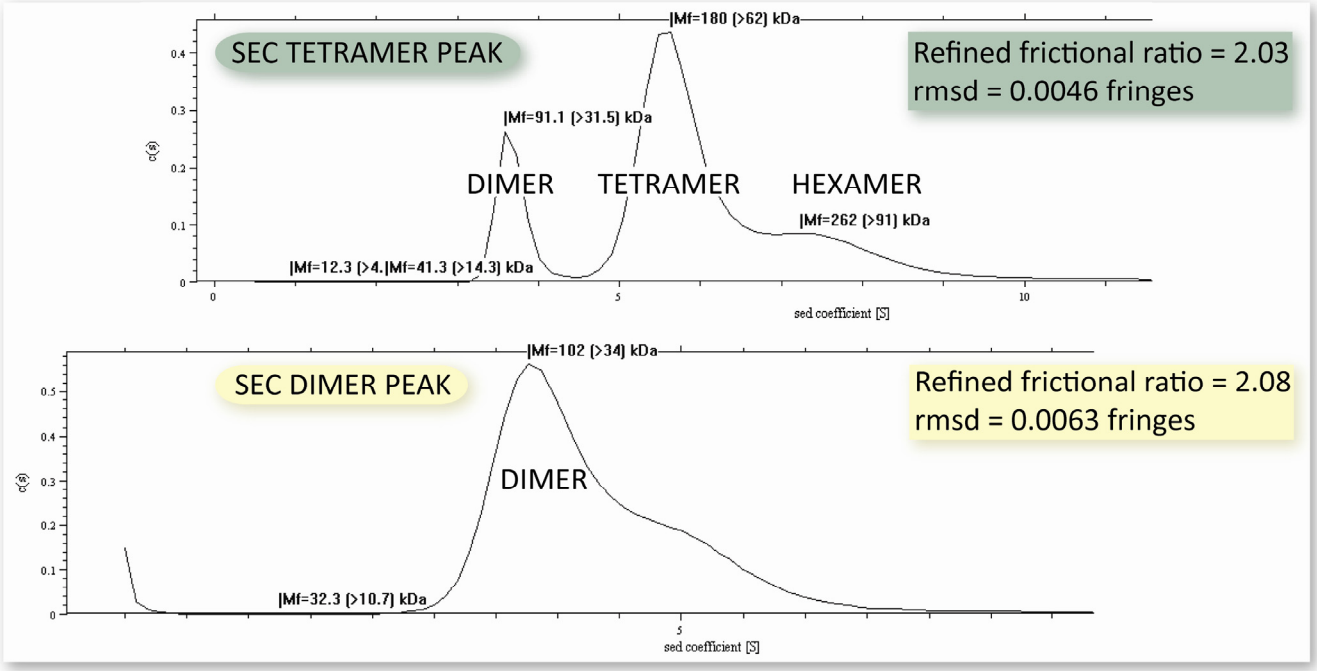

Note: the starting frictional ratio (f/f_0) was set to 1.3 and corresponded to the default value recommended for globular proteins using the program SedFit (179). The rmsd of a relevant fit should be significantly lower than 0.01 fringes.

4.5. CRYSTALLISATION AND DATA COLLECTION

The SEC tetramer and dimer peaks were subjected to initial crystallisation trials as described in Materials & Methods (chapter 8.8.). In comparison with material from the dimer peak, fewer and smaller colourless crystals or crystal-like material grew from the tetramer peak. Therefore, all the crystals presented in this section arose exclusively from the SEC dimer peak (eluting at 13 ml). All crystals shown were grown at 20°C. Only the crystals used to determine the structures presented in the next chapter (4.6.) are described. The resolution of the datasets as well as a summary of the crystallisation conditions of structures St_5-10 can be found in **table 4-6** of section 4.5.5., while those of structures St_1-4 are listed in part 3 (manuscript) **table S2**. The numbering of the structures was chosen according to the manuscript (see part 3) and therefore does not follow the order presented here.

4.5.1. NATIVE FL WT StSPL

Native FL WT StSPL, cloned either in pQE60 or pQE70, crystallised in a pH range from 8.0 to 8.5 in the presence of 0.15 potassium thiocyanate (KSCN) and in typically 16 to 18 % PEG 5K MME or 25 % PEG 2K MME (**figures 4-11**, **4-13**, **4-14**). In one single case, displayed in **figure 4-12**, crystals grew in the presence of Mg^{2+} from an initial heavy precipitate. This condition could not be reproduced to date. The crystals of StSPL grown in presence of Sr^{2+} grew at pH 7.5 in 0.3 M NaOAc and 15 % PEG 4K (**figure 4-15**). The crystals are yellow due to the presence of PLP. In all cases, the crystals producing high resolution datasets were plate- or needle-like shaped, appeared after one week and reached their full size after approximately two weeks. Crystals growing in the presence of Sr^{2+} reached their full size after approximately one month. Bulkier and bigger crystals appeared within one to two days but did not diffract to high resolution (pictures not shown).

Figure 4-11. Crystals of pQE70 FL WT StSPL **STRUCTURE St_1**

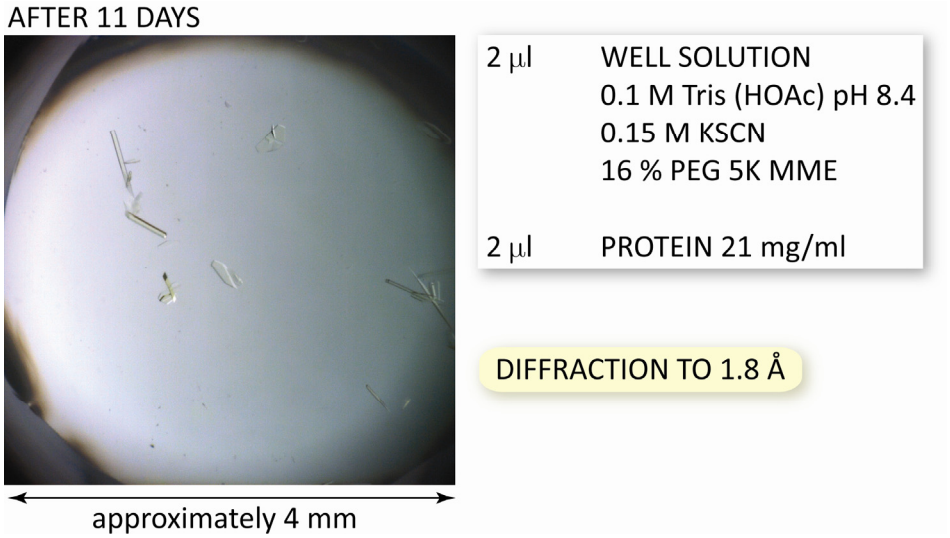

Figure 4-12. Crystals and diffraction pattern of pQE60 FL WT StSPL **STRUCTURE St_2**

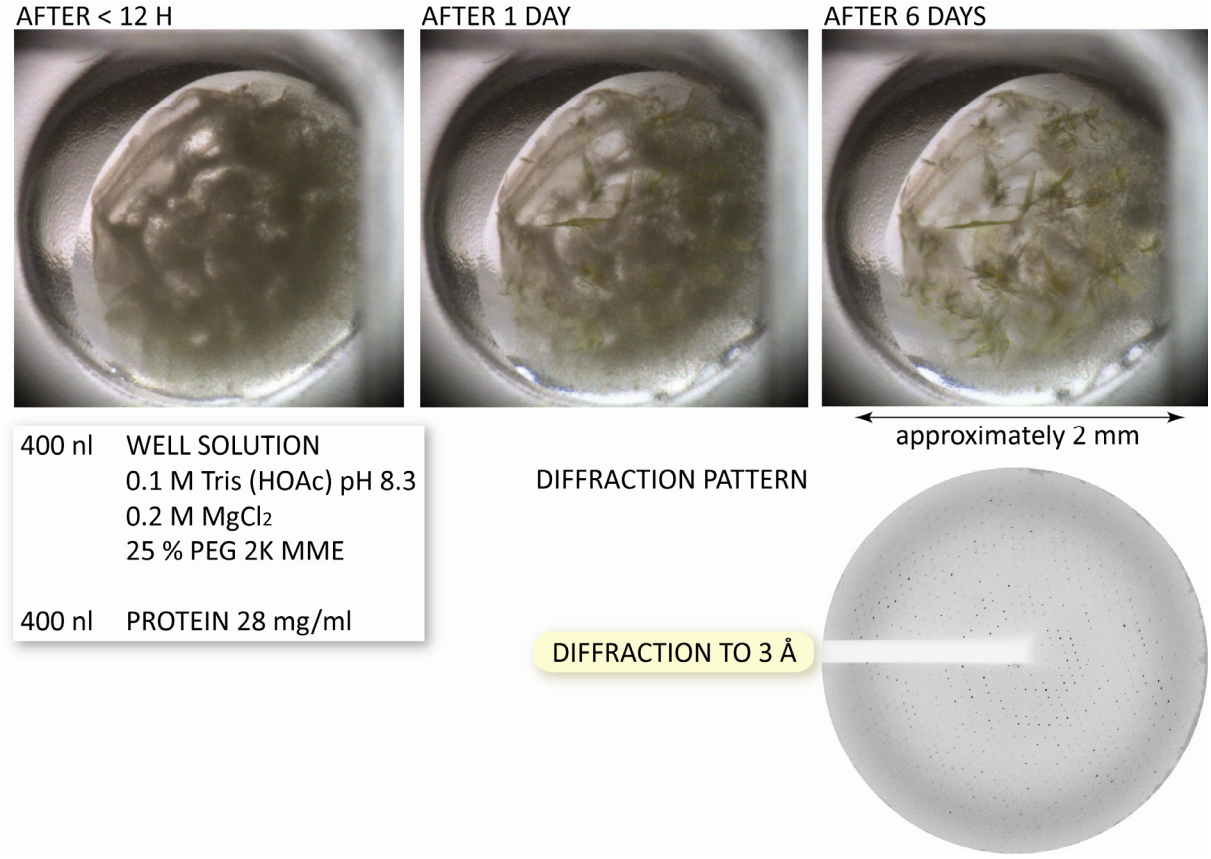

Figure 4-13. Crystals and diffraction pattern of pQE60 FL WT StSPL **STRUCTURE St_5**

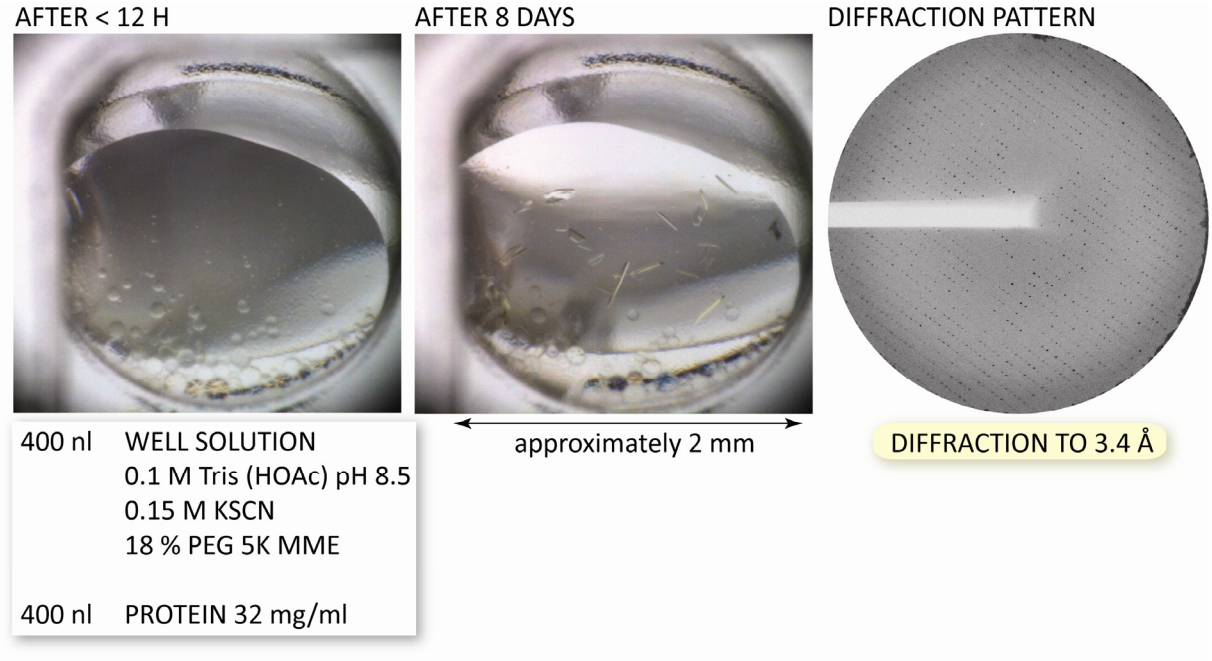

Figure 4-14. Crystals of pQE70 FL WT StSPL used for soaking trials with $MgCl_2$ resulting in **STRUCTURES St_6-8**

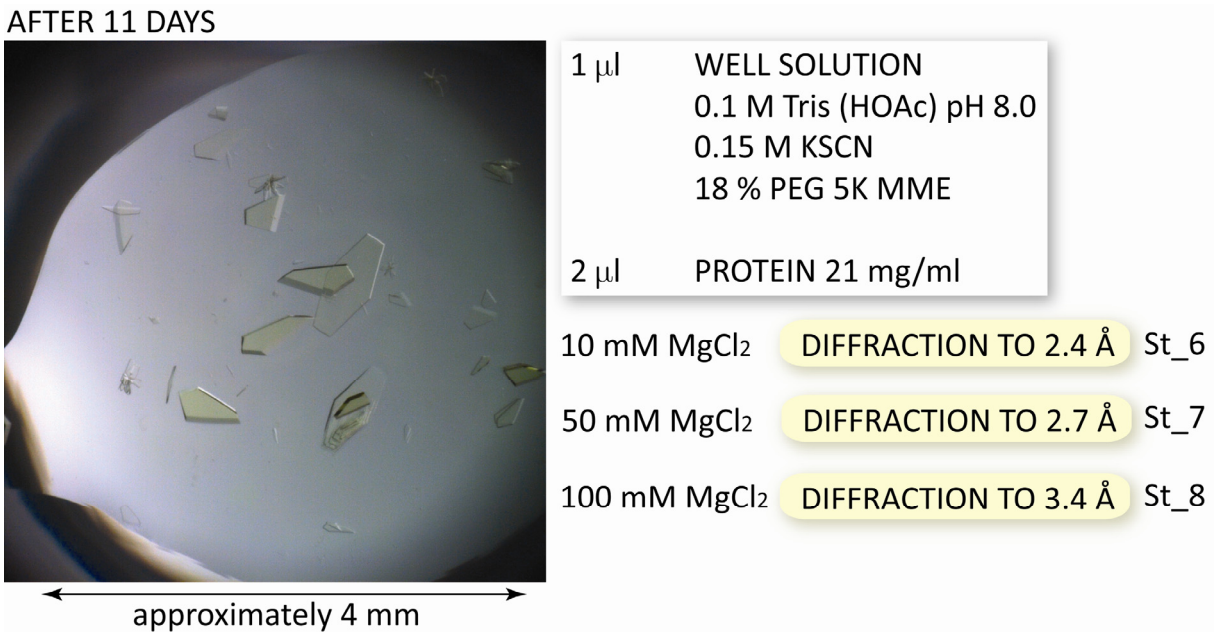

Figure 4-15. Crystals of pQE70 FL WT StSPL in presence of $SrCl_2$ resulting in **STRUCTURE St_9**

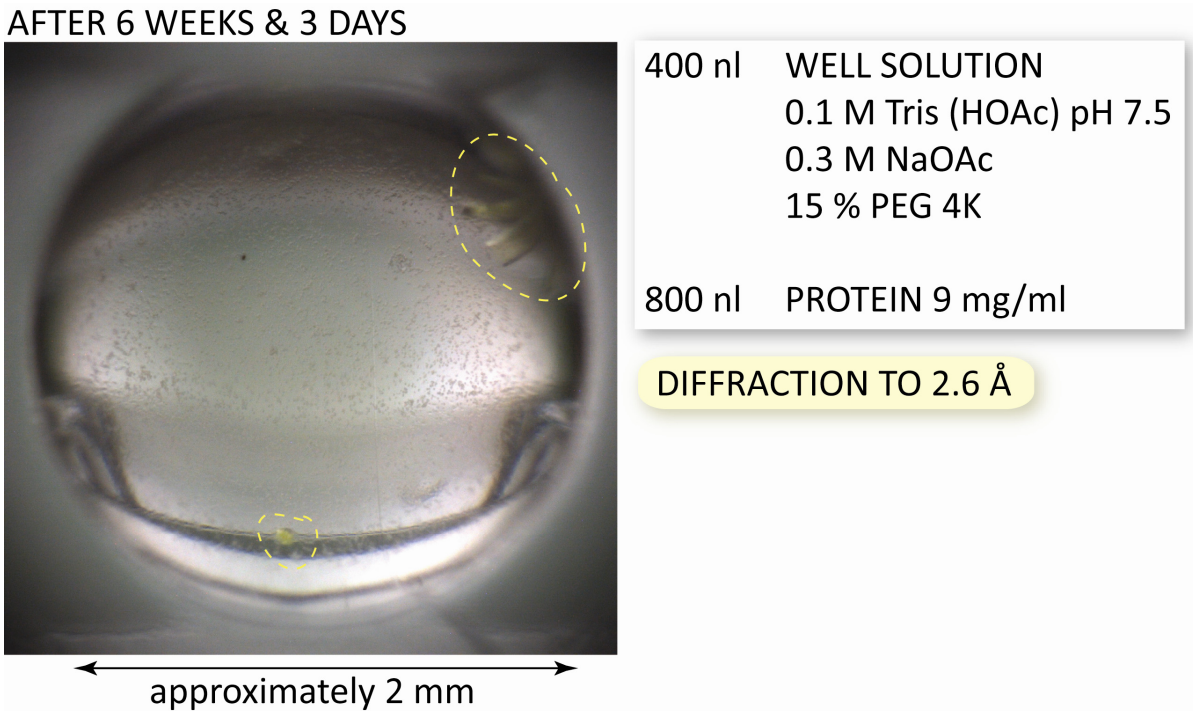

4.5.2. FL WT StSPL IN COMPLEX WITH SEMICARBAZIDE

Crystals of pQE70 FL WT StSPL in complex with the PLP-dependent enzymes inhibitor semicarbazide (see part 3 (manuscript) and section 4.7.1.) grew in conditions similar those of the native enzyme and exhibit similar shapes. Unlike those of the native enzyme, the crystals are colourless (**figure 4-16**).

Figure 4-16. Crystals of pQE70 FL WT StSPL in the presence of 10-fold molar excess of semicarbazide over monomer, resulting in **STRUCTURE St_4**

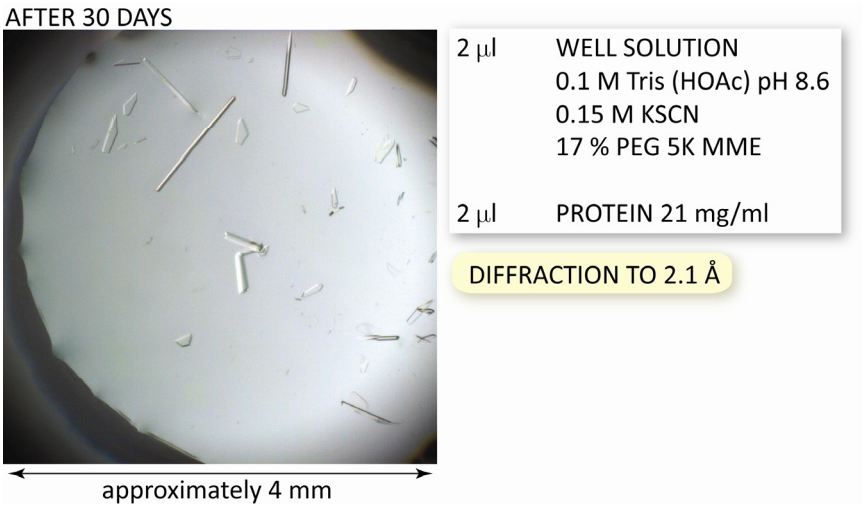

4.5.3. StSPL K311A IN COMPLEX WITH PE

After an overnight incubation at 4°C with PE, the spectrum of pQE70 StSPL K311A (FL) exhibits a new broad peak at 425 nm (**figure 4-17**) characteristic of an aldimine, like the internal aldimine of StSPL WT (**figure 4-6** section 4.4.1.). This indicates that PE formed a covalent complex with PLP (called thereafter external aldimine).

Figure 4-17. PE-induced spectral changes of StSPL K311A

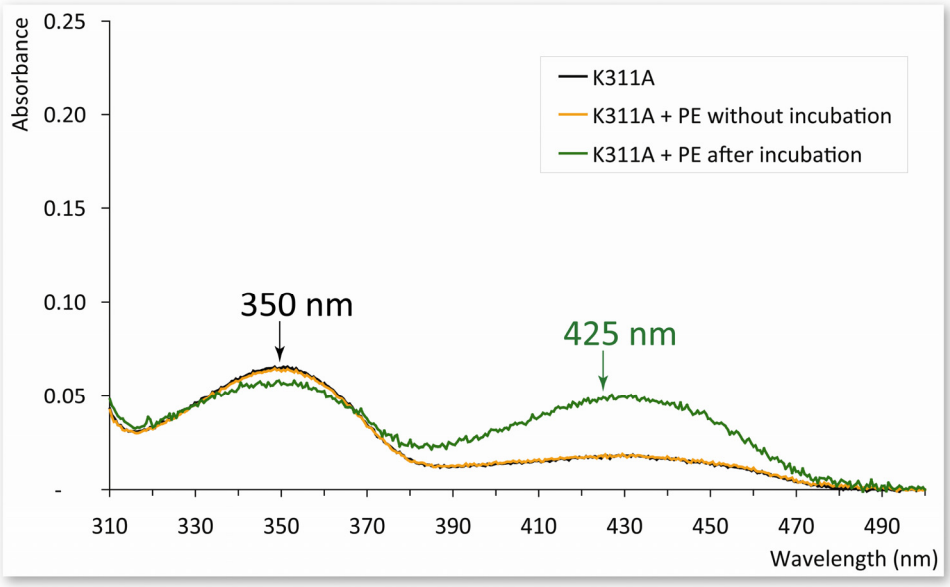

Crystals of the protein in complex with PE grew in similar conditions as the native enzyme and have similar shapes (**figure 4-18**).

Figure 4-18. Crystals of StSPL K311A in presence of PE, resulting in **STRUCTURE St_3**

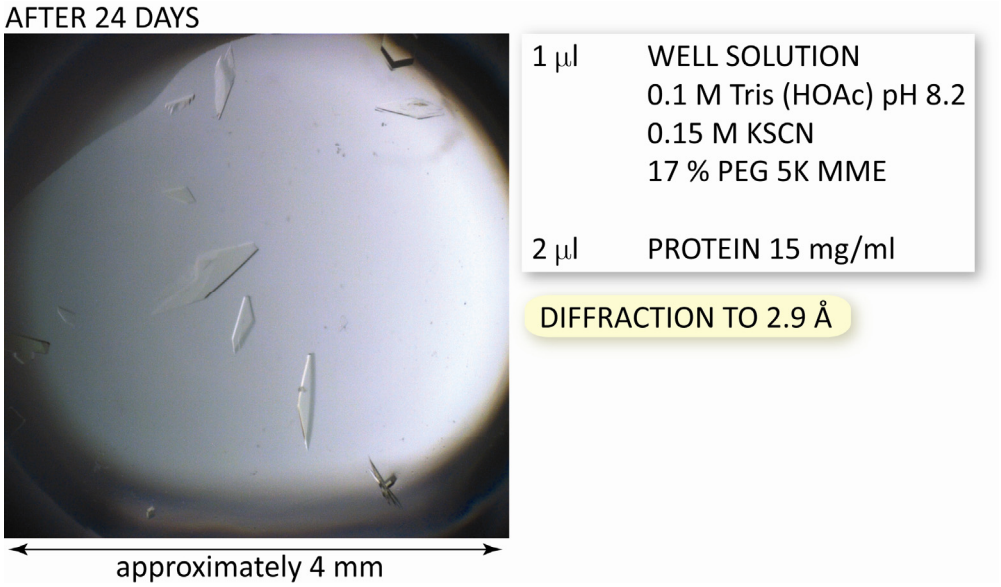

SOAKING TRIALS WITH A LONG-CHAIN ALDEHYDE

The purchased *cis*-11-hexadecenal (Fluka) was obtained as a suspension, which was diluted to 5 mM with Triton X-100 and used to soak crystals of StSPL K311A in complex with PE as described below for S1P in StSPL K311A (see section 4.5.4.). No high-resolution datasets were obtained from these attempts.

4.5.4. StSPL K311A IN COMPLEX WITH S1P

SOAKING TRIALS

Crystals of pQE70 StSPL K311A (FL) grew in similar conditions and had similar shapes as other crystals of WT StSPL that are not presented in section 4.5.1. These crystals were used for substrate soaking trials as described in Materials & Methods (section 8.8.5.). S1P was either suspended in the corresponding well solution (**figure 4-19**) or was solubilised in the well solution supplemented with 1 % Triton X-100 (not shown) before addition to the crystal. When Triton X-100 was present the crystals diffracted only to low resolution.

Figure 4-19. Crystal and diffraction pattern of StSPL K311A soaked with S1P, resulting in **STRUCTURE St_10**

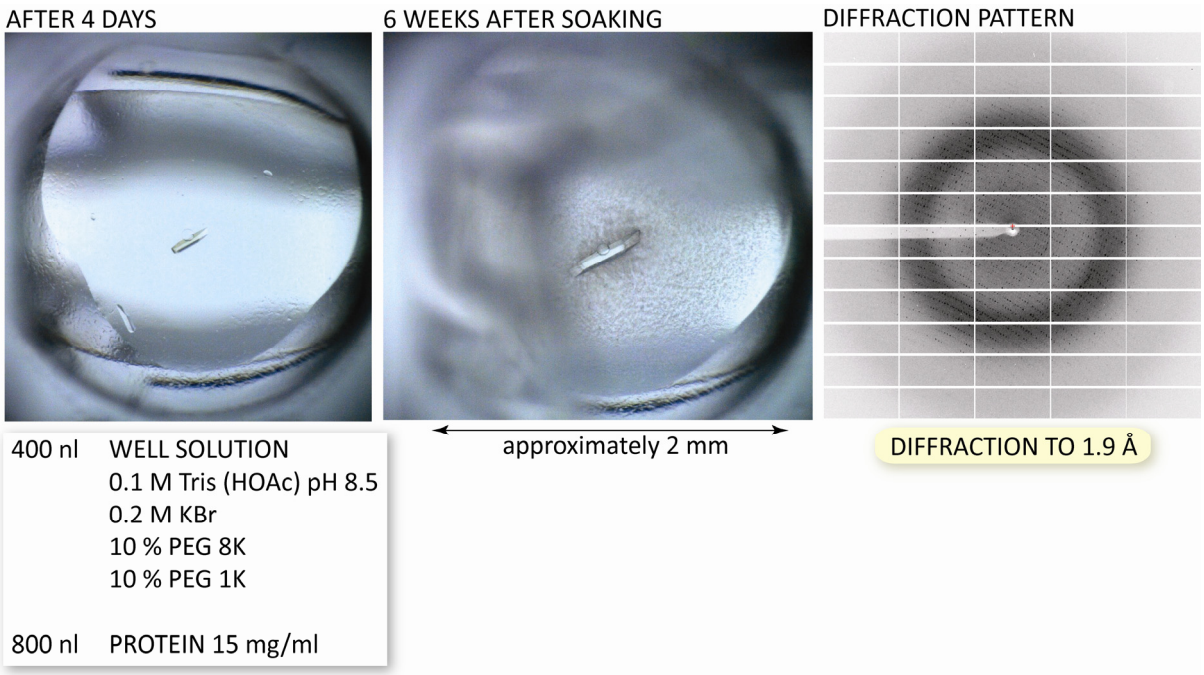

CO-CRYSTALLISATION TRIALS

The attempts and outcomes thereof are summarized in **table 4-5**.

Co-crystallisation with S1P either suspended in the protein solution or solubilised in Triton X-100 or ethanol prior to addition to the protein sample was attempted. Unexpectedly, no spectral changes were observed after overnight incubation at 4°C. The formation of the external aldimine with the substrate (that is the covalent complex between PLP and S1P) should result in spectral changes that can be monitored (180) (181), as for StSPL K311A mixed with PE (see section 4.5.3. **figure 4-17**). The co-crystallisation experiment was nevertheless continued. Increasing concentrations of Triton X-100 in the protein sample markedly reduced the number of crystals per drop and their size compared to native SPL. In one attempt, the protein sample mixed with Triton X-100-solubilised S1P was subjected to a SEC purification step to remove the detergent prior to crystallisation. High resolution datasets were obtained but no positive difference electron density corresponding to S1P was observed. This indicates that Triton X-100 has a deleterious effect on the crystal packing and should be removed for structural work.

Replacement of Triton X-100 with ethanol produced crystals diffracting to high resolution but their electron density maps lacked a significant signal for S1P.

Table 4-5. Outcome of the crystallisation trials of StSPL K311A in complex with S1P

ATTEMPT	METHOD	S1P	SOLVENT REMOVAL	CRYSTALS	HIGH-RESOLUTION DIFFRACTION	S1P VISIBLE
1	**SOAKING**	Suspended in well solution	***No solvent***	*Yes (survived)*	Yes	**No**
2		Solubilised in well solution supplemented with **1 % Triton X-100**	No		**No**	
3	**CO-CRYSTALLISATION**	Suspended in protein solution	***No solvent***	Yes	Yes	**No**
		Solubilised in **0.08 %** [(1)] **Triton X-100**	No	Yes[(2)]	**No**	
		Solubilised in 0.**16 %** [(1)] **Triton X-100**				
		Solubilised in 1 **%** [(1)] **Triton X-100**				
4		Solubilised in **1 % Triton X-100**	**SEC**	Yes	Yes	**No**
5		Solubilised in **50 % ethanol**	No	Yes	Yes	**No**
			30 min at **60°C**		**No**	

[(1)] Corresponding to 0.5, 1, and 6 times the CMC value of Triton X-100, respectively.
[(2)] A decreasing number of crystals per drop correlated with an increase of the Triton X-100 concentration and the crystals had different morphologies.

4.5.5. SUMMARY

Table 4-6. Crystallisation conditions and resolution of St_5-10

PART	STRUCTURE CODE	SAMPLE	PROTEIN CONC. [mg/ml]	RATIO PROTEIN:WELL SOLUTION	WELL SOLUTION [(1)]	CRYO [%EG (v/v)]	RES. (Å)
4.5.1.	**St_2**[(2)]						
	St_5	**Native pQE60** FL WT StSPL	32	1:1 (400 nl each)	0.1 M Tris (HOAc) pH 8.5 0.15 M KSCN 18% PEG 5K MME	20	3.4
	St_1[(2)]						
	St_6	pQE70 FL WT StSPL **soaked** in **10 mM Mg^{2+}**	21	2:1 (2 µl:1 µl)	0.1 M Tris (HOAc) pH 8.0 0.15 M KSCN 18% PEG 5K MME	20	2.4
	St_7	pQE70 FL WT StSPL **soaked** in **50 mM Mg^{2+}**					2.7
	St_8	pQE70 FL WT StSPL **soaked** in **100 mM Mg^{2+}**					3.4
	St_9	pQE70 FL WT StSPL **co-cryst.** with **Sr^{2+}**	9	2:1 (800 nl:400 nl)	0.1 M Tris (HOAc) pH 7.5 0.3 M Na-acetate 15% PEG 4K	25	2.6
4.5.2.	**St_4**[(2)]						
4.5.3.	**St_3**[(2)]						
4.5.4.	**St_10**	pQE70 StSPL **K311A** soaked with **S1P**	15	2:1 (800 nl:400 nl)	0.1 M Tris (HOAc) pH 8.5 0.2 M KBr 10% PEG 8K 10% PEG 1K	25	1.9

[(1)] All hits were obtained at 20°C.
[(2)] See part 3 (manuscript) **table S2**.

4.6. StSPL STRUCTURES

The statistics of the presented datasets are found in part 3 (manuscript) **table S3** (St_1-4 only) and in section 4.6.8 for St_5-10. For clarity, the disordered regions are not displayed on the figures. The disorder of St_5-10 was identical to that of St_1 (part 3), *i.e.* the Nt-FLEX domain (residues 1-57) was not visible.

4.6.1. FL WT StSPL HOMODIMER (STRUCTURE St_1)

See part 3 (manuscript).

4.6.2. FL WT StSPL HOMODIMER WITH CONFORMATIONAL HETEROGENEITIES (STRUCTURE St_2)

See part 3 (manuscript).

4.6.3. FL WT StSPL HOMOTETRAMER (STRUCTURE St_5)

Crystals containing two dimers in the asymmetric unit were found in the same drops as the above-described crystals with one dimer per a.u. (**figure 4-20**). Only one subunit of each dimer interacts with the other dimer to form the tetramer (subunits B and D, coloured dark grey on **figure 4-20**). PLP is present in all subunits, whereas phosphate ions are only found in subunits B and C. The interface area between two dimers spans about 520 Å^2, while it spans about 6280 and 6190 Å^2 between monomers A-B and C-D, respectively. The surface areas were calculated with the CCP4 version of PISA (182). For comparison, interface A-B of the St_2 homodimer, which exhibits conformational heterogeneities, spans 5340 Å^2.
Further analysis with the CRK tool (to be published) indicates that the tetramer most probably arises from a crystal contact and has no biological relevance. Mutants with a significantly decreased 4mer-to-2mer ratio on SEC are also found as tetramers, supporting the hypothesis of a non-biologically relevant oligomer (see structures St_3 and St_10 in sections 4.6.6. and 4.6.7., respectively, and the SEC profile of StSPL K311A in chapter 4.9.2. **figure 4-38** right panel).

Figure 4-20. Structure **St_5**

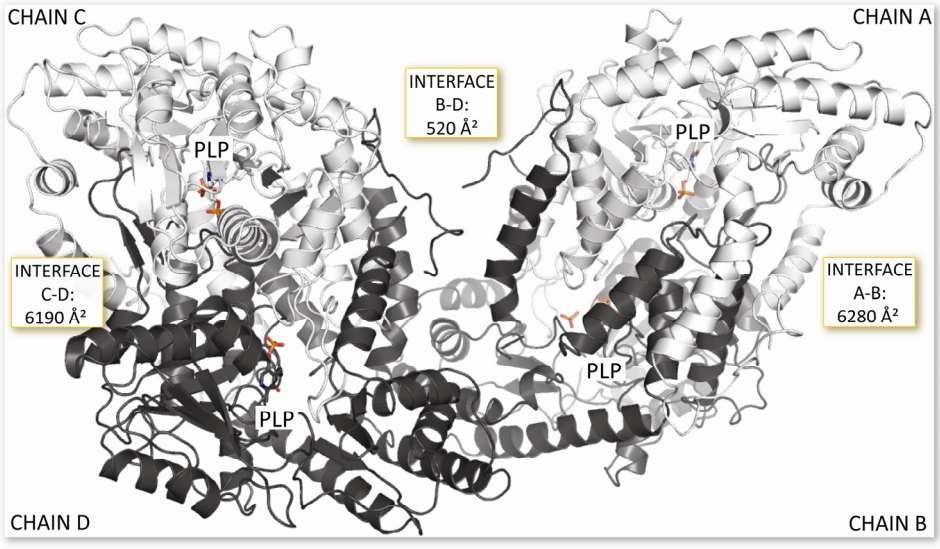

The N- and C-termini of subunits B and D are close to each other and might be involved in tetramer formation (**figure 4-21**). The first 57 residues (corresponding to the Nt-FLEX domain) that are not visible on the structure might extend the interface under particular biochemical conditions.

Figure 4-21. Localisation of N- and C-termini in the tetramer in structure St_5

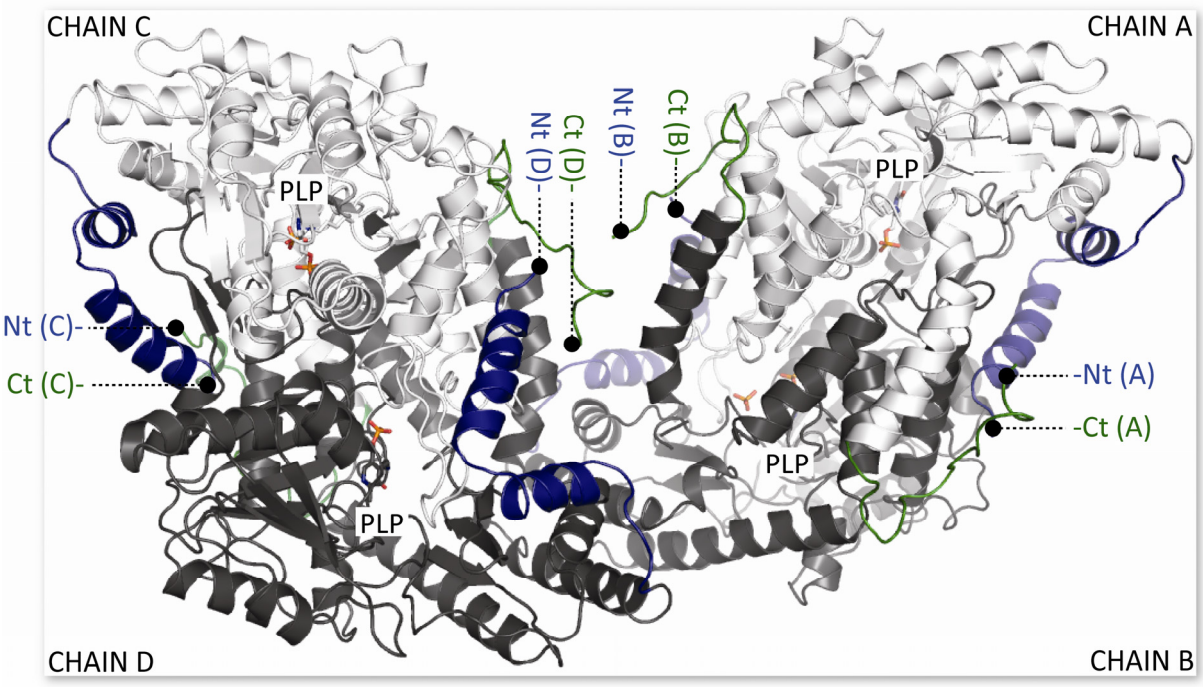

4.6.4. EFFECT OF DIVALENT CATIONS

Divalent cations such as Ca^{2+} and Zn^{2+} were reported to inhibit SPL activity (113) even if this could not be confirmed under the experimental conditions tested (see section 4.7.1.). It was nevertheless thought that Mg^{2+} present in the well solution triggered the conformational heterogeneities observed in structure St_2. To test this hypothesis, crystal soaking and co-crystallisation with divalent cations were attempted.

CRYSTAL SOAKING WITH Mg^{2+} (STRUCTURES St_6-8)

Crystals from the same drop were soaked with the well solution supplemented with 10, 50 and 100 mM Mg^{2+} and were found to diffract to 2.4, 2.7 and 3.4 Å, respectively. Assuming that this effect doesn't result from the initial properties of the respective crystal used for soaking, high concentrations of Mg^{2+} seem to promote conformational changes that disturb the crystal lattice. Unlike structure St_2, the protein is present as a tetramer and PLP and phosphate ions are found in all subunits of all three structures. The decreasing quality of diffraction data with increasing Mg^{2+} concentration makes comparisons of the three structures partly unreliable. In the case of the 50 mM and 100 mM structures, non-crystallographic symmetry restraints on the four subunits had to be imposed due to their poor observations-to-parameters ratio. A Mg^{2+} binding site is observed on the surface of the protein (carbonyl groups of residues R393, I395 and L398) (**figure 4-22**), with no apparent influence on conformation, as indicated by the low rmsd values between the three structures (**table 4-7**). Importantly, no conformational heterogeneities could be mapped.

Figure 4-22. Mg^{2+} binding site and residues involved in Mg^{2+} accommodation

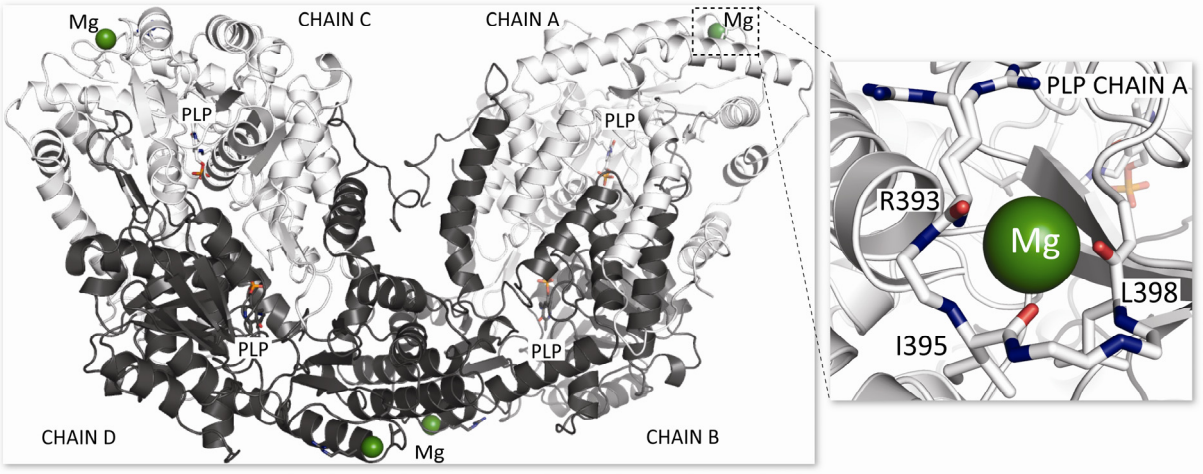

Table 4-7. Effect of Mg^{2+} on the conformation of FL WT StSPL (subunit A)

STRUCTURE 1	STRUCTURE 2	RMSD (Å)	ALIGNED Cα-ATOMS
St_6	**St_7**	**0.13**	446
	St_8	**0.25**	445
St_7		**0.24**	450

CO-CRYSTALLISATION WITH Sr^{2+} (STRUCTURE St_9)

To identify other putative binding sites of divalent cations, FL WT StSPL was co-crystallised with Sr^{2+} and a dataset was collected. St_9 is a dimer containing PLP and phosphate ions in both subunits. Unfortunately, no divalent cation could be localized and no significant conformational change was observed compared to the native protein, as indicated by a rmsd value of 0.25 Å over 450 aligned Cα-atoms between structures St_1 (native FL WT StSPL) and St_9. Presumably, only smaller cations like Mg^{2+}, Zn^{2+} and Ca^{2+} can bind to the protein (**table 4-8**).

Table 4-8. Pauling ionic radii of divalent cations

ELEMENT	ATOMIC RADIUS [pm](1)
Mg(II)	65
Zn(II)	74
Ca(II)	99
Sr(II)	113
Ba(II)	135

(1) Values found on http://www.webelements.com from (183).

4.6.5. SEMICARBAZIDE-INACTIVATED FL WT StSPL (STRUCTURE St_4)

See part 3 (manuscript).

4.6.6. StSPL K311A IN COMPLEX WITH PE (STRUCTURE St_3)

See part 3 (manuscript).

S1P EXTERNAL ALDIMINE MODEL

See part 3 (manuscript).

Figure 4-23. Accommodation of S1P modelled in the active site of StSPL K311A (stereo view)

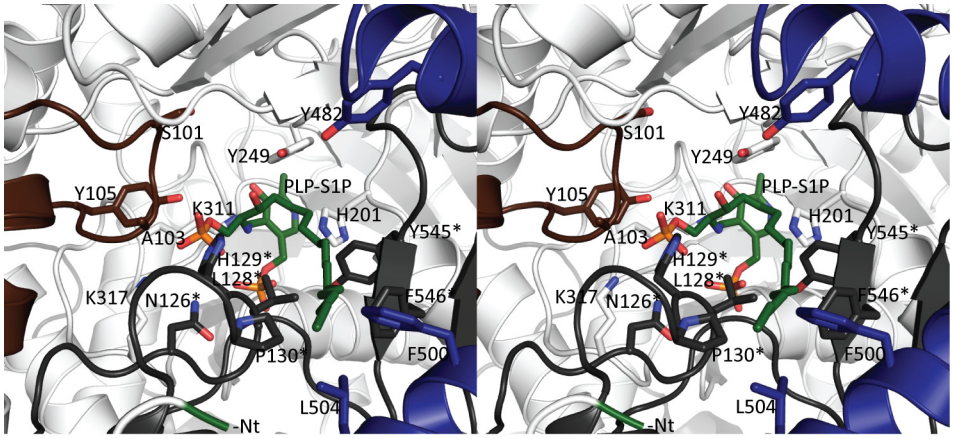

Note: See part 3 (manuscript) **Fig. 3*B*** for details.

4.6.7. StSPL INACTIVE MUTANT K311A: SOAKING WITH S1P (STRUCTURE St_10)

St_10 is a tetramer containing one cofactor molecule and one phosphate ion per subunit. The interface area between two dimers spans approximately 696 Å^2, while it spans 6313 and 6160 Å^2 between monomers A-B and C-D respectively. This mutant exhibits a significantly reduced tetramer-to-dimer peak ratio on SEC, confirming that the tetramer is in equilibrium with the dimer form (section 4.9.2. **figure 4-38** green line). No significant positive electron density is found in the active site of St_10 (**figure 4-24**). Likewise, no significant conformational changes can be observed, as indicated by a rmsd value of 0.27 Å over 451 aligned Cα-atoms between the chain A of structure St_1 (native FL WT StSPL) and St_10 and of 0.3 Å over 452 aligned Cα-atoms between the chain A of structure St_3 (StSPL K311A in complex with PE) and structure St_10.

Figure 4-24. Traces of S1P in the active sites of structure St_10

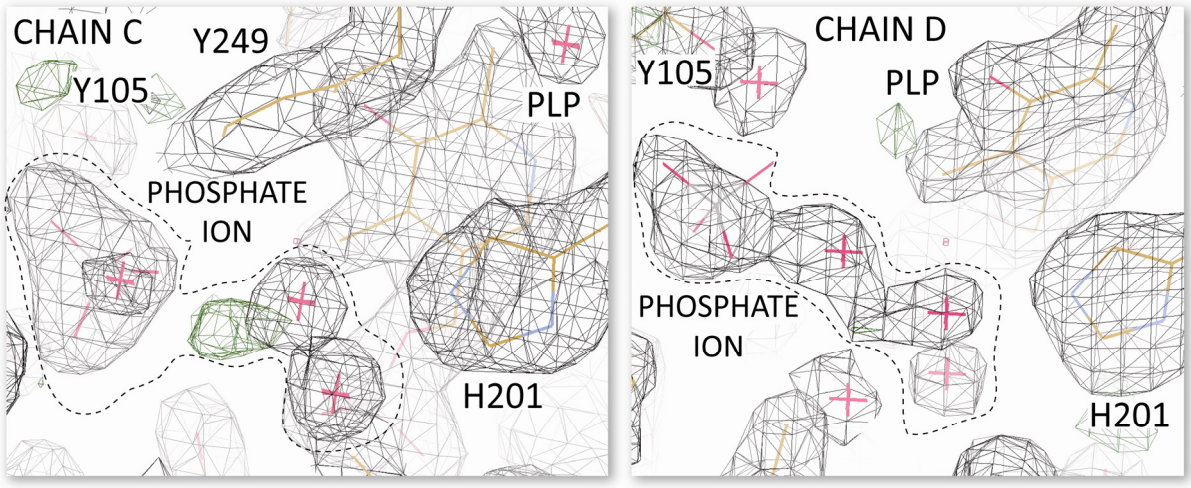

Note: the $2F_OF_C$ map was contoured at 1σ and depicted in black. The F_OF_C map was contoured at 3σ and is coloured green for positive electron density and red for negative. The putative trace of S1P is surrounded by a dashed line.

The active site is solvent-accessible, as shown in **Fig. S1*D*** in part 3 (manuscript). One single channel is observed in the structure, leading to the PLP. This channel might serve both for substrate entry and product exit; alternatively, the protein would have to undergo large conformational changes to build other defined compartments. Given the different physico-chemical properties of the substrate and the reaction products (see section 1.4.3.) the second hypothesis would make sense. In this respect, the N-terminal part (highlighted in green in **Fig. S1*D***), comprising Nt-FLEX (residues 1-57) and N-terminal domain (residues 58-97), and Ct-EXT (residues 472 to 507, highlighted in blue in **Fig. S1*D***) are the best candidates for compartmentalizing the reaction, as they are flexible (as seen in structure St_2 for Ct-EXT) and already line the single channel observed.

4.6.8. DATA COLLECTION AND REFINEMENT STATISTICS

Table 4-9. Data collection and refinement statistics for structures St_5-10. Refinement for these datasets was not brought to completion but only to the (advanced) level necessary to assess their significance in providing biochemical information.

STRUCTURE CODE	St_5	St_6	St_7	St_8	St_9	St_10
SPACE GROUP	$C222_1$	$C222_1$	$C222_1$	$C222_1$	$P2_1$	$C222_1$
UNIT CELL PARAMETER (Å/°)	a = 59.4 b = 244.9 c = 282.3	a = 59.6 b = 243.9 c = 283.2	a = 57.8 b = 245.8 c = 283.1	a = 61.3 b = 246.1 c = 282.1	a = 72.1 b = 85.0 c = 84.6 β=111.0	a = 59.3 b = 243.1 c = 281.3
RESOLUTION RANGE[(1)] (Å)	29.5-3.36 (3.5-3.36)	49.3-2.3 (2.4-2.3)	30-2.7 (2.8-2.7)	30-3.3 (3.4-3.3)	30.0-2.6 (2.7-2.6)	30.0-1.9 (20.0-1.9)
COMPLETENESS[(1)] (%)	95.9 (66.9)	97.4 (95.9)	96.4 (78.9)	99.5 (99.8)	99.7 (100.0)	97.7 (934)
REDUNDANCY	4.2	3.0	3.3	3.5	5.3[(2)]	3.8
UNIQUE REFLECTIONS	28831	172367	106691	61710	57 657	156574
I/σ [(1)] (%)	10.6 (3.1)	9.5 (1.9)	9.8 (2.4)	9.1 (1.5)	7.6 (3.8)	7.2 (2.0)
R_{SYM} [(1)] (%)	17.1 (49.7)	7.7 (56.5)	8.7 (40.3)	8.9 (82.7)	21.8 (43.3) [(2)]	12.6 (47.5)
No. OF REFLECTIONS (TEST)	28812 (1008)	172344 (2071)	106679 (2132)	61670 (1870)	57657 (2073)	156569 (1566)
No. OF ATOMS	13679	14339	13809	13805	6868	14 826
R_{WORK} (%)	22.1	21.4	20.9	25.4	20.8	20.7
R_{FREE} (%)	27.9	25.1	24.3	30.0	25.4	25.6
RMSD BONDS (Å)	0.007	0.008	0.006	0.008	0.008	0.009
RMSD ANGLES (°)	1.08	1.09	0.96	1.02	1.15	1.20
RAMACHANDRAN PLOT REGIONS						
FAVOURED %)	99.5	97.6	96.8	94.0	96.8	97.4
ALLOWED (%)	91.7	100	99.9	99.4	100	100
NUMBER OF OUTLIERS	9	0	2	10	0	0

[(1)] Into brackets: values for the outermost resolution shell.

[(2)] Data processing with anomalous signal; the Friedel pairs were treated as different reflections in the calculation of absorption correction factors.

4.7. ACTIVITY ASSAY

4.7.1. MONITORING OF UV-VIS SPECTRAL CHANGES (SPECTROPHOTOMETRIC ACTIVITY ASSAY)

See part 3 (manuscript).

As already pointed out in the introduction (section 1.4.3.), the poor solubility of S1P hinders precise biochemical investigations. The solubility of S1P was assayed in various solutions (as described in Materials & Methods (section 8.4.2.)) and the outcome is summarized in **table 4-10**. S1P was partly insoluble above approximately 0.05 mg/ml in all solutions tested. This means that a pellet was still visible after spinning down the sample at the end of the solubilisation procedure. Unfortunately, spectroscopic changes on FL WT StSPL could not be detected at this concentration of substrate (data not shown). Despite the partial insolubility of S1P, solutions at higher concentrations were used, with the disadvantage of ignoring the precise concentration of S1P (only an upper bound for the concentration is known, value reported in **Table 4-10**). The amount of solubilised S1P was maximal when S1P was initially suspended to at least 1 mg/ml, as reflected by a more intense 403 nm- and 420 nm-peaks after addition of the solution to FL WT StSPL (data not shown). Slight variations in solubility were observed for S1P purchased from different companies and from different batches.

Table 4-10. Influence of the S1P solubilisation procedure on the StSPL spectrophotometric activity assay outcome

SOLUTION	CMC	S1P MAXIMAL CONC.[(1)]	VOLUME ADDED (µl) [(2)]	403 & 420 nm-PEAKS	REMARK
1 % Triton X-100	6x	1	70	Yes	
		2			**REFERENCE** **figure 4-25** bottom right
0.16 % Triton X-100	CMC	1	70	Yes	
		2			
0.1 % DDM	10x	2	70	Less intense than REF.	
0.25 % digitonin	10x	2	70	Very faint	
100 % DMSO		1	70	Yes but aggregation	
		2	7	No	
			70	Less intense than REF. & aggregation	**figure 4-25** bottom left
100 % ethanol		1	30	Less intense than REF. & aggregation	
		2	10	No	
			15	Very faint	
			20	Less intense than REF.	
			30	Less intense than REF. & aggregation	**figure 4-25** upper panels
			35	Yes but strong aggregation	
50 % ethanol/water		1	20	No	
			40		
4 mg/ml BSA		0.5	70	No	
		1	35		
			70		

[(1)] In mg/ml. 0.5, 1 and 2 mg/ml S1P correspond to 1.3, 2.6 and 5.2 mM respectively.
[(2)] To 100 µl protein solution.

Interestingly, the aggregation observed upon addition of S1P solubilised in ethanol to SPL was less pronounced in a protein buffer lacking KP_i (**figure 4-25** upper left panel) than in 50 mM (**figure 4.25** upper right panel). This indicates that the solubility of S1P is prone to large variations and represents a bottle-neck in the study of SPL.

Figure 4-25. Transient changes on FL WT StSPL induced by S1P solubilised in ethanol in the presence (left panel) or absence (right) of 50 mM KP_i and by S1P solubilised in DMSO (bottom)

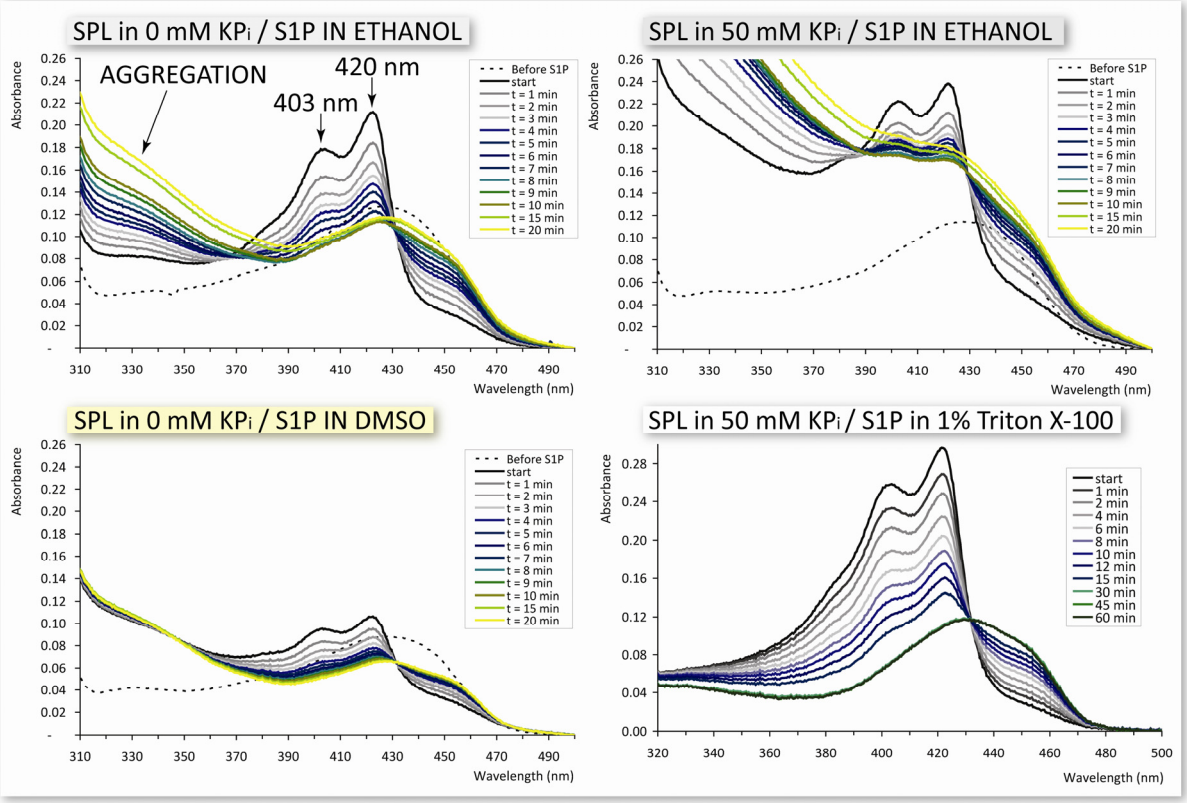

Note: the reference (FL WT StSPL) is shown in the bottom right panel.

Two approaches were used to validate the spectrophotometric activity assay. First, the assay was performed with the internal aldimine mutant K311A, a mutation known to inactivate PLP-dependent enzymes. When S1P was added to StSPL K311A under the same conditions as the WT, no spectral changes were observed (see part 3 (manuscript) **Fig. 4*B***). This indicates that mixing an inactive protein with S1P does not result in the formation of peaks at 403 and 420 nm. It must be mentioned that the test reflects changes occurring to the cofactor, changes that might be only indirectly linked to the cleavage of the substrate. Therefore, the absence of 403 nm and 420 nm-peaks does not necessarily correlate with enzyme inactivity. One can nevertheless safely assume that only an active protein can produce the characteristic transient peaks.

Semicarbazide (see part 3, **Fig. S5*B***), an inhibitor of PLP-dependent enzymes, was used to further validate the spectrophotometric activity assay. An equimolar amount, as well as 10-, 25- or 100-fold molar excess, respectively, of semicarbazide was added to FL WT StSPL. Spectra were recorded and S1P was added to the mixture either immediately after the inhibitor or after one hour incubation at room temperature protected from light. The

internal aldimine 425 nm-peak of native FL WT StSPL was progressively shifted towards 360 nm (see part 3, **Fig. S5*C***). When a 100-fold molar excess of semicarbazide over monomer was used, the equilibrium was reached after one hour. Semicarbazide is a carbonyl-reactive compound. The 360 nm-peak presumably corresponds to PLP-semicarbazone, a covalent complex between PLP and semicarbazide (see part 3, **Fig. S5*B***) (184) (185). In structure St_4 (see part 3, **Fig. S5*A***) PLP-semicarbazone has left the active site and residue Y249 partly takes the place of the pyridinium ring of PLP. FL WT StSPL incubated 30 minutes at room temperature with semicarbazide showed minor spectral changes at 420 nm upon addition of S1P (see part 3, **Fig. S5*D*** and **figure 4-26** left panel). When semicarbazide was added together with S1P to the enzyme, strong 403 nm- and 420 nm-peaks appeared (**figure 4-26** right panel), indicating that semicarbazide requires incubation to fully inhibit SPL.

Figure 4-26. FL WT StSPL inactivation by semicarbazide

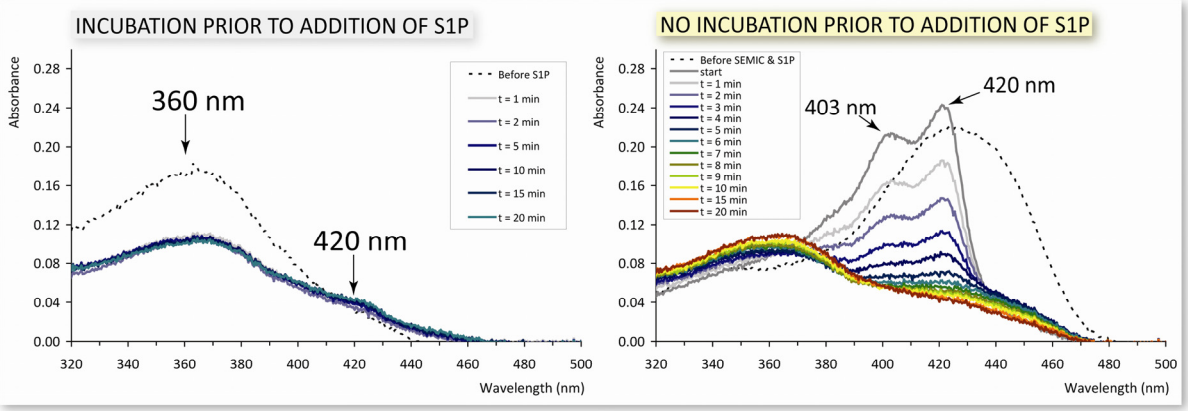

Iodoacetamide, a sulfhydryl reagent (section 1.4.3. **figure 1-19**), was reported to inhibit the activity of mouse SPL (113). It was tested as inhibitor of FL WT StSPL at 100-fold molar excess over active site under the same conditions as semicarbazide. Incubation with iodoacetamide did not result in alterations of the visible spectrum of the protein and 403 nm- and 420 nm-peaks appeared upon addition of substrate as for native FL WT STSPL (data not shown). Thus, iodoacetamide does not inhibit FL WT StSPL or it does it to a far lower extent than semicarbazide under the same experimental conditions; the compound may not be able to access its target site or cysteine residues may not strictly be required for the activity of StSPL.

The sensitivity of SPL from rat liver microsomes to BSA concentrations higher than 25 µM, to non-ionic and zwitterionic detergents (DDM, OG, CHAPS, LDAO) and to divalent metal cations (Ca^{2+}, Zn^{2+}, Mg^{2+}, Ni^{2+}, Mn^{2+}, Co^{2+}, Fe^{2+}, Cu^{2+}) was reported in 1991 (113) (reviewed in (132)). In the same study, SPL activity was shown to be stimulated by chelators such as EDTA. This effect might also arise from the inhibition of sphingosine kinase (present in rat liver microsomes) and not only from the stimulation of SPL. To date, no further evidence of either the inhibitory effect of divalent cations or of the stimulating effect of chelators on SPL has been published. The inhibition of FL WT StSPL by some of those compounds was assayed. A 20-min incubation in a 3-fold molar excess of BSA over FL WT StSPL active sites results in less intense 403 nm- and 420 nm-peaks (data not shown) confirming the inhibition of the enzyme by BSA. The zwitterionic detergent LDAO significantly increased the relaxation time of the FL WT StSPL spectrum, *i.e.* the time until no spectral changes occur anymore, at least by a factor 10 (data not shown). LDAO most probably competes with S1P for binding

within the active site. A 100-fold molar excess of Mg^{2+}, Sr^{2+}, Ba^{2+}, Ca^{2+} over FL WT StSPL active sites did not result in a significant inhibition (data not shown). The counter-ion of the divalent cation solutions used in the assay was chloride, as well as acetate for Ca^{2+} and Zn^{2+}.
THI (2-acetyl-4-tetrahydroxybutyl-imidazole), a compound present in the food colorant caramel colorant III was recently identified as an inhibitor of mouse thymic SPL (see section 1.4.3. **figure 1-20**) (78). In the assay, mice thymus extracted after intravenous injection of THI was used as source of SPL and the cleavage of radioactive substrate was estimated on thin-layer chromatography (TLC). Importantly, THI was recently shown to be unable to inhibit mouse SPL using the same assay when the mice had no prior contact to THI before tissue extraction (186). Thus, THI is assumed to undergo chemical modifications to become a potent inhibitor of SPL, for example phosphorylation or acylation. THI was nevertheless tested for its ability to inhibit FL WT StSPL. The compound was purchased and solubilised in either water or ethanol 100 % to 10 mM. The compound was poorly soluble in these solvents, even at 1 mM. The test was carried out as the assay with semicarbazide, except that the precise molar excess of THI over active site was unknown due its incomplete solubility. The incubation time before addition of substrate was set to 3 h at room temperature. Under those conditions, no significant inhibition of FL WT StSPL was observed (data not shown). Preliminary crystallographic analysis of StSPL K311A indicates that THI can access the active site and sits close to PLP and the phosphate ion (data not shown). This indicates either that THI is specific to human SPL (unlikely) or that THI must be modified to inhibit StSPL.
Fingolimod (FTY720) (140) and its phosphorylated form (P-FTY720), other inhibitors of human SPL, were assayed for their inhibition effect on FL WT StSPL *in vitro* using the above described spectrophotometric assay. Various solvents and detergent solutions were used, as described in Materials & Methods (section 8.4.4.). FTY720 and P-FTY720 behaved differently from S1P upon solubilisation. In all conditions tested, the addition of the FTY720 or P-FTY720 solution to FL WT StSPL resulted in strong aggregation, and in some case precipitation of the compound or of the protein (data not shown).

4.7.2. MASS SPECTROMETRY

MS activity assay was performed on mutants which did not exhibit peaks at 403 and 420 nm upon addition of substrate (see part 3 (manuscript) **Fig. S4**).

4.7.3. OTHER APPROACHES

Two further approaches were attempted to monitor the cleavage of S1P by FL WT StSPL. The first one involved the identification of the long-chain aldehyde product after derivatization with 2,4-dinitrophenylhydrazine (DNPH) using UV-Vis spectroscopy. Under the conditions tested, the control long-chain aldehydes hexenal (6C) and tridecenal (13C) produce a peak at 378 nm, absent when they are replaced with S1P (**figure 4-27**). When a FL WT StSPL reaction mixture before and after two different lipid extraction protocols (see Materials & Methods section 8.11.2.) was analysed under the same conditions, the long-chain aldehyde product of the SPL cleavage could not be detected (data not shown). Importantly, the peak intensities of the internal positive controls, that is hexenal and tridecenal added to the SPL reaction mixture and subjected to lipid extraction, were significantly lower than those of the corresponding external positive controls. They were in particular much lower for tridecenal than for hexenal. This indicates that the lipid extraction procedures used might not be suitable to isolate sufficient amounts of the C16-aldehyde resulting from the cleavage of S1P by FL WT StSPL. A recent functional study of SPL carried out with a fluorescent substrate and mice microsomes as a source of SPL (131) suggests that the long-chain aldehyde is in equilibrium with its cognate alcohol and carboxylic acid (see section 1.4.3. **figure 1-17**, left). Altogether, this indicates that the detection of the long-chain aldehyde product of SPL by DNPH is not a promising approach.

Figure 4-27. UV-Vis spectra of hexenal, tridecenal and S1P reacted with DNPH

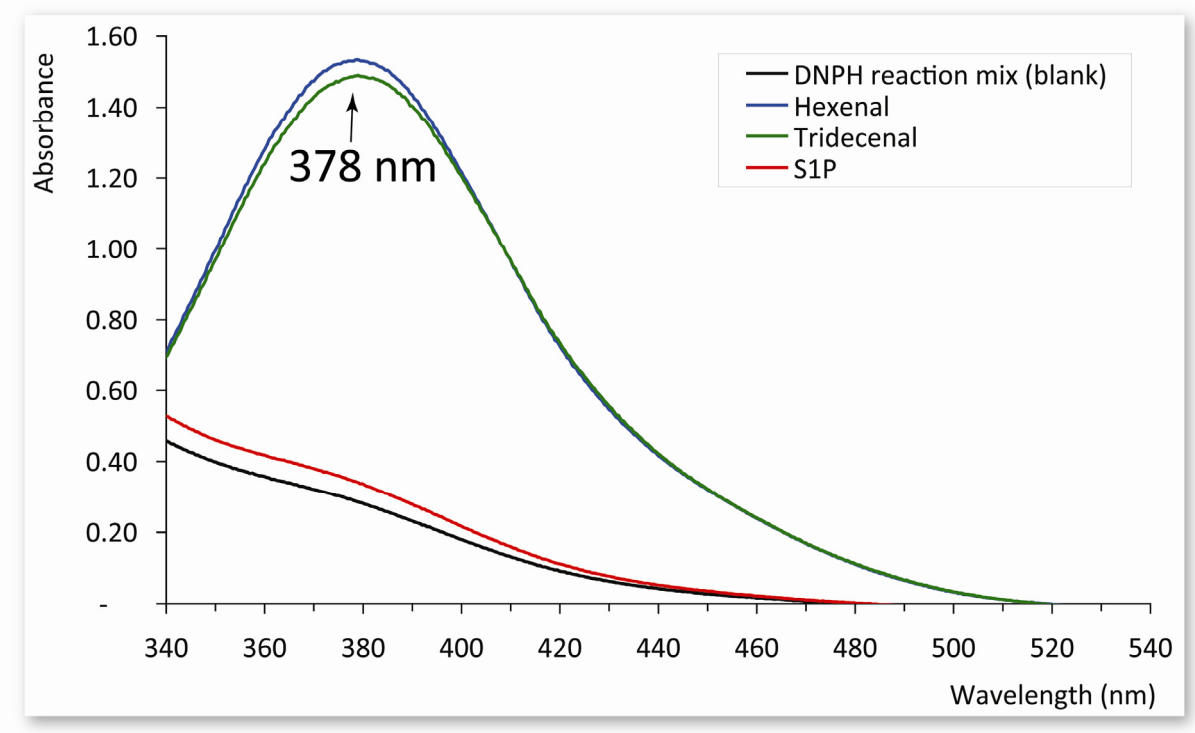

The second approach foresaw the identification of the uncleaved substrate (S1P), if any, and the soluble SPL product PE with naphthalene-2,3-dicarboxaldehyde (NDA). NDA is non-fluorescent until it reacts with a primary amine (in S1P as well as in PE) in the presence of an excess of cyanide (see Materials & Methods section 8.11.3.). NDA-derivatized S1P and PE are then separated using a HPLC C18 reverse-phase chromatography column. Assay parameters

such as solvent or detergent for S1P (ethanol or Triton X-100), concentration of KP_i in the reaction buffer, amount of NDA and cyanide, and incubation time at 50°C were optimized. The positive controls S1P and PE, theoretically set at the same concentration (corresponding to the maximal achievable concentration of S1P, see above), yielded signals of different intensities (**figure 4-28**). PE yields a 10-fold more intense signal than S1P when tested under the same experimental conditions. It is important to note that the PE reaction mixture was also supplemented with detergent. As a consequence, it appears that the effective S1P concentration is lower than the PE concentration or that the primary amine of S1P is less available for derivatization than that of PE. The latter effect might result from intermolecular interactions or interactions with the solvent or detergent.

Figure 4-28. UV-Vis spectra of PE and S1P reacted with NDA

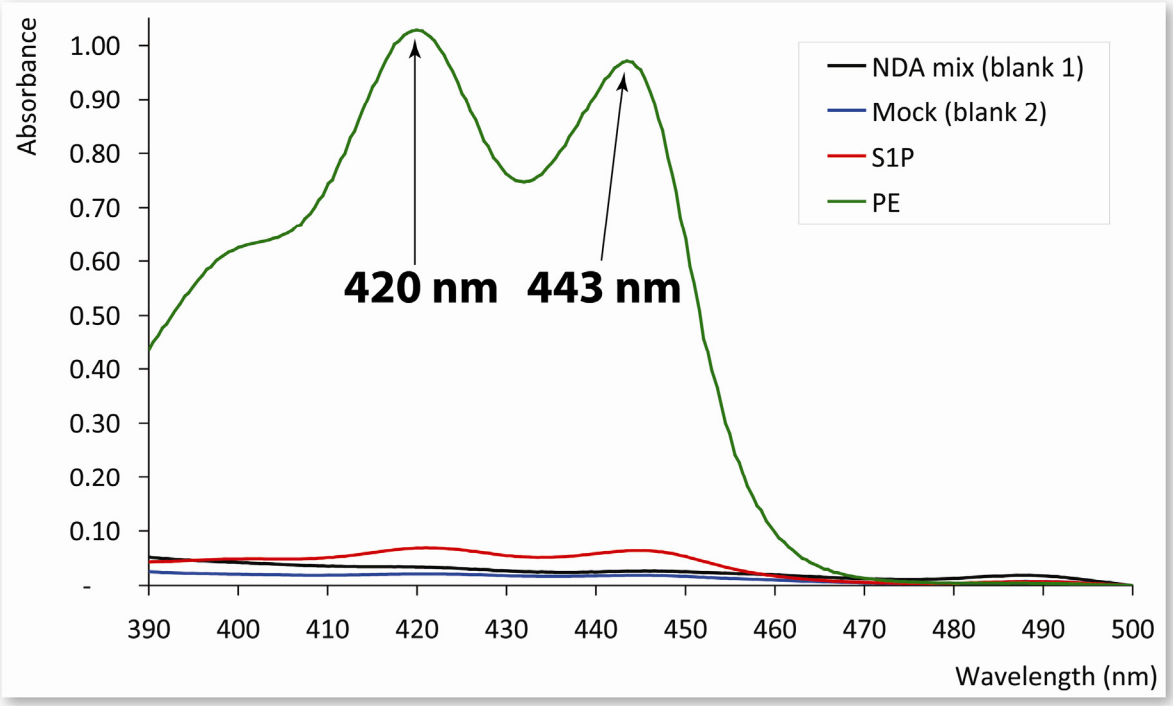

HPLC separation of NDA-S1P and NDA-PE was nevertheless attempted. In good agreement with the spectrophotometric measurements, PE produced a much stronger signal than S1P. PE-NDA eluted with a main peak at 13.3 min, a 150-fold weaker peak at 19.9 min and a 1000-fold weaker peak at 22.4 min (**figure 4-29** upper left). The main elution peak of S1P-NDA was found close to noise level at 22.4 min (**figure 4-29** upper right). The reaction mixture of SPL and S1P (solubilised in 1 % Triton X-100) after 3 hours incubation at 37°C originated two peaks that were close to noise level, at the retention times specific for PE and S1P (**figure 4-29** bottom). These were not present when SPL alone subjected to the derivatization procedure was eluted under the same conditions. This test indicates that FL WT StSPL is able to cleave S1P. The sensitivity of the test might be improved by detecting the NDA-derivatized species using fluorescence rather than UV-Vis absorption.

Figure 4-29. Elution profile of PE-NDA, S1P-NDA and FL WT StSPL reaction mix derivatized with NDA

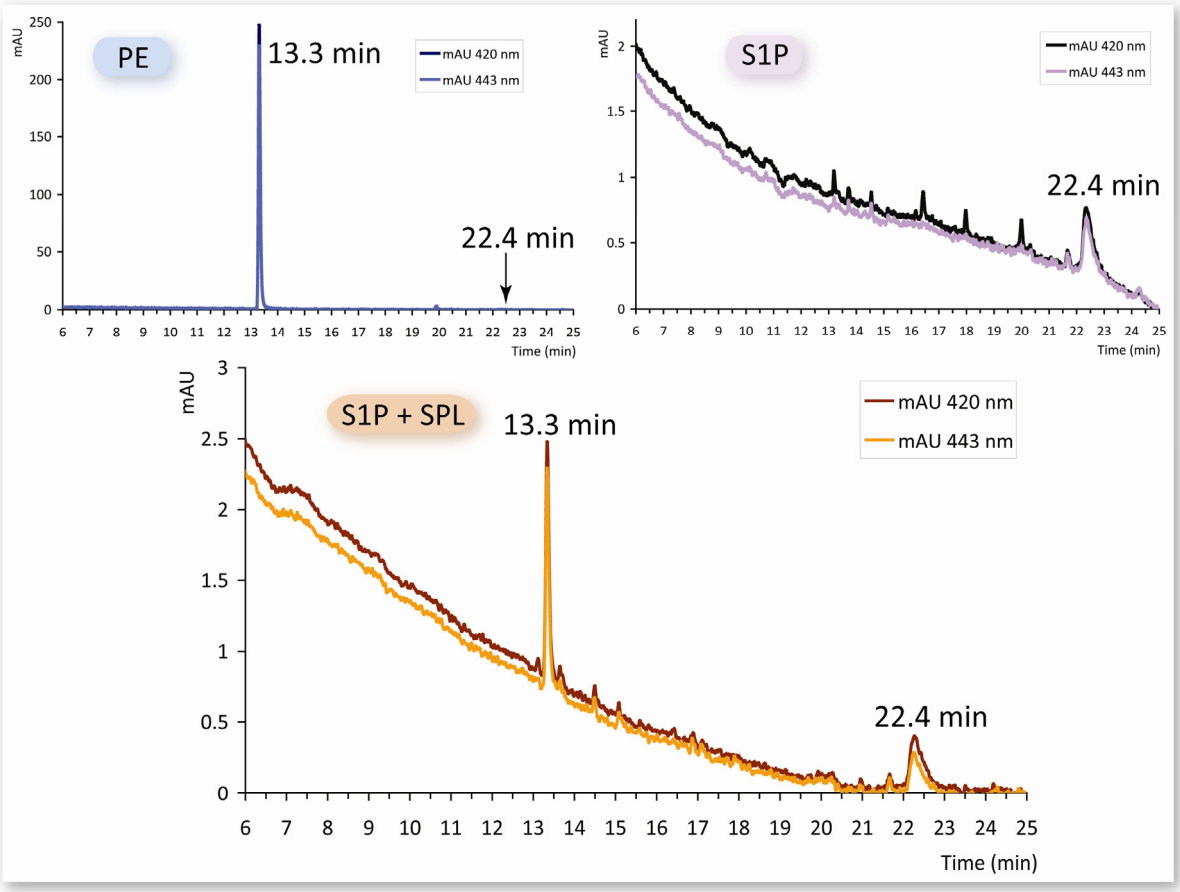

4.8. TRUNCATION STUDIES

4.8.1. PREDICTION- AND STRUCTURE-BASED DESIGN OF CONSTRUCTS

The first 60 residues of StSPL contain a strikingly high number of prolines (**figure 4-30**), suggesting a special structural or functional role. To test this hypothesis, N-terminal truncations were designed.

Figure 4-30. N-terminal 60 residues of FL WT StSPL

The first two N-terminal truncations were designed based on secondary structure prediction generated with the PSI-PRED server (187) (188) (http://bioinf.cs.ucl.ac.uk/psipred/psiform.html). The truncations started at residues P23 and P39, respectively. They lacked the predicted unstructured region preceding the first predicted helix and all residues until around the middle of the first helix (**figure 4-31**), respectively. Those two truncations, named Δ1-22 and Δ1-38 respectively, were cloned into pQE60 (**figure 4-32**).

Figure 4-31. PSIPRED secondary structure prediction of FL WT StSPL

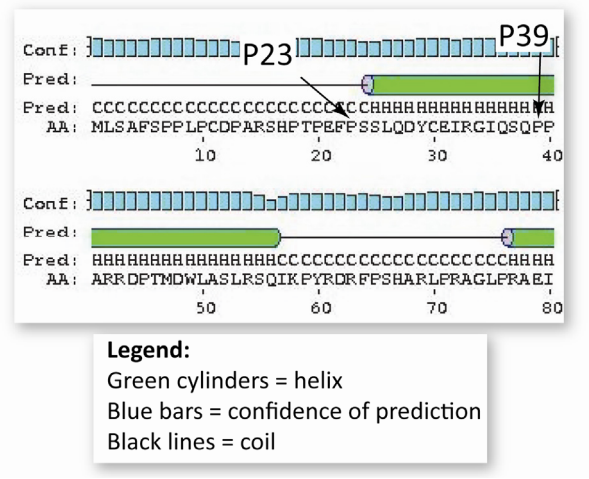

The next truncations were designed based on the available structural information (see part 3 (manuscript) **Fig. S1*A***). The Nt-FLEX domain (residues 1-57) is not visible or corresponds to disordered or below-average density in the electron density maps of all StSPL structures determined so far, indicating that these residues are, depending on conditions, either disordered or more flexible than the residues following them. The PSIPRED prediction indicates that a long helix should span residues 25 to 56. All residues until the end of this predicted helix were truncated and the corresponding construct was named ΔNt-FLEX (Δ1-57). The last two helices were removed in the construct named ΔCt-EXT (residues 1-471, that is Δ472-507) (see part 3 **Fig. S1*A***, coloured blue). This stretch extends over the putative active site channel entry and gets in contact with the N-terminus of the protein (coloured green in **Fig S1*A*** and ***D*** part 3). These residues are conserved among members of the SPL family (see chapter 2.3. **figure 2-5**) and are absent in *E. coli* GadB. The last residue of GadB corresponds to residue 471 of StSPL FL WT. Truncations ΔNt-FLEX and ΔCt-EXT were cloned into pQE70 (**figure 4-32**).

Figure 4-32. StSPL truncated variants cloned in pQE60 or pQE70

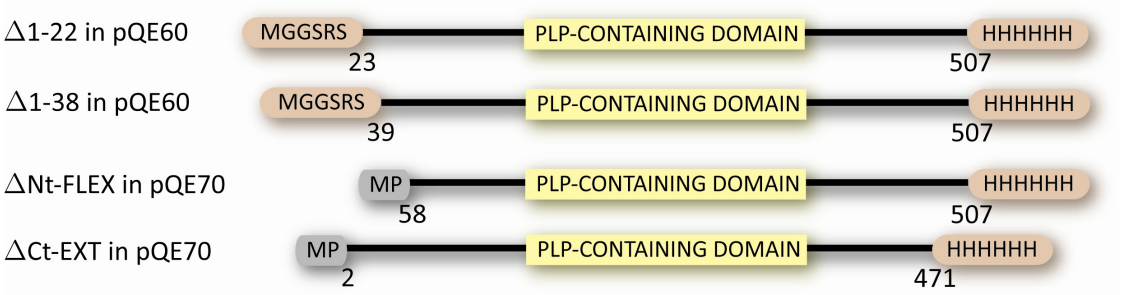

4.8.2. EXPRESSION IN *E. coli* AND PURIFICATION

The expression of pQE60 StSPL Δ1-22 and Δ1-38 was carried out according to the same protocol as FL WT StSPL (see Materials & Methods section 8.3.1. and part 3 (manuscript) SI *Text*). Neither truncation was expressed to a sufficient amount to be detected on a Coomassie-stained SDS-PAGE. Bands of StSPL Δ1-22 were hardly visible in the soluble fraction 4 h after induction using protein immuno-detection (**figure 4-33**). No signal is visible at all for StSPL Δ1-38. This indicates that both truncations are either not expressed or quickly degraded. It is difficult to determine whether this effect is due to the additional N-terminal residues MGGSRS (**figure 4-32**) that might destabilize the protein and promote its unfolding and subsequent degradation or is due to a crucial role that the residues 1-22 and 1-38 play in the folding and stability of StSPL. In light of the results showed thereafter on pQE70 StSPL ΔNt-FLEX, the first hypothesis seems more likely.

Figure 4-33. Expression of pQE60 FL WT StSPL, Δ1-22 and Δ1-38

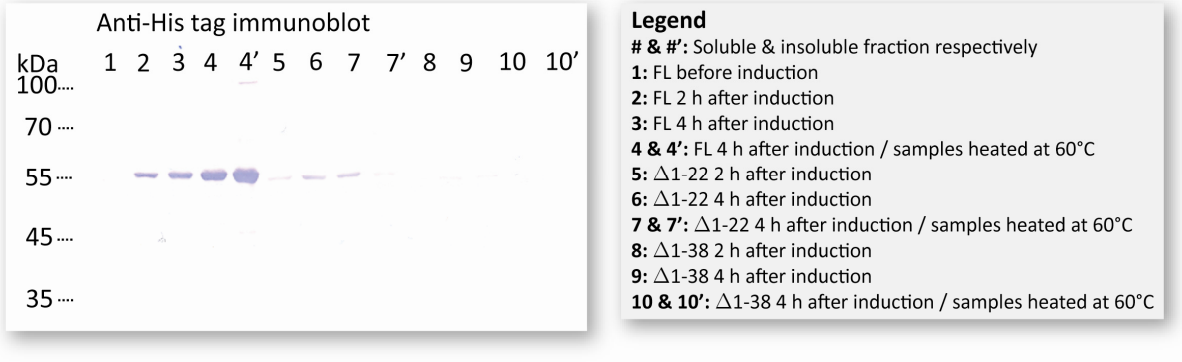

Unlike StSPL Δ1-22 and Δ1-38 cloned in pQE60, StSPL ΔNt-FLEX and ΔCt-EXT cloned into pQE70 were expressed in equal or slightly higher amounts as FL WT StSPL and were stable upon purification using the previously described protocol (**figure 4-34**). The three proteins showed slightly different SEC elution profiles. The 4mer-to-2mer peak ratio of both truncations was strikingly lower than for the FL protein, despite the fact that higher protein concentrations of truncated SPL were loaded onto the column (**figure 4-35**). This is in accord with the fact that residues 1 to 57 and 472 to 507 are involved in the tetramer formation, as seen from structure of the StSPL tetramer (see section 4.6.3. **figure 4-21**).

Figure 4-34. IMAC purification of pQE70 StSPL ΔNt-FLEX, ΔCt-EXT and FL

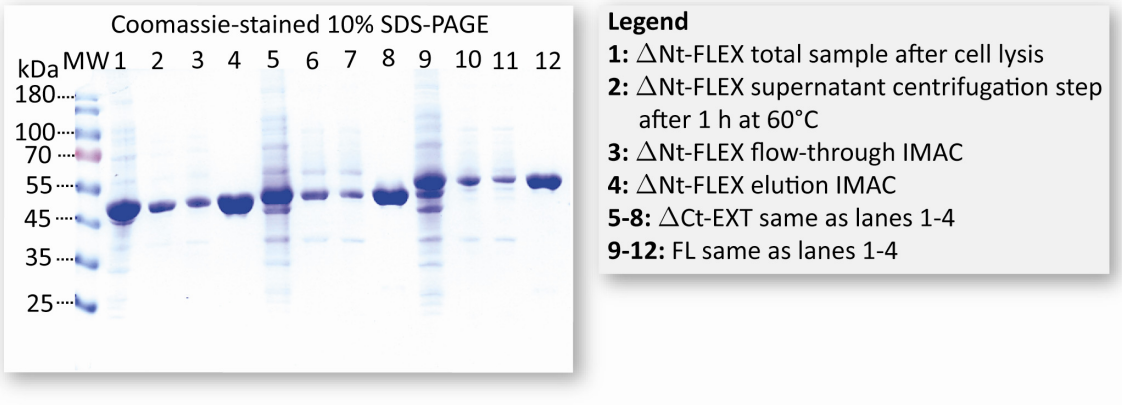

Figure 4-35. SEC purification of pQE70 StSPL ΔNt-FLEX, ΔCt-EXT and FL

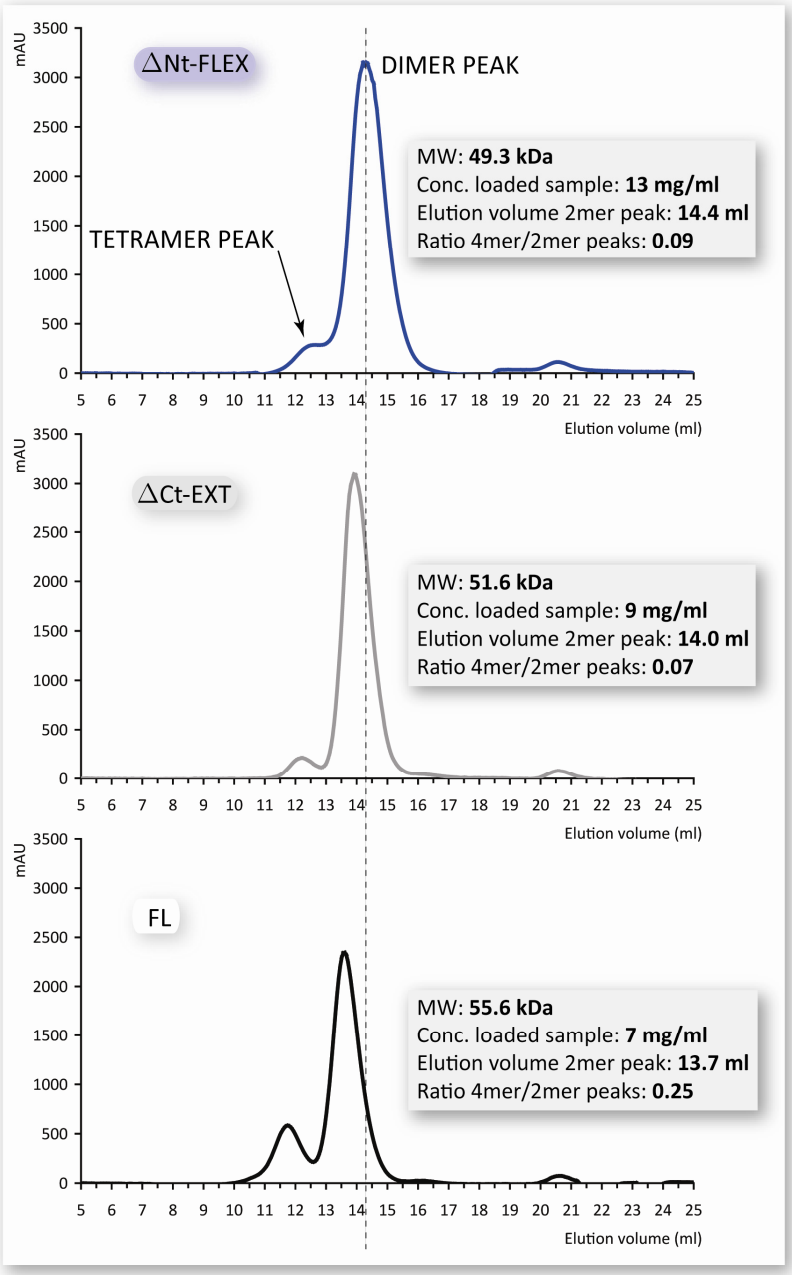

4.8.3. UV-VIS SPECTRA

StSPL ΔNt-FLEX and ΔCt-EXT produced altered visible absorption spectra compared to FL WT StSPL (**figure 4-36**). The spectrum of StSPL ΔNt-FLEX lacked the 345 nm small shoulder and StSPL ΔCt-EXT showed a broad peak at 345 nm with a shoulder at about 373 nm. Such differences observed in the latter SPL variant indicate that important changes occurred in the environment of the PLP (see section 4.4.1. figure 4-6).

Figure 4-36. UV-Vis spectra of StSPL ΔNt-FLEX, ΔCt-EXT and FL WT StSPL

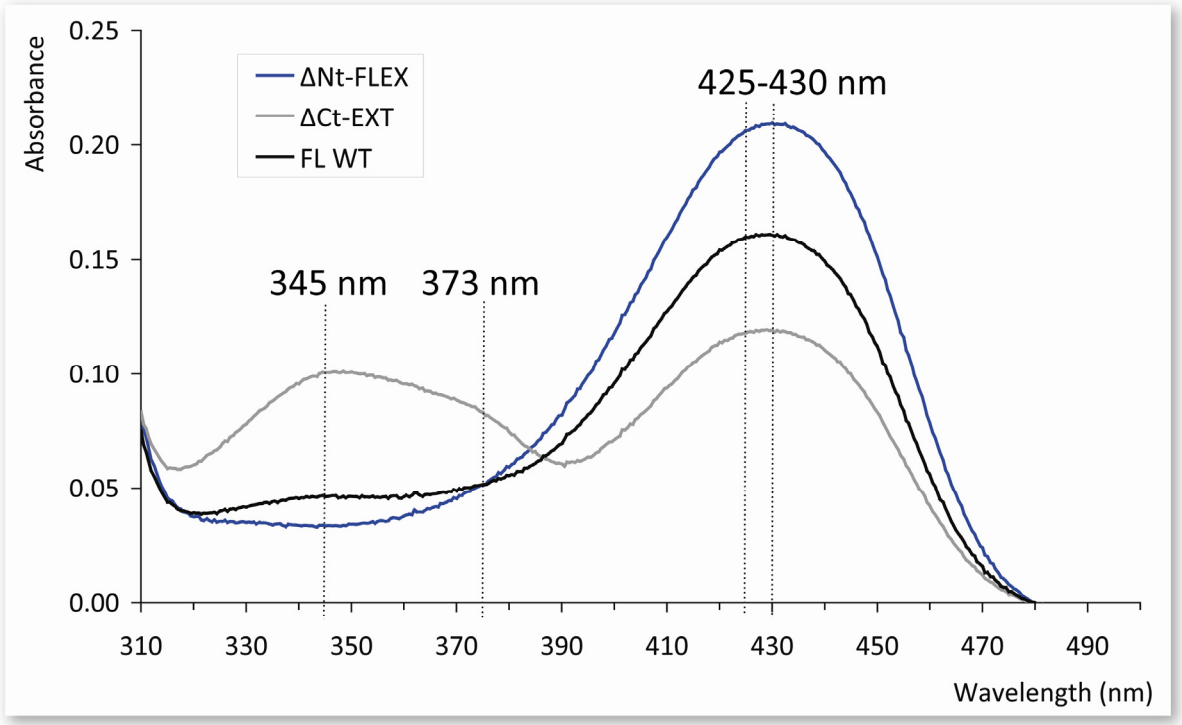

4.8.4. SPECTROPHOTOMETRIC ACTIVITY ASSAY

See part 3 (manuscript) **Fig. S4*A*** and ***B***.

4.9. MUTAGENESIS STUDIES

4.9.1. STRUCTURE-BASED DESIGN OF MUTANTS

StSPL mutants were designed with the aim to identify residues involved in activity, either in substrate polar head accommodation or in catalysis. Several sources were employed for the design. The structure of the PE-PLP complex and the derived model of S1P binding into the active site were used to localize residues presumably involved in substrate accommodation or close (within approximately 10 Å) to the bond to be cleaved (see part 3 (manuscript) **Fig. 3*B*** and section 4.6.6. **figure 4-23**). The structure of the dimer of FL WT StSPL with conformational heterogeneities (structure St_2) was used to design mutations by identifying residues on stretches that were either disordered or more flexible in the cofactor-lacking subunit, like S101, A103 and Y105 (**figure 4-37**). Serine, lysine, histidine, cysteine and tyrosine residues can act as nucleophiles or be involved in proton transfers. Glycine, alanine and proline may be important to define the degree of flexibility of a loop. H129* (coming from the other subunit) was chosen because it is located close to the polar head of S1P and has a higher B-factor in the active site lacking the cofactor (see part 3). Tyrosine 249 (**figure 4-37**) is seen to change conformation and partly replace the PLP in the structure of StSPL incubated with semicarbazide (structure St_4): it might also be involved in activity either in catalysis or in substrate accommodation, despite being replaced by phenylalanine in yeast and human SPLs (**table 4-11**). A recent mutagenesis analysis carried out on Dpl1p using an *in vivo* activity assay (112) showed that residues (StSPL numbering) C276, K311, K317 and Y482 (**figure 4-37**) are involved in activity to various extents. C276 had already been reported to be critical for activity of human SPL (where it corresponds to C317) (61). Human SPL was shown to be nitrosylated on residues Y356 and Y366 (128), corresponding to Y314 and Y324, respectively, in StSPL. This modification, which may be specific to higher eukaryotic SPL, might indicate that those residues, despite being relatively far away from the active site, are involved in activity or in conformational changes.

It should be mentioned that the present mutagenesis study was restricted to residues supposedly involved in catalysis or in the accommodation of the polar head of the substrate. Accommodation of the hydrophobic tail of the substrate was not addressed, since the structure of the protein with S1P was not known. The designed mutations, as well as the corresponding residues in yeast and human SPLs are listed in **table 4-11**.

Figure 4-37. Stereo view of WT StSPL active site showing the residues mutated in this study

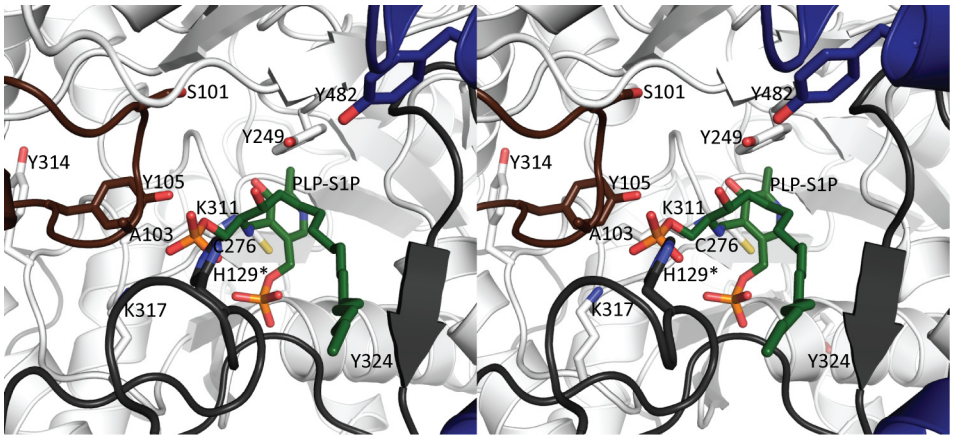

Table 4-11. FL StSPL mutagenesis studies (grey highlight)

StSPL	Mutation	Putative role(s)	Conservation	Dpl1p	HsSPL
S101	**S101A**	Active site loop conformation	Yes	S170	S146
A103	**A103P**	Active site loop conformation	No	A172	T148
Y105	**Y105F**	Catalysis/ Substrate polar head accommodation	Yes	Y174	Y150
N126		*Substrate polar head accommodation*	*Yes*	*N195*	*N171*
L128		*Substrate hydrophobic tail accommodation*	*Yes*	*L197*	*L173*
H129	**H129A**	Substrate polar head accommodation / Catalysis	Yes	H198	H174
P130		*Substrate hydrophobic tail accommodation / Active site conformation*	*Yes*	*P199*	*P175*
H201		*PLP pyridine ring stacking*	*Yes*	*H268*	*H242*
C276	**C276A**	Catalysis/ PLP pyridine ring stacking	Yes	C344	C317
Y249	**Y249F**	Catalysis / Substrate accommodation	No	F317	F390
H310		*Cofactor binding*	*Yes*	*H379*	*H352*
K311	**K311A**	Catalysis (internal aldimine)	Yes	K380	K353
Y312		*Active site conformation / Catalysis*	*Yes*	*Y381*	*Y354*
Y314	**Y314F**	Active site conformation (nitrosilation in corresponding HsSPL residue)	No	F383	Y356
K317	**K317A**	Catalysis / Substrate polar head accommodation	Yes	K386	K359
Y324	**Y324F**	Protein conformation (nitrosilation in corresponding HsSPL residue)	Yes	Y393	Y366
Y345		*Substrate accommodation / Catalysis*	*Yes*	*Y414*	*Y386*
F346		*Substrate hydrophobic tail accommodation*	*No*	*L413*	*I387*
Y482	**Y482A/F**	Substrate accommodation / Regulation of activity and local conformation	Yes	Y554	Y526
F500		*Substrate hydrophobic tail accommodation*	*Yes*	*F573*	*F545*
L504		*Substrate hydrophobic tail accommodation*	*Yes*	*L577*	*L549*

4.9.2. EXPRESSION IN *E. coli* AND PURIFICATION

FL SPL proteins carrying the desired mutation were cloned in pQE70, expressed in *E. coli* and purified according to the same protocol as WT StSPL (described in part 3 (manuscript) SI *Text* and in Materials & Methods section 8.3.1.). All mutants described below except A103P were expressed to a similar amount to that of WT StSPL. In comparison, the overall amount of StSPL A103P expressed was significantly lower. Purification of this mutant was nevertheless possible and the yield after SEC was similar to that of WT, as for all other mutants. The mutants A103P and K311A showed a significantly lower tetramer-to-dimer peak ratio on SEC than WT (**figure 4-38** blue, green and black traces, respectively).

Figure 4-38. SEC elution profile of StSPL WT, A103P and K311A

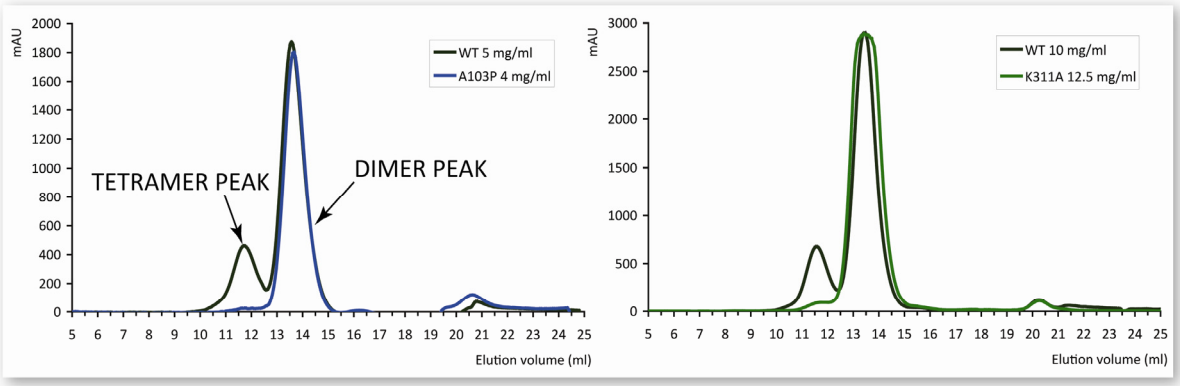

4.9.3. UV-VIS SPECTRA

All mutants except StSPL K311A (described in section 4.4.1.) and C276A exhibited a similar UV-Vis absorption spectrum as the WT. Compared to FL WT StSPL, C276A displayed a broad asymmetric peak at 335 nm and a lower peak at 425 nm (see part 3 (manuscript) **Fig. 4*A*** and ***E*** respectively).

4.9.4. SPECTROPHOTOMETRIC ACTIVITY ASSAY

StSPL mutants K311A, Y105F, Y482F, C276A, H129A, A103P, K317A and Y249F are described in part 3 (manuscript) **Fig. 4**, **S5** and **S6**.

StSPL mutants S101A, Y314F and Y324F behaved as WT StSPL upon addition of S1P (data not shown). StSPL S101A underwent spectral changes over time in the 380 nm region (**figure 4-39**). Similar changes were also observed in the inactive mutants A103P and K317A and also in the nearly inactive H129A (part 3, **Fig. S6**). Since S101 and A103 are presumably involved in the accommodation of the polar head of S1P, the shift at 380 nm might be explained by an impaired positioning of the substrate resulting in changes in the cofactor environment. K317 is at approximately 5 Å from the phosphate moiety, so it can shares with it a long-distance electrostatic interaction, and is likely involved in catalysis. StSPL Y482A behaved like Y482F (data not shown).

Figure 4-39. S1P-induced spectral changes of StSPL S101A

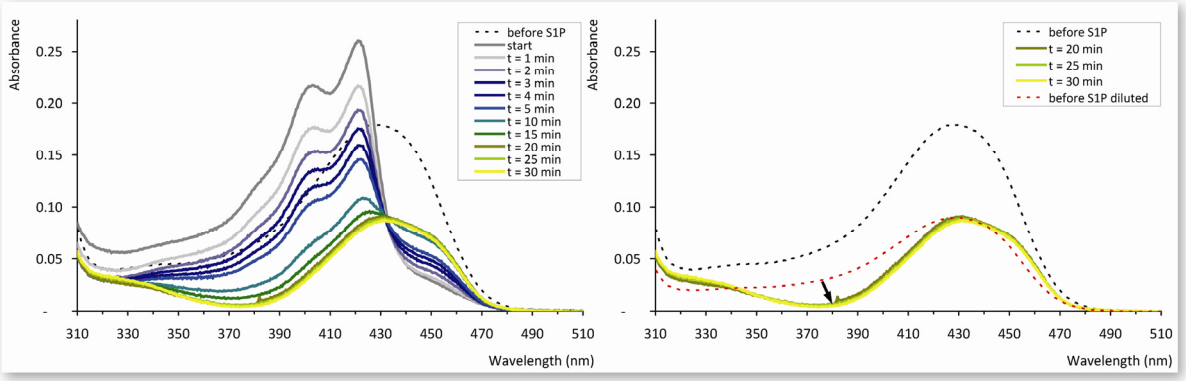

Table 4-12. Summary of StSPL truncation and mutagenesis studies

Variant	Reference	Native spectrum[1]	403 & 420 nm-peaks[2]	Relaxation time	Back to native spectrum[3]	ACTIVITY
ΔNt-FLEX	Part 3 Fig. S6*A*	Similar to FL	Yes	**Faster than FL**	Yes	**ACTIVE**
ΔCt-EXT	Part 3 Fig. S6*B*	**Shoulders at 345 & 373 nm & lower 425 nm-peak**	Yes	**Slower than FL**	**No**	**PARTLY ACTIVE**
S101A	Section 4.9.4.	Similar to WT	Yes	Similar to WT	**No**	**ACTIVE**
A103P	Part 3 Fig. S6*D*	Similar to WT	**No**		**No**	**INACTIVE**
Y105F	Part 3 Fig. 4	Similar to WT	**No**			**INACTIVE**
H129A	Part 3 Fig. S6*C*	Similar to WT	**Very faint**		**No**	**PARTLY ACTIVE**
C276A	Part 3 Fig. 4*E*	**Shoulder at 330 nm & lower peak 425 nm**	Yes	**Slower than WT**	**No**	**PARTLY ACTIVE**
Y249F	Part 3 Fig. S5*E*	Similar to WT	Yes	Similar to WT	Yes	**ACTIVE**
K311A	Part 3 Fig. 4*B*	**Shoulder at 330 nm**	**No**			**INACTIVE**
Y314F	Section 4.9.4.	Similar to WT	Yes	Similar to WT	Yes	**ACTIVE**
K317A	Part 3 Fig. S6*E*	Similar to WT	**No**		**No**	**INACTIVE**
Y324F	Section 4.9.4.	Similar to WT	Yes	Similar to WT	Yes	**ACTIVE**
Y482F/A	Part 3 Fig. 4*D* & section 4.9.4.	Similar to WT	Yes	**Slower than WT**	Yes	**PARTLY ACTIVE**

[1] The spectrum of FL WT StSPL is taken as reference.
[2] Upon addition of substrate.
[3] Within the measurement time (usually 60 minutes).

4.10. DISCUSSION AND PERSPECTIVES

4.10.1. EFFECT OF DIVALENT CATIONS

The conformational heterogeneities observed between the subunits of structure St_2 might be explained by the presence of 100 mM $MgCl_2$ in the crystallisation drop at plate setup. Crystals grew in one day following the appearance of the initial heavy precipitate (see section 4.5.1. **figure 4-12**). Those crystals could not be reproduced to date. Co-crystallisation trials were made in 100-fold molar excess of divalent cations over SPL active site that amounted to 10.7 mM divalent cations at plate setup. No bound cation was found and no significant conformational changes were observed in this structure (section 4.6.4. structure St_9) compared to the native enzyme (structure St_1). Soaking native crystals in solutions of increasing concentration of Mg^{2+} does not promote significant conformational changes (see section 4.6.4. structures St_6-8). Nevertheless, a decrease in resolution was observed with increased Mg^{2+} concentration in the soaking solution. This strongly suggests, but does not prove, that under the crystallisation conditions of St_6-8 binding of Mg^{2+} disturbs the crystal lattice.

4.10.2. CONFORMATIONAL HETEROGENEITIES (STRUCTURE St_2)

In structure St_2 (part 3 (manuscript) **Fig. 2**), a chloride ion is found in the active site instead of a phosphate ion in the other structures. The concentration of chloride in the drop at plate setup was 4 times higher (200 mM) than in the other structures that lack $MgCl_2$ and was 8 times higher than the phosphate concentration. Interestingly, chloride is found in the subunit containing PLP.
A regulation mechanism of mammalian glutamate decarboxylases (GAD) activity rests on modulating the protein affinity towards PLP. One fraction of one isoform of GAD frequently lacks PLP and the ratio between the holo- and apo-forms varies upon stimulation depending on the tissue (189). Serine palmitoyl-transferase (SPT, see section 1.5.5.) shares this feature since one subunit of the heterodimer strictly required for activity lacks PLP. This confirms that the conformational heterogeneities observed in the subunit lacking PLP in structure St_2 correspond to regions involved in activity and that StSPL activity might be regulated by modulating the affinity towards PLP.

4.10.3. PROPOSED REACTION MECHANISM

Based on the outcome of the mutagenesis studies, a reaction mechanism for the hydrolysis of S1P by StSPL can be proposed (**figure 4-40** and part 3 (manuscript) **Fig. S7**). The initial proton abstraction (**figure 4-40** ***step III***) may be carried out by residues K311, K317 or Y105, residues fulfilling both criteria of proximity to the proton on the C2 carbon atom of the substrate and of total inhibition upon mutation (mutant Y174F of Dpl1p, corresponding to StSPL Y105F, is however seen to be partly active). Mutant A103P is also fully inactive, confirming the role of residues 89 to 108 (see 4.6.2. and part 3 **Fig. 2** and **S6**), which are disordered on the subunit lacking PLP of structure St_2. The quinonoid reprotonation step (***step VI***) could be carried out by residues C276, K311 or by a water molecule. Mutation of C276 does not inactivate the enzyme, but slows down the enzyme turn-over. The residue C276 is eclipsed behind PLP in the resting state but the active site might undergo moderate rearrangements upon catalysis (for instance, rotation of the cofactor). The C2-C3 bond to be cleaved is expected to be perpendicular to the cofactor ring and parallel to its π system,

according to Dunathan's hypothesis (190). Mutating residue Y482 leads to a similar behaviour to that of the C276 mutant: given that Y482 is far from the cofactor and located in a region that is seen to undergo conformational asymmetry and disorder, it is tempting to speculate that this residue may involved in the regulation of enzymatic activity. Residue H129 is also very important for activity, even though the mutant H129A is not completely inactive in the spectrophotometric activity test. H129 is likely responsible for the accommodation of the phosphate head of the substrate (section 4.9.1. **figure 4-38**).

Figure 4-40. Proposed mechanism for the cleavage of S1P by StSPL

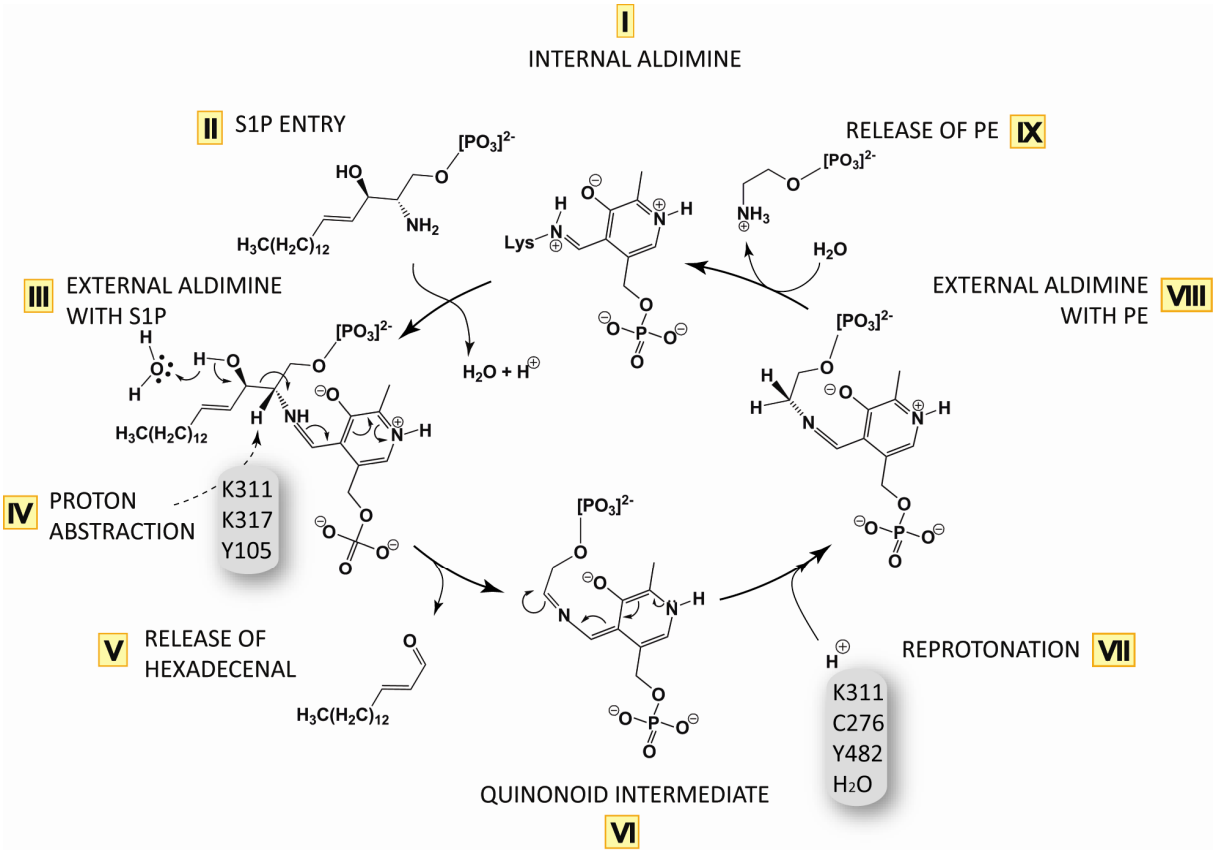

Further investigation of the role of other conserved residues among SPL, like N126, P130, H201, H310, Y312 and Y345 (see **table 4-11** and **figure 4-41**) may provide additional information on the reaction mechanism.

Figure 4-41. Additional residues of StSPL putatively involved in activity

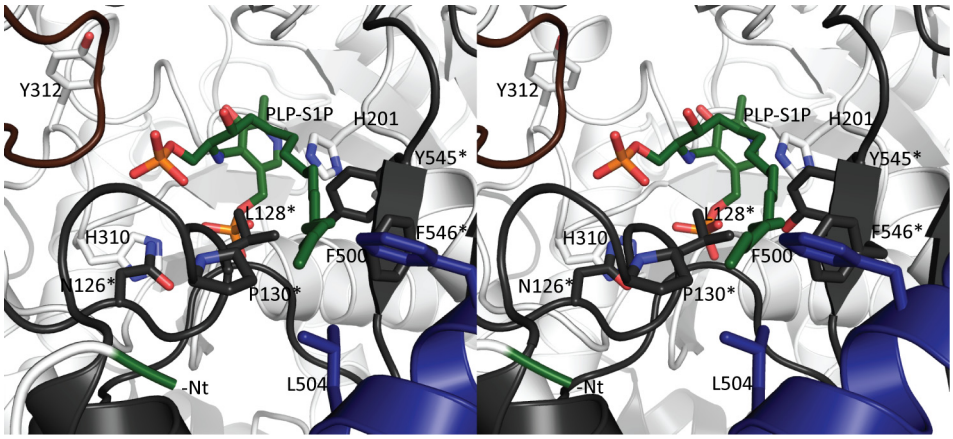

Kinetics data aimed at determining the dissociation constant K_M and the maximal enzymatic rate v_{max} are a prerequisite to validate the proposed reaction mechanism. To this purpose, a recently described fluorogenic substrate may be of interest (**figure 4-42**) (142).

Figure 4-42. SPL activity assay using a fluorogenic substrate

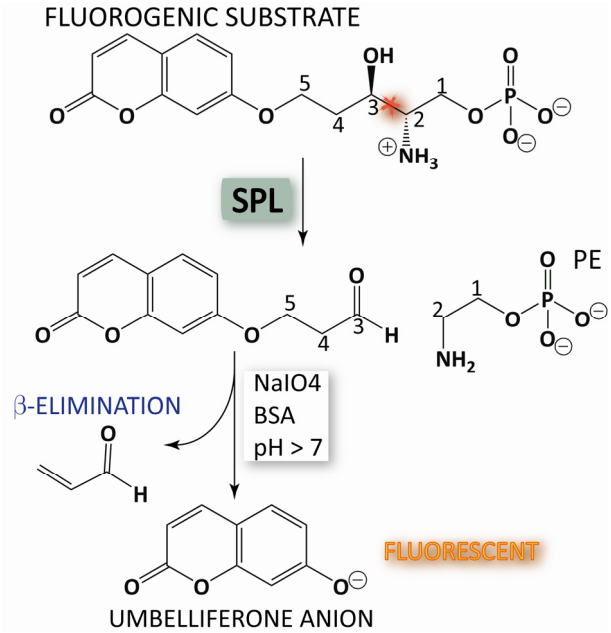

To discriminate between residues involved in substrate accommodation or in catalysis a S1P binding assay of StSPL WT and mutants may be performed using surface plasmon resonance (SPR) and isothermal titration calorimetry (ITC) (191). In all cases, optimized S1P solubilisation conditions are needed and SPL must be stable under those conditions. Circular dichroism (CD) may be a valuable technique to assess SPL folding and aggregation state under various conditions (192).

The precise binding mode of S1P within the active site must be precisely known to validate and extend the proposed mechanism. Large conformational changes upon substrate binding are likely to happen given the hydrophobicity of the substrate and the cytoplasmic localisation of the active site of SPL. Assuming that these conformational changes do not prevent crystallisation and diffraction to high resolution, co-crystallisation seems to be the

method of choice since the addition of the substrate solution to a crystal may disturb its lattice, thus leading to poor resolution in diffraction experiments. Several other approaches may be considered. Another mutant instead of K311A may be used for co-crystallisation experiments, like Y105F. A shorter, non-natural compound can be used instead of S1P (18C). Such a substrate is to date not commercially available. It should be kept in mind that the binding mode of a less hydrophobic substrate analogue might not reflect all the conformational changes undergone by the enzyme to accommodate the natural substrate.
Last but not least, the excess of S1P over active sites of SPL must be increased. At the maximal theoretical concentration of S1P (5 mM), the highest molar excess used in co-crystallisation experiments was 20-fold, whereas it reached 100-fold in the spectrophotometric activity assay (where the protein concentration was set to 1.2 mg/ml before addition of 70 µl of S1P and reached 0.7 mg/ml after). Since the protein does not crystallise below a concentration of approximately 5 mg/ml (after dilution with well solution), the solubility of S1P must be improved to reach the desired molar excess. Neutralizing the negative charges of the polar head of S1P by addition of acid significantly increases the solubility of S1P in organic solvent (to at least 20 mM in acidic DMSO). The drawback is that the absence of negative charges in the polar head might prevent the (correct) substrate accommodation within the active site, especially in light of the fact that positively charged residues like K317 and H129 are very likely to bind the polar head of S1P (see above). Moreover, SPL might unfold in acidic conditions or at least loose some activity. Detergents, with the exception of Triton X-100, seem to inhibit the enzyme. Organic solvents may destabilize SPL (SPL precipitates in concentrations of ethanol higher than 15%) and might bind S1P too strongly, restricting the access of SPL to the substrate. Reconstituting S1P into cholesterol and phospholipid liposomes may mimic natural conditions and offers an alternative to organic solvents and detergents.
Another approach is to add the complex PLP-S1P to an apo- StSPL inactive mutant (that is an enzyme lacking PLP). This approach was successfully used for the reported recently structure determination of LL-diaminopimelate aminotransferase (LL-DAP-AT) in complex with its substrate (193). Since PLP spontaneously forms a Schiff base with primary amines, as is the case with Tris (data not shown), a Schiff base between PLP and S1P is assumed to be formed similarly. The complex PLP-S1P is more hydrophilic than S1P and might allow reducing the amount of detergent or solvent required for its solubilisation. On the other hand, SPL might not be able to accommodate the bulkier and more hydrophilic complex, at least not *via* the same channel as S1P. Such a problem is not very likely to arise in light of the behaviour of the PLP-semicarbazide adduct, which is seen to be able to quantititatively leave the active site.

4.10.4. HOMOTETRAMER INTERFACE

The tetramer-dimer equilibrium of StSPL naturally lends itself to mutagenesis studies. Mutating residues involved in the dimer-to-dimer contacts might disrupt the tetramer. This is rather tedious work given the number of involved residues and can lead to enzyme inactivation (see section 4.6.3 structure St_5).
Both the N- and the C- terminal truncations lacking residues 1 to 57 and 472 to 507 (ΔNt-FLEX and ΔCt-EXT), respectively, have a significantly lower tetramer content compared to FL WT StSPL (see section 4.8.2 **figure 4-35**). Since StSPL ΔNt-FLEX is active whereas the activity of StSPL ΔCt-EXT is impaired, StSPL ΔNt-FLEX might be screened for a C-terminal truncation still producing an active dimer.
Varying the salt concentration and the surface net charges at different pHs might affect the relatively small interface (approximately 600 $Å^2$). Therefore, pH, ionic strength and salt content of the SEC buffer can be screened to monitor any changes in the tetramer-to-dimer peak ratio.

4.10.5. DISORDERED N-TERMINUS

The first 60 residues of StSPL (see section 4.8.1. **figure 4-30**) possess a high content of prolines and is conformationally disordered in the electron density maps examined to date. Amphipathic proline-rich peptides are known to penetrate lipid bilayers (recently reviewed in (194)) and to be involved in protein binding events, especially to SH3 domains of proteins (195) (196).
Intrinsically disordered regions, also called natively unfolded regions, are often involved in protein or lipid interactions (197). The N- and C-termini of the tumour suppressor p53 are intrinsically disordered (198). Its N-terminal disordered region contains a proline-rich repeat (PRR) which seems to be preferentially projected away from the core domain. Deletion of the PRR of the p53-related protein p63 abolishes its transactivation potential (199).
Surprisingly, StSPL ΔNt-FLEX seems to be more active *in vitro* than WT StSPL (see part 3 (manuscript) **Fig. S6*A***). This might support the hypothesis that the N-terminal stretch interacts with the membrane, either to position the protein for cleavage of S1P still embedded within the membrane or to extract the substrate from the bilayer. Such a mechanism is not required *in vitro*, since the substrate is solubilised in detergent or in organic solvent.
Additionally, Nt-FLEX might wrap onto Ct-EXT to close the active site (see part 3, **Fig. S1*D***). The lack of the active gate might facilitate access to the active site and increase the cleavage turn-over compared to WT StSPL. Small-angle X-ray scattering (SAXS) might be of interest to unravel the behaviour of StSPL Nt-FLEX.

4.10.6. SUBSTRATE ACCOMMODATION

SPL might bind its substrate by interacting with the membrane similarly to peripheral membrane proteins (which do not span the membrane, unlike integral membrane proteins). Phospholipases, protein kinases C, lipid kinases and lipid phosphatases translocate to and interact with cellular membranes upon stimulation (191) (200) and their activity depends on their affinity to the membrane. *E. coli* pyruvate oxidase (EcPOX) undergoes conformational changes upon binding of pyuvate that trigger membrane association most presumably according to ***mode II*** on **figure 4-43** (201). Recently, a report on the structure of *Aquifex aeolicus* sulphide:quinone oxidoreductase (SQR) and its putative membrane insertion mechanism was published (202). A helix-turn-helix motif penetrates into the membrane according to ***mode II*** to access the hydrophobic substrate quinone. Similarly, carnitine palmitoyltransferase 2 (CPT2) associates with the membrane (203) *via* a helix turn-helix motif composed of hydrophobic (tryptophan, phenylalanine, valine and leucine) and basic residues (lysine and arginine). In StSPL the first stretch of 60 residues (see section 4.8.1. **figure 4-30**) is indeed rich in proline and arginine, which might directly interact with S1P in the membrane while stabilizing the interaction by binding to the polar heads of phospholipids (***mode III***). *Bacillus subtilis* sphingomyelinase is assumed to interact with the membrane *via* a β-hairpin that might transport the substrate within the active site (***mode II***) (see section 1.5.1.).

Figure 4-43. Various modes of protein-membrane interaction

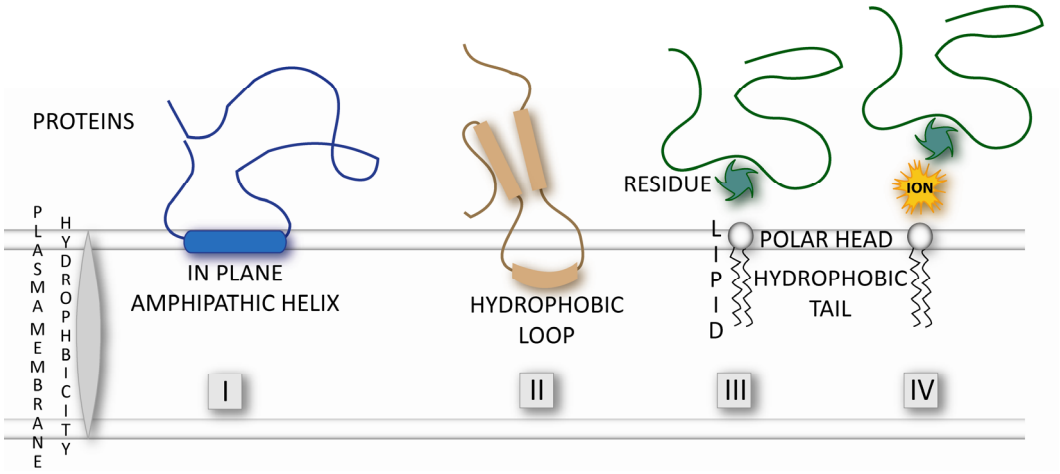

Once in contact with S1P still embedded into the membrane, SPL might cleave it or extract and accommodate it into the active site. This latter option might be possible since CERT (see section 1.5.3., ceramide transport protein) and GLTP (see section 1.5.4. glycolipid transfer protein) are able to extract sphingolipids from their natural environment. Alternatively, StSPL might interact with an S1P carrier similar to CERT and GLTP and able to deliver S1P to SPL.

5. RESULTS & DISCUSSION *Saccharomyces cerevisiæ* Dpl1p (Dpl1p)

5.1. HOMOLOGY MODEL-BASED TRUNCATIONS DESIGN

Unlike StSPL, Dpl1p possesses a predicted transmembrane helix spanning residues 58 to 81 (**figure 5-1**). Compared to *E. coli* GadB, both SPLs have a C-terminal extension (the Ct-EXT domain) corresponding to residue 542-589 in Dpl1p (see part 3 (manuscript) **Fig. S1*A*** and ***B***).

Figure 5-1. GadB, Dpl1p, and StSPL topology

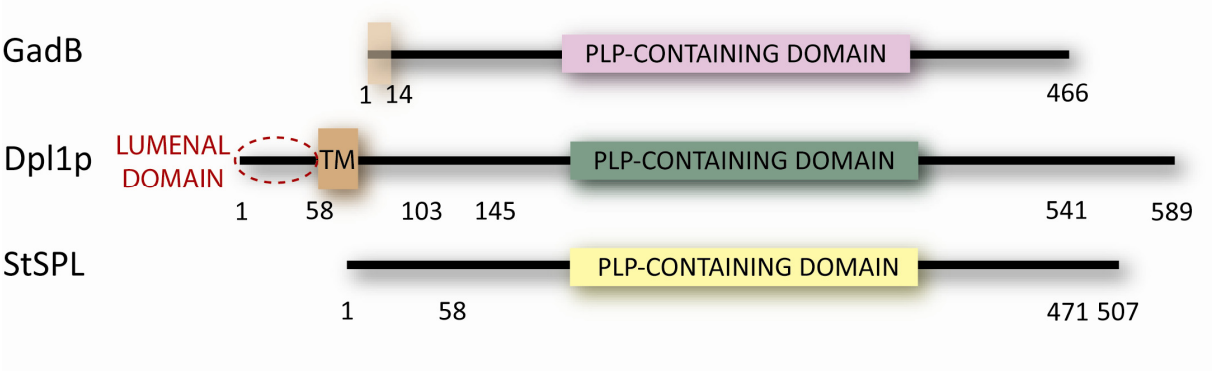

A preliminary homology model of Dpl1p was generated based on the structure of GadB and sequence analysis of the 1-145 region of Dpl1p. The program COILS (http://www.ch.embnet.org/software/COILS_form.html) (204) predicted a coiled-coil region for residues 106-135. An open question about this initial model is that a hexameric arrangement like in GadB implies the presence of two coiled-coil regions, followed by transmembrane and lumenal domains, departing axially from the hexamer in opposite directions (**figure 5-2** *left*): thus, the protein would have two transmembrane domains, one of which should be either unfolded or maybe binding to an unknown "shielding" protein with a hydrophobic surface. Such assumptions are of course not necessary for a dimeric arrangement (**figure 5-2** *right*).

Figure 5-2. Dpl1p predicted homology-model based topologies

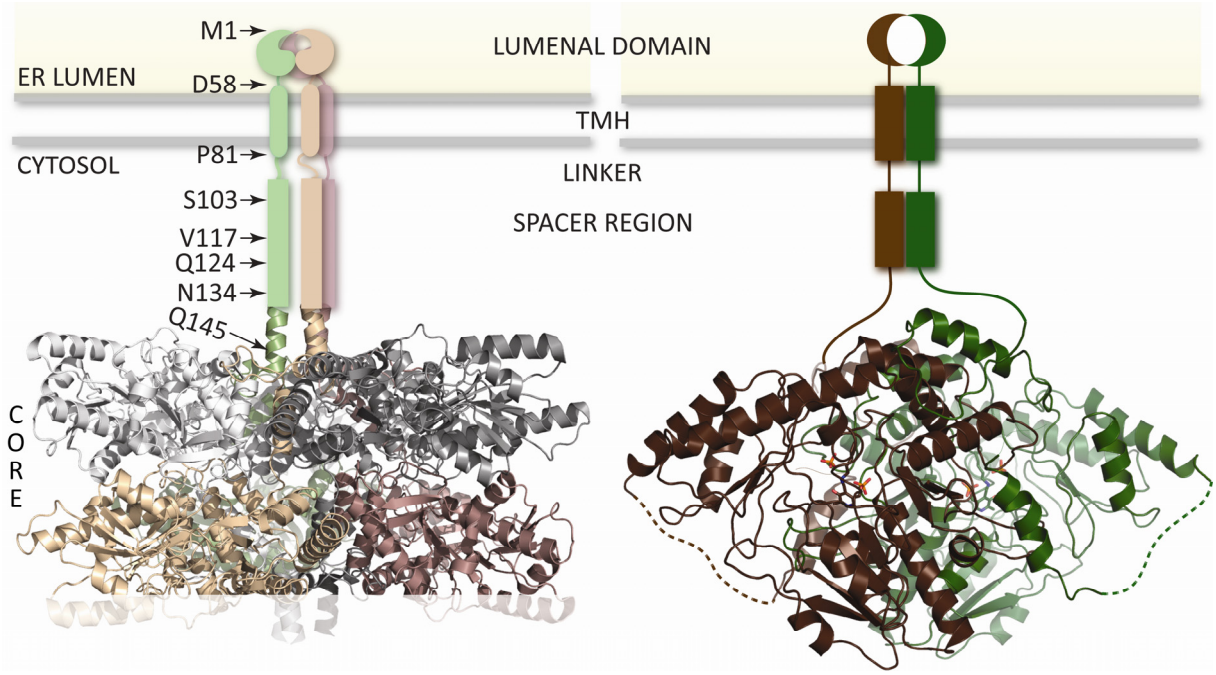

This initial model of Dpl1p served to design soluble truncations to avoid using detergents in protein production and in crystallisation trials and to remove predicted floppy stretches that could hinder crystallisation. All truncations designed and expressed in pET28a+ are listed in **table 5-1**. The additional residues resulting from cloning are shown in **figure 5-3**.

Table 5-1. Dpl1p truncations

TRUNCATION	STARTING / ENDING RESIDUE	FEATURES
Δ1-81	V82 / K589	Longest soluble construct
Δ1-102	S103 / K589	Start in the linker / spacer region
Δ1-116	V117 / K589	
Δ1-123	E124 / K589	
Δ1-133	N134 / K589	
Δ1-144	Q145 / K589	Core of the protein
Δ1-116:ΔCt-EXT	V117 / S541	Truncation of Ct-EXT
Δ1-133:ΔCt-EXT	N134 / S541	

Figure 5-3. Additional residues of Dpl1p truncations cloned into pET28a+

Note: constructs Δ1-81 and Δ1-116 have no additional G at their N-terminus.

5.2. EXPRESSION IN *E. coli*

The expression conditions were optimized for construct Dpl1p Δ1-116 as described in Materials & Methods section 8.3.2. and in part 3 (manuscript) SI *Text*: the resulting optimized conditions are summarized in **table 5-2**. Noteworthy, adding 10 mM glucose in the culture medium is a prerequisite for protein expression. Bacteria grown in a medium lacking glucose did not express the protein at all (data not shown). Supplementing the medium with 100 mM glucose reduced the protein expression level. Protein production was monitored by 10 % SDS-PAGE and anti-His tag protein immuno-detection (Western blot). The constructs displayed various expression patterns.

Table 5-2. Optimized expression conditions for Dpl1p truncations

Expression system	pET
***E. coli* strain**	HMS174(DE3)
Medium composition	LB (10 g tryptone, 5 g yeast extract, 10 g NaCl) 0.1 g/l pyridoxine 10 mM glucose Appropriate antibiotics
Starting $OD_{600\ nm}$ (500 ml medium)	0.02
$OD_{600\ nm}$ at induction	0.8
IPTG concentration	0.1 mM
Chemicals added at induction	0.1 g/l pyridoxine
Temperature	30°C
Expression duration	24 hours

Dpl1p Δ1-81 was not expressed in sufficient amounts to be visible on Coomassie-stained SDS-PAGE. N-terminal degradation was observed on anti-His tag immuno-blot 30 min after induction of expression in both HMS174(DE3) and BL-21(DE3), a protease-deficient strain (**figure 5-4** lanes 3, 4 and 6). The overall expression level in BL-21 was significantly lower than in HMS174. Dpl1p Δ1-81 was IMAC-purified from 2 L culture harvested 30 min after induction, with the aim of determining the starting residue of the degradation products by N-terminal sequencing. Only ***band B*** (**figure 5-4**) provided unambiguous signals corresponding to truncations Δ1-132 and Δ1-133 (data not shown). The estimated purity of the sample after IMAC was lower than 5 % and the yield of the Dpl1p-derived bands (A, B, C) lower than 0.05 mg per litre culture. Interestingly, truncation Δ1-81 expressed in yeast also seemed to undergo degradation, suggesting that this protein variant is intrinsically instable (see section 5.3.1.).

Figure 5-4. Soluble expression of Dpl1p Δ1-81 in *E. coli* HMS174(DE3) and BL-21(DE3)

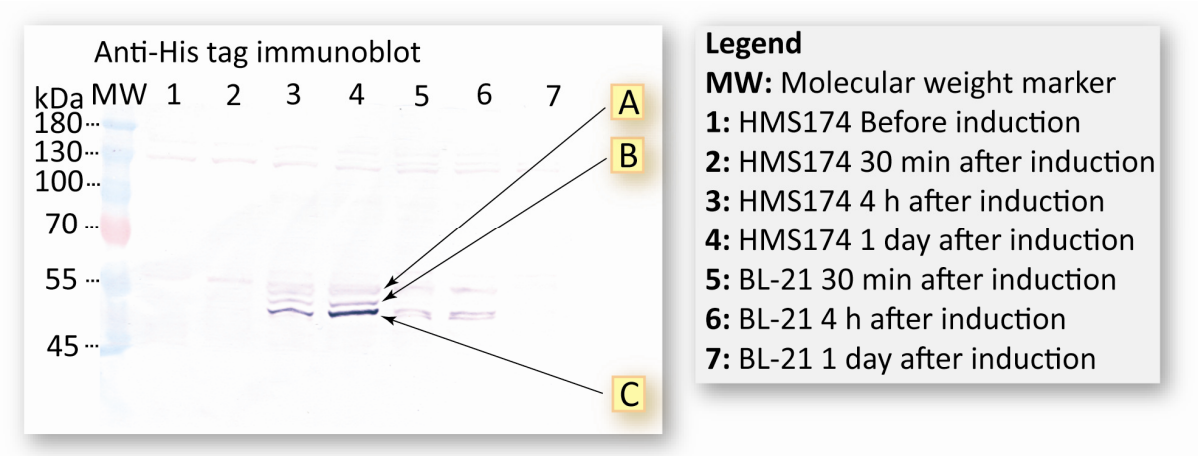

Dpl1p Δ1-133 was likewise expressed in *E. coli.* No sharp band corresponding to this truncation was visible on Coomassie-stained SDS-PAGE, suggesting either a low expression level or some degradation after expression. Since the construct did not undergo visible degradation on immuno-blot (data not shown), the construct was purified and used for crystallisation trials (see section 5.3.3.). Truncation Δ1-116 was the first construct initially designed based on the homology model of Dpl1p (**figure 5-2**). It turned out to be highly expressed in *E. coli* (**figure 5-5**) and stable upon purification (see section 5.3.2.).

Figure 5-5. Expression of Dpl1p Δ1-116 in *E. coli*

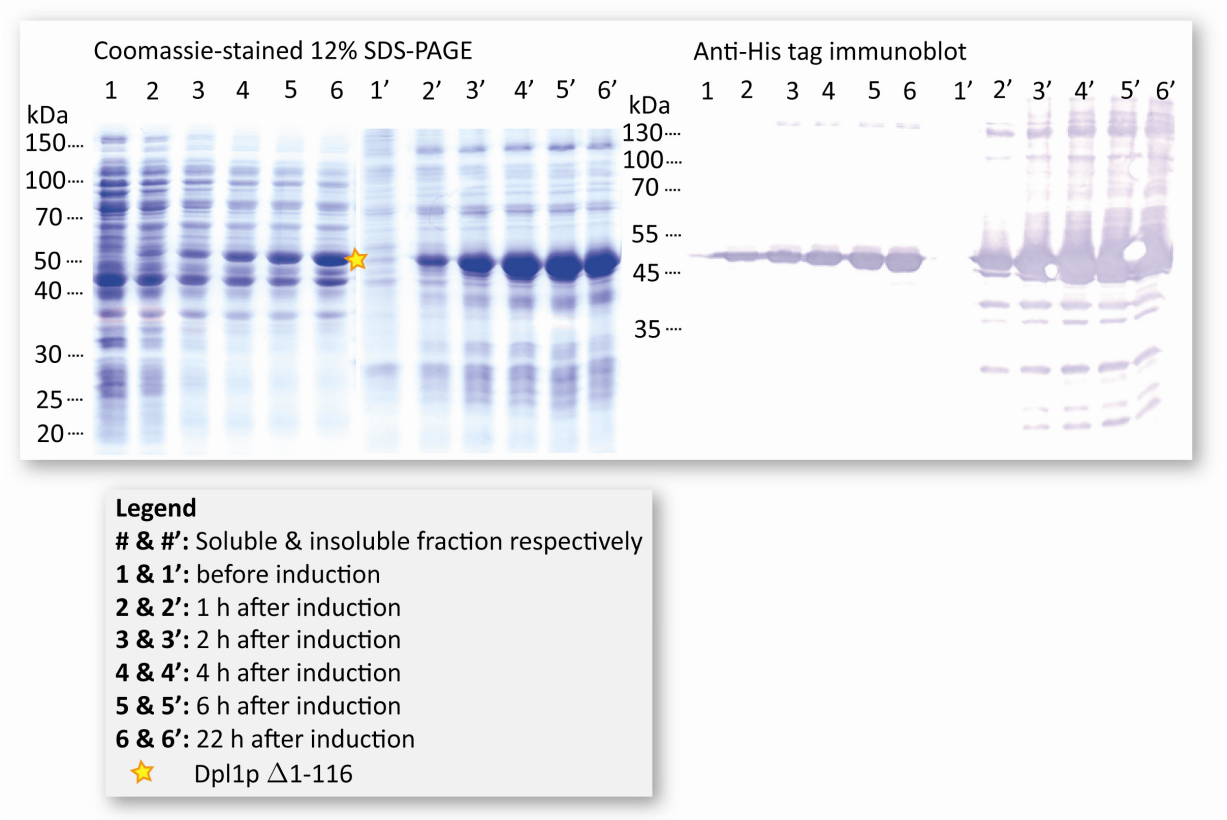

Note: the expression test shown was carried out with BL-21(DE3), but similar results were obtained with HMS174(DE3).

Interestingly, Δ1-116:ΔCt-EXT and Δ1-133:ΔCt-EXT were both expressed to a similar amount as Δ1-116, indicating that the last 45 residues might destabilize the truncation Δ1-133 when containing the Ct-EXT domain. Dpl1p Δ1-123 was designed with the aim of working with a construct as highly expressed as Δ1-116 and lacking any floppy stretches that might prevent crystallisation. Unfortunately, this construct was expressed similarly to Δ1-133 (data not shown). Dpl1p Δ1-144 was designed to be free from flexible loops which could prevent crystallisation. Unfortunately, the construct did not yield any signal in the soluble fraction on immuno-blot and only a faint signal in the insoluble fraction (data not shown). Dpl1p Δ1-102 was the last truncation designed based on the homology model and on the above presented results. The amount of Dpl1p Δ1-102 in the soluble fraction is similar to that of Δ1-116 (**table 5-3**). Interestingly, a significantly lower amount of protein is found in the insoluble fraction of Δ1-102 compared to Δ1-116 (data not shown).

Table 5-3. Overview of the expression in *E. coli*, purification and crystallisation outcome for Dpl1p truncations

TRUNCATION	**SOLUBLE EXPRESSION**[(1)]	**MAXIMAL YIELD** [mg per L culture]	**CRYSTALS**	**STRUCTURE**
Δ1-81	Low & Proteolysis	< 0.05 after IMAC		
Δ1-102	High	4 after SEC	Yes	Yes[(2)]
Δ1-116	High	5 after SEC	Spherulites	No
Δ1-123	Medium			
Δ1-133		0.3 after SEC	Tiny crystals & spherulites	No
Δ1-144	No			
Δ1-116:ΔCt-EXT	High	1 after SEC	No	
Δ1-133:ΔCt-EXT			No	

(1) Low expression means that no signal was seen on SDS-PAGE (protein was detected only using immuno-detection); High expression means that a clear intense band was seen; Medium expression means that a faint band was seen.

(2) The structure is presented in chapter 5.7.

5.3. PURIFICATION AND CRYSTALLISATION

5.3.1. Dpl1p FL AND Δ1-81 EXPRESSED IN *S. cerevisiæ*

Full-length Dpl1p (called thereafter FL Dpl1p) and Δ1-81 fused to a C-terminal FLAG tag (**figure 5-6**) were expressed in *S. cerevisiæ* and purified using affinity chromatography or ion-exchange chromatography by the laboratory of Prof. Howard Riezman in the University of Geneva (Switzerland). The elution fraction was then mailed to Zurich (on ice) and subjected to SEC prior to biophysical characterization and crystallisation trials.

Figure 5-6. Dpl1p FL and Δ1-81 constructs expressed in yeast

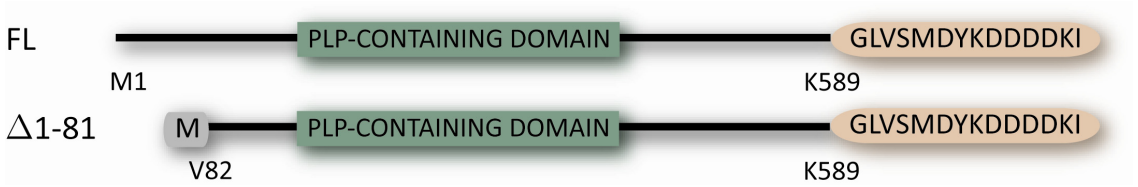

FL Dpl1p originated two close bands on Coomassie-stained SDS-PAGE in the range of the expected MW (67 kDa). The upper band disappeared after EndoH treatment, indicating that it corresponds to a glycosylated form of FL Dpl1p (data not shown). Several purification conditions were tested (**table 5-4**).

Table 5-4. Dpl1p FL purification trials

TRIAL	CULTURE [L]	DETERGENT	PURIFICATION	CONCENTRATION[1]	SEC BUFFER	YIELD[2] [mg]	FURTHER EXPERIMENT
1	15	DDM	ION-EXCHANGE (Tris buffer)	NO	KP_i	0.025	MS & Nterm. sequencing
2	5	Digitonin	AFFINITY (Tris buffer)	No	HEPES	0.025	MS
3	15	DDM	AFFINITY (HEPES buffer)	YES	HEPES	0.05	Crystallisation
4	20	DDM	AFFINITY (HEPES buffer)	YES	HEPES	0.08	AUC

[1] Performed in Zurich before SEC.
[2] Of protein of the 9 ml-shoulder (see **figure 5-7**).

SEC was performed under the same conditions as described for StSPL in Materials & Methods (section 8.3.1.) and in part 3 (manuscript) SI *Text*, using a Superdex-200 10/300 column. Buffer composition was screened with the aim of increasing the yield of protein after SEC (**table 5-5**).

Table 5-5. Dpl1p FL and Δ1-81 SEC buffers composition

FL Trial 1	**FL Trial 2**	**FL Trial 3**	**FL Trial 4**	**Δ1-81**
50 mM **KP_i** pH 7.2	50 mM **HEPES** pH 7.5			
100 mM NaCl			150 mM NaCl	
1 mM EDTA		0.25 mM EDTA	5 mM EDTA	
1 mM **AET**	1 mM **TCEP**		1 mM **DTT**	
10 µM PLP				
0.05 % (w/v) **DDM**[(1)]	0.05 % (w/v) **digitonin**[(2)]	0.05 % (w/v) **DDM**[(1)]		

[(1)] Corresponding to 5-fold CMC.
[(2)] Corresponding to 2-fold CMC.

The SEC elution profiles of trials 1 and 2 showed a main high MW peak eluting in the column void volume and a broad peak eluting at 9 ml (**figure 5-7**, grey and blue lines, respectively). The profile of the non-concentrated sample of trial 3 is similar to that of trial 1 (not shown). After concentration, an additional broad peak eluting at 11 ml appeared (**figure 5-7**, green line). The same behaviour was observed for trial 4 (not shown). When the 9-9.5 ml fraction of trial 2 was immediately reloaded onto the column without concentration, it produced a peak eluting also at 9 ml (data not shown), meaning that the higher-MW species was stable at 4°C without concentration, at least for a couple of hours. The fractions were analysed by SDS-PAGE (data not shown) and all peaks contained the characteristic pair of bands of FL Dpl1p. Based on a calibration run, the 9 ml and 11 ml peaks would correspond to species of 350 and 200 kDa respectively. Since the constitutive unit of PLP-dependent enzymes is a dimer, it is unlikely that the 11 ml peak corresponds to a trimer: rather the two peaks may correspond to a tetramer and a dimer, respectively, assuming a significant detergent contribution to the apparent MW. The slight variations in the elution profiles observed in various detergents could also arise from expression level and sample manipulation.

Figure 5-7. SEC in DDM or digitonin of FL Dpl1p expressed in yeast

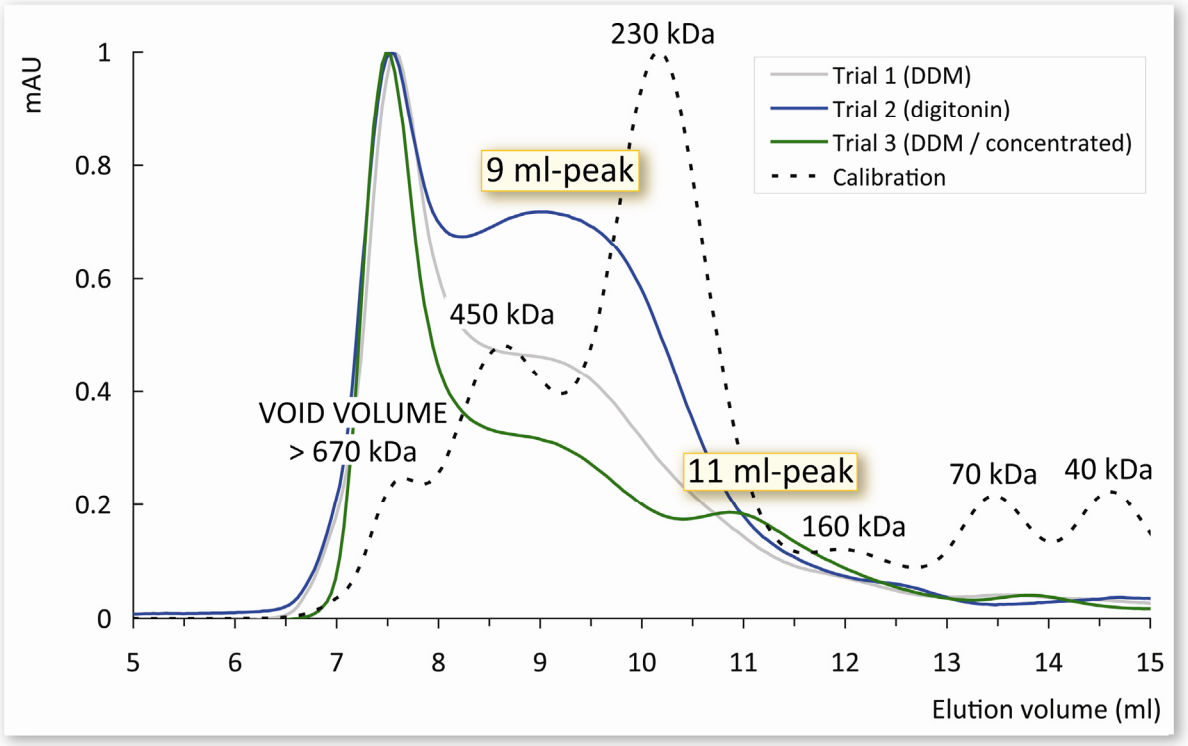

Note: the profiles were normalized to 1 mAU at their highest peak. The intensity of the 9 ml-peak of all trials was comprised between 5 and 50 mAU.

The yield was in all attempts below 0.1 mg of pure protein after SEC for 20 L culture in fermentor and did not vary significantly upon changing the buffer composition of the first purification step, the detergent used and the composition of the SEC buffer. This indicates that expression level is the limiting factor or that the protein is not stable upon purification. FL Dpl1p was nevertheless further characterized.

The identity of the protein from trial 2 was confirmed by mass spectrometry. Two peaks at 67157 Da and at 68862 Da were visible, most likely corresponding to the FLAG tagged protein (expected MW of 67161 Da) and its glycosylated form, respectively. The sample before SEC and the SEC 9-ml peak fractions of attempt 3 were subjected to crystallisation trials using a nanodrop crystallisation robot at 20°C and a commercial screen (Clear Strategy screen I & II pH 7.5 & 8.5, Molecular Dimensions Limited). Protein-to-well solution ratios of 3:1, 1:1, 1:3, for a total volume of 200 nl, were tested. Due to the low yield after SEC, the sample could not be concentrated to more than 0.5 mg/ml. No precipitate was visible on the plate (data not shown), even after plate equilibration (normally occurring after approximately two weeks).

The SEC fractions of attempt 4 were subjected to AUC with the aim of determining the oligomeric state of the protein from each SEC peak. Unfortunately, no monodisperse species could be detected (data not shown).

Dpl1p Δ1-81 was similarly expressed in yeast, where the construct underwent degradation, as in *E. coli* (see chapter 5.2. **figure 5-4**). The first SEC peak eluting with the column void volume mainly contained the expected protein (MW of 57.6 Da) as seen on SDS-PAGE (***band B***) (**figure 5-8**). A second broad peak eluting at 11 ml was a mixture of a 75-80 kDa species (***band A***) and a 50-55 kDa species (***band C***).

Figure 5-8. SEC of Dpl1p Δ1-81 expressed in yeast

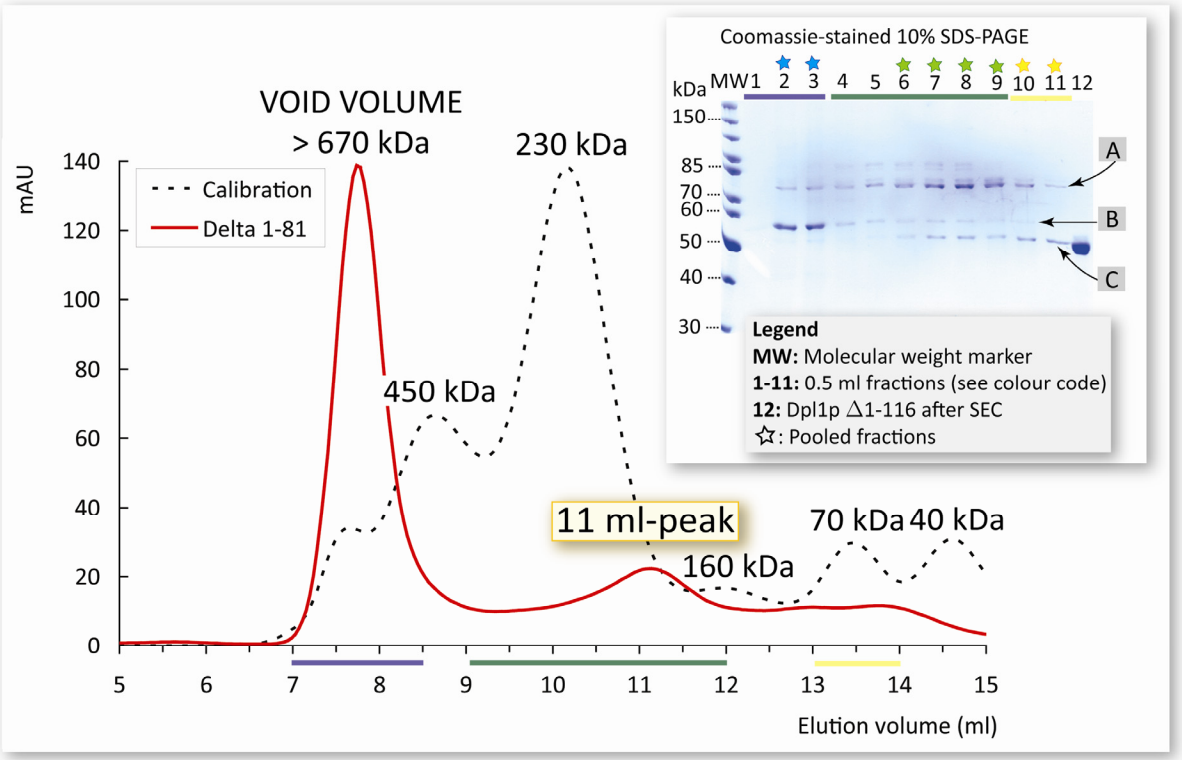

Note: the calibration curve was normalized to 140 mAU at its highest peak (230 kDa).

The fractions of the two main peaks (**figure 5-8** *blue* and *green stars* respectively) and the 13-14 ml-shoulder (*yellow stars*) were pooled and analysed by N-terminal sequencing and MS. Unexpectedly, a single MS peak at 69580 Da was found in all samples (data not shown). This most likely arise from wrong sample manipulation, since N-terminal sequencing of the samples in solution clearly identified Dpl1p Δ1-81 in the void volume peak (blue code) while the other samples (green and yellow stars) were too heterogeneous to give a clear sequence (data not shown). When bands A, B and C were sequenced after transfer onto PVDF membrane, Dpl1p Δ1-81 was only detected in band B, while bands A and C were too heterogeneous to be sequenced (data not shown).

5.3.2. Dpl1p Δ1-116 EXPRESSED IN *E. coli*

Like for StSPL, the purification of Dpl1p truncations expressed in *E. coli* was performed with IMAC and SEC (see Materials & Methods section 8.3.1. and part 3 (manuscript) SI *Text*). The protein eluted in SEC as a main sharp peak at 13 ml corresponding to an estimated MW of 110 kDa (**figure 5-9** *solid line*), based on column calibration with protein standards. Since the monomer of the construct has a MW of 53 kDa, this peak corresponded to a dimer. The average yield after SEC was in the range of 5 mg per L culture.

Figure 5-9. SEC elution profile and Coomassie-stained SDS-PAGE of Dpl1p Δ1-116

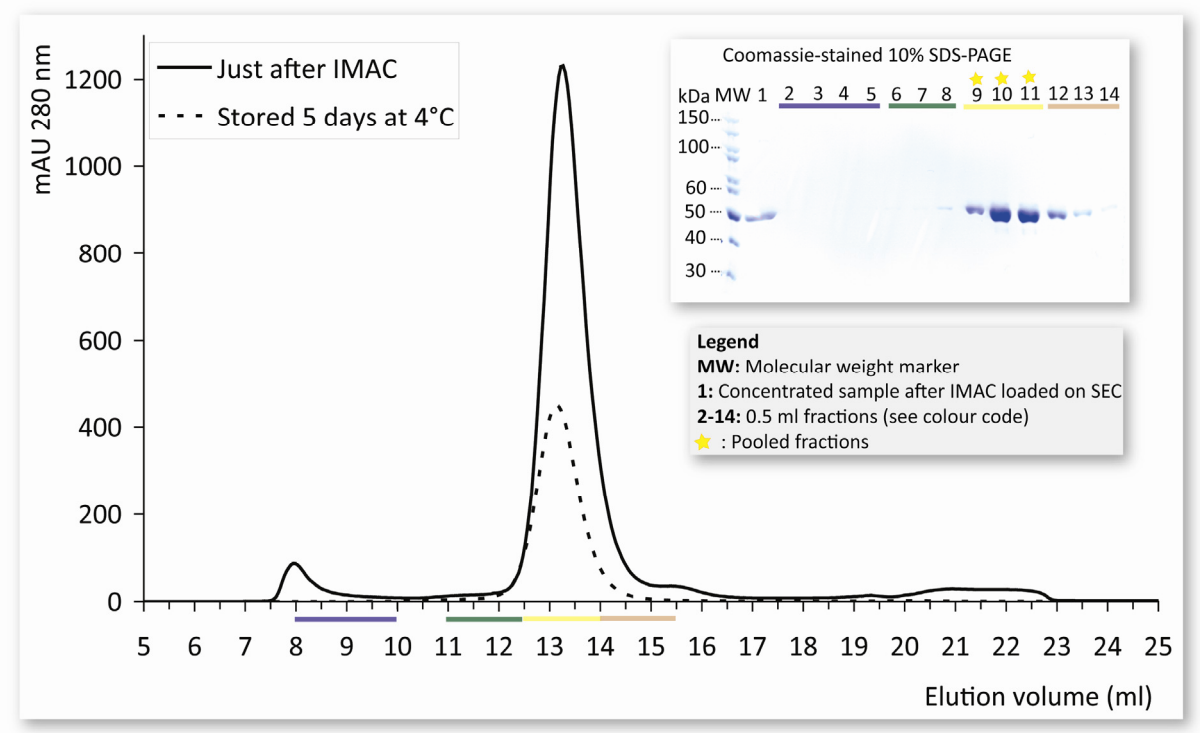

Note: the SEC buffer contained 50 mM HEPES-NaOH pH 7.5 instead of KP_i.

The identity of the main band was confirmed by protein immuno-detection (not shown). The oligomeric state was further analysed by AUC (not shown), which unambiguously confirmed that the construct is a dimer (measured MW of 100 kDa). N-terminal sequencing indicated that Met1 had been cleaved off. Pooled fractions stored for five days at 4°C without concentration were subjected again to SEC and displayed a single peak eluting at 13 ml (**figure 5-9** *dashed line*) Since faint bands were still present on SDS-PAGE after SEC, the integrity of the protein stored one month at 4°C was checked using N-terminal sequencing and MS. The analysis provided similar results to those after SEC (data not shown), indicating that the protein is stable and not degraded when stored for up to one month at 4°C. The UV-Vis spectrum was similar to that of Dpl1p Δ1-102 (see chapter 5.6.).

Despite extensive screening for crystallisation conditions, the construct only yielded spherulites (not shown). Importantly, when the SEC buffer contained HEPES instead of KP_i, no changes were observed in the purification outcome, but the protein did not yield any spherulites. This suggests that phosphate ions might influence and perhaps stabilize the conformation of the protein.

5.3.3. Dpl1p Δ1-133 EXPRESSED IN *E. coli*

The MW of a monomer of Dpl1p Δ1-133 is 50.9 kDa. The protein eluted as a broad tailed peak at 13.2 ml (**figure 5-10**), also corresponding to a dimer. The prominent peak at 8 ml corresponded to high MW contaminants and did not show any signal on immuno-blot (**figure 5-10** inset, lower picture). The yield after SEC was in the range of 0.3 mg per L culture.

Figure 5-10. SEC elution profile, Coomassie-stained SDS-PAGE and anti-His tag immuno-detection of Dpl1p Δ1-133

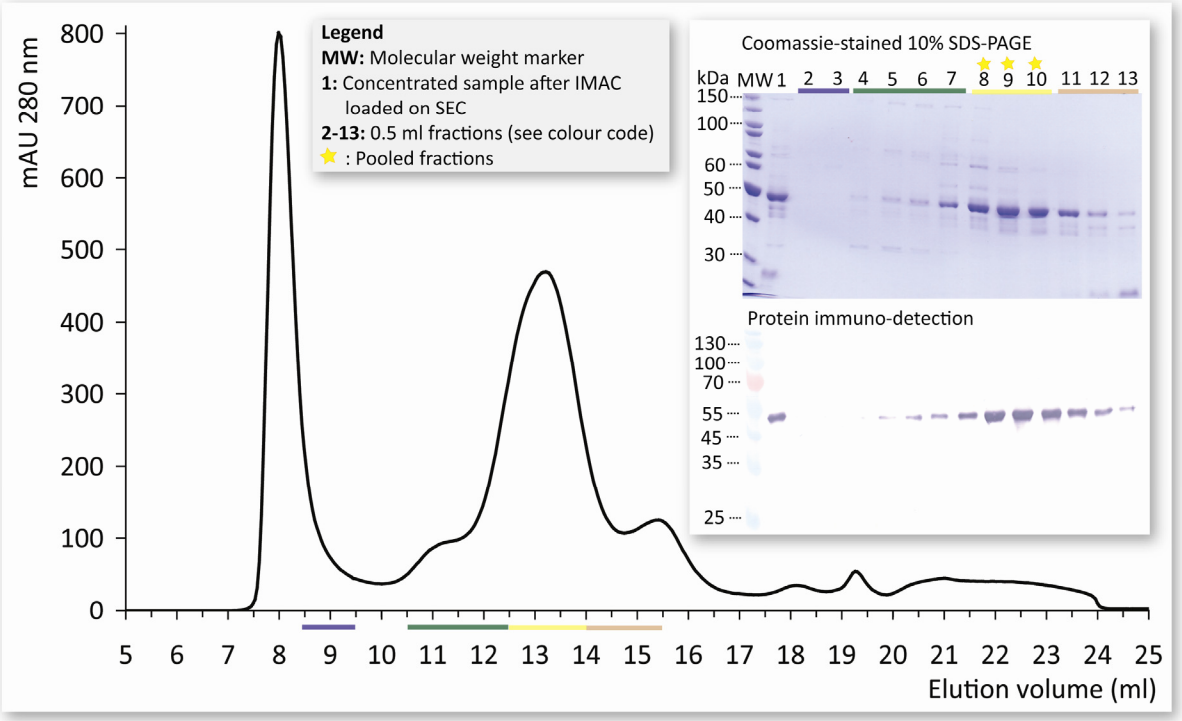

The pooled fractions after SEC were subjected to MS. Unlike Δ1-116, two peaks were found, one at the expected molecular mass and another at 25.1 kDa (data not shown), suggesting either that the sample was not pure or that Dpl1p Δ1-133 had undergone degradation. Indeed, compared to Δ1-116, the construct was prone to precipitation upon concentration, suggesting that this construct might expose hydrophobic patches that destabilize the protein. The UV-Vis spectrum was similar to that of Dpl1p Δ1-102 (see chapter 5.6.).
Spherulites and tiny needle-like crystals were found in the crystallisation drops (not shown). Those crystals were tested at the SLS but exhibited no diffraction.

5.3.4. Dpl1p Δ1-116:ΔCt-EXT AND Δ1-133:ΔCt-EXT EXPRESSED IN *E. coli*

Truncations of Ct-EXT (residues 542-589) combined with the two N-terminal truncations Δ1-116 and Δ1-133 were expressed and purified under the same conditions as described. Surprisingly the construct Δ1-133:ΔCt-EXT, unlike Δ1-133, was expressed at a similar amount to Δ1-116:ΔCt-EXT and Δ1-116 (data not shown). The SEC elution profile of Dpl1p Δ1-116:ΔCt-EXT was similar to that of Δ1-116 except that the main peak was broader (data not shown). The SEC elution profile of Dpl1p Δ1-133:ΔCt-EXT was similar to that of Δ1-133 (data not shown). The yield after SEC of both constructs amounted to 1 mg per L culture, *i.e.* about 5-fold lower than Dpl1p Δ1-116. This is most likely due to an impaired protein stability upon purification.
Neither crystals nor spherulites appeared in a preliminary crystallisation screen.

5.3.5. Dpl1p Δ1-102 EXPRESSED IN *E. coli*

Dpl1p Δ1-102 yielded the same amount of protein as Δ1-116 using IMAC and SEC as purification steps. The estimated protein purity after IMAC is around 95 % (**figure 5-11**, *lane 7*).

Figure 5-11. Dpl1p Δ1-102 IMAC purification

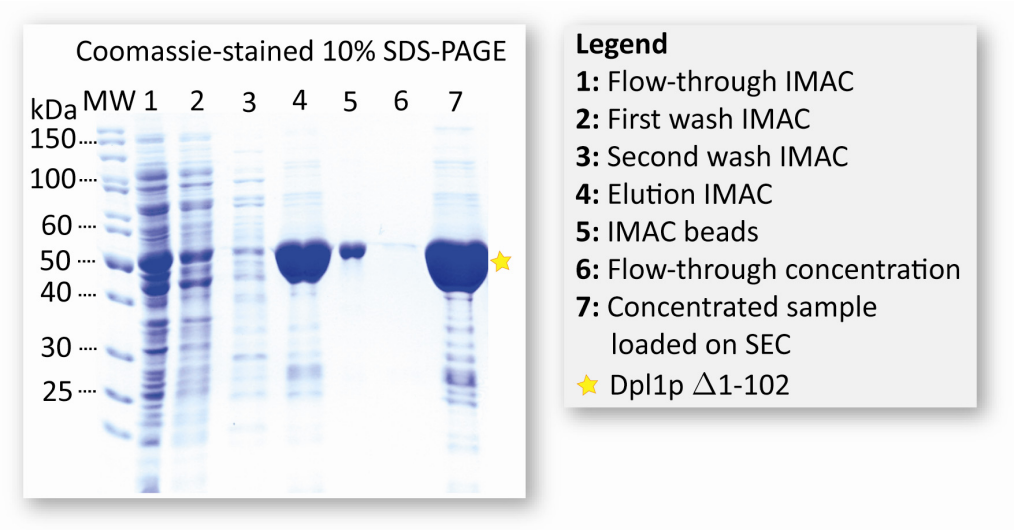

The protein (MW of 54.5 kDa) elutes from SEC as a single peak at 13 ml with a faint shoulder on the right (**figure 5-12**). When a new SEC column was used and higher sample concentration was loaded, two defined peaks (called thereafter peak 1 and peak 2) eluted at 12.9 and 13.1 ml, respectively (data not shown). The elution volumes corresponded to a MW of about 110 kDa. This value was confirmed by AUC (data not shown), indicating that Δ1-102 was present as a dimer in solution at the concentration tested. Like Δ1-116, the pooled fractions of both peaks of Δ1-102 stored for one month at 4°C eluted as a single sharp peak at the same elution volume as just after IMAC (data not shown). This confirmed the stability of both SEC peaks of Δ1-102 upon storage at 4°C. Fractions corresponding to peak 1 and peak 2 were analysed by MS and N-terminal sequencing. The MWs and N-terminal sequences of both peaks were identical and were in good agreement with the expected mass and sequence. Like all constructs expressed and analysed so far, Δ1-102 lacked Met1.

Figure 5-12. Dpl1p Δ1-102 SEC purification

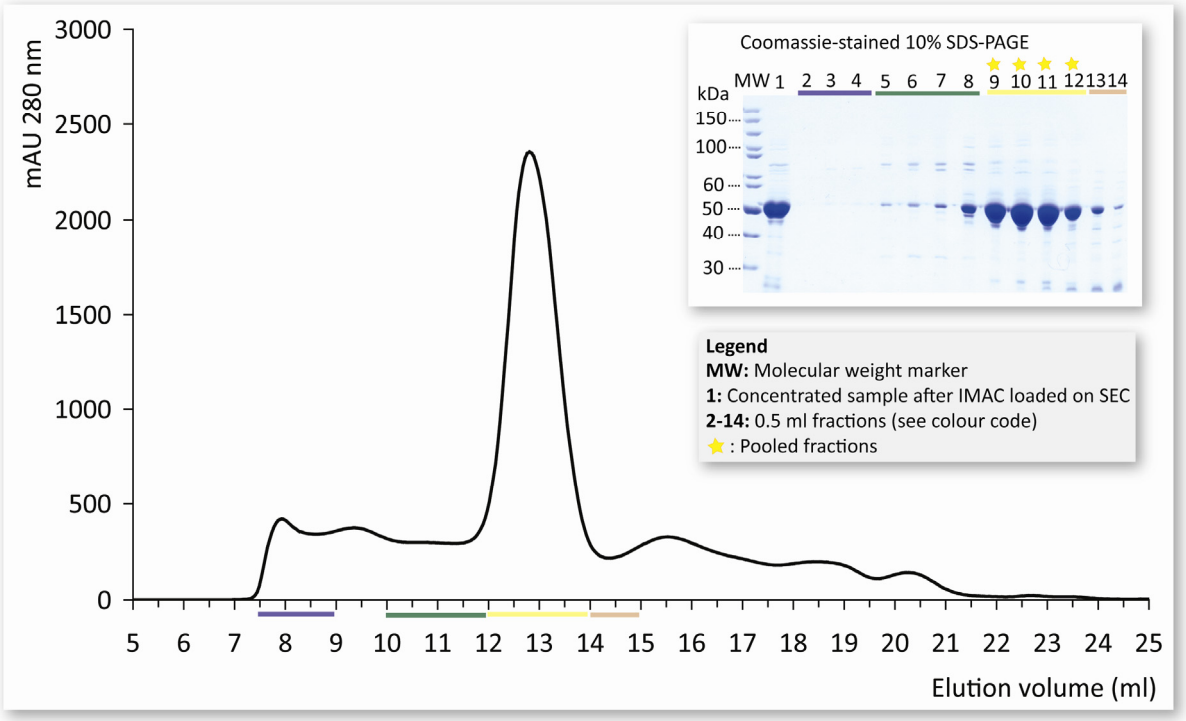

Note: the concentration of the sample loaded was about 30 mg/ml.

The yield after SEC was double in KP_i than in HEPES buffer and less prone to precipitation upon concentration. This suggests a stabilizing role of the phosphate ion on Dpl1p Δ1-102.

5.4. CRYSTALLISATION AND DATA COLLECTION OF Dpl1p Δ1-102

See part 3 (manuscript) **table** S2.

Crystallisation trials were carried out at 20°C and 4°C with protein exclusively in KP_i buffer. The crystals presented here were obtained at 20°C. Both SEC peaks 1 and 2 were subjected to crystallisation and both gave crystals. When only one single peak eluted from SEC, the fractions were pooled according to the example displayed in section 5.3.5. (**figure 5-12**, *yellow stars*). The crystals were yellow due to the presence of PLP in the active site (**figure 5-13**), as it was observed for native FL WT StSPL (see section 4.5.1.). Most of the crystals were found in conditions with a well solution containing Na-cacodylate at pH 6.1 to 6.7, 0.2 M Li_2SO_4 supplemented with various PEG lengths and concentrations. Some crystals of similar morphology were also obtained in NaOAc pH 5.5 or Na-cacodylate pH 6.5 and 40 % (v/v) MPD (hexylene glycol) or 35 % (v/v) isopropanol but they did not diffract to high resolution (data not shown). The crystal resulting in the Dpl1p structure was cryo-protected with 18 % EG.

Figure 5-13. Dpl1p Δ1-102 SEC peak 2 crystallisation resulting in **STRUCTURE Dpl1p**

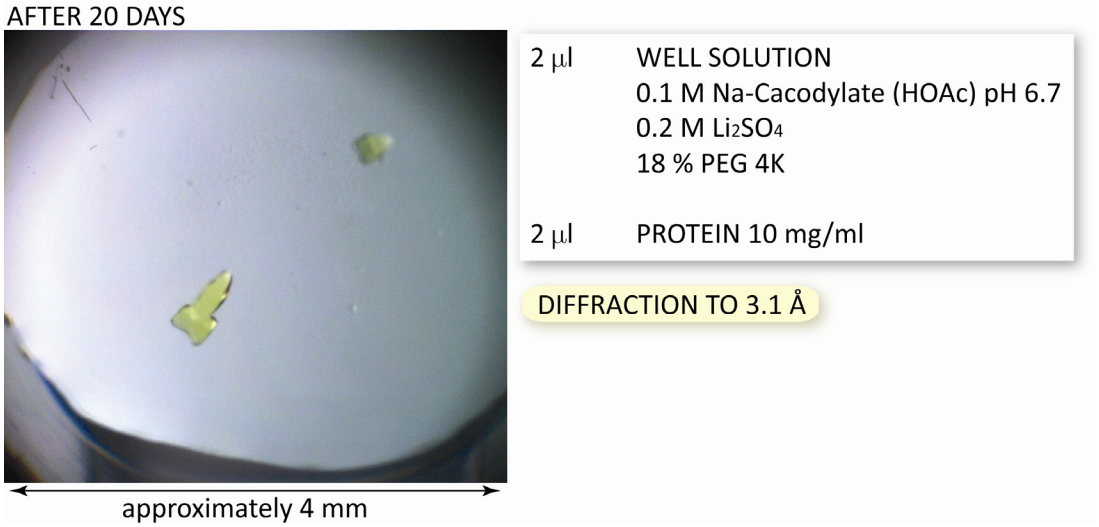

5.5. STRUCTURE DETERMINATION OF Dpl1p Δ1-102

See part 3 (manuscript) **Fig. 1*B*, S1** and **table S2**.

Two point mutations, I308V and N469D are present in the sequence and presumably arise from the genome used for cloning (see part 3 SI *Text*). Residue 308 is found in a hydrophobic region outside the active site (**figure 5-14**) and a mutation to valine is unlikely to induce large conformational changes or to inactivate the protein. Residue 469 is located at about 20 Å from the disordered part of Ct-EXT (residues 542 to 563, shown with a dashed line), region which is not visible on the electron density map (see part 3 (manuscript) **Fig. 1*B***). This stretch is presumably involved in substrate accommodation due to its flexibility and its location close to the active site entry (see part **Fig. S1*B*** and ***D***). Residue K484 interacts electrostatically with D469: this surface salt bridge does not appear, however, to have altered the local conformation, as seen by superposition with structure St_1 (which actually sports a salt bridge exactly at the same positions but with swapped charges: D469 corresponds to K399 and K484 corresponds to D413) (see part 3 **Fig. 1*B***).

Figure 5-14. Point mutations of Dpl1p Δ1-102

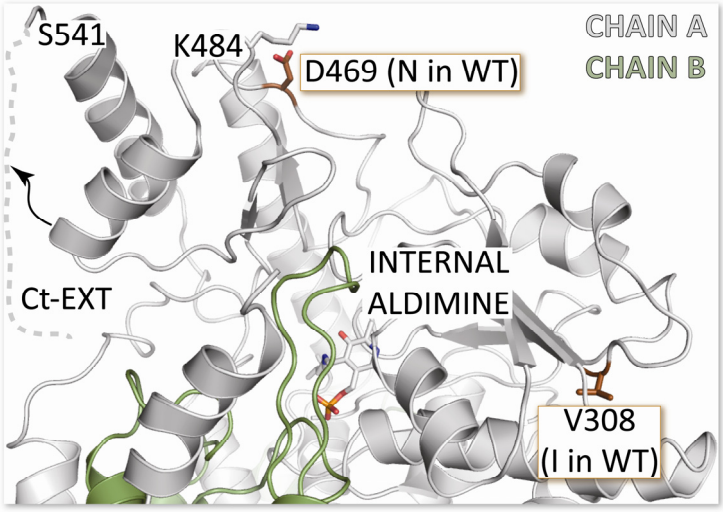

5.6. SPECTROPHOTOMETRIC ACTIVITY ASSAY OF Dpl1p Δ1-102

The visible spectrum of Dpl1p Δ1-102 is characterized by a broad peak centred at 425-430 nm (**figure 5-15** dashed line) also exhibited by Dpl1p Δ1-116, Δ1-133, Δ1-116:ΔCt-EXT and Δ1-133:ΔCt-EXT (data not shown) and by FL WT StSPL (section 4.4.1.). FL Dpl1p expressed in yeast and purified in either digitonin or DDM displayed a similar spectrum, except that the peak was centred at 415 nm (data not shown).

Figure 5-15. Dpl1p Δ1-102 visible spectrum and spectrophotometric activity assay with DHS1P

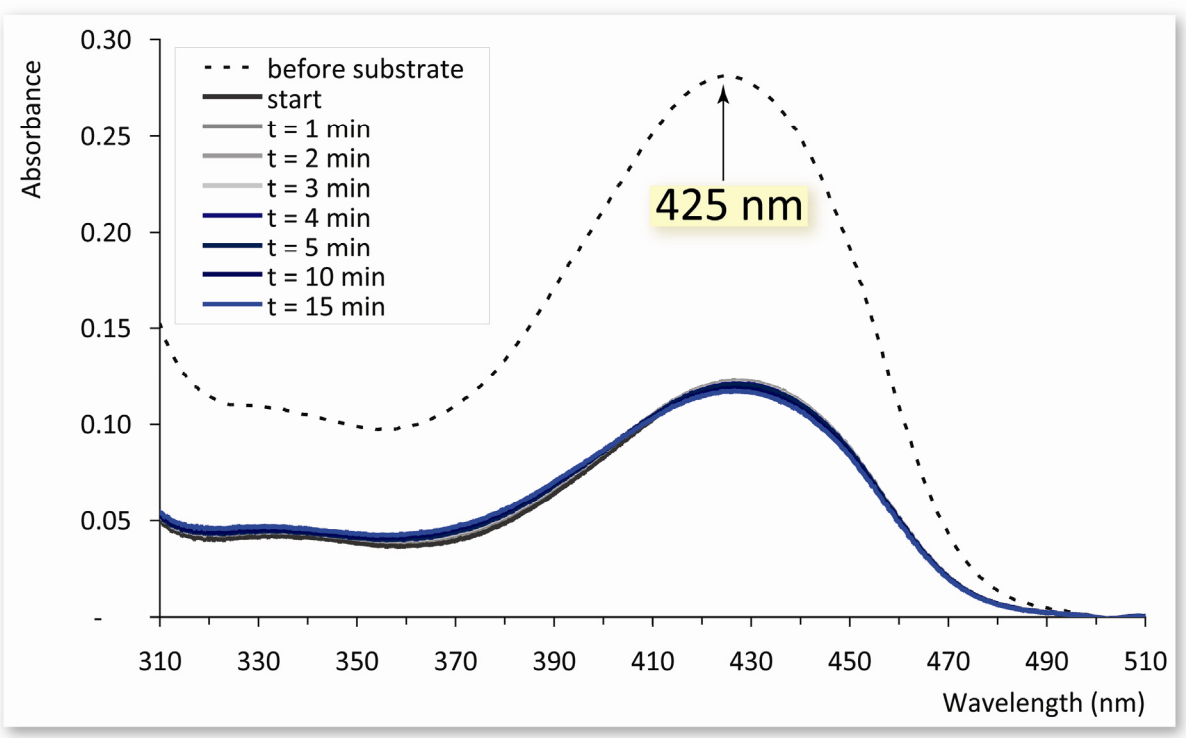

Note: the test was carried out in KP_i buffer with the pooled fractions from peak 2 of SEC.

When DHS1P, S1P and PS1P were added to the protein, the characteristic peaks at 403 and 420 nm (see part 3 (manuscript) **Fig. 4*A***) were not observed (**figure 5-15** full lines coloured grey to blue and part 3 (manuscript) **Fig. S6*J-L***). Slight changes in the 380 nm region occurred over time but were interpreted as insignificant. The test was carried out with pooled fractions from either peak of SEC in KP_i or HEPES buffer. The substrate was solubilised in either Triton X-100 or DDM or digitonin.
This result might suggest that Dpl1p Δ1-102 is inactive. For the above-described reasons, this result must be confirmed by measuring the activity of WT Dpl1p (that is, Dpl1p carrying residues I308 and N469). Activity must be assayed using the spectrophotometric and MS assays, as well as with the use of the fluorogenic substrate (see 4.10.3. **figure 4-42**).

5.7. MUTAGENESIS STUDY: SYNTHETIC LETHALITY TEST

5.7.1. STRUCTURE-BASED DESIGN OF MUTANTS

As controls, the lumenal domain truncation Δ1-57 (**figure 5-1**) and the mutants K380A, K386A, C344A and Y554F studied in (112) were included in the assay. Since the active sites of StSPL and Dpl1p are indistinguishable (**figure 5-16**), Dpl1p mutants corresponding to the StSPL mutants tested *in vitro* were chosen (**table 5-6**).

Figure 5-16. Dpl1p mutants assayed (stereo view)

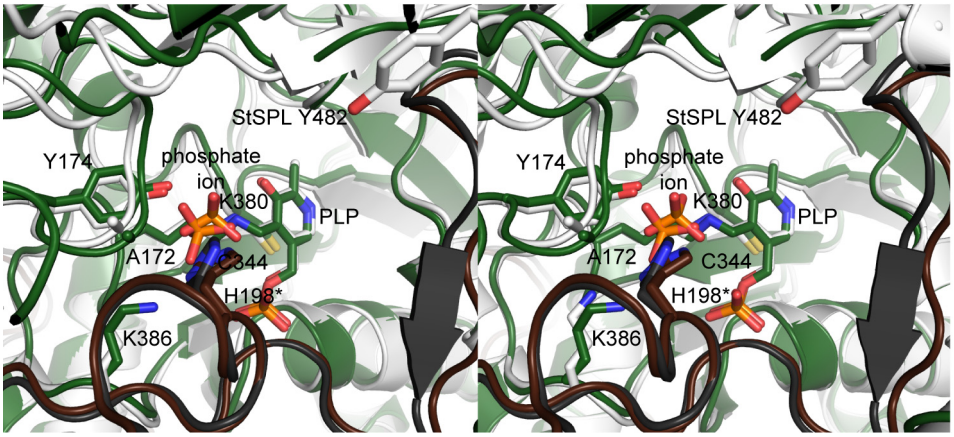

Note: Y554 sits on the disordered stretch of Ct-EXT spanning residues 542-563 and is therefore not visible in the structure. The location of StSPL Y482 might provide a hint on the position of Y554 in Dpl1p. For figure legend, see part 3 (manuscript) **Fig. 3*C*.**

Table 5-6. Dpl1p mutagenesis study

Dpl1	Activity[1]	Conservation[2]	Putative role(s)	*StSPL*	*Activity*[3]
A172P	**Not tested**	No	Active site loop conformation	*A103P*	*Inactive*
Y174F	**Not tested**	Yes	Catalysis / Substrate polar head accommodation	*Y105F*	*Presumably inactive*
H198A	**Not tested**	Yes	Substrate polar head accommodation / Catalysis	*H129A*	*Partly active*
C344A	Partly active	Yes	Catalysis / PLP pyridinium ring stacking	*C276A*	*Partly active*
K380A	Inactive	Yes	Catalysis (internal aldimine)	*K311A*	*Inactive*
K386A	Inactive	Yes	Catalysis / Substrate polar head accommodation	*K317A*	*Inactive*
Y554F	Partly active	Yes	Substrate accommodation / Regulation of activity and local conformation	*Y482F*	*Partly active*

[1] See reference (112).
[2] Compared to the bacterial and human counterparts. See **table 4-11** section 4.9.1.
[3] Of StSPL mutants using the spectrophotometric activity assay.

5.7.2. ASSAY PRINCIPLE

The genes *ura3, lcb3, leu2* and *dpl1* were knocked-out in the genome of the yeast strain used for the test. The genes *ura3* and *lcb3* were carried on a separate plasmid (**figure 5-17** upper left panel) and are both required for growth. The gene *lcb3* encodes a long-chain base phosphate phosphatase and *ura3* is involved in the synthesis of uracil. URA3 produces a toxic compound when 5-fluoroorotic acid (5-FOA) is used as a substrate (**figure 5-17** upper right panel). 5-FOA is not toxic in itself. This strain is transformed with a plasmid carrying a gene encoding for a Dpl1p variant (pRS415-Dpl1p) and the selection marker gene *leu2* which allows the strain to grow in the absence of leucine. The transformed strain is then grown on a medium containing uracil (**figure 5-17** bottom panel) but not leucine. Growth on 5-FOA is only possible for a strain lacking *ura3*, thereby *lcb3*, and expressing an active Dpl1p to complement the loss of LCB3. Colony size is the criterion to estimate the activity of the Dpl1p variant.

Figure 5-17. Principle of the synthetic lethality test

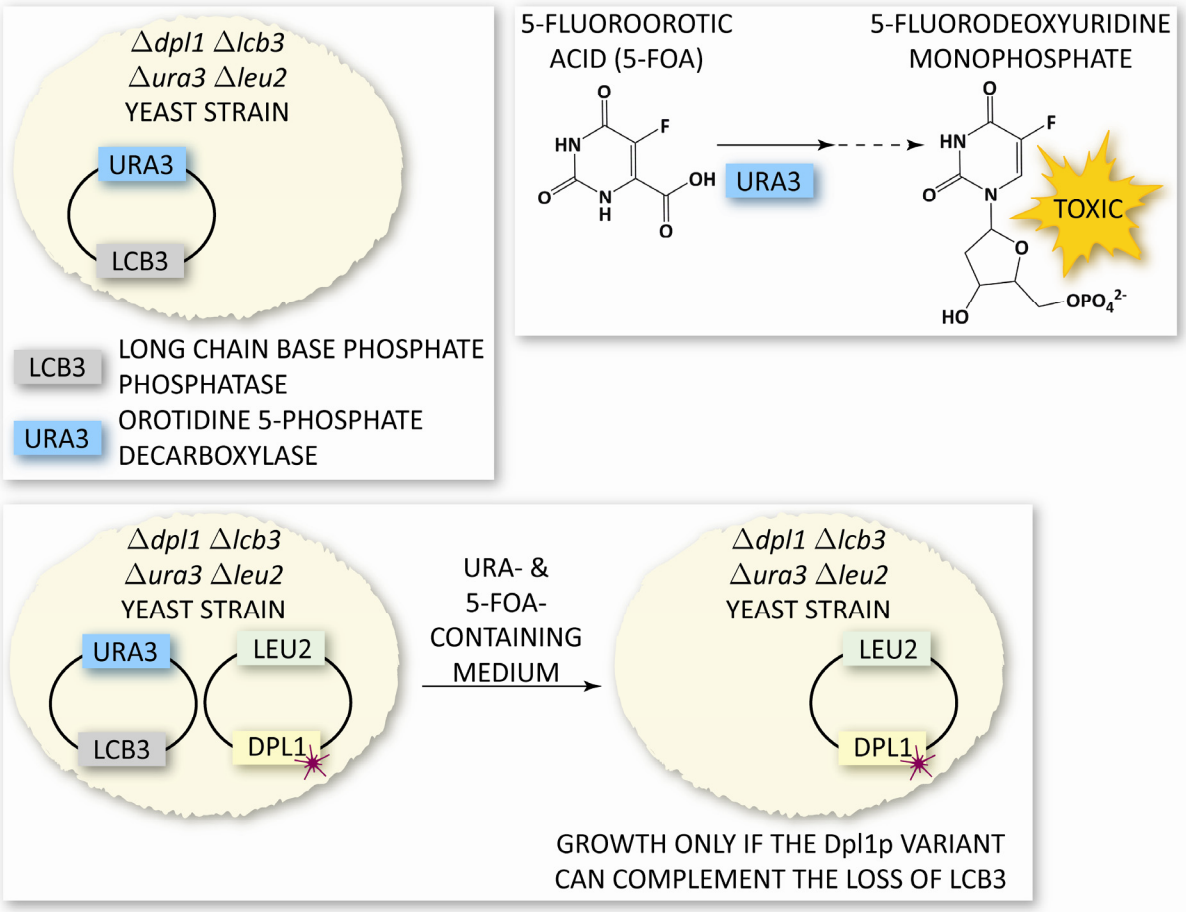

5.7.3. RESULTS

See part 3 (manuscript) **Fig. 5*B***.

5.7.4. SUMMARY

Table 5-7. Dpl1p activity: outcome and comparison with StSPL results of activity assay

Dpl1p	**Mutation Truncation**	***In vivo* activity**	***In vitro* activity**(1)	***StSPL***	***In vitro activity*(1)**
	Δ1-57	Partly active			
	Δ1-102		Inactive		
A172	**A172P**	Inactive		*A103P*	*Inactive*
Y174	**Y174F**	Partly active		*Y105F*	*Presumably inactive*
H198	**H198A**	Partly active		*H129A*	*Partly active*
C344	**C344A**	Partly active		*C276A*	*Partly active*
K380	**K380A**	Inactive		*K311A*	*Inactive*
K386	**K386A**	Inactive		*K317A*	*Inactive*
Y554	**Y554F**	Partly active		*Y482F*	*Partly active*

(1) Of Dpl1p Δ1-102 and StSPL mutants using the spectrophotometric activity assay.

5.8. DISCUSSION AND PERSPECTIVES

5.8.1. PROPOSED MECHANISM

Except for Y174F (StSPL Y105F), the results of the *in vivo* mutagenesis study of Dpl1p are in good agreement with those of the biochemical study on StSPL (**table 5-7**). As pointed out in section 4.7.1., the absence of the S1P-induced peaks in StSPL Y105F does not obligatorily correlate with enzyme inactivity. The enzyme activity of this mutant (and others) must be further investigated, for example with the use of a fluorogenic substrate (see 4.10.3. **figure 4-42**). Hence, the mechanism proposed in **figure 4-40** of section 4.10.3. for StSPL might be extended to Dpl1p. In case one assumes that StSPL Y105F is inactive, the discrepancies between yeast and bacterial SPL may be explained by their different biological context and role. Despite sharing more than 35 % sequence identity (see chapter 2.3. **table 2-1**), the two SPLs differ in cellular functions and, probably, in the regulation of activity. Given the importance of Dpl1p in yeast, one can assume that its activity must be fine-tuned. If the main role of StSPL is to degrade environmental sphingolipids as an energy source, the enzyme activity might have rather evolved towards a high turnover rate. *In vivo* activity studies of dpl1 P199, N195, H268, H379, Y381 and Y414 might provide further insights into the reaction mechanism (see **figure 4-41**), synergistically with the studies of the corresponding mutants of StSPL.

Although the function of WT Dpl1p, *i.e.* that carries I308 and N469, has to be tested to draw further conclusions, the fact that Dpl1p Δ1-102 is *in vitro* inactive (chapter 5.6.) is not surprising given that Dpl1p Δ1-57 is only partly active *in vivo* (**table 5-7**). It nevertheless should be mentioned that the requirements for *in* vivo and *in vitro* activity might differ since cellular activity may be linked with protein targeting to membranes. Dpl1p lacking the transmembrane helix might theoretically be active *in vitro* (see section 1.4.3. **figure 1-22**), similarly to human SPL as reported in (61). Unfortunately, Dpl1p Δ1-81 is degraded in *E. coli* (chapter 5.2.) and possibly also in yeast (section 5.3.1.). Other truncations starting between residue 82 and 102 may be assayed for expression and stability and might provide new insights about the role and conformation of the spacer region. The available outcomes of expression (see chapter 5.2.) and purification (see sections 5.3.2. to 5.3.5.) attempts of Dpl1p truncations clearly indicate that the linker and spacer regions (**figure 5-2**) bear important features for protein stability and presumably activity.

5.8.2. DISORDERED REGIONS

As for FL StSPL, some residues at the N-terminus are not or only faintly visible on the structure. It concerns Nt-EXT of FL StSPL (residues 1-57) and the first 26 residues of Dpl1p Δ1-102 (residues 103-128). Interestingly the first residue invariably visible in Dpl1p, D129, and in StSPL, K58, corresponds to the same residue in a pairwise alignment (**figure 5-18**). This indicates that the flexibility at the N-terminus is a conserved feature of both proteins and has probably a functional role.

Figure 5-18. N-terminal disorder found in FL StSPL and Dpl1p Δ1-102

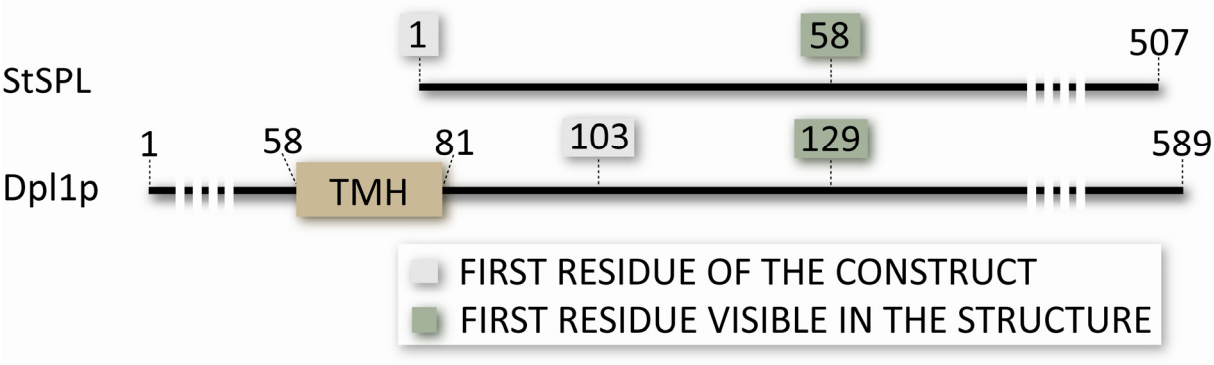

Residues 541-565 of Ct-EXT are not visible in the structure and might also play a functional role (see part 3 (manuscript) **Fig. S1*E***). One cannot exclude that this disorder is triggered by point mutation N469D (see chapter 5.5.), thus affecting substrate binding or correct positioning of residues required for activity, like Y554.
Lithium ions are found in all crystallisation conditions of Dpl1p Δ1-102 and might also play a role in the conformation of the protein. Further screening for different conditions might be useful to determine the role of these ions in the disorder of Ct-EXT.

5.8.3. OLIGOMERIC STATE OF FL Dpl1p

Dpl1p might be active in a higher oligomeric state, by analogy with GadB possibly a hexamer, and the oligomerization state might be modulated by a region missing (residues 1-102) in the truncated form. An alternative to working with FL Dpl1p might be to test the activity of a chimera of Dpl1p Δ1-102 fused to the N-terminal region of *E. coli* GadB or *A. thaliana* Gad1, also hexameric, as recently reported (205). This might provide hints about the requirement of oligomerization for Dpl1p activity. Similarly to StSPL, the SEC buffer composition might be screened with the aim of investigating the pH and salt-dependence of the oligomeric state of Dpl1p. The expression level of FL Dpl1p in yeast and its stability upon purification are not sufficient for biochemical and structural work (see section 5.3.1.). An alternative is the use of orthologues, like the recently described *Legionella pneumoniæ* LegS2 (117). Phylogenetic analysis attributes a protozoan that is, eukaryotic, origin to the *Legionella* protein. Interestingly, when expressed in COS7 mammalian cells, LegS2 targets to the mitochondrial membrane instead than to the ER as for yeast and human SPLs. Assuming that the protein expression level is higher than that of Dpl1p and that a suitable purification protocol is found, LegS2 might provide a useful tool to get insights into the structure and substrate accommodation mechanism of higher eukaryotic (like yeast and human) SPLs.
The question of whether Dpl1p is active as a dimer, like human GAD65/67 (206) or as a multiple thereof, for example a hexamer by analogy with *E. coli* GadB (164), is then still open. The first hypothesis is preferable for two reasons. First, the functional roles of *E. coli* GadB and Dpl1p differ. GadB is involved in acid resistance, and a hexamer possessing six active sites allows a faster turnover, thereby a faster decrease of pH in response to environmental changes. Such a speed advantage might not be required for Dpl1p since the substrate is a powerful cell messenger present in low amounts. Second, assuming that Dpl1p is a hexamer, the location of the second triple-helical coiled-coil spanning the membrane is an enigma (see **figure 5-2** *left*). For these reasons, we assume at present that Dpl1p is active as a dimer.

5.8.4. SUBSTRATE ACCOMMODATION

The presence of a predicted transmembrane helix in Dpl1p adds a level of complexity to the mechanism of substrate accommodation of StSPL reported in section 4.10.6. Three different modes are suggested here. In ***mode I*** (**figure 5-19** left panel), the transmembrane helices, presumably forming a double coiled-coil, would directly be involved in the accommodation of the substrate. Positively charged or polar residues (C65, K67, S70, N71) located in the predicted transmembrane helix (spanning residues 58 to 81) have recently been shown to be required for *in vivo* activity of Dpl1p (112). These residues might bind the polar head of the substrate and drive it into the active site through the spacer and the linker. This accommodation mode would be more likely in case that Dpl1p forms a higher oligomer, for example a hexamer implicating that the transmembrane domain is a triple-helical bundle, maybe allowing the building of a hydrophobic path from the membrane to the active site. The mechanism proposed in ***II*** (**figure 5-19** middle panel) is similar to ***I***, except that the substrate would be extracted from the membrane by positively charged residues of the spacer region. Alternatively, Dpl1p might start accommodating the substrate into the active site while still embedded within the membrane, as assumed for StSPL (**figure 4-43** section 4.6.10.) (but then the protein must be oriented differently from the way shown). The hypothesis of the existence of a yet unknown S1P carrier is illustrated in the ***mode III*** (**figure 5-19** right panel). The S1P importer CFTR (89) might be coupled to an S1P transport protein that would shuffle S1P into the active site of Dpl1p, as CERT transports ceramide from the ER to the Golgi (see section 1.5.3.). This last hypothesis is the most reasonable in terms of thermodynamics but requires the identification of the substrate carrier.

Figure 5-19. Possible substrate accommodation mechanisms of FL Dpl1p

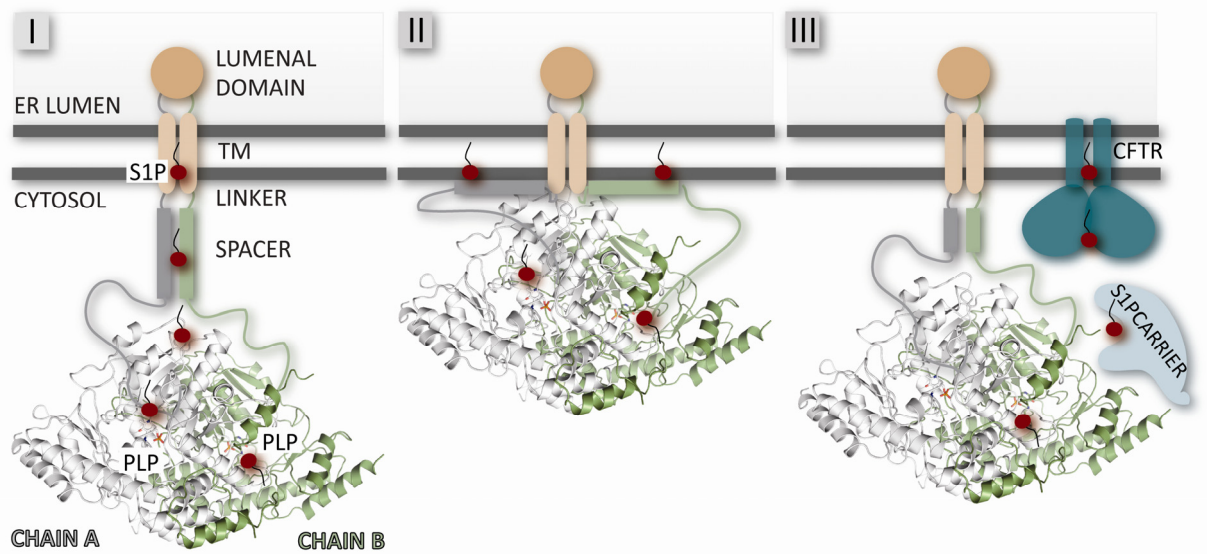

6. RESULTS & DISCUSSION HUMAN SPL (HsSPL)

6.1. TRUNCATIONS DESIGN AND EXPRESSION VECTOR

HsSPL truncations were designed based on a homology model (similar to that presented in chapter 5.1.) and on the behaviour of Dpl1p truncations upon expression (see chapter 5.2.). The constructs were first cloned into pQE60 for preliminary expression tests and the most promising among them were cloned into pET28a+, as described in Materials & Methods section 8.2.3. The additional residues resulting from the cloning are shown in **figure 6-1** and the constructs tested are listed in **figure 6-2**. The numbering shows the corresponding residues of Dpl1p and StSPL.

Figure 6-1. Additional residues of HsSPL truncations cloned into pQE60 and pET28a+

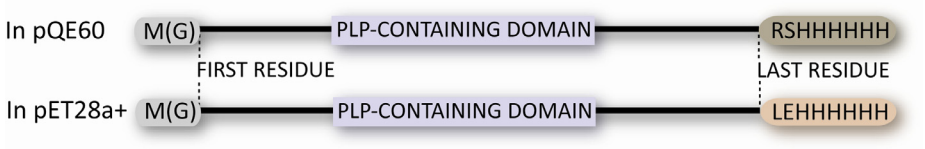

Figure 6-2. Residue correspondence in StSPL, Dpl1p and HsSPL and table of constructs designed and cloned (designed with a cross)

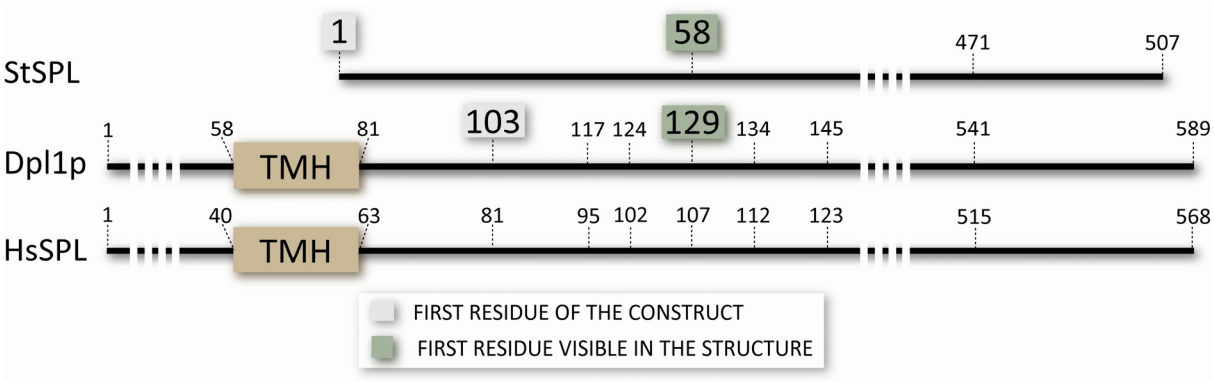

HsSPL TRUNCATION	pQE60	pET28a+
Δ1-63	X	
Δ1-80		X
Δ1-94		
Δ1-103		
Δ1-111		
Δ1-122		X
Δ1-94:Δ516-568		

6.2. EXPRESSION IN *E. coli* AND SOLUBILITY ASSAY

6.2.1. EXPRESSION

The conditions for expression were screened and optimized as described in Materials & Methods section 8.3.3. Parameters such as medium, temperature, vector, addition of ethanol at induction and various $OD_{600\ nm}$ were tested. All truncations were highly expressed but the protein was mainly found in the insoluble fraction of the cell, as shown in **figure 6-3** (lines 2' to 7') for HsSPL Δ1-80. Slight variations were observed in several expression conditions but the protein amount was invariably too low to be detected on Coomassie-stained SDS-PAGE (see **figure 6-3** lane 6, yellow star).

Figure 6-3. Expression test of pQE60 HsSPL Δ1-80 in *E. coli*

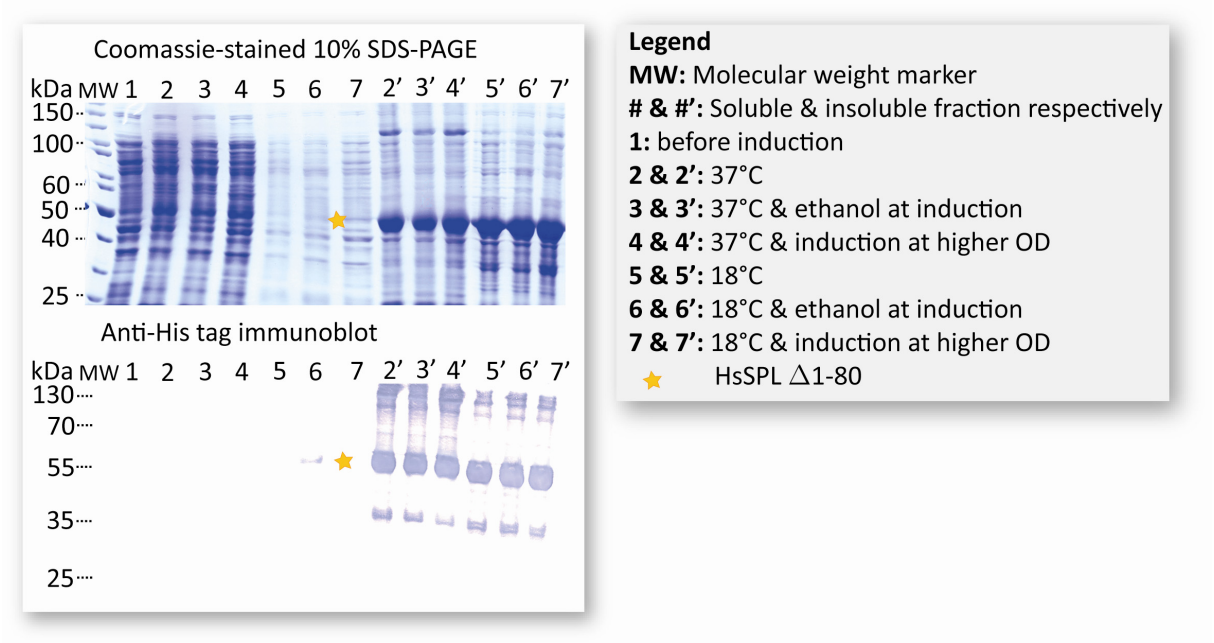

6.2.2. SOLUBILITY

The composition of the cell lysis buffer was screened to increase to amount of soluble protein. Addition of glycerol and Nonidet^{TM} P-40, a nonionic detergent, did not significantly increase the amount of protein in the soluble fraction, as opposite to NaCl (not shown) and Triton X-100 (see below). Lysing the cells at higher pH (see below) and heating the sample to 40°C (not shown) increased the amount of protein in the soluble fraction. Heat treatment was not used due to uncertainty about the stability of the protein. NaCl was routinely added at 250 mM concentration to all buffers used. The pH of the buffer with and without 0.1 % (corresponding to 2- to 6-fold CMC) Triton X-100, was screened (**figure 6-4**). The best solubility was achieved in KP_i pH 8.2, 250 mM NaCl and 0.1 % Triton X-100 (**figure 6-4** lane 3T).

Figure 6-4. pQE60 HsSPL Δ1-80 cell lysis buffer screen: pH and Triton X-100

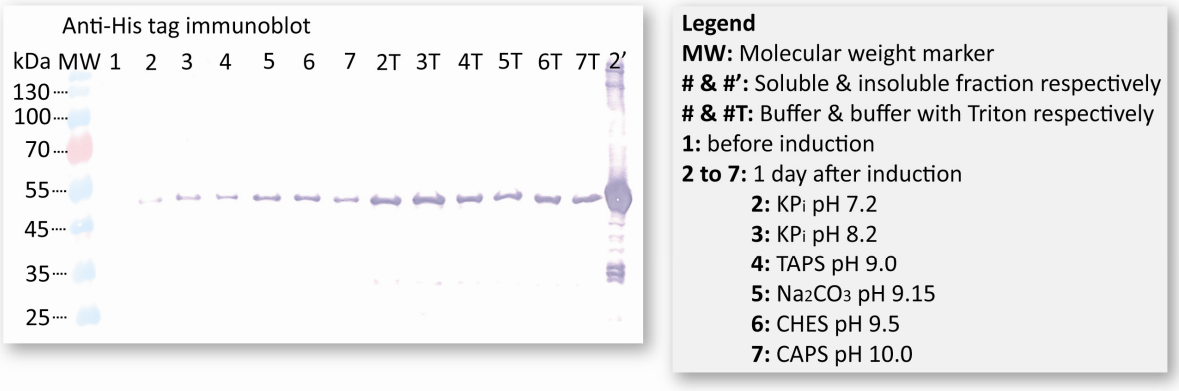

6.3. PURIFICATION

HsSPL Δ1-80 expressed in pQE60 was subjected to a purification attempt using IMAC and SEC. The same procedure as for StSPL (see part 3 (manuscript) SI *Text*) was used in a first trial (**table 6-1**, test 1), except that the buffers were supplemented with 250 mM NaCl. The sample eluted from IMAC was less that 1 % pure (data not shown) and SEC was not performed. The buffer composition was screened in a second trial (**table 6-1**, test 2). Since Dpl1p seemed more stable in the presence of phosphate than in HEPES (section 4.3.5.) 1 mM KP_i was added when CHES was used as buffering agent (**table 6-1**, tests 3 and 4). The SEC buffer was supplemented with 250 mM NaCl and did not contain Triton X-100. In all conditions tested, the purity was estimated to be lower than 5 % (data not shown).

Table 6-1. HsSPL Δ1-80 IMAC buffer composition

	Test 1	Test 2	Test 3	Test 4
50 mM KP_i pH 8.2	X	X		
1 mM KP_i (pH 8.2)			X	X
50 mM CHES pH 9.5			X	X
0.1 % Triton X-100		X		X

6.4. DISCUSSION & PERSPECTIVES

Truncations of eukaryotic Dpl1p can be efficiently expressed in *E. coli* (see chapter 5.2.) and its identity and similarity levels with HsSPL indicate a conserved fold. Interestingly, HsSPL seemed to behave differently than Dpl1p and StSPL upon expression in *E. coli* despite their sequence identity and similarity (see **table 2-1** chapter 2.3.). HsSPL exhibits features that cannot be deduced from the study of its bacterial and yeast counterparts. For all truncations tested most of the protein (estimated to be more than 99 %) is found in the pellet after centrifugation, suggesting that it is either insoluble or misfolded. The insolubility of the truncated variants of HsSPL can originate from the genetic material (gene sequence and plasmid), from the expression system and the conditions of expression, from the biophysical properties of the protein and its truncations or from the cell lysis and protein purification procedure.

The codons of HsSPL gene were optimized for expression in *E. coli* (see Material & Methods 8.2.3.). Although a high level of expression is achieved, the protein is mainly found in the insoluble fraction of the cell (**figure 6-3**), suggesting that the bacterial translation machinery might be overloaded. A similar outcome was observed for truncations of human Gad65 (data not shown) and for SIVA1, a 17 kDa human protein involved in apoptosis (Dr. Peer Mittl, communication in a group seminar). Thus, coding sequence optimisation might promote protein aggregation or sequestration into inclusion bodies (this could be checked by comparison with a non-codon optimized gene).

The type of plasmid and its promoter play a crucial role in protein overexpression. StSPL is significantly less expressed in the pET system than in pQE (data not shown). Both systems were used for HsSPL and yielded that same amount of protein in the soluble fraction, as opposite to StSPL. An auto-induction medium (207) (208) may provide a milder alternative and increase the amount of protein in the soluble fraction. *Lactobacillus lactis* and insect cells expression may provide an expression pattern different from that in *E. coli*. Cell-free (or *in vitro*) expression may be an interesting system to screen the solubility of HsSPL truncations if the properties of the protein are a bottle-neck for *in vivo* recombinant production.

Compared to StSPL and Dpl1p, FL HsSPL and truncated variants have a significantly higher isoelectric point (see **table 6-2**) and this feature might not be properly dealt with by *E. coli*. The pH and ionic force of the cell lysis buffer may therefore be critical parameters influencing the stability and solubility of the protein and have to be screened.

Other truncations may be designed based on more advanced bioinformatic methods. A truncation starting at V107 (Δ1-106) may improve the yield of soluble protein. HsSPL V107 corresponds to the first residue visible in all FL StSPL and in Dpl1p Δ1-102 electron density maps (respectively corresponding to K58 and D129) (see **figure 6-1**). A recently developed method using GFP as a folding indicator might be of help to probe the folding of HsSPL truncations expressed in *E. coli* (209).

Table 6-2. Theoretical isoelectric points of FL WT StSPL, Dpl1p and HsSPL including the additional residues from cloning

PROTEIN	VECTOR	pI[(2)]
FL WT StSPL	pQE70	6.1
StSPL ΔNt-FLEX (WT)		6.2
StSPL ΔCt-EXT (WT)		6.25
FL WT Dpl1p native sequence	-	8.2
Dpl1p Δ1-81[(1)]	pET28a+	7.4
Dpl1p Δ1-102[(1)]		6.8
Dpl1p Δ1-116		6.6
Dpl1p Δ1-133		6.9
Dpl1p Δ1-133:ΔCt-EXT		6.9
FL WT HsSPL native sequence	-	9.3
HsSPL Δ1-63	pQE60	9.4
HsSPL Δ1-80		9.3
	pET28a+	9.2
HsSPL Δ1-94	pQE60	9.1
HsSPL Δ1-94:ΔCt-EXT		9.2
HsSPL Δ1-111		9.2

[(1)] WT sequence, *i.e.* without point mutations I308V and N469V.
[(2)] The pI was calculated with ProtParam (http://www.expasy.org/cgi-bin/protparam) (178).

7. CONCLUSIONS

SPL exhibits structural similarity with serine-palmitoyl transferase (SPT) (see section 1.5.5.). Both SPL and SPT are PLP-dependent enzymes and share a similar fold: the rmsd between Dpl1p and the recently solved *S. paucimobilis* SPT is 2.5 Å over 296 aligned Cα atoms Interestingly, yeast and mammalian SPTs are presumably multimers of heterodimers. One subunit of the heterodimer, while strictly required for activity, lacks PLP and is therefore inactive. On the contrary, the above mentioned bacterial SPT is a homodimer with PLP bound in both active sites. Bacterial SPL exhibits, in one structure (St_2), conformational heterogeneity rather than the sequence heterogeneity observed in yeast and mammalian SPT. The conformational heterogeneity of St_2 affects cofactor binding, since one subunit does not contain PLP. Modulating the affinity of the protein towards the cofactor in one subunit might be a mechanism of regulation, as observed in human GAD65/67 (see section 4.10.2).

Similarly to SPT, the oligomeric state of SPL might not be conserved from prokaryotes to eukaryotes. Notably, FL WT SPL from *Symbiobacterium thermophilum* does not contain any predicted transmembrane helix, unlike its yeast and human counterparts. Eukaryotic SPL might be a homodimer, as observed in the crystal structure of Dpl1p Δ1-102, or a multiple thereof. If the oligomerization state is affected by the N-terminus of the protein, the *in vitro* inactivity of the Δ1-102 truncated variant could be related to its quaternary state. Noticeably, the lumenal domain of human SPL is about 20 residues shorter than that of Dpl1p, suggesting that the role of the very N-terminal part of the protein may vary across evolution. A truncated variant of Dpl1p (Δ1-57) lacking the lumenal domain is only partly active (see part 3 (manuscript) **Fig. 5*B***), while the activity of StSPL truncated until the first visible residue on the structure (ΔNt-FLEX) is not affected (see part 3 **Fig. S6*A***). Interestingly, the N-terminal regions of the bacterial and yeast enzymes are conformationally disordered until the same structurally aligned residue (see 5.8.2. **figure 5-18**), suggesting that this disorder or flexibility is a conserved feature from prokaryotes to eukaryotes even if its importance for activity varies across taxonomic domains. The conformational flexibility of the N-terminus of SPL might allow the region to interact with the membrane and help the accommodation of the substrate into the active site. In yeast and bacterial SPL, parts of the Ct-EXT domain are not visible in all structures, suggesting conformational flexibility in certain conditions. The Ct-EXT domains of both enzymes carry a conserved tyrosine involved in activity (482 in StSPL and 554 in Dpl1p). No autoinhibition *via* substituted aldamine was found in SPL and the structure of its C-terminal region does not allow for a GadB-like autoinhibition mode. Altogether, this indicates that the N- and C-termini are important to various extents for the activity of SPL from various organisms.

Assuming that the results observed are not biased by the expression and purification procedures, one can conclude that SPLs from *Symbiobacterium thermophilum*, yeast and human do not exhibit the same biophysical properties. While StSPL is stable and allows extensive functional and structural studies (see **table 7-1**), truncated variants of Dpl1p behave very differently upon expression in *E. coli* (see **table 7-2**) and the corresponding truncations in human SPL are not found in the soluble fraction of the cell (see **table 7-3**). Unlike the established signalling role of eukaryotic SPLs (see section 1.4.3.), the enzyme has most probably a function in *Symbiobacterium thermophilum* metabolism. These various functions must be linked with different regulatory mechanisms. Since the active sites of bacterial and yeast SPLs are very similar, the less conserved N-terminal region might be the

"fingerprint" of each SPL ortholog and affect various features of the protein, including stability. For example, a yeast SPL truncation lacking both the lumenal and transmembrane domains (Δ1-81 see chapter 5.2.), undergoes N-terminal cleavage upon expression in bacteria and presumably also in yeast (see 5.3.1.). Specific proteolysis of the N-terminus might therefore represent a regulation mechanism specific to yeast SPL. The observation that the lumenal domain truncation of yeast SPL (Δ1-57 see part 3 **Fig. 5*B***) is partially active *in vivo* may support this hypothesis.

Except for one residue (Y105 in bacterial SPL and Y174 in yeast SPL), the roles in enzyme activity of the residues tested in this study appear to be conserved between bacterial and yeast SPLs. Assuming that the residue (or residues) carrying out the proton abstraction on C2 (see section 4.10.3. **figure 4-40**) is strictly required for cleavage and that their mutation fully inactivates the protein, C276 in bacterial SPL and C344 in yeast SPL may not fulfil this function (see part 3 **Fig. 4*E*** and **5*B***). The mechanism proposed in 1993 assumed that a cysteine is the nucleophile (see section 1.4.3. **figure 1-23**) and was deduced from the sensitivity of rat SPL (from microsomes) to N-ethylmaleimide (NEM), a sulfhydryl reagent. This divergence with our experimental data may be explained in four ways. First, but not likely, mammalian SPLs might exhibit a different mechanism than yeast and bacterial SPLs. Second, NEM might indirectly affect the activity of SPL by altering the conformation of the active site, for instance by partly displacing the cofactor, that stacks against the side chain of C344. Third, partial activity, like in bacterial and yeast SPLs, might be retained after NEM treatment but might be below the detection threshold of the activity assay used for the 1993 study. Last, our data are biased. This is very unlikely, since both *in vitro* and *in vivo* assays on bacterial and yeast SPLs provided similar results.

Tyrosine 105 of bacterial SPL (Y174 for in the yeast enzyme) is located on a loop close to the S1P bond to be cleaved and forming part of the binding site of the phosphate moiety of the substrate. The Y105F mutant of bacterial SPL did not show activity bands when undergoing an *in vitro* spectrophotometric assay, while the Y174F mutant of yeast SPL was partly active *in vivo*. Assuming that these results are unbiased and their interpretation is correct, this would mean that the reaction mechanism (or regulation) is not completely conserved from bacteria to yeast.

The best candidate for proton abstraction in bacterial and yeast SPLs is the highly conserved lysine 317 (386 in yeast). The neighbouring H129 (H198 in yeast), also plays an important role, likely in substrate binding, since its alanine mutant is only slightly active (see part 3 **Fig. 4*E*** and **5*B***). Further analysis is required to decipher the precise role of all residues involved in the reaction mechanism of SPL.

Table 7-1. Summary of the main results obtained on StSPL

Construct	Vector	Soluble expression [1]	Oligomeric state	Crystals	Structure	Activity peaks[2]	Relaxation time	Activity by MS
FL WT	pQE60	YES	4mer-2mer	YES	YES			
Δ1-22		NO						
Δ1-38								
FL WT	pQE70	YES	4mer-2mer	YES	YES	YES	Reference	Active
ΔNt-FLEX			Less 4mer than FL WT				Faster	
ΔCt-EXT							Slower	
S101A							Similar	
A103P		Lower than WT		No hits		No peaks but spectral changes		Inactive / partly active
Y105F		YES	Similar to FL WT			NO		
H129A						Very small peaks & spectral changes	Faster	
Y249F						YES	Similar	
C276A							Slower	
K311A			Less 4mer than FL WT	YES	YES	NO		Inactive / partly active
K317A			Similar to FL WT			No peaks but spectral changes		
Y314F & Y324F						YES	Similar	
Y482A / F							Slower	

Note (**for all tables**):

[1] Corresponding to the amount of protein expressed in the soluble fraction of *E. coli*. A cross means that a band can be detected on Coomassie-stained SDS-PAGE.

(2) Corresponding to the appearance of the 403 nm- and 420 nm peaks using the spectrophotometric activity assay.

Table 7-2. Summary of the main results obtained on Dpl1p

Truncation	Point mutations	Expression	Soluble expression[(1)]	Yield after SEC[(3)]	Crystals	Structure	Activity peaks[(2)]
Δ1-81	$I_{308}V$ $N_{469}D$	Faint bands	Proteolysis / degradation (immuno-blot)	< 0.05			
Δ1-102		YES	YES	4	YES	YES	NO
Δ1-116	None			5	Spherulites Microcrystals	NO	
Δ1-123			NO				
Δ1-134				0.3	Spherulites Microcrystals	NO	
Δ1-145		Faint bands					
Δ1-116:Δ Ct-EXT		YES	YES	1	NO		
Δ1-134:Δ Ct-EXT							

Note on **Table 7-2**: Except for Y174F, the *in vivo* activity assay on Dpl1p (not included) provided similar results to those of StSPL *in vitro* (see **table 7-1**).

Table 7-3. Summary of the main results obtained on HsSPL

Truncation	Vector	Expression	Soluble expression[(1)]	Yield after SEC[(3)]
Δ1-63	pQE60	YES	NO	
Δ1-80	pQE60			< 0.01
	pET28a+			
Δ1-94	pQE60			
Δ1-103				
Δ1-111				
Δ1-122	pQE60			
	pET28a+			
Δ1-94:ΔCt-EXT	pQE60			

(3) Expressed in mg per L culture.

8. MATERIALS & METHODS

8.1. CHEMICALS

The plasmids and *E. coli* competent cells were purchased from Novagen (pET28a+ and HMS174(DE3)) and Qiagen (pQE60 and M15). The plasmid pQE70 was a kind gift from S. Savaresi (University of Zurich). The DNA polymerase was from Finnzymes. The restriction endonucleases and ligase were from New England Biolabs. The QuikChange site-directed mutagenesis kit was purchased from Stratagene. The oligonucleotide primers were from Microsynth. The Ni^{2+}-nitriloacetic acid agarose (Ni-NTA) beads were from Qiagen. All chromatography columns and systems were from GE Healthcare. The sphingolipids were purchased from Avanti Polar Lipids, Acros and Alexis Biochemicals. Unless otherwise stated, all chemicals were of the highest commercially available grade. The *Symbiobacterium thermophilum* genome was a kind gift from Dr. Kenji Ueda, Nihon University, Fujisawa, Japan. *Saccharomyces cerevisiæ* (baker's yeast) was purchased from a local supermarket (Migros AG), product code 1150.027 (EAN number 7610.2011).

8.2. CLONING FOR EXPRESSION IN *E. coli*

8.2.1. StSPL WT AND VARIANTS

See part 3 (manuscript) SI *Text* and **table S1**.

The constructs Δ1-22 and Δ1-38 were cloned into pQE60, as described for FL StSPL. The primers used to clone these truncations as well as the mutants S101A, Y314F, Y324F and Y482A are listed in **table 8-1**.

Table 8-1. Primers used for additional StSPL truncations and mutants

CONSTRUCT NAME	FORWARD (5') PRIMER	REVERSE (3') PRIMER
pQE60-StSPL Δ1-22	GGAAGATCTCCCTCCTCATTGCAGGACTATT	CCCAAGCTTACTAGTGATGGTGATGGTGATGCACCTCGTACAGCAGGTCG
pQE60-StSPL Δ1-38	GGAAGATCTCCGCCTGCGAGGAGGGA	
pQE70-StSPL FL S101A	CTATGCCGCCGGCGCCG	CGGCGCCGGCGGCATAG
pQE70-StSPL FL Y314F	GTACGGCTTCGGGGCCA	TGGCCCCGAAGCCGTAC
pQE70-StSPL FL Y324F	GATCCTCTTCCGCAGAC	GTCTGCGGAAGAGGATC
pQE70-StSPL FL Y482A	GCCCCGGTCGCCGGCATGGCC	GGCCATGCCGGCGACCGGGGC

8.2.2. DPL1P TRUNCATIONS

The cloning procedure is identical to that reported in part 3 (manuscript) SI *Text* and the primers are listed in **table 8-2**.

Table 8-2. Primers used for Dpl1p truncations expressed in *E. coli*

CONSTRUCT NAME	FORWARD (5') PRIMER	REVERSE (3') PRIMER	POINT MUTATIONS
pET28a+-Dpl1p Δ1-81	CATGCCATGGTGAGGTT AGCAGTGAGAAC	CCGCTCGAGCTTGGTGG CGGTATCCTCT	I308 => **V**308 N469 => **D**469
pET28a+-Dpl1p Δ1-116	CATGCCATGGTCAAACA ATCGATCGAAGAC		None
pET28a+-Dpl1p Δ1-123	CATGCCATGGAACTAAT TAGATCGGACTCT		
pET28a+-Dpl1p Δ1-133	CATGCCATGGGAAATTT CCCACAGTTGCCATCC		
pET28a+-Dpl1p Δ1-144	CATGCCATGGGACAGGA TGATGTTATTGAAGAGC		
pET28a+-Dpl1p Δ1-116:ΔCt-EXT	Same as above	CCGCTCGAGTGATTCGC TCTTCAACTCTTG	
pET28a+-Dpl1p Δ1-133:ΔCt-EXT	Same as above		

8.2.3. HsSPL TRUNCATIONS

Various N-terminal and C-terminal truncations of the human *spl* gene were amplified by PCR using a synthetic sequence optimized for expression in *E. coli* (GenScript) based on the DNA sequence deposited by Van Veldhoven *et al.* (61) in the NCBI database under the accession number NP_003892. To clone the PCR products into pQE60 (Qiagen), NcoI and BglII restriction enzyme cleavage sites were incorporated into the forward (5') and reverse (3') primer, respectively (**table 8-3**). Some clones contained an additional G residue at the 5' (N-terminal end of the protein) and all clones an additional RSHHHHHH at the 3' (C-terminal end) that resulted from cloning. Positive clones after ligation were sequenced to confirm the integrity of the construct. The pQE60-HsSPL plasmids were transformed into *E. coli* M15 competent cells (Qiagen) and selected on LB agar containing 100 µg/ml of ampicillin and 50 µg/ml of kanamycin. Single colonies were then used for protein expression. Similarly, some truncations of the *spl* gene were amplified by PCR and inserted into pET28a+ (Novagen) using the restriction enzymes NcoI and XhoI. The protein transcribed from pET28a+ contains the same additional residues as from pQE60 at the N-terminus and an additional LEHHHHHH stretch of residues at the C-terminus. The primers used are listed in **table 8-3**.

Table 8-3. Primers used for HsSPL truncations

CONSTRUCT NAME	FORWARD (5') PRIMER	REVERSE (3') PRIMER	ADDITIONAL N-TERMINAL RESIDUE
pQE60-HsSPL Δ1-63	CATGCCATGGAGTCGCTGT GGTCTCGCT	GGAAGATCTATGCGGCTTC GGCGAACCG	None
pQE60-HsSPL Δ1-80	CATGCCATGGGAAGCCCAA TTATTGGACGTAAGATC		GS
pQE60-HsSPL Δ1-94	CATGCCATGGGAACTAAAG ACGATATCAGCAAAAAT		G
pQE60-HsSPL Δ1-103	CATGCCATGGGATCTTTCCT GAAAGTAGATAAAGA		G
pQE60-HsSPL Δ1-111	CATGCCATGGGATATGTGA AAGCGCTGCCTTCT		G
pQE60-HsSPL Δ1-122	CATGCCATGGGAAGCTCGG CAGTACTGGAAAAA		G
pQE60-HsSPL Δ1-94:ΔCt-EXT (516-568)	Same as above	GGAAGATCTAGGATTTTTC ATAATTTGAGTAACG	G
pET28a+-HsSPL Δ1-80	Same as above	CCGCTCGAGATGCGGCTTC GGCGAACCG	GS
pET28a+-HsSPL Δ1-122	Same as above		G

8.3. EXPRESSION AND PURIFICATION

8.3.1. StSPL

The total and soluble expression levels of StSPL variants in *E. coli* were assessed using 4 ml-cultures. Various cell culture parameters, like medium, temperature, cell density at induction, amount of inducer, harvesting time, as well as composition of the cell lysis buffer were optimized to obtain the highest amount of soluble protein. The cells from culture samples measured at regular intervals were spun for 5 min at 12000 *g* at room temperature and suspended in 50 µl buffer (buffer 1_St (**table 8-4**) or another one) per 1 $OD_{600\ nm}$ unit. The suspension was frozen and thawed twice at -20°C. An equal amount of buffer 2_St (**table 8-4**) was then added. The samples were incubated 1 h at room temperature. Care was taken to protect them from light, due to the light sensitivity of the enzyme cofactor, PLP. A second incubation for 1 h at 60°C followed. The cells were then spun 30 min at 12000 *g* at room temperature. The supernatant, representing the soluble fraction of the lysed cells, was separated. The pellet, representing the insoluble fraction and unlysed cells, was resuspended in the same amount of buffer as the supernatant, and both fractions were mixed with SDS-PAGE loading dye and applied on 10 % SDS-PAGE for analysis. Anti-6x His tag immunoblot was performed according to standard procedure to confirm the identity of the protein (210).
The expression conditions used for protein production are described in part 3 (manuscript) SI *Text*.

Table 8-4. Buffers used for the purification of StSPL and Dpl1p

CHEMICAL	BUFFER 1_St	BUFFER 1_Sc	BUFFER 2_St	BUFFER 3	BUFFER 4	BUFFER 5	BUFFER 6
KP_i pH 7.2 (KOH, 20°C) [mM]	50						
NaCl [mM]	-						100
IMIDAZOLE [mM]	-				10	100	
EDTA-NaOH [mM]	-			1		5	1
DTT [mM]	-	1	2	1			
PLP [µM]	-	200	400	200			10
PROTEASE INHIBITOR COCKTAIL WITHOUT EDTA	-	1x	2x	0.5x	0.5x	1x	
CHICKEN EGG WHITE LYSOZYME	-	100 000 U/ml	200 000 U/ml				
DNase I	-	10 µg/ml	20 µg/ml				

8.3.2. Dpl1p

To assess the total and soluble expression of each Dpl1p variant, the same procedure as for StSPL was followed with minor variations. The cell pellets were frozen and thawed and then suspended in 100 µl buffer (buffer 1_St (**table 8-4**) or another one) per 1 $OD_{600\ nm}$ unit. The samples, protected from light, were incubated for 1 h on ice and subjected to two freezing/thawing cycles before separating the soluble and insoluble fractions by centrifugation as previously described.
The expression conditions used for protein production are described in part 3 (manuscript) SI Text.

8.3.3. HsSPL

To assess the total and soluble expression of each human SPL variant, the same procedure as for Dpl1p was employed except that the various cell lysis buffers were tested for their ability to efficiently lyse the cells and solubilise the protein.
Human SPL Δ1-80 carried by pQE60 was expressed in *E. coli* M15 in TB (12 g/l bacto-tryptone, 24 g/l bacto-yeast extract, 0.4 % v/v glycerol, pH brought to 7.3 (20°C) with H_3PO_4) supplemented with the appropriate antibiotics. The procedure was the same as for Dpl1p with the following modifications: the 100 ml-preculture was grown at 30°C, the culture grown at 37°C before and at 18°C after induction.
The cell pellet of 1 L culture (≈ 7.5 g wet cells) was resuspended in twice its volume of buffer 1_Sc supplemented with 250 mM NaCl (**table 8-4**). The following steps were similar to the purification of Dpl1p except that the beads were washed twice in buffer 3 containing 250 mM NaCl, before elution with buffer 4 containing the same amount of NaCl. Other buffers were also tested for their ability to increase the yield of soluble protein. SEC was performed with buffer 6 supplemented with 250 mM NaCl.

8.4. SPECTROPHOTOMETRIC MEASUREMENTS

8.4.1. StSPL AND DPL1P NATIVE SPECTRA

This part is described in part 3 (manuscript) SI *Text*.

8.4.2. SPECTROPHOTOMETRIC ACTIVITY ASSAY

This part is described in part 3 (manuscript) SI *Text*.

For solubility screening, the phosphosphingolipids were solubilised in 1 or 0.16 % (w/v) Triton X-100, 0.1 % (w/v) dodecylmaltoside (DDM), 0.25 % digitonin (Sigma), 100 % dimethyl-sulfoxide (DMSO), 100 % ethanol, 50 % (v/v) ethanol in water, and 4 mg/ml bovine serum albumin (BSA) (Fluka) in water. The solution or solvent was added to the phospholipid powder to reach a maximal concentration of 0.05, 0.5, 1 or 2 mg/ml (≈ 0.125, 1.3, 2.6 and 5 mM respectively). It must be mentioned that insoluble material was invariably observed in all conditions and concentrations tested. In addition, variations in the amount of soluble material after solubilisation in one given solution or solvent were frequently observed, presumably due to discrepancies in the properties of the lipid batch and to the inherently difficult reproducibility of the solubilisation procedure.

8.4.3. FL WT StSPL INHIBITED WITH SEMICARBAZIDE AND IODOACETAMIDE

The procedure for inhibition of StSPL by semicarbazide is described in part 3 (manuscript) SI *Text*.

Similarly the inhibition ability of iodoacetamide (Fluka) has been tested at 100-fold molar excess iodoacetamide over protein monomer after 15 min incubation at room temperature.

8.4.4. FL WT StSPL INCUBATED WITH HUMAN SPL INHIBITORS

2-acetyl-4-tetrahydroxybutyl-imidazole (THI) (Matreya) was solubilised to a maximal concentration of 10 mM in 100 % ethanol or water using the same procedure as for the phosphosphingolipids (see section 8.4.2.) except that the incubation step at 37°C was omitted and that also the compound was protected from light, because of the light-sensitive imidazole ring. THI was only partly soluble under the conditions tested. The test set up was similar to semicarbazide, except that the precise concentration of THI was unknown. THI was added to a 14 µM protein solution and the mix was incubated for time spans ranging from 0 to 3 h at room temperature before addition of substrate.
P-FTY720 was a kind gift from Dr Volker Brinkmann, Novartis Pharma AG, Basel, Switzerland. Various solubilisation methods were employed. In a first attempt, the compound was solubilised to 1 mM (same protocol as described for the phosphosphigolipids) in 100 % ethanol, 50 % ethanol in water, 100 % DMSO, and 1 or 0.16 % (w/v) Triton X-100. In another attempt, P-FTY720 was solubilised to 50 mM in DMSO containing 2 M HCl, vortexed and spun down as described for the phospholipids. No insoluble material was observed. This stock solution was then diluted to 1 mM in 100 % ethanol, 50 % ethanol in water, 100 % methanol, 100 % DMSO, 1 or 0.16 % (w/v) Triton X-100 and various amounts of these solutions were added to the protein. In a third trial, the compound was first dissolved to 1 mM in 100 % methanol and incubated for 30 min at 60°C including 1 min vortex every 4 min. The solution was then sonicated for 10 min, extensively vortexed and spun down as described. Aliquots were dried at 60°C and a 4 mg/ml BSA solution was added to reach either 1 mM or 2 mM P-FTY720. The sample was then solubilised as described for the phospholipids.
FTY720 was either a kind gift from Dr Volker Brinkmann or purchased from Cayman Chemical. The compound was solubilised to 20 mg/ml in 1 or 0.16 % (w/v) Triton X-100, 100 % ethanol, 100 % DMSO, vortexed and spun down 10 min at 14000 *g* at room temperature. The supernatant was kept for further analysis.

8.4.5. EFFECT OF DIVALENT CATIONS AND LDAO ON FL WT StSPL ACTIVITY

The test was carried out similarly to the previous inhibition tests. Briefly, an EDTA-free 16 µM protein solution was mixed with various amounts of Mg-, Sr-, Ba-, Ca- and $ZnCl_2$ and then mixed with the substrate under spectrophotometric monitoring. Ca- and ZnOAc have also been used. The spectra of the mix were directly recorded, without incubation.
Similarly, spectra were recorded in presence of a final concentration of 10 mM lauryldimethylamine-oxide (LDAO) (Fluka).

8.5. ANALYTICAL ULTRACENTRIFUGATION

A sedimentation velocity experiment was performed on an analytical ultracentrifuge ProteomeLab XL-I (Beckman-Coulter). The first peak (elution around 11 ml) of the SEC chromatogram of pQE60 FL WT StSPL was concentrated and set at 15 and 0.4 mg/ml whereas the second peak (elution around 13 ml) was set at 33 and 0.4 mg/ml. Dpl1p Δ1-102 was concentrated to 44 mg/ml and diluted to 2 mg/ml. The samples were sedimented at 30000 rpm (rotor An-50 Ti) at 4°C. The samples at 0.4 mg/ml were detected using UV-visible absorbance at 320 nm and those at 2, 15 and 33 mg/ml using interference. The spectra were analysed with the program SedFit (National Institutes of Health) with refinement of the frictional coefficient (179).

8.6. MASS SPECTROMETRY

The mass of proteins after SEC was confirmed by MS. The samples in solution were desalted with C_4 ZipTip® pipettes tips (Millipore) and diluted first in water and further with 50 % acetonitrile, 0.2 % formic acid pH 2 before injection. Protein masses were measured in the positive mode on a quadrupole mass spectrometer equipped with an electrospray ionization (ESI) source and a time of flight (TOF) ion separation device (Q-TOF Ultima API, Waters Corporation). Multiple-charged protein ion signals were deconvoluted to produce zero-charge spectra using the Maximum EntropyTM 1 (MaxEnt1) algorithm in the Micromass MassLynx software package (Thermo Scientific).

8.7. N-TERMINAL AMINO ACID SEQUENCE DETERMINATION

SDS-PAGE protein bands corresponding to the protein after SEC were transferred to a polyvinylidene fluoride (PVDF) membrane (Immobilon-P, Millipore) by means of a Mini-Trans Blot® electrophoretic transfer cell (Bio-Rad) according to the manufacturer's instructions. After transfer, the membrane was stained with 0.1 % Coomassie in water/ethanol/acetic acid (60/39/1) to identify the proteins of interest and allowed to dry at room temperature. The 55 kDa bands were excised to have their 6 to 10 N-terminal residues sequenced by the Edman degradation method (211) with a Procise® 492cLC protein sequencer (Applied Biosystems).

8.8. CRYSTALLISATION

In all cases, suitable crystallisation conditions were screened for using a nanodrop crystallisation robot (Honeybee 963, Digilab Genomic Solutions) starting from commercially available (Molecular Dimensions Limited, Clear Strategy Screens I & II) and hand-made crystallisation screens, using the sitting-drop vapour diffusion method in 96 well plates (Crystalquick, Greiner bio-one) at 4 and 20°C. Various ratios of protein sample to well solution and various protein concentrations were tested. Conditions where the largest crystals had grown were scaled-up in 24 well plates (Cryschem, Hampton Research). The crystals from either 96 or 24 well plates were mounted in a cryo loop (Hampton Research) and transferred into a mixture of well solution and ethylene glycol (EG) for cryo-protection (see part 3 (manuscript) **table S2** and section 4.5.5. **table 4-6**). In the case of soaking and co-crystallisation experiments, the cryo-protection solution was supplemented with the corresponding compound at the appropriate concentration. Crystals were then flash-frozen by rapid immersion in liquid propane and stored in liquid nitrogen until data collection.

8.8.1. NATIVE FL WT StSPL

Initial crystals were found in various conditions at 20°C incubation by diluting a 21-32 mg/ml protein sample with either an equal (1:1 drop) or half a volume (2:1 drop) of well solution. They usually appeared after two to fifteen days.

8.8.2. FL WT StSPL IN COMPLEX WITH DIVALENT CATIONS

SOAKING
Native protein crystals obtained as described above were transferred to a mixture of well solution supplemented with 10, 50 and 100 mM final concentration of $MgCl_2$. The crystals were incubated for 1 h 10, 1 h 15 to 1 h 20 min, respectively, before cryo-protection and freezing.

CO-CRYSTALLISATION
A molar excess of 100-fold of $MgCl_2$, $BaCl_2$ and $SrCl_2$ over protein subunit was added to the protein (set at 9 mg/ml). The samples were centrifuged for 10 min at 14000 *g* at room temperature and crystallised as described.

8.8.3. FL WT StSPL IN COMPLEX WITH SEMICARBAZIDE (CO-CRYSTALLISATION)

This part is described in part 3 (manuscript) SI *Text* and **table S2** (structure St_4).

8.8.4. StSPL K311A IN COMPLEX WITH PE (CO-CRYSTALLISATION)

This part is described in part 3 (manuscript) SI *Text* and **table S2** (structure St_3).

SOAKING TRIALS WITH A LONG-CHAIN ALDEHYDE
Similarly to the S1P soaking procedure, crystals resulting from co-crystallisation of the K311A mutant with PE were soaked in a 5 mM solution of *cis*-11-hexadecenal (Fluka) in 1 % Triton X-100.

8.8.5. StSPL K311A IN COMPLEX WITH S1P

SOAKING

Crystals of the inactive mutant K311A were obtained as described for the WT enzyme. Several soaking methods were tried. In a first trial, no solvent or detergent was added to the sample. Powder of S1P (Acros) was suspended in the corresponding well solution and intensively vortexed. 2 µl of the suspension were added to the well (0.8 µl). The well was closed and incubated for 6 h at 20°C before cryo-protection and freezing. In a second trial, crystals were incubated in S1P solubilised in the well solution (supplemented with 1 % Triton X-100). The mixture was incubated from 6 h to 6 weeks at 20°C before being transferred into a cryo-protection solution.

CO-CRYSTALLISATION

In a first trial, a 5 mg/ml protein solution was mixed with 1 mg of S1P powder and incubated for 17 h under orbital shaking, either at room temperature or at 4°C in either 10 or 100 µM PLP. The sample was concentrated five times before crystallisation.

In a second trial, 0.5 ml of 2 mg/ml S1P in 1 % Triton X-100 and 0.5 ml of a protein solution at 5 mg/ml were mixed and incubated for 2 h at room temperature, followed by a 18 h-long step of orbital shaking at 4°C. The sample was subjected to a SEC purification step aiming at removing the detergent from the sample, as described in 8.3. The protein was then concentrated to 15 mg/ml and crystallised as described.

In a third trial, 1 ml S1P solubilised in 1 % Triton X-100 was added to 0.7 ml protein solution concentrated to 20 mg/ml. The final concentration of detergent amounted to 0.6 %, that is approximately 3.6 times its critical micelle concentration (CMC) and the protein concentration was 8 mg/ml. The plates were set up with a sample-to-well solution ratio of 2:1, without incubation. A similar experiment was carried out using S1P solubilised in 0.16 % and 0.08 % Triton X-100 instead of 1 % that corresponds respectively to its CMC and half its CMC. The samples were incubated for 17 h at 4°C under orbital shaking and concentrated 2.5 times before crystallisation.

S1P solubilised in 50 % ethanol in water (v/v) was similarly diluted with respect to the protein until a final ethanol concentration of 15 % (v/v). The mixture was then incubated for 30 min without stirring either at room temperature within a closed tube or at 60°C in an open tube to allow for evaporation of ethanol. The mixtures were centrifuged, concentrated to reach 10 mg/ml and crystallised as already described. This procedure was repeated at 4°C.

8.8.6. OTHER MUTANTS OF StSPL

The A103P mutant was subject to crystallisation trials according to the same protocol as described for native FL WT StSPL.

8.8.7. Dpl1p Δ1-102

This part is described in part 3 (manuscript) SI *Text* and **table S2** (structure Dpl1p).

8.8.8. OTHER TRUNCATIONS OF Dpl1p

The truncated variants Δ1-116, Δ1-133, Δ1-116:ΔCt-EXT, Δ1-133:ΔCt-EXT were subjected to crystallisation trials under the same conditions as Dpl1p Δ1-102. The truncation Δ1-116 yielded only spherulites and Δ1-133 thin needles, which didn't diffract. The truncations Δ1-116:ΔCt-EXT and Δ1-133:ΔCt-EXT did not yield any crystals.

8.9. DATA COLLECTION

Datasets were collected at 100K at the X06SA beamline of the Swiss Light Source (SLS), Villigen, Switzerland. Care was taken to limit radiation damage to the crystals by using appropriate beam filtering. All datasets were collected on the high-resolution diffractometer of the beamline, using a PILATUS 6M detector, with the exception of datasets St_1 and St_2, collected on a MD2 micro-diffractometer using a MAR225 CCD detector.

8.9.1. Sr, Mg, Ba ANOMALOUS SIGNALS (CO-CRYSTALLISATION)

These datasets were collected with the aim of detecting the small anomalous scattering signal deriving from divalent cations (Sr^{2+}, Mg^{2+}, Ba^{2+}) bound to the protein. To this end, care was taken to collect redundant datasets with heavy beam filtering, in order to increase the accuracy of the anomalous differences and to reduce the effects of radiation damage. Processing with XDS (see also chapter 8.10) was carried out with the option **STRICT_ABSORPTION_CORRECTION= TRUE**, treating the Bijvoet pairs as distinct symmetry-related reflections in the calculation of the absorption correction coefficients.

8.10. STRUCTURE DETERMINATION, REFINEMENT AND MODEL VALIDATION

The models used for molecular replacement are listed in **table 8-5**.

8.10.1. StSPL STRUCTURES St_1-4

The refinement statistics of St_1-4 are found in part 3 (manuscript) SI *Text* and **table S3**.

8.10.2. OTHER StSPL STRUCTURES

The refinement statistics of St_5-10 are found in section 4.6.8. **table 4-9**.

8.10.3. Dpl1p STRUCTURE

This part is described in part 3 (manuscript) SI *Text* and **table S3**.

Table 8-5. Structure determination of the high-resolution datasets

STRUCTURE CODE	SAMPLE	RESOLUTION [Å]	NUMBER OF POLYPEPTIDE CHAINS PER a.u.	MOLECULAR REPLACEMENT SEARCH MODEL	NCS(1)
St_2	pQE60 FL WT StSPL native	3.0	2	polyS GadB	YES
St_5	pQE60 FL WT StSPL native	3.4	4	St_2 (subunits A & B)	YES
St_1	pQE60 FL WT StSPL native	2.0	2	St_10 (subunits A & B)	NO
St_6	pQE70 FL WT StSPL soaking in 10 mM Mg^{2+}	2.4	4	St_10 (subunits A & B)	NO
St_7	pQE70 FL WT StSPL soaking in 50 mM Mg^{2+}	2.7	4	St_10 (subunits A & B)	NO
St_8	pQE70 FL WT StSPL soaking in 100 mM Mg^{2+}	3.4	4	St_2 (subunits A & B)	YES
St_9	pQE70 FL WT StSPL co-cryst. with Sr^{2+}	2.6	2	St_10 (subunits A & B)	NO
St_3	pQE70 StSPL K311A co-cryst. with PE	2.9	4	St_10 (subunits A & B)	YES
St_4	pQE70 StSPL K311A co-cryst. with SEMIC	2.0(5)	2	St_10 (subunits A & B)	NO
St_10	pQE70 StSPL K311A soaked with S1P	1.9	4	St_2 (subunits A & B)	NO
Dpl1p	pET28a+ Dpl1p Δ1-102 native	3.1(5)	4	St_10 (subunits A & B)	YES

(1) NCS applied (using Phenix): note that St_5, 6, 7, 8, 9 and 10 were not refined to completion. Application of NCS may change in a complete refinement protocol for datasets St_6,7 and 9.

8.11. S1P CLEAVAGE ASSAYS

8.11.1. DETECTION OF SUBSTRATE AND REACTION PRODUCT BY MS

This experiment is described in part 3 (manuscript) SI *Text*.

8.11.2. LONG-CHAIN ALDEHYDE DERIVATIZATION TRIALS

The long-chain aldehyde end product of the SPL reaction was subjected to derivatization with dinitrophenylhydrazine (DNPH) after lipid extraction, carried out using two different protocols described in (212) and in (113), (131), respectively. Chloroform was replaced by dichloromethane in the lipid extraction attempt based on (212). Dried material from the organic phase was resuspended in 20 µl 100 % methanol and derivatized with DNPH as described in (131) and (143). The internal and external standards used were *trans*-2-hexenal (Acros) and *trans*-2-tridecenal (Sigma-Aldrich). The corresponding 2,4-dinitrophenylhydrazone derivatives were detected spectrophotometrically by monitoring the absorbance increase at 378 nm and not on HPLC as performed in (131). A DNPH derivatization test omitting the lipid extraction was also tried. For this, 20 µl of reaction mixture was used instead of 20 µl of organic phase resuspended in methanol.

8.11.3. S1P DERIVATIZATION AND HPLC SEPARATION

Derivatization of the primary amine of S1P and PE with naphthalene-2,3-dicarboxaldehyde (NDA) (Invitrogen) was carried out as described in (213) with some modifications. Instead of the lipid extraction step, S1P solubilised in either 100 % ethanol or 0.16 % Triton X-100 was separated from the enzyme in a Vivaspin-500 50000 MWCO concentrator (Sartorius Stedim) according to the manufacturer's instructions. The same test omitting the separation step was also tried. The flow-through was used in the same way as the lipid extract as explained in (213) except that 10 mM NDA and sodium cyanate (NaCN) solutions were used instead of 5 mM. 20 µl of derivatization mixture were separated using a C18 reverse-phase HPLC column (Macherey-Nagel) calibrated with S1P and PE standards. Mobile phase A was 50 mM KP_i pH 6.5, while mobile phase B was acetonitrile. The gradient program was 0-25 min 100-40 % A, 0-60 % B; 25-35 min 100 % A. The separation was carried out at 40°C at a flow rate of 1 ml/min. The derivatives were detected at 420 and 443 nm. The HPLC system was from Agilent and the chromatograms were analysed using the software ChemStation (Agilent).

8.12. YEAST SYNTHETIC LETHALITY TEST

This experiment is described in part 3 (manuscript) SI *Text*.

The plasmid pRS415- Dpl1p fl wt as well as pRS415 plasmids carrying Dpl1p mutants were a kind gift from Prof. Howard Riezman (University of Geneva, Switzerland).

9. REFERENCES

1. van Meer G, Voelker DR, & Feigenson GW (2008) Membrane lipids: where they are and how they behave. *Nat Rev Mol Cell Biol* 9:112-124.
2. Marsch M & Helenius A (2006) Virus entry:open sesame. *Cell* 124:729-740.
3. Marsh D (2007) Lateral pressure profile, spontaneous curvature frustration, and the incorporation and conformation of proteins in membranes. *Biophys J.* 93:3884-3899.
4. Hla T, Lee MJ, Ancellin N, Paik JH, & Kluk MJ (2001) Lysophospholipids--receptor revelations. *Science* 294:1875-1878.
5. Daum G (1985) Lipids of mitochondria. *Biochim Biophys Acta* 822:1-42.
6. Strauss JFr, Kishida T, Christenson LK, Fujimoto T, & Hiroi H (2003) START domain proteins and the intracellular trafficking of cholesterol in steroidogenic cells. *Mol Cell Endocrinol.* 202:59-65.
7. Devaux PF & Morris R (2004) Transmembrane asymmetry and lateral domains in biological membranes. *Traffic.* 5:241-246.
8. Pomorski T & Menon AK (2006) Lipid flippases and their biological functions. *Cell Mol Life Sci.* 63:2908-2921.
9. Anglin TC, Liu J, & Conboy JC (2007) Facile lipid flip-flop in a phospholipid bilayer induced by gramicidin A measured by sum-frequency vibrational spectroscopy. *Biophys J.* 92:L01-03.
10. López-Montero I*, et al.* (2005) Rapid transbilayer movement of ceramides in phospholipid vesicles and in human erythrocytes. *J Biol Chem.* 280:25811-25819.
11. Daleke DL (2007) Phospholipid flippases. *J Biol Chem.* 282:821-825.
12. Aye IL, Singh AT, & Keelan JA (2009) Transport of lipids by ABC proteins: interactions and implications for cellular toxicity, viability and function. *Chem Biol Interact* 180:327-339.
13. Baumann NA*, et al.* (2005) Transport of newly synthesized sterol to the sterol-enriched plasma membrane occurs via nonvesicular equilibration. *Biochemistry* 44:5816-5826.
14. Sleight RG & Pagano RE (1983) Rapid appearance of newly synthesized phosphatidylethanolamine at the plasma membrane. *J Biol Chem* 258:9050-9058.
15. Kaplan MR & Simoni RD (1985) Intracellular transport of phosphatidylcholine to the plasma membrane. *J Cell Biol* 101:441-445.
16. Voelker DR (1990) Characterization of phosphatidylserine synthesis and translocation in permeabilized animal cells. *J Biol Chem* 265:14340-14346.
17. Warnock DE, Lutz MS, Blackburn WA, Young WWJ, & Baenziger JU (1994) Transport of newly synthesized glucosylceramide to the plasma membrane by a non-Golgi pathway. *Proc Natl Acad Sci U S A* 91:2708-2712.
18. Hanada K*, et al.* (2003) Molecular machinery for non-vesicular trafficking of ceramide. *Nature* 426:803-809.
19. Hanada K, Kumagai K, Tomishige N, & Kawano M (2007) CERT and intracellular trafficking of ceramide. *Biochim Biophys Acta* 1771:644-653.
20. Kudo N*, et al.* (2008) Structural basis for specific lipid recognition by CERT responsible for nonvesicular trafficking of ceramide. *Proc Natl Acad Sci U S A* 105:488-493.
21. van Veldhoven PP & Mannaerts GP (1993) Sphingosine-phosphate lyase. *Adv Lipid Res* 26:69-98.

22. Merrill AHJ, Wang MD, Park M, & Sullards MC (2007) (Glyco)sphingolipidology: an amazing challenge and opportunity for systems biology. *Trends Biochem Sci.* 32:457-468.
23. Bartke N & Hannun YA (2009) Bioactive sphingolipids: metabolism and function. *J Lipid Res* 50 91-96.
24. Linn SC*, et al.* (2001) Regulation of de novo sphingolipid biosynthesis and the toxic consequences of its disruption. *Biochem Soc Trans* 29:831-835.
25. Pewzner-Jung Y, Ben-Dor S, & Futerman AH (2006) When do Lasses (longevity assurance genes) become CerS (ceramide synthases)?: Insights into the regulation of ceramide synthesis. *J Biol Chem* 281:25001-25005.
26. Causeret C, Geeraert L, Van der Hoeven G, Mannaerts GP, & Van Veldhoven PP (2000) Further characterization of rat dihydroceramide desaturase: tissue distribution, subcellular localization, and substrate specificity. *Lipids* 35:1117-1125.
27. Raas-Rothschild A, Pankova-Kholmyansky I, Kacher Y, & Futerman AH (2004) Glycosphingolipidoses: beyond the enzymatic defect. *Glycoconj J* 21:295-304.
28. Wijesinghe DS*, et al.* (2005) Substrate specificity of human ceramide kinase. *J Lipid Res* 46:2706-2716.
29. Tafesse FG, Ternes P, & Holthuis JC (2006) The multigenic sphingomyelin synthase family. *J Biol Chem* 281:29421-29425.
30. Marchesini N & Hannun YA (2004) Acid and neutral sphingomyelinases: roles and mechanisms of regulation. *Biochem Cell Biol* 82:27-44.
31. Xu R*, et al.* (2006) Golgi alkaline ceramidase regulates cell proliferation and survival by controlling levels of sphingosine and S1P. *FASEB J* 20:1813-1825.
32. Hait NC, Oskeritzian CA, Paugh SW, Milstien S, & Spiegel S (2006) Sphingosine kinases, sphingosine 1-phosphate, apoptosis and diseases. *Biochim Biophys Acta* 1758:2016-2026.
33. Johnson KR*, et al.* (2003) Role of human sphingosine-1-phosphate phosphatase 1 in the regulation of intra- and extracellular sphingosine-1-phosphate levels and cell viability. *J Biol Chem* 278:34541-34547.
34. Bandhuvula P & Saba JD (2007) Sphingosine-1-phosphate lyase in immunity and cancer: silencing the siren. *Trends Mol Med* 13:210-217.
35. Horibata Y & Hirabayashi Y (2007) Identification and characterization of human ethanolaminephosphotransferase1. *J Lipid Res.* 48:503-508.
36. Dobrosotskaya IY, Seegmiller AC, Brown MS, Goldstein JL, & Rawson RB (2002) Regulation of SREBP processing and membrane lipid production by phospholipids in Drosophila. *Science* 296:879-883.
37. Hakomori S (2000) Traveling for the glycosphingolipid path. *Glycoconj J* 17:627-647.
38. Tani M, Ito M, & Igarashi Y (2007) Ceramide/sphingosine/sphingosine 1-phosphate metabolism on the cell surface and in the extracellular space. *Cell Signal* 19:229-237.
39. Romiti E*, et al.* (2000) Characterization of sphingomyelinase activity released by thrombin-stimulated platelets. *Mol Cell Biochem* 205:75-81.
40. Duan RD*, et al.* (2003) Identification of human intestinal alkaline sphingomyelinase as a novel ecto-enzyme related to the nucleotide phosphodiesterase family. *J Biol Chem* 278:38528-38536.

41. Johnson KR, Becker KP, Facchinetti MM, Hannun YA, & Obeid LM (2002) PKC-dependent activation of sphingosine kinase 1 and translocation to the plasma membrane. Extracellular release of sphingosine-1-phosphate induced by phorbol 12-myristate 13-acetate (PMA). *J Biol Chem* 277:35257-35262.
42. Don AS & Rosen H (2009) A lipid binding domain in sphingosine kinase 2. *Biochem Biophys Res Commun* 380:87-92.
43. Spiegel S & Milstien S (2003) Sphingosine-1-phosphate: an enigmatic signalling lipid. *Nat Rev Mol Cell Biol* 4:397-407.
44. Yatomi Y*, et al.* (1997) Sphingosine 1-phosphate, a bioactive sphingolipid abundantly stored in platelets, is a normal constituent of human plasma and serum. *J Biochem* 121:969-973.
45. Hänel P, Andréani P, & Gräler MH (2007) Erythrocytes store and release sphingosine 1-phosphate in blood. *FASEB J* 21:1202-1209.
46. Mitra P*, et al.* (2006) Role of ABCC1 in export of sphingosine-1-phosphate from mast cells. *Proc Natl Acad Sci U S A* 103:16394-16399.
47. Boujaoude LC*, et al.* (2001) Cystic fibrosis transmembrane regulator regulates uptake of sphingoid base phosphates and lysophosphatidic acid: modulation of cellular activity of sphingosine 1-phosphate. *J Biol Chem* 276:35258-35264.
48. Goñi FM & Alonso A (2002) Sphingomyelinases: enzymology and membrane activity. *FEBS Lett* 531:38-46.
49. Tani M & Kuge O (2009) Sphingomyelin synthase 2 is palmitoylated at the COOH-terminal tail, which is involved in its localization in plasma membranes. *Biochem Biophys Res Commun* 381:328-332.
50. Vacaru AM*, et al.* (2009) Sphingomyelin synthase-related protein SMSr controls ceramide homeostasis in the ER. *J Cell Biol* 185:1013-1027.
51. Monick MM*, et al.* (2004) Cooperative prosurvival activity by ERK and Akt in human alveolar macrophages is dependent on high levels of acid ceramidase activity. *J Immunol* 173:123-135.
52. Ferlinz K*, et al.* (2001) Human acid ceramidase: processing, glycosylation, and lysosomal targeting. *J Biol Chem* 276:35352-35360.
53. Ohlsson L*, et al.* (2007) Purification and characterization of human intestinal neutral ceramidase. *Biochimie* 89:950-960.
54. Bose R*, et al.* (1995) Ceramide synthase mediates daunorubicin-induced apoptosis: an alternative mechanism for generating death signals. *Cell* 82:405-414.
55. Hornemann T, Wei Y, & von Eckardstein A (2007) Is the mammalian serine palmitoyltransferase a high-molecular-mass complex? *Biochem J* 405:157-164.
56. Han G*, et al.* (2009) Identification of small subunits of mammalian serine palmitoyltransferase that confer distinct acyl-CoA substrate specificities. *Proc Natl Acad Sci U S A* 106:8186-8191.
57. Hanada K*, et al.* (1997) A mammalian homolog of the yeast LCB1 encodes a component of serine palmitoyltransferase, the enzyme catalyzing the first step in sphingolipid synthesis. *J Biol Chem* 272:32108-32114.
58. Giussani P*, et al.* (2006) Sphingosine-1-phosphate phosphohydrolase regulates endoplasmic reticulum-to-golgi trafficking of ceramide. *Mol Cell Biol* 26:5055-5069.
59. Sutherland CM*, et al.* (2006) The calmodulin-binding site of sphingosine kinase and its role in agonist-dependent translocation of sphingosine kinase 1 to the plasma membrane. *J Biol Chem* 281:11693-11701.

60. Stahelin RV*, et al.* (2005) The mechanism of membrane targeting of human sphingosine kinase 1. *J Biol Chem* 280:43030-43038.
61. Van Veldhoven PP, Gijsbers S, Mannaerts GP, Vermeesch JR, & Brys V (2000) Human sphingosine-1-phosphate lyase: cDNA cloning, functional expression studies and mapping to chromosome 10q22(1). *Biochim Biophys Acta* 1487:128-134.
62. Toledo MS, Suzuki E, Handa K, & Hakomori S (2005) Effect of ganglioside and tetraspanins in microdomains on interaction of integrins with fibroblast growth factor receptor. *J Biol Chem* 280:16227-16234.
63. Bollinger CR, Teichgräber V, & Gulbins E (2005) Ceramide-enriched membrane domains. *Biochim Biophys Acta* 1746:284-294.
64. Ray PE (2009) Shiga-like toxins and HIV-1 'go through' glycosphingolipids and lipid rafts in renal cells. *Kidney Int* 75:1135-1137.
65. Hannun YA & Obeid LM (2008) Principles of bioactive lipid signalling: lessons from sphingolipids. *Nat Rev Mol Cell Biol* 9:139-150.
66. Spiegel S & Milstien S (2002) Sphingosine 1-phosphate, a key cell signaling molecule. *J Biol Chem* 277:25851-25854.
67. Gouaze-Andersson V & Cabot MC (2006) Glycosphingolipids and drug resistance. *Biochim Biophys Acta* 1758:2096-2103.
68. Smith ER, Merrill AHJ, Obeid LM, & Hannun YA (2000) Effects of sphingosine and other sphingolipids on protein kinase C. *Methods Enzymol* 312:361-373.
69. Venable ME, Lee JY, Smyth MJ, Bielawska A, & Obeid LM (1995) Role of ceramide in cellular senescence. *J Biol Chem* 270:30701-30708.
70. Obeid LM, Linardic CM, Karolak LA, & Hannun YA (1993) Programmed cell death induced by ceramide. *Science* 259:1769-1771.
71. Chalfant CE & Spiegel S (2005) Sphingosine 1-phosphate and ceramide 1-phosphate: expanding roles in cell signaling. *J Cell Sci* 118:4605-4612.
72. Hinkovska-Galcheva V*, et al.* (2005) Ceramide 1-phosphate, a mediator of phagocytosis. *J Biol Chem* 280:26612-26621.
73. Hla T (2004) Physiological and pathological actions of sphingosine 1-phosphate. *Semin Cell Dev Biol.* 15:513-520.
74. Johnson KR*, et al.* (2005) Immunohistochemical distribution of sphingosine kinase 1 in normal and tumor lung tissue. *J Histochem Cytochem* 53:1159-1166.
75. Shida D, Takabe K, Kapitonov D, Milstien S, & Spiegel S (2008) Targeting SphK1 as a new strategy against cancer. *Curr Drug Targets* 9:662-673.
76. French KJ*, et al.* (2006) Antitumor activity of sphingosine kinase inhibitors. *J Pharmacol Exp Ther* 318:596-603.
77. Taha TA, Argraves KM, & Obeid LM (2004) Sphingosine-1-phosphate receptors: receptor specificity versus functional redundancy. *Biochim Biophys Acta* 1682:48-55.
78. Schwab SR*, et al.* (2005) Lymphocyte sequestration through S1P lyase inhibition and disruption of S1P gradients. *Science* 309:1735-1739.
79. Liu H, Chakravarty D, Maceyka M, Milstien S, & Spiegel S (2002) Sphingosine kinases: a novel family of lipid kinases. *Prog Nucleic Acid Res Mol Biol* 71:493-511.
80. Hobson JP*, et al.* (2001) Role of the sphingosine-1-phosphate receptor EDG-1 in PDGF-induced cell motility. *Science* 291:1800-1803.
81. Shu X, Wu W, Mosteller RD, & Broek D (2002) Sphingosine kinase mediates vascular endothelial growth factor-induced activation of ras and mitogen-activated protein kinases. *Mol Cell Biol* 22:7758-7768.

82. Young KW*, et al.* (2003) Ca2+/calmodulin-dependent translocation of sphingosine kinase: role in plasma membrane relocation but not activation. *Cell Calcium* 33:119-128.
83. Xia P*, et al.* (2002) Sphingosine kinase interacts with TRAF2 and dissects tumor necrosis factor-alpha signaling. *J Biol Chem* 277:7996-8003.
84. Edsall LC, Cuvillier O, Twitty S, Spiegel S, & Milstien S (2001) Sphingosine kinase expression regulates apoptosis and caspase activation in PC12 cells. *J Neurochem* 76:1573-1584.
85. Birchwood CJ, Saba JD, Dickson RC, & Cunningham KW (2001) Calcium influx and signaling in yeast stimulated by intracellular sphingosine 1-phosphate accumulation. *J Biol Chem* 276:11712-11718.
86. Rivera J, Proia RL, & Olivera A (2008) The alliance of sphingosine-1-phosphate and its receptors in immunity. *Nat Rev Immunol* 8:753-763.
87. Kobayashi N*, et al.* (2006) Sphingosine 1-phosphate is released from the cytosol of rat platelets in a carrier-mediated manner. *J Lipid Res* 47:614-621.
88. Sato K*, et al.* (2007) Critical role of ABCA1 transporter in sphingosine 1-phosphate release from astrocytes. *J Neurochem* 103:2610–2619.
89. van Meer G & Lisman Q (2002) Sphingolipid transport: rafts and translocators. *J Biol Chem* 277:25855-25858.
90. Kim RH, Takabe K, Milstien S, & Spiegel S (2009) Export and functions of sphingosine-1-phosphate. *Biochim Biophys Acta* 1791:7692-7696.
91. Lee MJ*, et al.* (1998) Sphingosine-1-phosphate as a ligand for the G protein-coupled receptor EDG-1. *Science* 279:1552-1555.
92. Liu Y*, et al.* (2000) Edg-1, the G protein-coupled receptor for sphingosine-1-phosphate, is essential for vascular maturation. *J Clin Invest* 106:951-961.
93. Kupperman E, An S, Osborne N, Waldron S, & Stainier DY (2000) A sphingosine-1-phosphate receptor regulates cell migration during vertebrate heart development. *Nature* 406:192-195.
94. Brinkmann V*, et al.* (2002) The immune modulator FTY720 targets sphingosine 1-phosphate receptors. *J Biol Chem* 277:21453-21457.
95. Mandala SM*, et al.* (2002) Alteration of lymphocyte trafficking by sphingosine-1-phosphate receptor agonists. *Science* 296:346-349.
96. Graeler M, Shankar G, & Goetzl EJ (2002) Cutting edge: suppression of T cell chemotaxis by sphingosine 1-phosphate. *J Immunol* 169:4084-4087.
97. Pappu R*, et al.* (2007) Promotion of lymphocyte egress into blood and lymph by distinct sources of sphingosine-1-phosphate. *Science* 316:295-298.
98. Venkataraman K*, et al.* (2008) Vascular endothelium as a contributor of plasma sphingosine 1-phosphate. *Circ Res* 102:669-676.
99. Yatomi Y (2008) Plasma sphingosine 1-phosphate metabolism and analysis. *Biochim Biophys Acta* 1780:606-611.
100. Schwab SR & Cyster JG (2007) Finding a way out: lymphocyte egress from lymphoid organs. *Nat Immunol* 8:1295-1301.
101. Ledgerwood LG*, et al.* (2008) The sphingosine 1-phosphate receptor 1 causes tissue retention by inhibiting the entry of peripheral tissue T lymphocytes into afferent lymphatics. *Nat Immunol* 9:42-53.
102. Matloubian M*, et al.* (2004) Lymphocyte egress from thymus and peripheral lymphoid organs is dependent on S1P receptor 1. *Nature* 427:355-360.

103. Mao C, Wadleigh M, Jenkins GM, Hannun YA, & Obeid LM (1997) Identification and characterization of Saccharomyces cerevisiae dihydrosphingosine-1-phosphate phosphatase. *J Biol Chem* 272:28690-28694.
104. Mandala SM*, et al.* (1998) Sphingoid base 1-phosphate phosphatase: a key regulator of sphingolipid metabolism and stress response. *Proc Natl Acad Sci U S A* 95:150-155.
105. Mao C, Saba JD, & Obeid LM (1999) The dihydrosphingosine-1-phosphate phosphatases of Saccharomyces cerevisiae are important regulators of cell proliferation and heat stress responses. *Biochem J* 342 Pt 3:667-675.
106. Mandala SM*, et al.* (2000) Molecular cloning and characterization of a lipid phosphohydrolase that degrades sphingosine-1- phosphate and induces cell death. *Proc Natl Acad Sci U S A* 97:7859-7864.
107. Ogawa C, Kihara A, Gokoh M, & Igarashi Y (2003) Identification and characterization of a novel human sphingosine-1-phosphate phosphohydrolase, hSPP2. *J Biol Chem* 278:1268-1272.
108. Le Stunff H*, et al.* (2002) Characterization of murine sphingosine-1-phosphate phosphohydrolase. *J Biol Chem* 277:8920-8927.
109. Le Stunff H, Milstien S, & Spiegel S (2004) Generation and metabolism of bioactive sphingosine-1-phosphate. *J Cell Biochem* 92:882-899.
110. Saba JD, Nara F, Bielawska A, Garrett S, & Hannun YA (1997) The BST1 gene of Saccharomyces cerevisiae is the sphingosine-1-phosphate lyase. *J Biol Chem* 272:26087-26090.
111. Fyrst H & Saba JD (2008) Sphingosine-1-phosphate lyase in development and disease: sphingolipid metabolism takes flight. *Biochim Biophys Acta* 1781:448-458.
112. Mukhopadhyay D, Howell KS, Riezman H, & Capitani G (2008) Identifying key residues of sphinganine-1-phosphate lyase for function in vivo and in vitro. *J Biol Chem* 283:20159-20169.
113. Van Veldhoven PP & Mannaerts GP (1991) Subcellular localization and membrane topology of sphingosine-1-phosphate lyase in rat liver. *J Biol Chem* 266:12502-12507.
114. Reiss U*, et al.* (2004) Sphingosine-phosphate lyase enhances stress-induced ceramide generation and apoptosis. *J Biol Chem* 279:1281-1290.
115. Ikeda M, Kihara A, & Igarashi Y (2004) Sphingosine-1-phosphate lyase SPL is an endoplasmic reticulum-resident, integral membrane protein with the pyridoxal 5'-phosphate binding domain exposed to the cytosol. *Biochem Biophys Res Commun* 325:338-343.
116. Zhou J & Saba JD (1998) Identification of the first mammalian sphingosine phosphate lyase gene and its functional expression in yeast. *Biochem Biophys Res Commun* 242:502-507.
117. Degtyar E, Zusman T, Ehrlich M, & Segal G (2009) A Legionella effector acquired from protozoa is involved in sphingolipids metabolism and is targeted to the host cell mitochondria. *Cell Microbiol* 11:1219-1235.
118. Skrzypek MS, Nagiec MM, Lester RL, & Dickson RC (1999) Analysis of phosphorylated sphingolipid long-chain bases reveals potential roles in heat stress and growth control in Saccharomyces. *J Bacteriol* 181:1134-1140.
119. Gottlieb D, Heideman W, & Saba JD (1999) The DPL1 gene is involved in mediating the response to nutrient deprivation in Saccharomyces cerevisiae. *Mol Cell Biol Res Commun* 1:66-71.

120. Grote E, Vlacich G, Pypaert M, & Novick PJ (2000) A snc1 endocytosis mutant: phenotypic analysis and suppression by overproduction of dihydrosphingosine phosphate lyase. *Mol Biol Cell* 11:4051-4065.
121. Chen WV, Delrow J, Corrin PD, Frazier JP, & Soriano P (2004) Identification and validation of PDGF transcriptional targets by microarray-coupled gene-trap mutagenesis. *Nat Genet* 36:304-312.
122. Alvarez RH, Kantarjian HM, & Cortes JE (2006) Biology of platelet-derived growth factor and its involvement in disease. *Mayo Clin Proc* 81:1241-1257.
123. Ito K*, et al.* (2007) Lack of sphingosine 1-phosphate-degrading enzymes in erythrocytes. *Biochem Biophys Res Commun* 357:212-217.
124. Oskouian B*, et al.* (2006) Sphingosine-1-phosphate lyase potentiates apoptosis via p53- and p38-dependent pathways and is down-regulated in colon cancer. *Proc Natl Acad Sci U S A* 103:17384-17389.
125. Oskouian B & Saba J (2007) Sphingosine-1-phosphate metabolism and intestinal tumorigenesis: lipid signaling strikes again. *Cell Cycle* 6:522-527.
126. Hibbs K*, et al.* (2004) Differential gene expression in ovarian carcinoma: identification of potential biomarkers. *Am J Pathol* 165:397-414.
127. Seo EY*, et al.* (2006) Identification of the target genes of atopic dermatitis by real-time PCR. *J Invest Dermatol* 126:1187-1189.
128. Zhan X & Desiderio DM (2006) Nitroproteins from a human pituitary adenoma tissue discovered with a nitrotyrosine affinity column and tandem mass spectrometry. *Anal Biochem* 354:279-289.
129. Kariya Y*, et al.* (2005) Products by the sphingosine kinase/sphingosine 1-phosphate (S1P) lyase pathway but not S1P stimulate mitogenesis. *Genes Cells* 10:605-615.
130. Zhang K*, et al.* (2007) Redirection of sphingolipid metabolism toward de novo synthesis of ethanolamine in Leishmania. *Embo J* 26:1094-1104.
131. Bandhuvula P, Fyrst H, & Saba JD (2007) A rapid fluorescence assay for sphingosine-1-phosphate lyase enzyme activity. *J Lipid Res* 48:2769-2778.
132. Van Veldhoven PP (2000) Sphingosine-1-phosphate lyase. *Methods Enzymol* 311:244-254.
133. Stoffel W, LeKim D, & Sticht G (1969) Distribution and properties of dihydrosphingosine-1-phosphate aldolase (sphinganine-1-phosphate alkanal-lyase). *Hoppe Seylers Z Physiol Chem* 350:1233-1241.
134. Stoffel W & Grol M (1974) Chemistry and biochemistry of 1-desoxysphinganine 1-phosphonate (dihydrosphingosine-1-phosphonate). *Chem Phys Lipids* 13:372-388.
135. Boumendjel A & Miller SP (1994) Synthesis of sphingosine-1-phosphate and dihydrosphingosine-1-phosphate. *J Lipid Res* 35:2305-2311.
136. Stoffel W, Bauer E, & Stahl J (1974) The metabolism of sphingosine bases in Tetrahymena pyriformis. Sphingosine kinase and sphingosine-1-phosphate lyase. *Hoppe Seylers Z Physiol Chem* 355:61-74.
137. Billich A*, et al.* (2003) Phosphorylation of the immunomodulatory drug FTY720 by sphingosine kinases. *J Biol Chem* 278:47408-47415.
138. Paugh SW, Payne SG, Barbour SE, Milstien S, & Spiegel S (2003) The immunosuppressant FTY720 is phosphorylated by sphingosine kinase type 2. *FEBS Lett* 554:189-193.
139. Mullershausen F*, et al.* (2009) Persistent signaling induced by FTY720-phosphate is mediated by internalized S1P1 receptors. *Nat Chem Biol* 5:428-434.

140. Bandhuvula P, Tam YY, Oskouian B, & Saba JD (2005) The immune modulator FTY720 inhibits sphingosine-1-phosphate lyase activity. *J Biol Chem* 280:33697-33700.
141. Sasaki H, Arai H, Cocco MJ, & White SH (2009) pH dependence of sphingosine aggregation. *Biophys J* 96:72727-72733.
142. Bedia C*, et al.* (2009) Synthesis of a fluorogenic analogue of sphingosine-1-phosphate and its use to determine sphingosine-1-phosphate lyase activity. *Chembiochem* 10:820-822.
143. Bandhuvula P, Li Z, Bittman R, & Saba JD (2009) Sphingosine 1-phosphate lyase enzyme assay using a BODIPY-labeled substrate. *Biochem Biophys Res Commun* 380:366-370.
144. Shimojo T, Akino T, Miura Y, & Schroepfer GJJ (1976) Sphingolipid base metabolism. Stereospecific uptake of proton in the enzymatic conversion of sphinganine 1-phosphate to ethanolamine 1-phosphate. *J Biol Chem* 251:4448-4447.
145. Openshaw AE, Race PR, Monzó HJ, Vázquez-Boland JA, & Banfield MJ (2005) Crystal structure of SmcL, a bacterial neutral sphingomyelinase C from Listeria. *J Biol Chem* 280:35011-35017.
146. Obama T*, et al.* (2003) His151 and His296 are the acid-base catalytic residues of Bacillus cereus sphingomyelinase in sphingomyelin hydrolysis. *Biol Pharm Bull* 26:920-926.
147. Ago H*, et al.* (2006) Structural basis of the sphingomyelin phosphodiesterase activity in neutral sphingomyelinase from Bacillus cereus. *J Biol Chem* 281:16157-16167.
148. Murakami MT*, et al.* (2006) Structural insights into the catalytic mechanism of sphingomyelinases D and evolutionary relationship to glycerophosphodiester phosphodiesterases. *Biochem Biophys Res Commun* 342:323-329.
149. Murakami MT, Fernandes-Pedrosa MF, Tambourgi DV, & Arni RK (2005) Structural basis for metal ion coordination and the catalytic mechanism of sphingomyelinases D. *J Biol Chem* 280:13658-13664.
150. Inoue T*, et al.* (2009) Mechanistic insights into the hydrolysis and synthesis of ceramide by neutral ceramidase. *J Biol Chem* 284:9566-9577.
151. Tani M, Iida H, & Ito M (2003) O-glycosylation of mucin-like domain retains the neutral ceramidase on the plasma membranes as a type II integral membrane protein. *J Biol Chem* 278:10523-10530.
152. Malinina L, Malakhova ML, Teplov A, Brown RE, & Patel DJ (2004) Structural basis for glycosphingolipid transfer specificity. *Nature* 430:1048-1053.
153. Malinina L*, et al.* (2006) The liganding of glycolipid transfer protein is controlled by glycolipid acyl structure. *PLoS Biol* 4:e362.
154. Airenne TT*, et al.* (2006) Structural evidence for adaptive ligand binding of glycolipid transfer protein. *J Mol Biol* 355:224-236.
155. Hornemann T*, et al.* (2009) The SPTLC3 subunit of serine-palmitoyltransferase generates short chain sphingoid bases. *J Biol Chem* 284:26322-26330.
156. Ikushiro H, Hayashi H, & Kagamiyama H (2003) Bacterial serine palmitoyltransferase: a water-soluble homodimeric prototype of the eukaryotic enzyme. *Biochim Biophys Acta* 1647:116-120.
157. Ikushiro H, Islam MM, Tojo H, & Hayashi H (2007) Molecular characterization of membrane-associated soluble serine palmitoyltransferases from Sphingobacterium multivorum and Bdellovibrio stolpii. *J Bacteriol* 189:5749-5761.

158. Yard BA*, et al.* (2007) The structure of serine palmitoyltransferase; gateway to sphingolipid biosynthesis. *J Mol Biol* 370:870-886.
159. Shiraiwa Y, Ikushiro H, & Hayashi H (2009) Multifunctional role of his159in the catalytic reaction of serine palmitoyltransferase. *J Biol Chem* 284:15487-15495.
160. Raman MC*, et al.* (2009) The External Aldimine Form of Serine Palmitoyltransferase: STRUCTURAL, KINETIC, AND SPECTROSCOPIC ANALYSIS OF THE WILD-TYPE ENZYME AND HSAN1 MUTANT MIMICS. *J Biol Chem* 284:17328-17339.
161. Ikushiro H, Fujii S, Shiraiwa Y, & Hayashi H (2008) Acceleration of the substrate Calpha deprotonation by an analogue of the second substrate palmitoyl-CoA in Serine Palmitoyltransferase. *J Biol Chem* 283:7542-7553.
162. Ikushiro H*, et al.* (2009) Structural Insights into the Enzymatic Mechanism of Serine Palmitoyltransferase from Sphingobacterium multivorum. *J Biochem* 146:549-562.
163. De Biase D, Tramonti A, Bossa F, & Visca P (1999) The response to stationary-phase stress conditions in Escherichia coli: role and regulation of the glutamic acid decarboxylase system. *Mol Microbiol* 32:1198-1211.
164. Capitani G*, et al.* (2003) Crystal structure and functional analysis of Escherichia coli glutamate decarboxylase. *Embo J* 22:4027-4037.
165. Gut H*, et al.* (2006) Escherichia coli acid resistance: pH-sensing, activation by chloride and autoinhibition in GadB. *Embo J* 25:2643-2651.
166. Altschul SF*, et al.* (1997) Gapped BLAST and PSI-BLAST: a new generation of protein database search programs. *Nucleic Acids Res* 25:3389-3402.
167. Boutet E, Lieberherr D, Tognolli M, Schneider M, & Bairoch A (2007) UniProtKB/Swiss-Prot. *Methods Mol Biol* 406:89-112.
168. Ohno M*, et al.* (2000) Symbiobacterium thermophilum gen. nov., sp. nov., a symbiotic thermophile that depends on co-culture with a Bacillus strain for growth. *Int J Syst Evol Microbiol* 50:1829-1832.
169. Nishida H, Beppu T, & Ueda K (2009) Symbiobacterium lost carbonic anhydrase in the course of evolution. *J Mol Evol* 68:90-96.
170. Ueda K*, et al.* (2001) Distribution and diversity of symbiotic thermophiles, Symbiobacterium thermophilum and related bacteria, in natural environments. *Appl Environ Microbiol* 67:3779-3784.
171. Sugihara T*, et al.* (2008) Distribution of Symbiobacterium thermophilum and related bacteria in the marine environment. *Biosci Biotechnol Biochem* 72:204-211.
172. Ueda K*, et al.* (2004) Genome sequence of Symbiobacterium thermophilum, an uncultivable bacterium that depends on microbial commensalism. *Nucleic Acids Res* 32:4937-4944.
173. Sahu SK, Rajasekharan A, & Gummadi SN (2009) GroES and GroEL are essential chaperones for refolding of recombinant human phospholipid scramblase 1 in E. coli. *Biotechnol Lett* 31:1745-1752.
174. Eliot AC & Kirsch JF (2004) Pyridoxal phosphate enzymes: mechanistic, structural, and evolutionary considerations. *Annu Rev Biochem* 73:383-415.
175. Toney MD (2005) Reaction specificity in pyridoxal phosphate enzymes. *Arch Biochem Biophys* 433:279-287.
176. Cook PD, Thoden JB, & Holden HM (2006) The structure of GDP-4-keto-6-deoxy-D-mannose-3-dehydratase: a unique coenzyme B6-dependent enzyme. *Protein Sci* 15:2093-2106.

177. Sharif S*, et al.* (2007) 15N nuclear magnetic resonance studies of acid-base properties of pyridoxal-5'-phosphate aldimines in aqueous solution. *J Phys Chem B* 111:3869-3876.
178. Gasteiger E*, et al.* (2005) Protein Identification and Analysis Tools on the ExPASy Server. *John M. Walker (ed): The Proteomics Protocols Handbook, Humana Press* 571-607.
179. Lebowitz J, Lewis MS, & Schuck P (2002) Modern analytical ultracentrifugation in protein science: a tutorial review. *Protein Sci* 11:2067-2079.
180. Webster SP*, et al.* (2000) Mechanism of 8-amino-7-oxononanoate synthase: spectroscopic, kinetic, and crystallographic studies. *Biochemistry* 39:516-528.
181. Ikushiro H, Hayashi H, Kawata Y, & Kagamiyama H (1998) Analysis of the pH- and ligand-induced spectral transitions of tryptophanase: activation of the coenzyme at the early steps of the catalytic cycle. *Biochemistry* 37:3043-3052.
182. Krissinel E & Henrick K (2007) Inference of macromolecular assemblies from crystalline state. *J Mol Biol* 372:774-797.
183. Huheey JE, Keiter EA, & Keiter RL eds. (1993) *Inorganic Chemistry : Principles of Structure and Reactivity* (HarperCollins, New York, USA).
184. Cordes EH & Jencks WP (1962) Semicarbazone formation from pyridoxal, pyridoxal phosphate, and their Schiff bases. *Biochemistry* 1:
185. Srivastava SK & Beutler E (1973) A new fluorometric method for the determination of pyridoxal 5'-phosphate. *Biochim Biophys Acta* 304:765-773.
186. Bagdanoff JT*, et al.* (2009) Inhibition of sphingosine-1-phosphate lyase for the treatment of autoimmune disorders. *J Med Chem* 52:3941-3953.
187. Jones DT (1999) Protein secondary structure prediction based on position-specific scoring matrices. *J Mol Biol* 292:195-202.
188. Bryson K*, et al.* (2005) Protein structure prediction servers at University College London. *Nucleic Acids Res* 33:W36-38.
189. Kaufman DL, Houser CR, & Tobin AJ (1991) Two forms of the gamma-aminobutyric acid synthetic enzyme glutamate decarboxylase have distinct intraneuronal distributions and cofactor interactions. *J Neurochem* 56:720-723.
190. Dunathan HC (1966) Conformation and reaction specificity in pyridoxal phosphate enzymes. *Proc Natl Acad Sci U S A* 55:712-716.
191. Cho W, Bittova L, & Stahelin RV (2001) Membrane binding assays for peripheral proteins. *Anal Biochem* 296:153-161.
192. de Andrade SA*, et al.* (2005) Conformational changes of Loxosceles venom sphingomyelinases monitored by circular dichroism. *Biochem Biophys Res Commun* 327:117-123.
193. Watanabe N*, et al.* (2008) Mechanism of substrate recognition and PLP-induced conformational changes in LL-diaminopimelate aminotransferase from Arabidopsis thaliana. *J Mol Biol* 384:1314-1329.
194. Pujals S & Giralt E (2008) Proline-rich, amphipathic cell-penetrating peptides. *Adv Drug Deliv Rev* 60:473-484.
195. Williamson MP (1994) The structure and function of proline-rich regions in proteins. *Biochem J* 297:249-260.
196. Yu H*, et al.* (1994) Structural basis for the binding of proline-rich peptides to SH3 domains. *Cell* 76:933-945.
197. Fink AL (2005) Natively unfolded proteins. *Curr Opin Struct Biol* 15:35-41.

198. Wells M*, et al.* (2008) Structure of tumor suppressor p53 and its intrinsically disordered N-terminal transactivation domain. *Proc Natl Acad Sci U S A* 105:5762-5767.
199. Helton ES, Zhang J, & Chen X (2008) The proline-rich domain in p63 is necessary for the transcriptional and apoptosis-inducing activities of TAp63. *Oncogene* 27:2843-2850.
200. Lomize AL, Pogozheva ID, Lomize MA, & Mosberg HI (2007) The role of hydrophobic interactions in positioning of peripheral proteins in membranes. *BMC Struct Biol* 7:pages not indicated.
201. Neumann P, Weidner A, Pech A, Stubbs MT, & Tittmann K (2009) Structural basis for membrane binding and catalytic activation of the peripheral membrane enzyme pyruvate oxidase from Escherichia coli. *Proc Natl Acad Sci U S A* 105:17390-17395.
202. Marcia M, Ermler U, Peng G, & Michel H (2009) The structure of Aquifex aeolicus sulfide:quinone oxidoreductase, a basis to understand sulfide detoxification and respiration. *Proc Natl Acad Sci U S A* 106:9625-9630.
203. Rufer AC*, et al.* (2007) Carnitine palmitoyltransferase 2: analysis of membrane association and complex structure with a substrate analog. *FEBS Lett* 581:3247-3252.
204. Lupas A, Van Dyke M, & Stock J (1991) Predicting coiled coils from protein sequences. *Science* 252:1162-1164.
205. Gut H*, et al.* (2009) A Common Structural Basis for pH- and Calmodulin-mediated Regulation in Plant Glutamate Decarboxylase. *J Mol Biol* 392:334-351.
206. Fenalti G*, et al.* (2007) GABA production by glutamic acid decarboxylase is regulated by a dynamic catalytic loop. *Nat Struct Mol Biol* 14:280-286.
207. Sivashanmugam A*, et al.* (2009) Practical protocols for production of very high yields of recombinant proteins using Escherichia coli. *Protein Sci* 18:936-948.
208. Fox BG & Blommel PG (2009) Autoinduction of protein expression. *Curr Protoc Protein Sci* Chapter 5:Unit 5.23.
209. Geertsma ER, Groeneveld M, Slotboom DJ, & Poolman B (2008) Quality control of overexpressed membrane proteins. *Proc Natl Acad Sci U S A* 105:5722-5727.
210. Lindner P*, et al.* (1997) Specific detection of his-tagged proteins with recombinant anti-His tag scFv-phosphatase or scFv-phage fusions. *Biotechniques* 22:140-149.
211. Edman P & Begg G (1967) A protein sequenator. *Eur J Biochem* 1:80-91.
212. Andréani P & Gräler MH (2006) Comparative quantification of sphingolipids and analogs in biological samples by high-performance liquid chromatography after chloroform extraction. *Anal Biochem* 358:239-246.
213. He X, Huang CL, & Schuchman EH (2009) Quantitative analysis of sphingosine-1-phosphate by HPLC after napthalene-2,3-dicarboxaldehyde (NDA) derivatization. *J Chromatogr B Analyt Technol Biomed Life Sci* 877:983-990.

10. ACKNOWLEDGMENTS

First of all, I would like to thank Markus Grütter for making this project possible and for all his support during the entire thesis. The scientific advices and state-of-the-art lab infrastructure he provided me were invaluable.

I am indebted to Guido Capitani. He initiated the project and followed it throughout its course. I appreciated so much his expertise, advices, support and patience. He guided me and taught me so many things (especially in crystallography) that he would actually deserve much more than four lines of acknowledgments!

Special thanks go to Prof. Howard Riezman, for the very nice collaboration, his help, and for expertise in functional assays and data analysis.

I thank Prof. Antonio Baici and Prof. Raimund Dutzler to be in my thesis committee.

I thank Prof. Daniela De Biase to share her expertise in spectroscopy. Her help was invaluable.

I'm very grateful to Christophe Briand, Beat Blattmann, Céline Stutz-Ducommun, Serge Chesnov and Bernd Roschitzki for their expertise, flexibility, motivation and enthusiasm. I thank my colleagues from the "L70 office", Heinz Gut, Christian Stirnimann, and our "guest" Oliv Eidam, for the excellent professional working atmosphere, advices and help. I extend these acknowledgments to all my colleagues from the Grütter group, as well as the Dutzler group.

I don't forget Prof. Peter Schürmann. I thank him for having accompanied my first steps into research and my (rapidly) growing interest for research. I enjoyed so much the wonderful master thesis project he offered me! I also thank my lab- and study mate Dominique Glauser for the fantastic five years of studies and practical work in Neuchâtel and especially for the collaboration during the last year.

My colleagues at PSI were fantastic: Daniela (thank you so much for your help and support!) and Antonietta, Remo, and Yannick.

Special thanks go to my friends the crazy Doucette and Guillaume, for opening my horizons and taking care of me, and to Céline (again!), Beatrice, Carine and Patrick for the great (too scarce!) time together.

I would like to deeply thank my family for their love, support and patience. They could cope with my (very frequent) mood fluctuations linked to research. I am so lucky to have you!

Last but not least, I thank Steve, the biggest and the most beautiful surprise of my life. He has shared my time for more than two years, heard, helped and supported me so well. Part of this thesis goes to you. You are simply brilliant!

11. *CURRICULUM VITÆ*

Personal data

Name	Bourquin
First names	Florence Evelyne
Date of birth	December 10th, 1979
Place of birth	La Chaux-de-Fonds (NE), Switzerland
Citizenship	Buttes, Les Verrières, La Côte-aux-Fées (NE), Switzerland

Education

1995-1998	High school (scientific section) in La Chaux-de-Fonds (NE), Switzerland
1998-2002	Undergraduate studies in biology, specialisation in biochemistry and plant physiology, at the University of Neuchâtel (NE), Switzerland
2002-2003	Diploma thesis at the Plant Biochemistry Laboratory, University of Neuchâtel Supervisor: Prof. Peter Schürmann Title: "Mutagenèse dirigée de la ferrédoxine:thiorédoxine réductase de *Synechocystis*: Aspects fonctionnels et interaction avec la ferrédoxine et les thiorédoxines f et m"
2003	Degree: Dipl. Biol.
2003-2005	Research associate at Paul Scherrer Institute (PSI), Villigen (AG), Switzerland Supervisors: Prof. Fritz K. Winkler, Dr. XiaoDan Li Subject: Structural studies of i-CLiPs (intra-membrane cleaving proteases)
2005-2009	PhD studies at the Department of Biochemistry, University of Zürich (ZH), Switzerland within the framework of the *NCCR Structural Biology* program Supervisors: Prof. Markus G. Grütter, Dr. Guido Capitani Collaboration: Prof. Howard Riezman, University of Geneva (GE), Switzerland
2009	Dissertation Title: "Questioning the Sphinx: Structural and functional studies of sphingosine-1-phosphate lyase"

Publications

Characterization of ferredoxin:thioredoxin reductase modified by site-directed mutagenesis. Glauser DA[*], Bourquin F[*], Manieri W, Schürmann P (2004).
J Biol Chem. **279**(16): 16662-9.
[*] equal contribution

Spectroscopic characterization of site-specific [Fe(4)S(4)] cluster chemistry in ferredoxin:thioredoxin reductase: implications for the catalytic mechanism. Walters EM, Garcia-Serres R, Jameson GN, Glauser DA, Bourquin F, Manieri W, Schürmann P, Johnson MK, Huynh BH. (2005).
J Am Chem Soc. **127**(26): 9612-24.

Structural snapshots along the reaction pathway of ferredoxin-thioredoxin reductase. Dai S, Friemann R, Glauser DA, Bourquin F, Manieri W, Schürmann P, Eklund H. (2007).
Nature. **448**(7149): 92-6.

Role of histidine-86 in the catalytic mechanism of ferredoxin:thioredoxin reductase. Walters EM, Garcia-Serres R, Naik SG, Bourquin F, Glauser DA, Schürmann P, Huynh BH, Johnson MK. (2009).
Biochemistry. **48**(5): 1016-24.

Structural basis for activity of eukaryotic and prokaryotic sphingosine-1-phosphate lyase, a key enzyme of sphingolipid metabolism
Bourquin F *et al.* (2009)
Manuscript submitted.

Courses and meeting contributions

2003	NCCR Practical course *"Characterization and Crystallization of Soluble and Membrane Proteins"*, 13-17.10.2003, University of Zürich, Switzerland
2009	7th NCCR Symposium on New Trends in Structural Biology, 07-08-09.2009, Zürich, Switzerland (poster contribution: Structural studies of sphingosine-1-phosphate lyase)